# WEAR AND CORROSION OF MECHANICAL SEALS

KAMALJEET SINGH SAGOO

Doctor of Philosophy

THE UNIVERSITY OF ASTON IN BIRMINGHAM

December 1988

The University of Aston in Birmingham

# Wear and Corrosion of Mechanical Seals

Kamaljeet Singh Sagoo
Doctor of Philosophy
December 1988

Summary

Mechanical seals are used extensively to seal machinery such as, pumps, mixers and agitators in the oil, petrochemical and chemical industries. The performance of such machinery is critically dependent on these devices. Seal failures may result in the escape of dangerous chemicals, possibly causing injury or loss of life.

Seal performance is limited by the choice of face materials available. These range from cast iron and stellited stainless steel to cemented and silicon carbides. The main factors that affect seal performance are the wear and corrosion of seal faces. This research investigated the feasibility of applying surface coating / treatments to seal materials, in order to provide improved seal performance.

Various surface coating / treatment methods were considered; these included electroless nickel plating, ion plating, plasma nitriding, thermal spraying and high temperature diffusion processes. The best wear resistance, as evaluated by the Pin-on-Disc wear test method, was conferred by the sprayed tungsten carbide/nickel/tungsten-chromium carbide deposit, produced by the high energy plasma spraying (Jet-Kote) process. In general, no correlation was found between hardness and wear resistance or surface finish and friction. This is due primarily to the complexity of the wear and frictional processes. Wear mechanisms observed in the investigation included adhesive transfer, oxidation, plastic deformation, ploughing, fracture and delamination.

Corrosion resistance was evaluated by Tafel extrapolation, linear polarisation and anodic potentiodynamic polarisation techniques. The best corrosion performance was exhibited by an electroless nickel/titanium nitride duplex coating due to the passivity of the titanium nitride layer in the acidified salt solution. The surface coating / treatments were ranked using a systematic method, which also considered other properties such as, adhesion, internal stress and resistance to thermal cracking.

The sealing behaviour of surface coated / treated seals was investigated on an industrial seal testing rig. The best sealing performances were exhibited by the Jet-Kote and electroless nickel silicon carbide composite coated seals. The failure of the electroless nickel and electroless nickel/titanium nitride duplex coated seals was due to inadequate adhesion of the deposits to the substrate. Abrasion of the seal faces was the principal wear mechanism. For operation in an environment similar to the experimental system employed (acidified salt solution) the Jet-Kote deposit appears to be the best compromise.

Key Words: Mechanical seals, surface coatings, wear resistance, corrosion resistance, friction.

# DEDICATION

This thesis is dedicated to Sant Baba Puran Singh Ji, Sant Norang Singh Ji, my father, my late mother, my wife and my son Attar.

## ACKNOWLEDGEMENTS

I would like to thank the Science and Engineering Research Council and Flexibox Ltd. for their financial support of this project.

I would also like to thank my supervisor, Dr.J.K.Dennis for his guidance and encouragement throughout the course of this work. Thanks are also due to members of the staff and technicians of the Department of Mechanical and Production Engineering of Aston University for their assistance and valuable advice.

CONTENTS

Page No.

Page No.

Page.No.

## LIST OF FIGURES

## LIST OF TABLES

# CHAPTER I

## 1.0 INTRODUCTION

Seals are mechanical devices used to prevent leakage of liquids, solids or gases. They may be classified into two major categories, static and dynamic. Static seals comprise of three major groups, known as gaskets, sealants and direct contact seals. In this category, sealing takes place between surfaces which do not move relative to each other, e.g. cylinder head gasket (motor car). Dynamic seals can also be subdivided into two basic groups designated as seals for rotating shafts and seals for reciprocating shafts; a piston ring is a typical example from the latter group. General classification for all seals is shown in Figure 1.

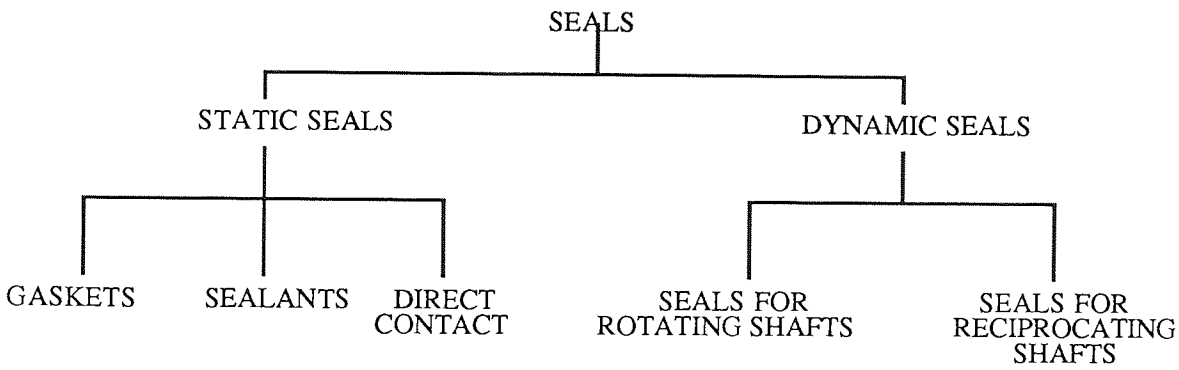


Figure 1 General Seal Classification

Rotating shaft seals comprise of two principal groups. interfacial seals and interstitial seals. The former group is subdivided into axial seals and radial seals, as shown in Figure 2. Interstitial or clearance seals are used for sealing gases where minimum power loss is required and speeds are high, e.g. compressors and turbines. In this

group, sealing components have no direct mechanical contact with the rotating shaft, and consequently the leakage is high compared with interfacial seals.

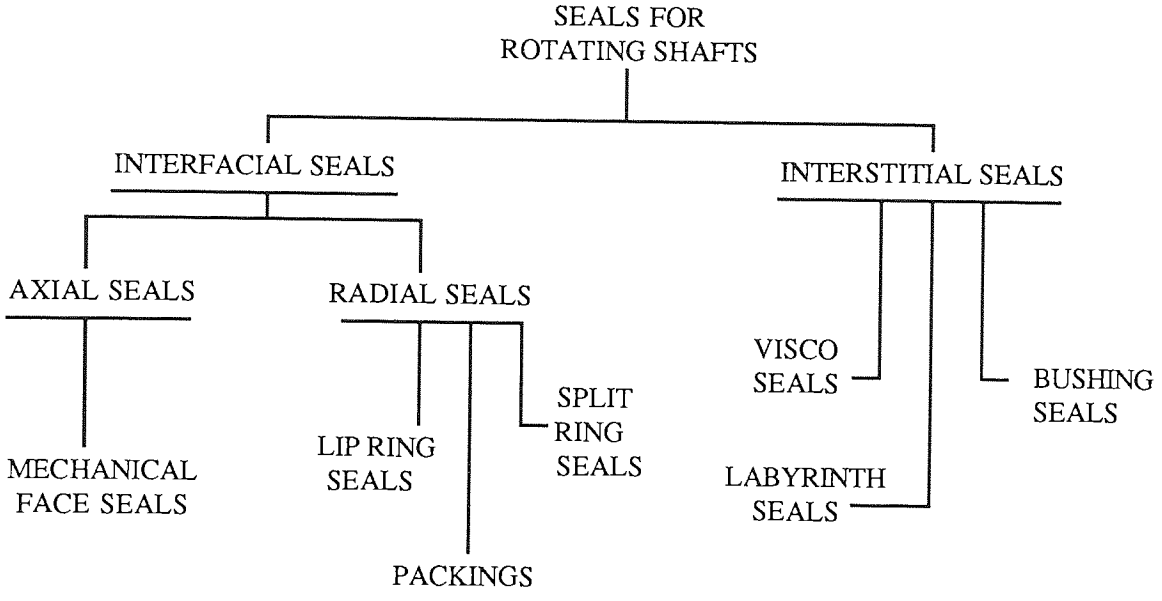


Figure 2. Classification Chart for Rotating Shafts Seals

Interfacial seals represent a very large family of industrial sealing devices that establish a direct contact between the sealing components and the rotating shaft. Lip seals are primarily used to seal oil splash with shaft using rolling element bearings, e.g. gearboxes. However, they have the following limitations:

(a) Low pressure limits (1 $MN/m^2$) sealed pressure)

(b) Poor tolerance for shaft defects

(c) Elastomeric lip seal materials tend to thermally degrade above 90°C.

The other type of radial seals are packed glands, these provide low cost sealing at moderate pressures and speeds, e.g. pumps and agitators. However, they are limited to sealing fluids at moderate pressures (3 $MN/m^2$). Furthermore, relatively high power loss and shaft wear can occur. With mechanical seals these problems can be overcome

and they are used to handle a wide diversity of fluids, temperatures (up to 500°C), pressures (10 $MN/m^2$) and speeds. Moreover, they impart low leakage, higher reliability and longer life (three times) compares with packed glands.

Mechanical seals are used in machinery such as centrifugal pumps, injection pumps, mixers and compressors, in such industries as petro-chemical, chemical, oil and food manufacturing. The performance of the pump is critically dependent on mechanical seals. Seal failure may result in the escape of dangerous chemicals, possibly causing injury or loss of life.

It may necessitate costly plant shutdown until a repair is completed. In general, mechanical seals exhibit unpredictable service life and reliability. For example, some of the comments made by the U.K. process industries are as follows[1]:

Esso Petroleum: "Mechanical seal failure is unquestionably the most frequent cause of pump failure."

B.P. Chemicals: "60 percent of all the company's plant breakdown are due to mechanical seal failure."

I.C.I. : "The mechanical seal is one of the most unreliable items of equipment on process plants."

Various surveys have been conducted to quantify seal failure rates; these are summarised as follows:

(1) Buck[2] studied refinery seals and concluded that "most seals fail prematurely." Less than 10 percent of his 36 failed seals had worn out.

(2) Summer-Smith[3] studied centrifugal pumps, his results were presented as Weibull charts. The Weibull indices, $\beta$, for the seals ranged between 0.7 and 1.1, indicating a mixture of infantile mortality ($\beta = 0.5$) and random mid-life failure ($\beta = 1.0$), but not the wear out situation ($\beta = 3.4$).

(3) The British Hydromechanic Research Association (B.H.R.A.)[4-8] investigated seal failures in a variety of pump applications, their survey showed the following salient points.

(a) Discontinuous seal operation leads to a notably short life.

(b) The type of fluid being sealed was found to have direct bearing on the life expectancy of a seal, and the life achieved by mechanical seals operating on different classes of fluids. . If the fluid concerned was corrosive or a polymer, most seals required replacement within six months.

(c) High vibration levels in pumps resulted in reduced seal life.

(d) High fluid pressures and/or temperatures adversely affect seal life.

Seal performance is limited by the choice of seal face materials available. These range from cast irons and stellited stainless to cemented carbides and silicon carbides. The main objectives of this research are as follows:

(1) Critically review the literature to ascertain potential surface coatings / treatments for mechanical seal application.

(2) Evaluation of the wear and corrosion properties of the surface coatings / treatments selected above, using appropriate laboratory tests.

(3) To investigate the feasibility of applying surface coatings / treatments to seal components, by evaluating their performance on an industrial seal testing rig.

# CHAPTER II

## 2.0 MECHANICAL SEALS

Mechanical seals comprise of rotating and stationary elements in "rubbing contact" to form a sealing face with a minimal leakage. Buchter's (9) book on "Industrial Sealing Technology" covers a wide range of sealing devices and includes a good review on the fundamentals and application of mechanical seals. Mayer's (10) book on "Mechanical Seals" provides a wealth of information and is regarded by many, as a handbook on the subject.

### 2.1 Principles of Operation

An unbalanced mechanical seal is shown in Figure 3. It consists of the following components:

1) Primary Seal Rings

2. Secondary Seal Rings

3. Spring

The primary seal ring faces have a lapped surface finish and are optically flat to within two light bands. One of the primary seal rings (usually a Ceramic or Cemented Carbide) is attached to the shaft and rotates with it, which is termed the rotor. Whilst the other primary ring (usually Graphite) is held resiliently in the gland housing and is stationary; this is termed the stator. Secondary sealing components are by definition designed to seal the primary seal rings in order to prevent leakage along the shaft and the cavity of the gland plate to atmosphere.

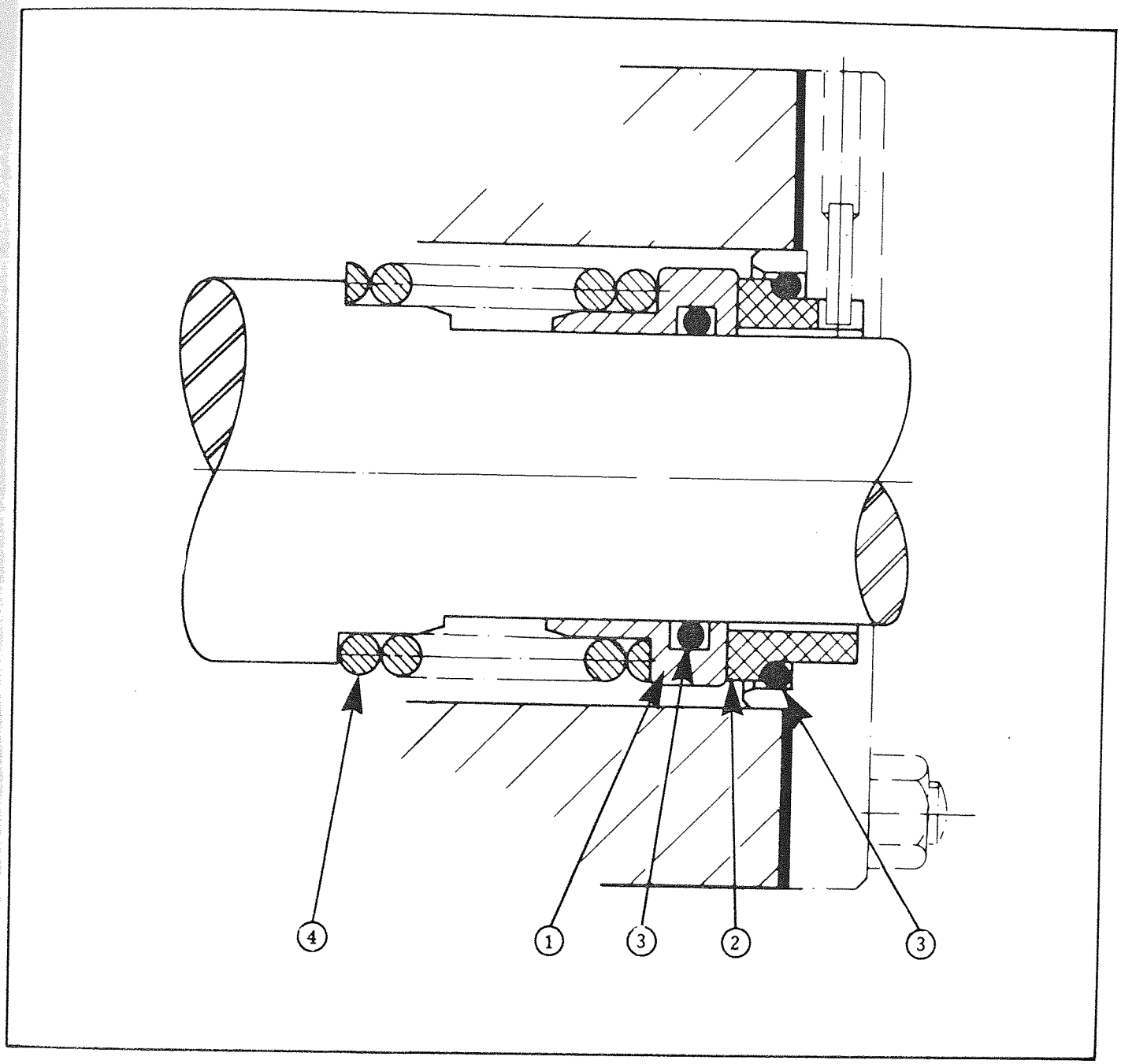


SEAL COMPONENTS

1. ROTARY SEAL RING
2. STATIONARY SEAL RING
3. SECONDARY SEAL RING
4. SPRING

Figure 3. An unbalanced mechanical seal(13).

Initial seal face contact is maintained by the spring. An interference fit between the spring and the shaft at one end provides a positive resilient drive.

The system fluid pressurises the entire seal unit and, due to the extreme flatness of opposing primary rings, intimate rubbing contact results. Thus, any kind of leakage of the system fluid must pass across the rubbing interface, hence, mechanical seals are not zero leakage devices but exhibit a controlled leakage which is dependent on the nature of the fluid being sealed, operating parameters of the pump and maximum permissible leakage rate. The key to good sealing is the formation of a thin lubricant film across the rubbing interface. Before considering in more detail the lubrication in mechanical seals, it is necessary to consider the effect of the system fluid pressure on the primary seal rings.

### 2.1.1 Hydraulic Balance (9-12)

A hydrostatic fluid pressure is generated at the rubbing interface and results in the formation of a pressure wedge which opposes seal face contact. The term hydraulic balance, when applied to mechanical seals, is used to denote the relationship between the pressure being sealed and seal face contact pressure. Seals are classified as balanced or unbalanced, but within each classification there is variation of degree of balance. In both types of seals, the initial face load is provided by the seal spring. Hydraulic balancing is a design manipulation whereby the seal face contact pressure can be reduced, with respect to pressure being sealed. Unbalanced mechanical seals are used to seal fluids up to 10 bar, whereas balanced seals can be used up to 85 bar. The variation

of hydraulic balance is illustrated in Figure 4. The diameter of the seal sleeve shoulder, S, represents the effective sealing diameter. The hydraulic piston area, A, of the rotor and the contact face of the sealing faces, B, are shown. In arrangement (i), all the contact face area B is disposed outside the effective sealing diameter S and the hydraulic piston area A is equal to the contact face area B. In this design, the average face contact pressure will be exactly one hundred percent of the hydraulic pressure sealed.

In arrangement (ii), all contact face area B is disposed outside the effective sealing diameter S and the hydraulic piston area A is greater than the contact face area B. In this case, the average face contact pressure will be more than one hundred percent of the hydraulic pressure sealed. Arrangement (iii), shows the relationship of most balanced seals, here a part of the contact face area, B, designated as B1, is disposed outside the effective sealing diameter, S, the total seal face area B, will be equal to the sum of B1 and B2. The unit face loading will be less than pressure sealed, in accordance with the ratio of the two areas i.e.

$$\frac{B1}{B1 + B2} = \frac{A}{B} \qquad (1)$$

This value, expressed as a percentage indicates the degree of balance of the seal. In balanced seals, lowering of the seal face pressure allows a thicker fluid film between the faces, thus reducing the friction and consequent heat generation. Hence, a balanced seal is able to tolerate more arduous conditions and higher fluid pressures than an unbalanced seal. However, balanced seals typically cost 10 to 50% more than unbalanced seals for the same application because of closer tolerances and more

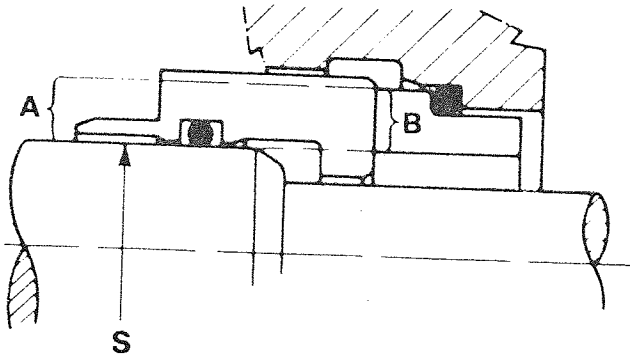


ARRANGEMENT (1)

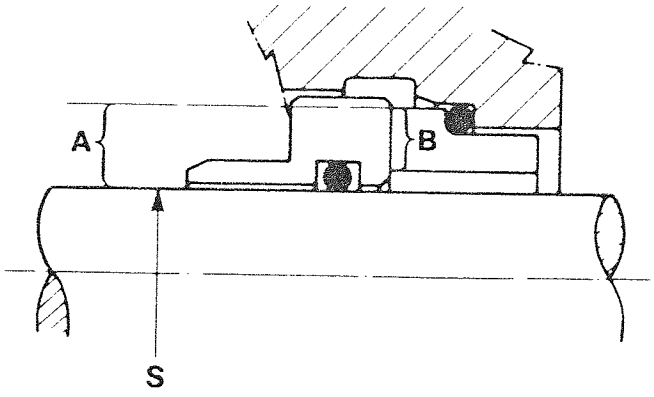


ARRANGEMENT (11)

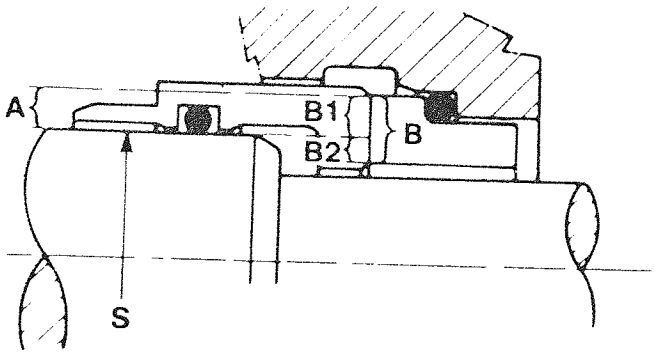


ARRANGEMENT (111)

Figure 4. Hydraulic balancing of mechanical seals(13)

complex seal shapes. Moreover, they are subject to catastrophic failure, if the operating conditions do not closely match design conditions. A key factor in evaluating seal operation is the P.V. factor, the product of seal contact pressure and the sliding velocity.

### 2.1.2 P.V. Factor [9-12]

Seal manufacturers use the so called "P.V. factor" to characterise the ability of the material to resist wear. This parameter determines the suitability of material combination for seal faces, and specifically the amount of heat generated at the face.

$$P.V. = \text{pressure} \times \pi \times \text{seal diameter} \times \text{rotational speed} \quad (2)$$

units normally applicable are:-

$$\text{bar m/sec} = \text{bar} \times \pi \times \text{m} \times \text{rev/sec.} \quad (3)$$

Typical values of the P.V. capability of different face material combinations are given below [13].

| Stator Vs Rotor | P.V bar m/sec) |
|---|---|
| Carbon Vs hard faced stainless steel | 190 |
| Carbon Vs leaded bronze | 190 |
| Carbon Vs nickel iron | 400 |
| Carbon Vs tungsten carbide | 900 |

### 2.1.3 Lubrication in Mechanical Seals

Hydrodynamic lubrication is generally believed to be most widely applicable, when the seal is running normally at speed. However, when the speed is low, as when starting or stopping, or when the operating fluid is a particularly poor hydrodynamic lubricant, then the boundary lubrication mode takes over. It is for this reason that a good boundary lubricant such as carbon-graphite is used for primary seal rings (stators). The key question that arises is, how can hydrodynamic fluid pressures be generated between two optically flat primary seal rings?

Various workers [14-16] have shown that a hydrodynamic pressure larger than the hydrostatic is generated in the fluid film due to effects of waviness, misalignment and vibration of the faces. For example waviness provides the necessary convergent geometry for hydrodynamic pressure generation. Waviness takes the form of gentle variation of flatness around the seal face, with separation of the high spots of the undulation of the order 20mm and amplitude of only few light bands (0.25 microns). .

How does the concept of hydrodynamic lubrication of mechanical seals relate to actual seal operation; in view of the seal failure problem outlined in the introduction. Mechanical seals handle a wide diversity of fluids as mentioned earlier. The viscosity of the fluid is important, fluids which are more viscous tend to be better hydrodynamic lubricants. However, for very viscous fluids, shearing of the fluid film may result in increased friction and possibly rupturing of carbon-graphite (stator) rings. Secondly, it is necessary for a stable fluid film to exist between the faces, for efficient running of seals. If this film stability is destroyed, excessive wear takes place leading to rapid seal

failure. If the sealed fluid is volatile, e.g. ammonia, or if the heat generated at the seal interface is not conducted away efficiently, stable lubricant film is unlikely to form. Finally, as the hydrodynamic film is very thin, 1-3 microns, slight distortion of seal faces, resulting from hydraulic forces on the seal or from thermal stresses (due to temperature gradients), could disrupt the film.

### 2.1.4 Leakage

There are various causes for face seal leaks, these normally take place through the radial gap formed by the two sliding surfaces. The main factors influencing the distortion of the seal gap are:

(1) Axial forces

(2) Radial forces

(3) Temperature gradients.

The net effect of the above factors is to cause distortion of the seal ring, such that it alters the position of seal face contact, as shown in Figure 5.

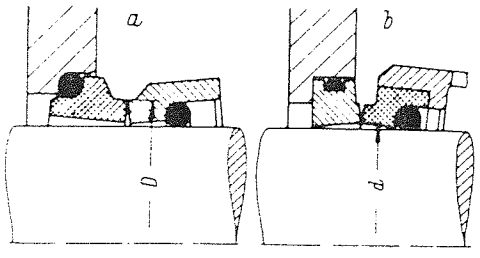


*(a) contact at outside diameter D; (b) contact at inside diameter d*

Figure 5. Mechanical and Thermal distortions of Seal rings[10]

If, for instance, because of distortion a gap has formed which permits the liquid under pressure to enter the gap, then hydrostatic load relief occurs which results in increased leakage. If the closing force is still sufficient, the subsequent wear will produce a parallel gap. Thus, wear is the stabilising influence which tries to control the shape of the seal gap. In mechanical seals, the running in process can take several minutes or up to several months. The period depends mainly upon the degree of distortion, the resistance to wear and the net load.

## 2.2 Materials for Mechanical Seals

The books by Buchter [9] and Mayer [10] cover broadly the materials commonly used for the components in mechanical seals. Papers by Schoeherr [17] and Field [18] look at materials for seal faces and secondary sealing rings. Bayliss [19] has examined various elastomeric materials for secondary sealing rings and compares their mechanical and chemical properties. Whately [20] reviews the latest advances in materials for seal faces. The main materials commonly used for seal faces are as follows:

(1) Carbon-graphite

(2) Metals and alloys

(3) Ceramics

(4) Metal carbides.

### 2.2.1 Primary Seal Ring Materials

#### 2.2.1.1 Carbon-Graphite:

Carbon-graphite is inert to most common chemicals and has an inherent quality of self-

lubrication not readily found in other seal ring materials. Carbon has excellent resistance to thermal shock. It provides very good wear characteristics desirable for seal performance. Its coefficient of friction varies from 0.04 to 0.25, depending on grade and type of application.

Carbon graphite, either plain or impregnated with resins, inorganic salts, polymers, or metals such as lead, babbit, antimony or silver, is used in large quantities for primary rings in combination with a variety of metal alloys, alumina, ceramics and tungsten carbides. Impregnation imparts additional strength to the structure, higher resistance to general face wear, and higher resistance to increased hydrostatic pressure. In an attempt to increase the wear resistance of carbon-graphite, siliconised graphite has been developed.

2.2.1.2 Siliconised-Graphite:

This is essentially a thin layer of SiC on carbon-graphite rings which is claimed to have superior wear resistance. Siliconised graphite rings are prepared by reacting machined graphite rings with a source of silicon at temperatures of 1900-2500 K. i.e.

$$SiO + 2C \rightarrow SiC + CO \qquad (4)$$

Silicon monoxide vapour diffuses into the pores of the machined graphite reacting with the graphite to form silicon carbide. Reaction is greatest at the surface and less in the interior. The thickness of reacted zone is approximately 0.5-1mm.

Properties claimed for siliconised-graphite:

(1) Good corrosion resistance (acids and alkalis)

(2) Outstanding thermal shock resistance

2.2.1.3 Metals and Alloys

Cast iron, nickel resist and certain types of tool steels are used for primary seal rings under low pressure conditions at low rotational velocities when corrosion is not a factor. Bearing and leaded bronzes are used in certain applications where the low tensile strength and low modulus of elasticity of carbon-graphite are disadvantageous because of seal deflection problems.

In the presence of mild corrosive atmospheres hardenable stainless steels and/or stellites (cobalt-nickel-base alloys) can be used. Stellite is an excellent material for seal faces where fluids with good lubricity and lower temperatures are used and steady operating conditions are guaranteed. Stellite is very susceptible to the phenomena of heat checking. The other non-ferrous metals/alloys which are often used in seals for corrosive situations are, aluminium bronze, Hastelloy C and titanium.

Aluminium bronze is often used as seal mating material when salt solutions and sea water have to be handled. However, it has been found that selective attack of the Kappa phase occurs in sea water. Various nickel alloys are also used, such as Inconel, Monels and Hastelloy C. Monel is nickel-copper alloy which has high corrosion resistance to acids, alkalis, brine, water, food products and the atmosphere. Hastelloys are nickel-chromium-molybdenum-iron based alloys which are characterised by their high corrosion resistance to oxidising acids such as nitric, chromic, and sulphuric acids. However, these particular alloys are expensive and have a moderate hardness (200-300 B.H.N.) and consequently are unlikely to have sufficient wear resistance for arduous situations.

#### 2.2.1.4 Ceramics

The oxides of magnesium, aluminium and silicon are used as sliding face materials for their extreme chemical inertness and high hardness (1500-1750Hv). Ceramics are generally acceptable for most acidic environments, however, they are prone to attack in alkalis; due to the amphoteric nature of the oxides. Furthermore ceramics are brittle and are sensitive to impact loads and thermal shock. They are also particularly prone to severe heat checking.

#### 2.2.1.5 Metal Carbides

This group includes carbides of tungsten, silicon and boron and they are particularly notable for their high hardness and wear resistance. Tungsten carbide has been advocated for seals in abrasive environments [21]. However, the cobalt binder is prone to selective leaching in corrosive environments . Although binders such as chromium-cobalt have been proposed [22] and are claimed to be more corrosion resistant Lashway [23] has suggested the use of silicon carbide for corrosive wear seal face applications. Essentially there are two types of silicon carbide:

(1) Sintered SiC ($\alpha$ or $\beta$ crystals, no free silicon)

(2) Reaction bonded SiC (SiC + 10-20% silicon).

##### 2.2.1.5.1 Sintered Silicon Carbide

This contains small amounts of sintering aids such as aluminium or boron or their compounds, e.g. aluminium carbide. Aluminium carbide is subject to corrosion, therefore, may cause a drop in strength (similar to the leaching of Co). Since it contains no free silicon it therefore, exhibits excellent corrosion resistance. Small, evenly

distributed pores which are not interconnected are preferred.

#### 2.2.1.5.2 Reaction Bonded Silicon Carbide

This is manufactured by subjecting a compact of alpha ($\alpha$) silicon carbide and carbon to liquid silicon at high temperatures. The liquid silicon penetrates the compact and reacts with the carbon to form beta silicon carbide which bonds the original alpha silicon carbide grains together. A free silicon content (10-20%) fills the remaining porosity, this results in an impermeable material.

Lashway et al [24] have investigated the corrosion resistance of various grades of silicon carbide and other face materials in corrosive fluids. Sintered silicon carbide exhibited a much better corrosion resistance than reaction bonded silicon carbide; attack of the free silicon, in the latter, is largely responsible for the poor corrosion resistance.

## 2.3 Failure of Seals

Seal failure is often caused by loss of the lubricating film, resulting in high wear and friction, and manifests as either excessive leakage or seizure of the pump. A useful guide to seal failures and their causes and remedies has been given by Neale [25]. Wear of the seal faces is influenced by alteration of a major factor such as lubrication conditions, interface loading, rubbing speed, temperature, lubricating property of the media, properties of solids in suspension, etc.

2.3.1 Wear of Seal Faces

Mayer [9] has classified seal face wear into five groups:

(1) Adhesive wear from attractive surface forces.

(2) Abrasive wear from the filing effect of the rough surface or foreign bodies in the seal gap.

(3) The corrosive wear which is initiated by chemical and especially high interface temperature.

(4) Surface wear which is caused by either thermal stress or fracture in the sliding faces.

(5) Radial wear which can be caused by the erosive effect of liquids and gases at high fluid rates.

In general, carbon-graphite, being relatively soft, is subject to abrasive wear; particularly when there is no lubricating film between seal faces, or if there are abrasives present in the fluid. Figure 6 shows schematically the appearance of seal faces after dry running and in the presence of abrasives, respectively. Besides being highly susceptible to abrasive attack, carbon-graphites are also prone to failure by sludging and carbon blistering.

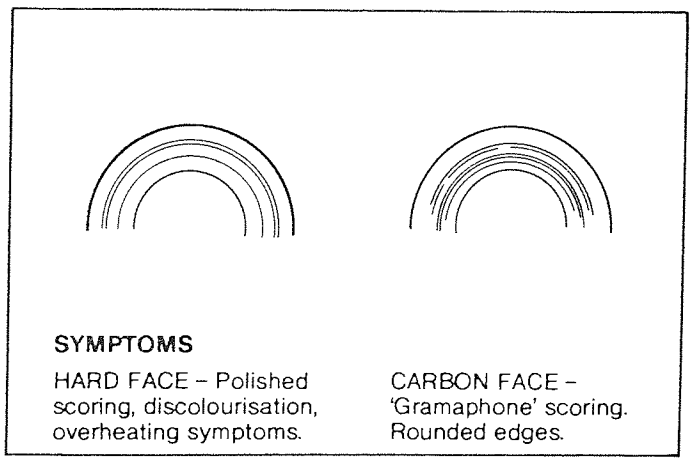


Figure 6. Dry running of Seal faces[13].

Sludging often occurs when sealing high viscosity fluids. When the shear stress between the seal faces exceeds the rupture strength of the carbon, particles are pulled out of the face [26]. This problem is quite prevalent in the case of pumps sealing hydrocarbons. Carbon blistering tends to occur on pumps sealing oil and petroleum products. "Blistering" usually appears as glossy areas and/or pits in the running face of the carbon. Strugala [27] suggests that carbon blistering, is mainly due to transient expansions of the oil which has penetrated the pores in the carbon, due to thermal cycling. This results in the formation of sub-surface cracks, which leads to exfoliation of sub-surface layers.

Merrick and Brooks [28,29] investigated the mechanism of wear of nickel and nickel molybdenum alloys against themselves. They tried to simulate contact that would occur in face seals during shutdown or start up when lubrication is not operative. Scanning electron microscopy revealed that worn surfaces were plastically deformed and exhibited a smeared and layered topography. Furthermore, they noted the presence of raised areas, termed wedges, which were thought to be formed by shearing of local contact junctions. Moreover, these 'wedges' could work harden and act as abrasive particles. In the case of a harder material against a softer material, severe smearing and abrasion of the latter was observed. Adhesive transfer of the softer material occurred on the harder counterface. Roan and Brooks [30] investigated the wear behaviour of Hastelloy B against graphite. This combination is recommended for wear applications in corrosive environments. In the low wear regime, graphite smeared over the counterface, and acted as a solid lubricant. At a higher PV factor, corresponding to heavy wear, the counterface exhibited numerous ploughing marks. This abrasive action was thought to be due to SiC particles in the graphite counterface. Hard face materials,

such as metal carbides, are not as afflicted by abrasive wear as the materials mentioned above. However, they are susceptible to thermocracking and corrosion.

### 2.3.2 Thermocracking

One of the greatest dangers in mechanical seals is the formation of thermal stress cracks on the sliding faces. Thermocracking is illustrated schematically in Figure 7 (a,b, c) .

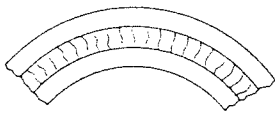

(a) parrallel radial cracks

(b) radial cracks with blisters

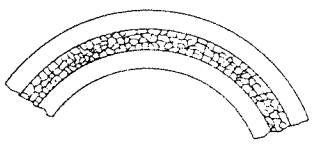

(c) surface crazing

Figure 7. Thermocracking of Mechanical Seals [25]

Mayer [10] suggests that these cracks may be caused by momentary overload due to dry running, as a result of failure of coolant or by a large load or speed variation. The cracks lead to increased wear and can act as paths for leakage. Sibley[31] has suggested that thermal stress cracks are caused by hot spots on sliding faces. Thus, due to differential thermal expansion, surface stresses are set up, which, when high enough lead to crack formation. Hence, the presence of thermal gradients across the seal width are important. Properties such as thermal conductivity and diffusivity influence the magnitude of the thermal gradient, and therefore the mismatch.

The thermal stress parameter (T.S.P.) expresses the tendency of the material to crack radially under a thermal gradient [33]. The thermal stress parameter is as follows:

$$\text{T.S.P.} = \frac{\text{T.D} \times \text{U.T.S}}{\text{Y.M} \times \text{C.E}} \qquad (5)$$

where:

T.D= Thermal conductivity

U.T.S= Ultimate tensile strength

Y.M.= Youngs modulus

C.E.= Coefficient of linear expansion.

In general, the higher the T.S.P., the greater the resistance to thermocracking. Table 1 shows typical values of T.S.P. for various materials.

Table 1 Thermal stress parameters for various materials

| Material Thermal Shock Parameter | Cal / cm/ s |
|---|---|
| Sintered silicon carbide | 60 |
| Reaction bonded silicon carbide | 59 |
| Tungsten carbide (6% Co) | 48 |
| Aluminium oxide | 7 |
| Mechanical carbon | >50 |

The actual mechanism of thermocracking is still not understood fully. Abar [32], using thermocouples behind stationary carbon, found that for materials which exhibited cyclic carbon temperatures (e.g. SiC), there was a tendency for thermocracking. It was suggested that this may be due to repetitive partial or complete loss of lubrication which consequently results in variation of frictional heat produced. Another view is that a high rate of heat generation (high friction) at the seal face and intermittent cooling, are necessary for thermocracking to occur [33]. Intermittent cooling is thought to be caused by face seal deflections, e.g. thermal deflection.

Since mechanical seals are often subjected to complex environments, potential causes of failure are difficult to isolate. Metcalfe [34] has classified failure of mechanical seals in Nuclear Service applications into the following three categories:

(1) Design failure

(2) Installation failure

(3) Operator failure.

For example, inadequate lapping is a manufacturing failure, which leads to inadequate overall flatness and consequently excessive leakage. Inadequate lapping is a prime cause of early seal failure. If seal faces and other surfaces which the seal relies upon for support, are not lapped sufficiently, then excessive leakage and/or friction may cause failure, often immediately. Spherical and saddle shaped surfaces are two examples of inadequately lapped surfaces. It has been recommended that flatness tolerance for seal faces should be within one light band per 70mm seal diameter using the optical interference technique.

### 2.3.3. Corrosion of Seals

Although hard carbides have extremely high resistance to abrasion, they are attacked by various chemicals. The following carbide mechanism has been proposed [35].

Sintered hard carbide alloys are powder metallurgical products made of refractory metal elements combined with low melting point matrix or binder material, e.g. cobalt. When the sintered tungsten carbide corrodes, the cobalt binder dissolves, leaving the skeletal structure of the tungsten carbide intact. The corrosion removes the binder from the seal ring, resulting in rapid wear, leakage and weakening of the carbide ring.

The following forms of corrosion apply to carbide seal rings [36]

(1) Galvanic or two metal corrosion

(2) Concentration cell corrosion

(3) Erosion

(4) Direct chemical attack

(5) Oxidation.

2.3.3.1 Galvanic

When an electrolytic fluid is being sealed, tungsten carbide seal rings may be attacked by galvanic action. For example, if a WC/Co seal ring is used in a seal containing an electrolyte, such as NaCl, with a mating ring or seal housing or other components of metallic copper in the near vicinity of the rings, severe galvanic corrosion will occur.

2.3.3.2 Erosion-Corrosion

If the seals are separated at high pressures, the fluid radial velocity across the seal can be extremely high, causing erosion of the seal face. When the material being sealed is also corrosive to the seal face, the carbide grain can be loosened by dissolution of the binder. The result may be extreme erosion of the carbide so that radial grooves are formed on the face of the carbide.

To improve the corrosion resistance of tungsten carbides, alternative binders to cobalt have been suggested, such as Co-Cr and Ni binders. However, from an electrochemical viewpoint, the above binders would lead to the formation of dissimilar metal corrosion cells. Field experience has shown that nickel is no better than cobalt as the binder [37].

2.3.3.3 Concentration Cell Corrosion / Differential Aeration

Concentration cell or crevice type corrosion may occur in stagnant areas of seals where solution accumulates, local anode - cathode cells are set up and subsequent corrosion takes place. Differential oxygen concentration cells may also be set up; an interesting

example of this form of corrosion has been cited by Hirano [38]. He investigated the problem of excessive starting torque of mechanical seals (stainless steel versus graphite) used for centrifugal pumps. After standstill for a long period the machine could no longer be driven easily by its own electric motor. Results of experimental investigation indicated that sealing surfaces were stuck together as a result of black pitting spots on the stainless steel surface. These junctions resisted shearing at the start. The passive oxide film on the stainless steel was broken down by rubbing action. The presence of an oxygen concentration cell across the seal width promotes crevice corrosion on the steel surface.

## 2.4 Design, Materials and Applications

The establishment and maintenance of a liquid film between two sealing members is very important, particularly in adverse conditions, to optimise the seal life. The chemical/physical properties of the fluid to be sealed, operating conditions and degree of danger implied by an ineffective seal should be considered in depth at the design stage.

It may be difficult to establish a stable film, for example, seals used in handling super heated water. In this case, a drop in pressure across the seal face combined with an increase in temperature generated by face friction reduces the stability of the interface film. Wilkinson [39] lists two factors which influence the interface film temperature:

(1) Friction heat generated at point of rubbing.

(2) Heat soak via the pump casing, shaft and shaft sleeve.

Wilkinson advocates the use of heat exchangers built into the seal housing adjacent to the rubbing faces to dissipate the frictional heat. However, the overall cost of sealing increases, hence the above method should be used only where it is economically viable. In chemical, petroleum and related industries, numerous fluids are handled that can, under no condition, be considered lubricants between the rubbing contact areas of the seal. A similar situation exists when the fluids contain abrasives or any foreign particles that could affect the seal faces.

In the chemical (40), and petrochemical industry (50), the use of double and tandem seals is advocated for arduous sealing applications.

### 2.4.1 Double Seals

In this configuration two single seals are arranged back to back to maintain a liquid barrier fluid. The inner seal operates on the barrier fluid which is kept at a pressure higher than the product, and therefore any leakage is of the barrier fluid and not the pump product. The barrier fluid, to some extent, contaminates the product; thus, both fluids should be compatible with each other. Double seals are often used when product leakage is unacceptable for economic or hazardous reasons. A typical double seal is shown in Figure 8.

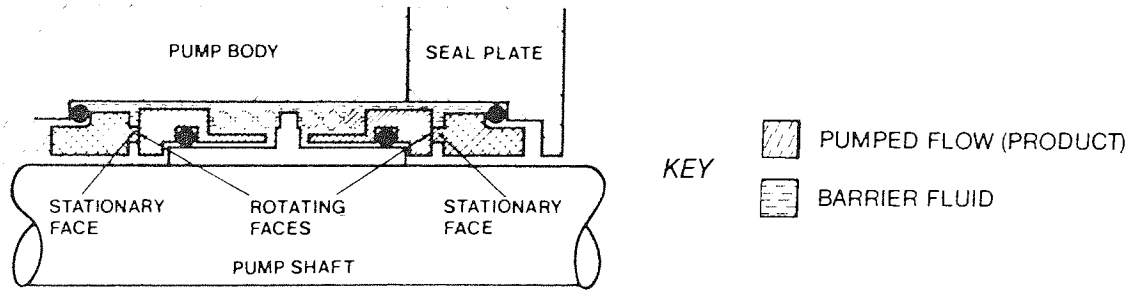


Figure 8 . Double Seal arrangment for Mechanical Seals (13).

### 2.4.2 Tandem Seals

Tandem seals are used when the contamination of the product by the barrier fluid is undesirable. In this design, both seals are faced in the same direction rather than back to back, as for double seals. Furthermore, the barrier fluid pressure is less than that of the product pressure at the inner seal. Thus, the pumped product leaks into the barrier fluid, thereby avoiding the contamination of the product.

When mechanical seals are confronted with handling abrasive fluids, erratic leakage, excessive face wear and relatively short life can be expected. Various methods have been developed to keep the solid particles away from the seal parts. Norton [42] and Tankus [43] has suggested the use of the following techniques.

(1) Double seals

(2) Single seals with flushing gland

(3) Grease lubricated seals

(4) Centrifugal separators.

Trytek [44] has discussed the problem of sealing hot water, apart from the difficulty in establishing a stable fluid film between the seal faces, the presence of suspended solids in water, can be problematic. A carbon-graphite stator and tungsten carbide rotor, operating on a hot water system containing suspended solids, failed after six months, only one quarter of its design life. The carbon-graphite seal face exhibited severe abrasive wear. Trytek [44] also advocates the use of some of the above methods to divorce the abrasive particles from the seal faces. In the above case fluids are inherently abrasive, whereas certain fluids in chemical and petrochemical fields show tendency to crystallise

when subjected to certain thermal environments.

e.g. ammonium nitrate

pthalin hydrides, and

malic hydrides.

Hence, when equipment handling these fluids is shut down and permitted to attain ambient temperatures, the film remaining between the faces is transformed into crystalline matter. Abrasive wear takes place on seal faces when equipment is switched on. As heat is generated, these crystals revert to fluids. Hence, there is a need to promote some means of temperature control around the seal area before start up. Various heating methods have been discussed by Tankus [43].

N.B. Temperature of crystalline dissipation must be attained prior to permitting any dynamic action of the seal chamber.

The above discussion has mainly dealt with various design techniques to combat abrasion, whilst for seals in corrosion/wear situations much of the work has been done on selection and development of new face materials.

Shiro and Schoenherr [45] describe the problem of sealing highly corrosive boric acid (12%) at 106°C with mechanical seals in nuclear plants. Apart from its potent corrosive nature, with boric acid there is a likelihood of precipitation of boric acid between the sealing faces, and consequently abrasive wear conditions. The results with different seal face materials are as follows:

(1) Binderless tungsten carbide (chipping and scoring of surface).

(2) A chromium oxide coating on 316 stainless steel (heat checking)

(3) Hard chromium plating (badly worn)

(4) $Al_2O_3$ (ceramic) (high leakage).

A boron carbide ($B_4C$) stationary ring and carbon graphite rotating ring were tested for over 1,000 hours in 12% boric acid at 82°C. The boron carbide ring was in excellent condition with no signs of corrosive attack at the end of the test.

Carbon-graphite systems have good 'self' lubricating properties but are 'softer' relative to hard face materials and are susceptible to more wear, particularly in abrasive environments. Siliconised graphite has been proposed as an alternative to carbon-graphites because the former is claimed to have better wear resistance.

Paxton et al [46] reported that siliconised graphite produced lower rates of wear on the carbon seal nose than either tungsten / carbide or fused alumina. Mowrey [47] using a test rig, evaluated the wear and leakage characteristics of siliconised graphite and solid silicon carbide, both in the stator position, running against a tungsten carbide rotor in salt water. He found that the seal nose wear for siliconised graphite was approximately eight times less than for solid silicon carbide. The surface of the siliconised graphite contains islands of graphite; both Paxton et al and Mowrey [47] attribute the good sealing performance, to hydrodynamic lift off effects originating from these islands. However, it is more likely that these islands provide good boundary lubrication and the silicon carbide areas confer wear resistance.

Another member of the silicon family which is thought to have potential in abrasive applications is reaction bonded silicon carbide. Various seal face combinations were

tested in a rig using fluid containing a high proportion of dissolved salts (33). The maximum PV factors were determined as shown in Table 2.

Table 2. The maximum PV factors determined for various Seal Face materials (33).

| Face Rubbing Tests Limiting Pressures and Pressure/Velocity Factor (PV) | | | |
|---|---|---|---|
| Face | Counterface | Max. Pressure ($MN \cdot m^{-2}$) | Max. PV ($MN \cdot m^{-2} \times m/s$) |
| carbon | Co-Cr-W-C alloy (solid) | 9.0 | 24.5 |
| | chrome oxide coating | 5.5 | 15.8 |
| | tungsten carbide coating | 9.7 | 28.0 |
| | tungsten carbide (solid) | 11.0 | 35.0 |
| | SiC:S | 11.0 | 175.0 |
| | alumina oxide | 6.7 | 17.5 |
| tungsten carbide (solid) | tungsten carbide (solid) | 1.4 | 4.2 |
| | SiC:S | 6.2 | 17.5 |
| Co-Cr-W-C alloy (solid) | SiC:S | 0.5 | 8.8 |
| SiC:S | SiC:S | 4.8 | 14.0 |

It can be seen that tungsten carbide in friction against reaction bonded silicon carbide, and the latter against itself, gave the most promising results as far as the PV factor is concerned. Schopplein (48) has also advocated the use of reaction bonded silicon carbide (against itself) in slurry applications. Although, reaction bonded silicon carbide is a very abrasion resistant material, its corrosion resistance is questionable, as previously discussed in Section 2.2.1.5.2.

Very little has been reported on the use of surface coatings/treatments, although as mentioned earlier, Shiro and Schoenherr (45) have tried hard chromium and chromium oxide (thermally sprayed) coatings. By measuring the resistance across the film, Tribe(49) has shown for seal and bearing applications, that thermally sprayed coatings such as chromium oxide and tungsten carbide are porous. The latter reflecting the conductivity and, therefore, a continuous path. Hence, these types of coating may not confer corrosion protection to the substrate.

To summarise this section, mechanical seals are essentially two flat surfaces in intimate rubbing contact, and as such are subject to wear. If the pumped fluid is corrosive, then corrosion of the seal faces may also occur. Hence, the two major criteria for the selection of surface coatings and surface treatments for mechanical seals are good wear and corrosion resistance. However, before considering any suitable surface coatings/treatment, it is essential to understand how material degradation occurs, as a result of wear and/or corrosion.

# CHAPTER III

## 3.0 WEAR- LITERATURE REVIEW

### 3.1 Introduction

Wear may be defined as the unintentional removal of material from rubbing surfaces. Usually wear is one of the major factors creating industrial and engineering problems. It necessitates high expenditure for replacement of components and assemblies. Wear reduces the operating efficiency by increasing power losses, oil consumption and the rate of component replacement. To summarise, wear is one of the most destructive influences to which materials are exposed. Various mechanisms of wear and wear models have been proposed.

Wear encountered in industrial situations can be broadly classified [50] :

| | |
|---|---|
| Abrasive | 50% |
| Adhesive | 15% |
| Erosion | 8% |
| Fretting | 8% |
| Chemical | 5% |

Wear, however, is rarely the result of a single mechanism. Hence, two or more of the independent wear mechanisms may occur simultaneously and interact. Wear is the subject of reviews by Lancaster [51], de Gee [52] and Yust [53] .

## 3.2 Adhesive Wear

This is the basic form of wear which always occurs when two surfaces slide over one another. All real surfaces, no matter how carefully prepared and polished, are rough on a molecular scale. As two surfaces are brought into contact, therefore, only a relatively few asperites actually touch, and the real area of contact, $A_r$, is only a small fraction of the apparent contact area, $A_a$ (see Figure 9.a).

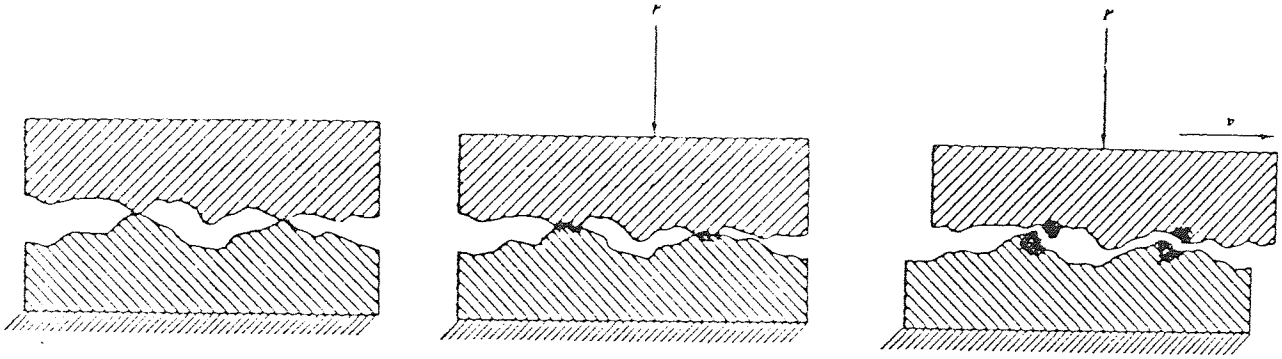

(9.a) $A_r << A_a$ (9.b) Microwelding of asperites (9.c) Shearing of microwelds

Figure 9. Schematic representation of elastic / plastic asperity interaction resulting in formation and shearing of microwelds.

It has been deduced [54] from electrical conductance experiments that for the usual range of engineering design loads the real to apparent contact area ratio $A_r / A_a$, is in the range from $10^{-2}$ to $10^{-5}$. When two surfaces are brought into contact their asperites yield both elastically and plastically until they are able to support the entire applied load. The latter causes minute welds to form at each of the local contact areas [55-58] (Figure 9.b).

The weld might shear at the original junction in which case no wear can occur. On the other hand, there is a finite probability that the junction will shear away from the original interface and material from one of the surfaces will have been transferred to the other. (Figure 9.c). Moreover, because the asperites tend to come in contact repeatedly as the operating cycle is repeated, small amounts of deformation continue to take place. The result is the work hardening of the asperites, with a consequent decrease in ductility of the metals. After a time, depending on the amount of deformation at each contact, the asperites become brittle and tend to break off.

Archard[59] proposed the idea of a certain probability existing for a wear particle to be formed as a result of junction shear allows the wear rate to be expressed in terms of a simple equation. The factor, K, represents the fraction of the friction junctions producing wear. If K is 1, it means that every junction involved in friction process produces a wear fragment.

$$W = \frac{KL}{3p} \qquad (6)$$

where:

W = Worn volume/unit distance of sliding

L = Applied load

p = Flow pressure of the metal.

Typical values of K are given in Table 3 below:

Table 3 Typical value of Archard's Constant.(59)

| Rubbing material | Coefficient of friction $\mu s$ | K |
|---|---|---|
| Gold on gold | 2.5 | 0.1 to 1 |
| Mild steel on mild steel | 0.6 | $10^{-2}$ |
| Brass on hard steel | 0.3 | $10^{-3}$ |
| Polythene on hard steel | 0.6 | $10^{-7}$ |

Archard's model (59) of adhesive wear is based on the following assumptions:

(1) Asperites are of hemispherical shape

(2) Each asperity encounter produces a wear particle of dimension comparable with the dimension of the contact.

(3) The hemispherical asperites are deformable but the flat counterface is non-deformable.

The amount of adhesive transfer is affected significantly by the nature of the surfaces and the ambient conditions. Cleanliness of the surface greatly facilitates adhesive wear. In contrast, presence of absorbed films or tribo-oxidation products (58,60,61) reduces this tendency.

Wear under adhesive conditions, unlike abrasive wear, is subject to sharp transitions in behaviour. Variations in load and speed may bring about marked thermal changes

which precede, and cause, wear changes. Welsh(62) was one of the first to systematically examine the concept of mild wear (oxidative) and severe wear (metallic), and the sharp transitions between these (Figure 10) which he referred to as T1 and T2 transitions.

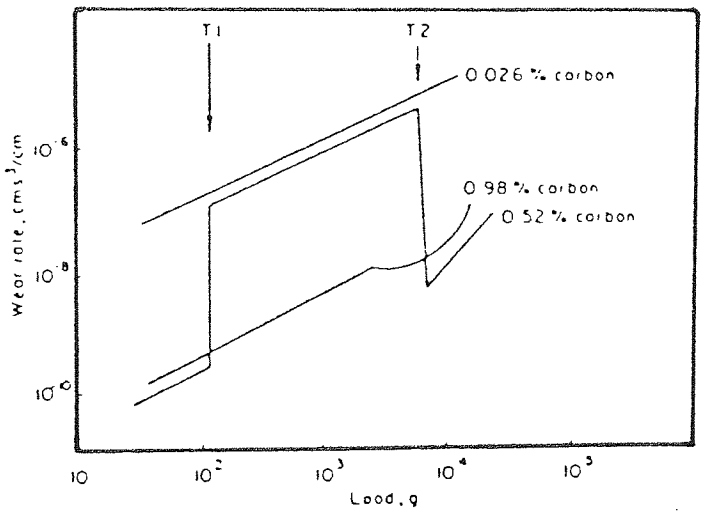


Figure 10. Transitional wear behaviour of different steels (62).

Below T1, wear occurs by the removal of oxide debris from an oxidised surface supported on a work hardened substrate. T1 is a transition to severe wear initiated by the breakdown of the protective surface oxide produced at lower loads. Plastic deformation of the substrate occurs due to a higher bulk temperature, and the wear rate increases considerably with production of metallic debris. Between T1 and T2 severe wear occurs. At the T2 transition, the surface temperature is high enough for phase hardening to produce a hard 'white layer' structure which prevents deformation and helps to establish an oxidised surface once more. At sufficiently low loads, it is claimed that wear may effectively cease. The main propounder of this theory is Rabinowitz (63)

who explains his proposal in terms of a theory of wear based upon interfacial energies. Critically, wear particles will only become detached if the stored elastic energy exceeds the increase in surface energy created by the formation of a new surface. He argues that at sufficiently light loads, the junction area will be so small that maximum stored energy in a possible wear fragment cannot exceed the surface energy required to release it and so no wear can occur. However, with the advent of the 'thin layer activation' (TLA) (64) technique to measure wear, the above statement may not be true. TLA relies on the ability to tag components with small amounts of radioactivity, the activity is confined to a thin surface layer, typically 30-300 μm deep. Sensitive counting methods detect the change in level of radiation, due to removal of the active layer by wear. The main feature of this technique is its ability to measure very small surface losses on a wide variety of materials. The measurement of low wear rates is important in many instances, for example, the wear of magnetic discs for computers.

## 3.3 Delamination Wear

The term delamination wear was introduced by Suh (65). In principle, delamination wear, which takes the form of regular detachments of thin plate like particles from the wearing surface(s), is due to the influence of high tangential (friction) forces on the surface zones of the material, under such conditions adhesive transfer does not occur.

The model of delamination wear is based on the following reasoning:

(a) During wear, the material at and very near the surface has a low dislocation density. This means that this layer strain hardens less than sub-surface layers.

(b) An accumulation of lattice defects (dislocations) due to repeated asperity contact

occurs just below the metal and not at the surface.

(c) Accumulation and coalescence of subsurface defects leads to nucleation of voids and cracks parallel to the surface.

(d) When the cracks reach their critical size, the metal surface layers shear in the form of sheet like particles.

## 3.4 Abrasive Wear

In this type of wear, the removal of solid material from a surface is accomplished by being ploughed or gouged out by a much harder surface or body. In general, abrasive wear takes place whenever hard, foreign particles, such as metal grit, metallic oxide and dust from the environment are present between the rubbing surfaces. Small particles produced by adhesive wear may be sufficiently work hardened that they can abrade either of the two parent surfaces.

The primary requirement for the occurrence of abrasive wear is that there must be a great dissimilarity in hardness between the sliding surfaces.

There are two types of abrasive wear referred to in the literature, namely, 'two-body' and 'three body' abrasion. They are not, however, distinct forms of wear since the action of abrasion is the same in each case. In abrasive wear, relative motion between soft and hard surfaces causes the asperity or particle to plough out or cut a groove in the softer material.

The equation for linear abrasive wear (66) due to a hard cone ploughing a soft material is:

$$W = \frac{K.L\ (2 \tan \alpha)}{H\ .\ \pi} \qquad (7)$$

Where, H, $\alpha$, K and L represents the indentation hardness, base angle of cone, the proportion of the groove volume which appears as loose wear debris and the sliding distance respectively.

Hence, equation (7) implies that the wear volume will increase linearly with load and sliding distance. Furthermore, an inverse relationship between the wear volume, W, and hardness, H, exists. Although this is true for pure metals it is not for alloys. This trend is shown schematically in Figure 11.

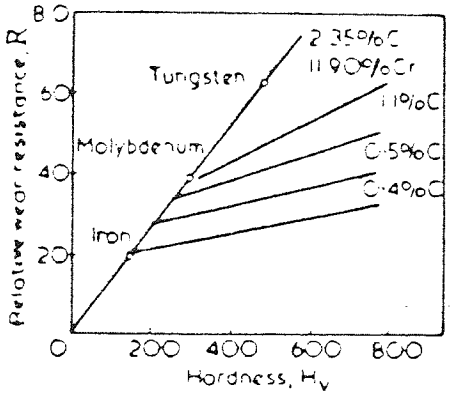


Figure 11. Relative wear resistance, R, as related to hardnes

Richardson's work (68) emphasised the importance of considering the hardness of abrasive particles. He showed that the hardness of the surface resisting wear must be greater than half the hardness of the abrasive if any real improvement in wear resistance is to be achieved, i.e.

$$KT = \frac{\text{Hv of Surface}}{\text{Hv of abrasive}} > 0.5 \qquad (8)$$

However, it is unnecessary to increase the hardness of the material beyond 1.3 times that of the abrasive, because no further significant improvement will be obtained. If the surface is made too hard it may also become too brittle. In sliding of metals the main cause of abrasion is hard articles that may be present in one of the surfaces (e.g. carbides or inclusions in steels), work hardened fragments or the formation of very hard oxide films, i.e. $Al_2O_3$.

## 3.5 Fretting Wear

Fretting is a form of surface wear which occurs when two surfaces undergo very small amplitude oscillatory or vibrational slip. Fretting is characterised by the production of a finely oxidised debris which often flows out of the contact area. The debris on ferrous metals has a cocoa-like appearance and consists of ferric oxide. The fretted surfaces are generally pitted, the pits being shallow, fully oxidised and surrounded by debris.

With reference to mechanical seals, high vibration levels lead to reduced seal life[69,70]. Furthermore, vibration in pump machinery can lead to fretting wear of the shaft sleeve, resulting in shaft hang up, as illustrated in Figure 12.

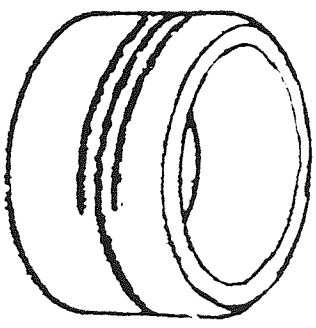

Figure 12. Schematic representation of fretting wear of the shaft sleeve [13].

### 3.5.1 Mechanism of Fretting Wear

There are extensive reviews on fretting wear by Hurricks[71], Waterhouse[72] and Gould [73], however, there is no general agreement about the mechanism.

Tomlinson[74] showed that relative motion between contact surfaces was necessary and that the reciprocating nature of fretting was responsible for the major damage. Tomlinson thought that fretting wear was due to molecular rubbing rather than abrasion. Moreover, the cohesive forces between molecules, as they touched briefly caused detachment of wear particles. These particles then oxidised spontaneously.

Godfrey[75] and Barnatt[76] were of the opinion that fretting wear is initiated by loosening, due to inherent adhesive forces, of extremely finely divided material. The latter is extruded from the contact area and reacts with oxygen simultaneously. However, Godfrey's[75] experiments showed that platinum produces a fine black powder of the virgin metal, which does not oxidise under atmospheric conditions. Moreover, fully oxidised quartz and ruby may be fretted readily. This negated the role of oxygen. In contrast, Feng and Uhlig[77] found the damage to steel in nitrogen to be only one-sixth that in oxygen; in nitrogen the debris was metallic iron, whereas, in the presence of air, oxide was formed.

Uhlig[78] considered fretting to comprise of wear and chemical factors. The latter, reflecting asperities scraping off oxide layers exposing clean active metal, which rapidly oxidises. The mechanical factor reflects the asperities which plough beneath the oxide layer and results in microwelding. Metallic debris removed in this manner may be

oxidised. On the above models Uhlig[78] derived the following equation:

$$W(total) = (k_o L1/2 - k_1 L)\frac{C}{f} + k_2 l L C \qquad (9)$$

W(total) =Total wear volume

L =Load

C =No° of cycles

f =Frequency

l =Total slip

ko, k1, k2 =Constants

Considering the above equation (9), first two terms represent the corrosion factors and third term, the mechanical factor. Thus, depending upon the numerical values of the above dependent variables, equation (9) can be used to evaluate contributions from corrosion and/or mechanical wear regimes.

Haliday and Hirst[79] investigated the fretting corrosion of mild steel. They found that initially high values of friction corresponded plastic flow and formation of microwelds, as time proceeded, these microwelds rupture leading to production of loose metallic debris; this led to abrasive wear of the opposite face. Oxidation of the initial surface and loose wear debris was postulated; to account for the low coefficient of friction observed after the initially high value.

Ohmae and Tsukizoe[80] studied the fretting wear of mild steel and their results show similar trends to Haliday and Hirst[79]. Ohmae and Tsukizoe[80] showed that at small slip amplitudes (0-70μm), fretting oxidation was predominant, as envisaged by Uhlig's[78] model. However, at larger slip amplitudes (greater than 70μm) a combination of adhesion, abrasion and oxidation of loose virgin metal was observed. Abrasion of fretted surfaces was also noted by Feng and Rightmare[81]. However, the above workers[79,80,81] postulated that abrasion is by loose oxide debris. Furthermore, they did not attach any significance to the possibility that wear debris may be sufficiently work hardened to act as an abrasive particle.

The mechanism of fretting is further complicated, according to observations made by Waterhouse[82] and Sproles[83], that the wear mechanism is in accordance with the delamination theory of wear[65]. However, Kayaba and Iwabuchi[84] studied the fretting wear of 0.6%C steel and noted that adhesion and abrasion were the primary mechanisms. Although plate-like particles were observed, they argued that delamination wear was not the sole mechanism but is another contributing factor.

In general, fretting can lead to a reduction in fatigue strength of a material. The presence of an alternating shear stress in the surface, arising from frictional force, may lead to initiation of fatigue cracks[85]. The delamination theory predicts sub-surface cracks parallel to the surface, whereas, fatigue cracks propagate perpendicular to the surface.The question arises whether fatigue cracks are the precursors of fretting, or is it delamination cracks? Clearly, fretting wear/fatigue is a complex phenomena and should not be generalised by a single theory.

# CHAPTER IV

## 4.0 CORROSION

There are many definitions of metallic corrosion, but in essence they state that it is the reaction between a metal and its environment which invariably leads to a degradation in the metal's mechanical and physical properties. There are two basic types of corrosion, namely, aqueous corrosion and 'dry' corrosion; the former is more important with respect to mechanical seals.

### 4.1 Aqueous Corrosion

#### 4.1.1 The Basic Corrosion Cell

Aqueous corrosion is an electrochemical process, i.e. a chemical effect which induces the passage of an electric current. In order to produce a continuous flow of current, a complete cell must be set up comprising two half-cells. The components of such a cell are:- (i) an anode, the site at which a metal is corroded (dissolved); (ii) a cathode, which is not consumed in the corrosion; (iii) a conductor, if the anode and cathode are not in contact; and (iv) an electrolyte, which permits flow of ions between electrodes. The basic electrochemical cell is shown in Figure 13. Electrons are produced at the anode by the reaction:

$$M \rightarrow M^{n+} + ne \qquad (10)$$

The fundamental cathodic process is the consumption of electrons, but this may be achieved in a number of ways depending on the environment. A common cathodic

reaction is the hydrogen evolution reaction (H.E.R.):

in acid solutions: $2H^+ + 2e \rightarrow H_2$ (11)

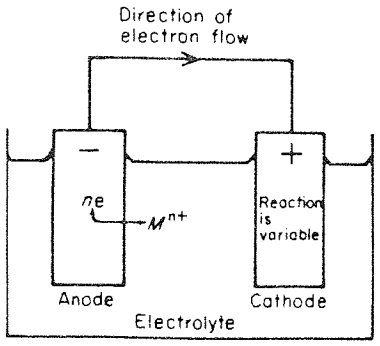


Figure 13. The basic electrochemical corrosion cell.

In practice, anodes and cathodes are not as shown in Figure 13, except in bimetallic contact. In the simplest case they arise from two different metals contacting each other, the surface of one becoming anodic with respect to the other. In general, in any electrochemical reaction, the most negative or active half-cell tends to be oxidised and the most positive or noble half-cell tends to be reduced. Redox potentials are useful in predicting corrosion behaviour. Advantage is taken of this effect in the cathodic protection of iron by zinc (galvanising): zinc is anodic to iron and, therefore, dissolves in preference to iron which is, therefore, protected. More usually corrosion cells are very small and numerous and occur at different points on the same metal surface. In this case anodes and cathodes arise from local differences in the metal structure and environment. Wranglen[86] has classified corrosion cells into the following categories:

1. Macro-cells, leading to localised macro-attack.
2. Micro-cells, leading to localised attack.

3. Submicro-cells, leading to general corrosion.

Corrosion cells leading to localised attack may be classified as follows:

1. Galvanic macro-cells, metal-metal: Galvanic corrosion.
2. Galvanic micro-cells within a metal, for example:
   a) intercrystalline corrosion
   b) graphitic corrosion
   c) pitting and crevice corrosion.
3. Oxygen concentration cells, usually macro-cells.
   a) waterline attack
   b) crevice corrosion
   c) deposit corrosion
   d) filiform corrosion.

4) Metal concentration cells (macro-cells).

Detailed mechanism of the above forms of corrosion are discussed in books by Wranglen[86], Shreir[87] and Fontana[88].

Various methods can be used to prevent corrosion, some of these are as follows:

1) Alloy additions
2) Anodic protection
3) Cathodic protection
4) Use of inhibitors.

Additions of titanium and niobium to austenitic stainless steels reduce the tendency to

weld decay, a form of intergranular corrosion. If the basic metal can be passivated, however, and if the electrolyte favours passivation, contact with a more noble metal may promote passivation still further. This is the general concept of anodic protection. Noble metal alloying acts by raising the electrode potential of the base metal so that it is raised into and stays in the passivity range. In stainless steels alloying additions of 0.1% Pd or 1% Cu bring about a strong reduction of the corrosion rate in sulphuric acid.

Proper design should keep contact with corroding agents to a minimum. Joints should be designed correctly to reduce the tendency for liquids to enter and be retained. Contact between materials far apart in the electrochemical (redox) series should be avoided. If this cannot be achieved, they should be separated by rubber or plastic to reduce the possibility of galvanic corrosion. An excellent book by Pludik[89] covers various design manipulations to prevent and control corrosion.

Inhibitors are substances that, where corrosion occurs in moist environments, are added to lower the corrosion rate by retarding anode or cathode processes. An anodic inhibitor increases the anode polarisation and hence moves the corrosion potential in the positive direction, whereas, a cathodic inhibitor in the corresponding manner displaces the corrosion potential in the negative direction.

In view of the electrochemical nature of corrosion, two notable electrochemical techniques have been developed to evaluate corrosion resistance of materials:

1) Tafel extrapolation technique

2) Linear polarisation technique.

2) Linear polarisation technique.

## 4.2 Electrochemical Corrosion Testing

### 4.2.1 Tafel Plot Technique

In this technique, a controlled potential scan is typically applied to a sample of the material, starting at the corrosion potential ($\phi_{corr}$), and extending in either the anodic or cathodic direction for a few hundred millivolts.. When the resultant potential-current function is plotted on semi-log paper, it characteristically exhibits a linear region. A projection of the linear region defines the corrosion current density ($I_{corr}$) at the intersection with $\phi_{corr}$ and therefore, the corrosion rate may be determined. Figure 14 shows a typical Tafel plot.

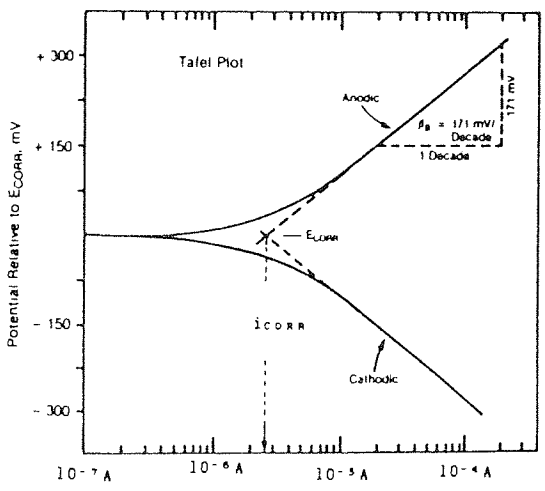


Figure 14. Tafel extrapolation technique.

The theory of Tafel extrapolation is given in Appendix I. The technique is affected by two, interfering phenomenon: concentration polarisation and resistance drop effects.

species cannot reach or be removed from the electrode surface at a sufficiently rapid rate. The reaction becomes diffusion controlled. The effect of concentration polarisation is minimised by stirring the solution. Resistance drops across the solution can also cause non-linear Tafel behaviour at high currents. The effects of concentration polarisation and resistance drops are most serious when $I_{corr}$ is large and high currents are needed to verify Tafel behaviour. As a general rule, linearity over two decades of current is desired. To overcome some of the limitations of Tafel extrapolation technique, the linear polarisation method has been developed.

## 4.3 Linear Polarisation Technique

Skold and Larson[90] in their studies of the corrosion of steel and cast iron in natural water found that a linear relationship existed between the applied potential and the anodic and cathodic current densities, providing the values of the latter were low. However, the recognition of the importance of these observations is due to Stern and Geary[91] who used the term 'Linear Polarisation' to describe the linearity of the potential-current relation, in the region of the corrosion potential. The slope of the linear curve ($\Delta\phi - \Delta I$) is termed the polarisation resistance, $R_p$, which has the unit of Ohms. In general, the higher the value of $R_p$, the lower the corrosion rate of the material.

A typical linear polarisation plot is illustrated in Figure 15. The polarisation resistance, $R_p$, together with Tafel constants can be used to evaluate the corrosion current density via the Stern-Geary[91] equation. The derivation of this equation is given in Appendix II.

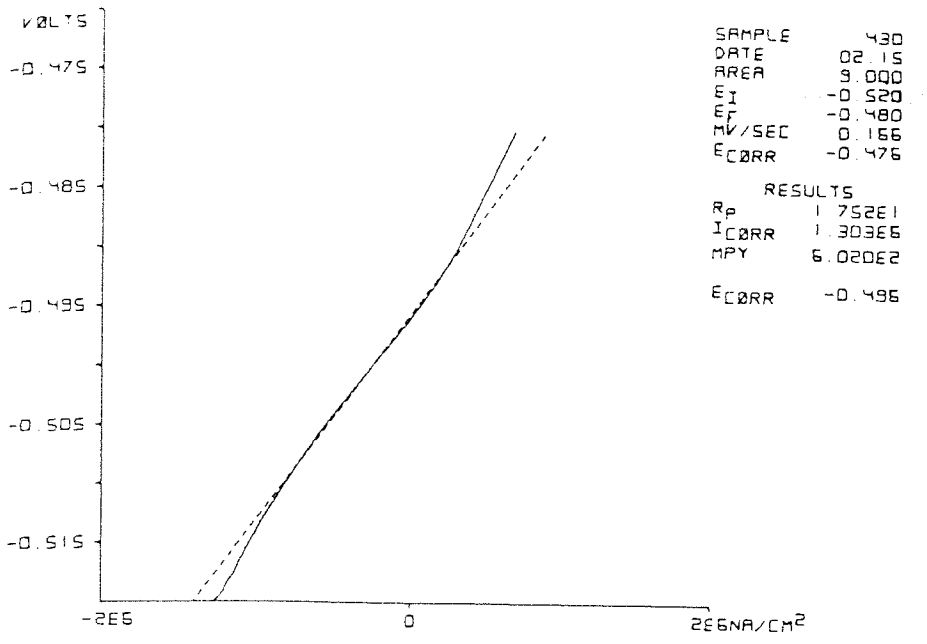


Figure 15. Linear Polarisation technique[88].

Stern-Geary equation:

$$I_{corr} = \frac{B_A \cdot B_C}{2.3 \cdot R_p \cdot (B_A + B_C)} \qquad (12)$$

where, $B_A$ and $B_C$ are the anodic and cathodic Tafel constants respectively.

The linear polarisation technique has two major limitations:

1) The technique requires prior knowledge or assumed values of the Tafel constants.

2) There is evidence, as discussed later, that suggests linear polarisation plots are curved and not linear.

Hoar[92] pointed out that the Tafel constants $B_A$ and $B_C$ have to be determined from a full polarisation curve which also leads to the corrosion current and therefore, makes

additional corrosion current measurements, such as polarisation resistance, unnecessary. However, Hoar did not consider the following advantages of linear polarisation. The technique offers significant advantages over Tafel extrapolation because an experiment can be completed in a matter of minutes and because the small polarisation from the corrosion potential does not disturb the system, thereby permitting the periodic monitoring of instantaneous corrosion rates. In addition, very low corrosion rates can be measured with the same precision and degree of accuracy obtained in measuring high corrosion rates[93]. Significant applications have included the study of inhibitors in solution[94], localised corrosion[95] and the adaptability of the linear polarisation technique is evident from in situ measurements in soil[96]. The shape of the linear polarisation plot may be given by the parameter $I/I_{corr}$ and is determined by the ratio of the Tafel constants. Equation (A1.1., Appendix I) may be expressed as:

$$\frac{I}{I_{corr}} = \exp\left(\frac{2.3\phi}{B_A}\right) - \exp\left(\frac{-2.3\phi}{B_C}\right) \qquad (13)$$

Figures (16) show the effect of Tafel constants on the shape and range of linear polarisation plots.

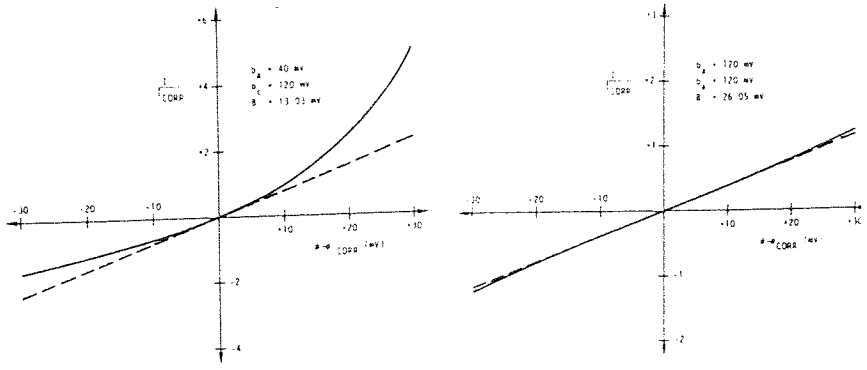

Figure 16. Polarisation-Current plots for various combinations of Tafel slopes[97].

However, irrespective of the shape of a given plot, the polarisation resistance $R_p$, can be determined with sufficient accuracy by drawing a tangent to the measured curve at the corrosion potential. It is on this principle that Leroy[98,99] used the error to be expected in the corrosion current which is derived from the slope of the best least square line through the experimental data as a criterion of the validity of linear polarisation method.

Oldham and Mansfeld[100] proposed a graphical technique to evaluate the corrosion current density, this method does not require the prior knowledge of Tafel constants. However, this technique involves drawing tangents to the polarisation plots and means that the latter must show some non-linearity. Mansfeld[101] suggested a method whereby the corrosion current density and Tafel slopes could be simultaneously determined from the polarisation plot.

In the Mansfeld method the value of $R_p$, the polarisation resistance, is calculated from the polarisation curve as a tangent at the corrosion potential. The 2.3 $R_p$ I vs potential curve is constructed which enables a graphic evaluation of the best of the various combinations of $B_A$ and $B_C$ pairs to be made for calculating the corrosion current density from $R_p$, $B_A$ and $B_C$. In 1978 Roy and Sircar[102] suggested an alternative method to determine Tafel slopes and corrosion current density. Their method consists essentially of a graphical comparison, by means of a nomogram, of the experimental curves obtained with a series of external cathodic polarisation curves taken up to only 60 mV, with the 'theoretical' curves corresponding to equation (A.1.1) for various values of the parameters $B_A$ and $B_C$ and a corrosion current density of 1 $mA/cm^2$.

Je.de. Damborena et al[103] describe a computer programme to facilitate and improve the graphical method of Roy and Sircar[102]. However, Je.de.Damborena points out that the solution determined by computer programmes may not be unique. This lack of discrimination is observed better in the graphical methods since various curves may be sufficiently close to the experimental values.

In general, the problem of the lack of knowledge of the Tafel constants has been solved, as described above.

The strongest criticism of the linear polarisation theory, came from Oldham and Mansfeld[104] who showed that differentiation of equation (A.2.17) to give the 2nd differential:

$$\frac{d^2 I}{d \phi^2} = I_{corr} \left( \frac{1}{B_A^2} - \frac{1}{B_C^2} \right) \qquad (14)$$

Hence, from the above equation the curvature is only zero when $B_A$ and $B_C$ are equal. Oldham and Mansfeld suggested that, in general, polarisation curves have curvature at the corrosion potential, except in the unlikely case that the anodic and cathodic Tafel slopes are equal. However, Leroy[98.99] concluded that two circumstances can give a zero or negligible curvature of the polarisation curve at the corrosion potential:

(1) $B_A = B_C$ as pointed out by Oldham and Mansfeld.

(2) If the Tafel constants are large, the numerical value of the 2nd differential tends towards zero. Figure (17) shows the dependence of the curvature of polarisation curves at the corrosion potential, on the anodic and cathodic Tafel constants. Leroy[98,99] argued that because of the latter effect the linear polarisation technique is valid for many corroding systems.

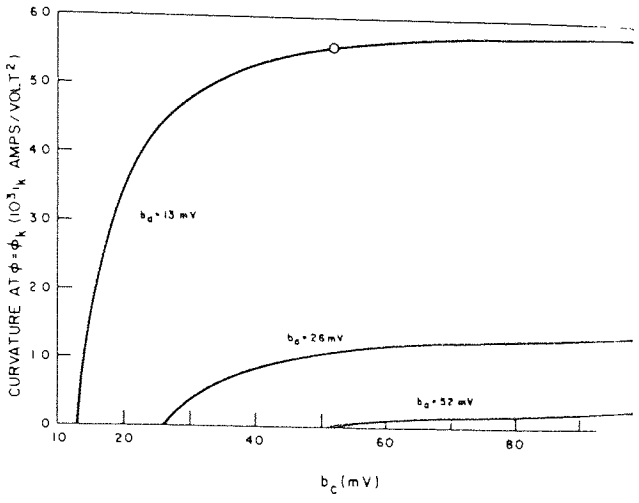


Figure 17. Dependence of the curvature of polarisation curves at the corrosion potential, on the anodic and cathodic Tafel constants[98].

In summary, Tafel extrapolation and linear polarisation techniques are based on the electrochemical nature of corrosion. The main disadvantage of the former, namely, non-Tafel behaviour, has been overcome by linear polarisation; which relies on potential-current measurements in the vicinity of the corrosion potential. However, both techniques were employed and the determined Tafel constants were used, in conjunction with the Stern-Geary equation to evaluate instantaneous corrosion rates.

# CHAPTER V

## 5.0 SURFACE TREATMENTS AND SURFACE COATINGS- LITERATURE REVIEW

### 5.1 Introduction

There are several comprehensive reviews on properties and applications of surface treatments and/or coatings. These include the Department of Trade and Industry publication[105], Tribology Handbook[25], I.M.F. publication[106], Fulmer Materials Optimiser[107] and by Child[108]. The latter is more orientated towards surface treatments. The surface coatings and/or treatments investigated in this research are listed below:

1) Thermochemical processes e.g.
   a) Boriding
   b) Toyota Diffusion Process

2) Electroless or Autocatalytic coatings
   a) Electroless nickel
   b) Electroless nickel codeposited with silicon carbide particles.

3) Welding techniques e.g.
   a) Plasma arc spraying of nickel-chromium-boron and chromium oxide deposits.

b) Tungsten carbide (25%) / 5% nickel / tungsten / chrome carbides deposited via Jet-kote process.

4) Physical Vapour Deposition e.g.

a) Duplex coating of electroless nickel with an overlay of titanium nitride via Ion Plating process.

b) Plasma nitriding

## 5.2 Boriding

### 5.2.1 Introduction

Boriding is a technique which enables extremely hard iron boride layers (1800 - 2100 Hv) to be formed on steels of various kinds. The hard layer is formed by the diffusion of boron into steel.

Boron combines with iron to form two borides, $Fe_2B$ and FeB, and one ($Fe_2B$) or both of these are found in the diffusion layer. The layer is generally in the form of needles which penetrate the substrate. The boron source may be a gas, a molten salt or a solid pack or paste.

The process is conducted in the temperature range 850 - 1050°C for 1 - 8 hours, a layer of iron borides, generally up to 0.15 mm thick, is formed. The process can be applied to ferrous or non ferrous metals.

### 5.2.2 Properties of Borided Layers

Two iron borides can be formed, FeB and $Fe_2B$, the latter is much harder and brittle than FeB. FeB is generally undesirable in boride coatings as it may spall during wear. Table 4 compares the surface hardness of borided steels with other representative materials.

Table 4 Comparison of the surface hardness of borided steels with other representative materials[110]

| Material | Hardness (Hv) |
|---|---|
| Tool steel | 750 |
| Carburised steel | 900 |
| Nitride steel | 1200 |
| Tungsten carbide + 6% Co | 1700 |
| Borided mild steel | 1600 |
| Borided H13 | 1800 |

Borided layers on mild or low alloy steels are typically acicular. The acicular structure is a useful characteristic because the area of contact between boride layer and the substrate is higher than a corresponding layer with a uniform interface[109,110]. High alloy steels, particularly stainless steels, produce a uniform front and consequently there is a greater tendency for the borided layer to flake off.

As the alloy content of the substrate material increases, the depth of borided layer in a given treatment decreases. In general, thicker coatings may be produced on lower carbon steels. The optimum thickness of a boride layer is not necessarily the thickest, but depends upon the application.

a) Thick layers are recommended to combat erosive wear. (e.g. for extrusion tooling used for abrasive fillers such as glass or asbestos fibres).

b) Thin layers are advocated for protection against adhesive wear. A layer of 5 microns would be adequate in theory to prevent this type of wear, but, because of the tooth-shaped form of $Fe_2B$, layers of 15-20 μm minimum are recommended.

5.2.2.1 Wear Resistance

Wear testing by Fichtl[111] and Linial and Lavella[112] has shown that borided surfaces have much reduced wear (approximately 1/100th) compared with the steel substrate. The static coefficient of friction is reduced by borided surfaces to levels comparable with the Suflinuz processes.

Using the Pin-on-disc test, Eyre and Morri[113] showed that steel in the carburised or normalised condition undergoes a transition from mild to severe wear, whilst the borided steel does not. Moreover, it exhibits a considerable improvement in wear rate, varying from two to three orders of magnitude. Eyre[114] has also compared the wear life of borided layers with those from other surface treatments, such as Tufftriding, and showed that borided is superior to other treatments.

Habig[61] has shown that, in contrast to both hardened tool steel and vanadised steel, borided steel showed a reduction in pin wear with sliding velocity. This is attributed to the development of tribo-oxidation products on the borided steel surface.

The developments of oxidation products with borided coatings is a distinct feature in minimising the extent of adhesive wear at high temperatures in comparison with other thermochemically treated surfaces, such as nitrided ones. Similar results have been reported for gas borided steel by Takeuchi et al [115].

Sridhar and Iyer[116] showed that abrasion resistant borided mild steel was far superior to the unborided steel; using the sand blasting method. However, results were not compared with known thermochemical treatments and, therefore, precludes the usefulness of their results. Eyre and Morri[113] investigated the abrasion resistance of carburised, borided and normalised steel by calculating the volume displaced from a 50 mm scratch made by a diamond indenter. Their results suggest that borided is more effective than carburising in resisting abrasion.

#### 5.2.2.2 Corrosion Resistance

Very little has been published on the corrosion resistance of borided layers, however, they are claimed to be resistant to acids. According to Fichtl[117] borided austenitic steels are much more resistant to hydrochloric acid than non borided ones. This is probably because austenitic stainless steels are prone to chloride attack. Boride layers are resistant to molten zinc and find a useful application in steel hooks; to suspend work for hot dip galvanising[110].

### 5.2.3. Limitations of Boriding

1. May cause thermal distortion of complex shape components.

2. Boride layers are porous, therefore, from a corrosion view point, this may be a disadvantage.

3. Boriding increases the dimensions to the component, by an amount related to the thickness of layer. If the component is out of tolerance, diamond lapping may be used but is difficult.

## 5.3 Toyota Diffusion Process

### 5.3.1 Introduction

In this process, developed in Japan, a uniform and pore free layer of vanadium, niobium or chromium carbide, is formed on the surface of a steel by immersion in a fused borax salt bath containing the appropriate ferro alloy. The thickness of the layer is typically four to ten microns. The bath temperature is selected around the hardening temperature of the substrate steel ranging from 800 - 1250°C. The carbide layer forms by reaction of the metal dissolved in the salt bath with carbon in the steel. The process is covered by various patents[118].

5.3.2 Properties of Toyota Diffusion Layers(119-122).

Although there is a distinct straight boundary between the substrate and carbide layer, the carbide forming elements do diffuse into the substrate and form a metallurgically bonded structure. Very high hardnesses, up to 3500 Hv, are produced dependent on the carbide formed. Figure 18 shows a hardness comparison of coated carbides on steels with other processes that impart wear resistance to steel.

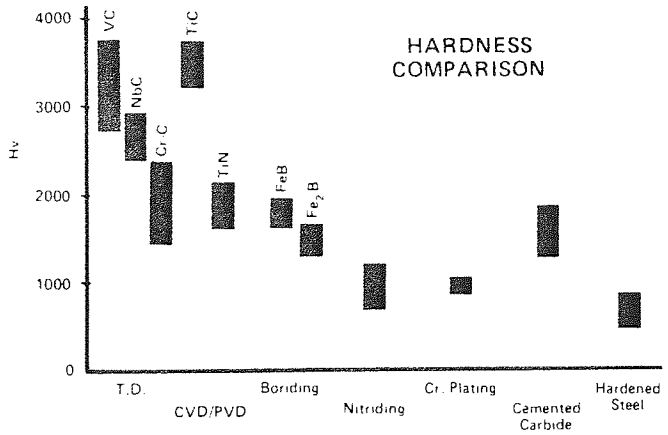


Figure 18 Hardness comparison of various surface treatments / coatings (121).

5.5.2.1. Wear Resistance

Wear tests showed that carbide coated steels are superior to those treated by nitriding, hard chromium plating and thermal spraying, as shown in Figure 19. Falex wear tests conducted by Arai(121) showed that vanadium carbide coated blocks started to seize under much heavier loads than hardened tool, nitrided or chromium plated steels.

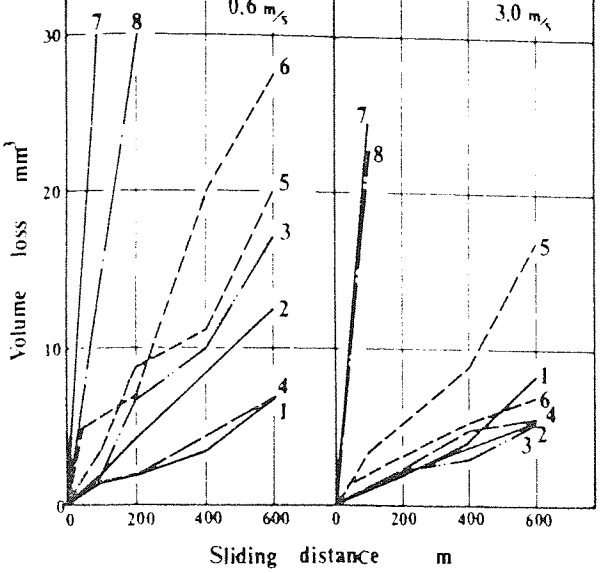


Key: 1 VC coated; 2 TiC coated; 3 NbC coated; 4 cemented WC + Co; 5 thermal sprayed WC + Co; 6 Cr plated; 7 nitrided; 8 hardend 1.5/12Cr die steel.
Test machine – Ohgoshi type; counter material – annealed Cr-Mo structural steel 30×3mm; final load – 3.3kg; sliding velocity – 0.6 or 3.0m/sec.

Figure 19 Wear resistance of carbide coated steels(120)

5.3.2.2. Corrosion Resistance

Little is published on the corrosion resistance of carbide layers, but they are recommended for corrosive applications.

5.3.3 Limitations of Toyota Diffusion Process

1. The process is applicable to steels containing at least 0.4% carbon.

2. It may cause thermal distortion of complex shaped components.

3. Post lapping is restricted because of extreme hardness of T.D. layers.

4. For hot working applications, reversion of the carbide layer could occur i.e. carbon diffusing back into the substrate. However, according to Plumb(123) this does not take place.

5. Selective areas cannot be treated.

## 5.4 Titanium Nitride Coatings

### 5.4.1 Introduction

Titanium nitride (TiN) coatings may be synthesised by physical vapour deposition (P.V.D.) or chemical vapour deposition (C.V.D.). However, P.V.D. techniques are characterised by their lower deposition temperatures and, therefore, minimise thermal distortion and the need for post-hardening treatment. In general, titanium nitride coatings are characterised by their golden colour, high hardness and chemical inertness. It is not proposed to give process details and mechanisms of deposition, as these are discussed elsewhere[123,124]. The main application for titanium nitride coatings is for high speed steel cutting tools.

### 5.4.2 Properties of Titanium Nitride Coatings

The coating thickness, in general, is dependent upon the deposition technique and process parameters, for P.V.D. thicknesses of 3-5 μm are typical. The most notable property of titanium nitride is its hardness; typically 2500 - 3000 Hv. The high hardness is thought to be associated with the presence of $Ti_2N$[125-127] in the coating and not TiN. Hard titanium nitride coatings (≈ 2500Hv) have a mixed phase structure composed of almost equal proportions of TiN and $Ti_2N$ phases[128]. However, according to Hibbs et al[129] maximum hardness is associated with single phase TiN deposits.

Different morphologies tend to form at substrate temperatures in the range T < 0.3 Tm < 0.45 Tm < Tm, where Tm is the melting point of the source(130). The transition between ranges is not sharp but gradual. The form of structures are shown schematically in Figure 20.

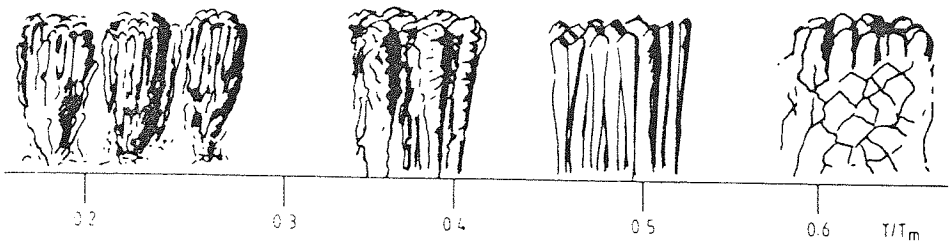


Figure 20. Schematic temperature dependence of microstructure morphology as the temperature of the substrate is varied. $T_m$ is the melting point of the plated metal(130).

Tapered crystallites are produced in the range 0.2 - 0.3, which have an intercrystalline porosity. As the T/Tm ratio increases elongated columnar grains with definite crystals and grain boundaries are formed. Deposits produced by ion plating have considerably less porosity than by evaporation and sputtering.

### 5.4.2.1 Wear Resistance

Studies by Hinterman(131) suggest two prime factors that may impair the wear resistance of thin hard coatings. These are as follows:

1) The presence of shear-stresses at coating substrate interfaces. This may lead to failure by cracking or spalling if adhesion is poor.
2) Good adhesion to the substrate is very important. Any protective coating is only as

good as its adhesion to the substrate.

Wear tests conducted by Hinterman[131] on TiN produced by C.V.D. and ion plating indicate that they both have high load carrying capacity. These results are in agreement with those of Kobayashi and Doi[81] who found that inserts coated by an ion plating process show a wear rate similar to that of inserts from the C.V.D. process.

Ramalingam et al[128] showed that thin films of reactively sputtered TiN, typically 5 μm thick, provide good wear resistance. Moreover films deposited at 150°C reduced the crater wear of cemented carbide tool inserts. This low temperature of deposition would seem to have high potential because it is well below the tempering temperature of many tool steels. Pin on disc tests[132] on TiN (4 μm thick) coating, produced by ion plating, gave a coefficient of friction of 0.2 at 0.5N loading. At a load of 1N, the coating wore through after a sliding distance of 150m.

Sundquist et al [132] and Sirvio et al[133] studied the abrasive wear of ion plated TiN coatings using the dry sand/rubber abrasion tester. Their results may be concluded as follows:

1) The abrasion resistance of a coated $D_3$ tool steel was increased by 77%.
2) As the surface roughness (Ra) of ion plated TiN increases, so does the wear.
3) Subsurface hardening such as plasma nitriding prior to ion plating does not improve the abrasion resistance.

The relationship between coating thickness and surface roughness is important, if they

are of the same order of magnitude rapid wear occurs. The coating wears off at tips of the asperites revealing the base material. It is important to ensure that the coating thickness is a few times greater than the Ra value of the surface roughness.

### 5.4.3 Limitation of Titanium Nitride Coatings Deposited by P.V.D. Techniques

1. Line of sight process, blind holes and recesses may be difficult to coat.

2. Adhesion to substrate is questionable, particularly deposits layed down by evaporation and sputtering techniques.
3. Deposits are porous to a certain degree, this may be disadvantageous from a corrosion view point.

## 5.5 Electroless Nickel

### 5.5.1 Introduction

Electroless nickel is deposited by the catalytic reduction of nickel ions with sodium hypophosphite in baths at pH 4.5 to 5 and 85 to 95°C. The deposits usually contain 7 to 11 per cent phosphorous by weight. Originally, it was thought that as-plated electroless nickel deposits were amorphous[134], however, Graham et al [135] concluded, on the basis of electron diffraction patterns, that the deposits can be described as supersaturated solid solutions of phosphorus in a microcrystalline nickel matrix.

### 5.5.2 Properties of Electroless Nickel

Deposit uniformity is a unique characteristic of all electroless plating processes. Unlike electroplating, uniform deposition can be obtained on irregular surfaces such as threads and on complex shaped parts.

Electroless nickel has the property of controllable hardness (within certain limits) with the maximum hardness approaching that of hard chromium. The hardness of electroless nickel is 450-500 Hv as deposited. The hardness reaches a maximum at about 400°C and is virtually independent of the phosphorus content[136].

#### 5.5.2.1. Wear Resistance

Parker[137], using the Falex wear tester, showed that the wear of electroless pins was less after heat treatment than that of hard chromium pins when run against ($H_{r20}/H_{rc}60$). steel blocks. Moreover, using the Alpha (LFW-1) test an electroless nickel plated ring, heat treated for one hour at 400°C to maximum hardness (1,000 $H_{r100}$), had the best wear resistance and least abrasiveness.

Randin and Hintermann[136], using a ball and disc machine, examined the influence that the phosphorus content of the coating had upon the un-lubricated wear. It was found that maximum wear took place in the as-deposited state for a coating containing 7 wt% phosphorus. Increasing the temperature of heat treatment reduced the wear and at

heat treatment temperatures above 400°C the wear decreased as the level of phosphorus decreased. Tope et al[138] obtained data using results from a lubricated cross-cylinders wear test rig to conclude that thin, 10μm, rather than thick as-deposited electroless coatings were more wear resistant.

As mentioned above, maximum hardness is generally associated with best wear resistance. Ma and Gawne[139] investigated the influence of counterface materials running against electroless nickel, using the Falex wear tester. High wear rates were noted with electroless nickel pins running against austenitic stainless steel and lower wear rates with 0.4% carbon steel and hard chromium plated counterface blocks.

It was postulated that the higher wear rates observed with austenitic stainless steel counterface blocks and electroless pins were due to greater mutual solubility between them, compared to other wear couples investigated. Moreover, electroless nickel pins (heat treated at 400°C) exhibited a higher wear than those treated at 600°C, when considering austenitic stainless steel counterface blocks. This strange result could be explained by the following hypotheses:

Electroless nickel (heat treated at 400°C) is much harder than austenitic stainless steel. Initially hard asperites, on the electroless nickel surface, would plough through the softer austenitic stainless steel surface. The latter work hardens, due to plastic deformation, a situation may occur where the work hardened wear junctions become brittle and fragment. This may lead to a predominantly abrasive wear situation. Alternatively, with electroless nickel heat treated at 600°C, surface work hardening of

austenitic stainless steel may be less due to lower hardness of the former. As deposited electroless nickel and electroless nickel (heat treated at 600°C) have similar hardnesses and one would expect similar rates, but Ma and Gawne's[139] results were not indicative of this. However, the contradiction in results may be due to the different levels of adhesion. Heat treatment of electroless nickel deposits at 600°C results in improved adhesion due to the formation of an Fe-Ni intermetallic layer at the substrate-coating interface[140]. Thus, adhesion of coatings may be important when there are strong adhesive forces between rubbing surfaces.

5.5.2.2 Corrosion Resistance

Electroless nickel confers corrosion protection to the substrate by acting as an exclusion barrier. Electroless nickel coatings are of the non-sacrificial type. The chemical resistance of these deposits to a wide variety of chemicals has been reported[140].

Exposure tests conducted by Deminjer and Brenner[141] showed that electroless nickel coatings, from an acid bath, protected steel against rusting better than electrodeposited nickel coatings. Mallory[142] investigated the corrosion behaviour of electroless nickel deposits using the salt (A.A.S.S.) spray test. Better corrosion resistance was afforded by deposits with:

a) Higher phosphorus content.

b) Greater thickness.

c) Lower porosity.

Studies by M.Sadeghi et al[143] on the effect of heat treatment on the corrosion resistance of electroless nickel revealed the following salient points:

a) Heat treatment over the range 250°C - 400°C causes a drastic reduction in corrosion resistance due to several factors, including:-

   - phosphide precipitation which causes anisotropic dimensional changes in the deposit which results in stress cracking.
   - differential thermal expansion between the electroless nickel and the substrate which further impairs deposit integrity.

b) Heat treatment above 400°C, typically 600 - 800°C results in a significant improvement in corrosion resistance. This is due to formation of hard protective tenacious oxide film on the surface and Fe-Ni alloy at the interface between the coating and the substrate.

Sadeghi et al [143] suggest that electroless nickel formulations based on organic stabilisers and accelerators confer better corrosion resistance than those based on trace heavy metal stabilisers and sulphur accelerators. However, the former deposit contained 13% P and the latter 8.5% P, which casts doubt on the usefulness of their comparison. However, work carried out by Trudgeon[144] and Van Gool et al[145] conclusively proves that formulations based on sulphur based stabilisers impair corrosion resistance.

### 5.5.3 Electroless Nickel Composites

These are coatings produced by the codeposition of particles in electroless nickel alloys. In general, composite coatings confer better wear resistance and abrasion resistance.

Moreover, wear resistance may be enhanced by suitable post ageing treatments.

A comprehensive review on the current state of art of electroless composite coatings has been written by N.Feldstein et al (146), which includes the following salient points:

1) Electroless coatings codeposited with polycrystalline diamond offer better wear resistance than those codeposited with natural diamond.

2) Composite coatings containing alumina had better wear resistance than coatings containing silicon carbides. This contradicts the results published by Parker(137). Inclusion of alumina appears to provide superior wear resistance even though the testing time was longer and silicon carbide is double the hardness of alumina. Anchoring of the particles within the matrix, particularly in the wear mode, is thought to be important. It might be some morphological difference between alumina and silicon carbide which aids mechanical clamping of the particles.

3) Inclusion of particulate matter within the electroless metal increases the surface roughness. This parameter is important in application of composite coatings which require precise frictional levels.

A recent development is the production of electroless nickel / P.T.F.E. composite coatings(147,148). These coatings are claimed to confer non-stick, dry lubrication and lower coefficient of friction. Typical values of coefficient of friction, (against chromium steel counterface) are (0.2 - 0.3) and (0.2 - 0.5) for as-plated and heat treated deposits respectively.

Tulsi[147,148] heat treated the electroless nickel P.T.F.E. composite deposits at 400°C for 4 hours. However, thermal degradation of P.T.F.E. occurs at approximately 320°C, and this could impair wear and frictional characteristics, if deposits are heat treated as described above. Pin-on-disc wear tests conducted by Thomas[149] would seem to support this hypothesis. Table 5 shows pin-on-disc wear test results for electroless nickel / P.T.F.E. coated pins against Sursulf treated discs.

Table 5. Wear results of electroless nickel / P.T.F.E. coated pins against Sursulf treated discs[149]

| | Wear rate g/cm X $10^{-8}$ | Coefficient of friction | Hardness Hv (20g) |
|---|---|---|---|
| As-plated Electroless nickel P.T.F.E. | 5.06 | 0.36 | 352 |
| Electroless nickel P.T.F.E. heat treated at 300°C for 4 hours | 10.53 | 0.71 | 642 |

Load = 4 kg Sliding velocity = 0.5 $ms^{-1}$

## 5.6 Plasma Nitriding

### 5.6.1 Introduction

Nitriding is the generic name for processes which rely on the diffusion of atomic nitrogen into surface, to form a wear resistance surface. Nitriding can be carried out in several ways:

1) Gas nitriding in retorts using ammonia with catalytic decomposition at the steel surface.
2) Salt bath nitriding in cyanide based salts, commercially known as Tufftride, Sulphinuz, Sursulf, etc.
3) Plasma nitriding.

Essentially diffusion of nitrogen into a suitable steel substrate results in the formation of:

1) Compound layers, which are mainly iron nitrides, typically 0.02 mm thick.
2) Diffusion layer, consisting of alloy nitrides (0.2 - 0.7 mm thick), with a peak hardness of 900 - 1100 VPN.

Conventional gas nitriding results in a compound layer which consists of $\gamma'$ (F.C.C.) and $\varepsilon$ (C.P.H.) iron nitrides, often termed 'white layer'(151.152). This compound layer is brittle and could spall, leading to abrasive wear in service. Brittleness is thought to be due to stresses generated between the different crystal structures. In general, white layer is removed by grinding or by chemical treatments, both of which are very expensive.

Beneath the compound layer, nitrogen diffuses into the underlying steel to form finely dispersed needles of alloy nitrides, and by reaction with carbon in the steel, carbo-nitrides are formed. Hence, in order to achieve an appreciable hardening effect by nitriding, steel must contain nitride forming elements such as aluminium, titanium, chromium, molybdenum and vanadium[151,152].

In plasma nitriding it is possible, by controlling the process parameter, to produce essentially a monophase $\gamma'$ compound layer. This monophase layer is strongly adherent with good lubricity characteristics and need not be removed from components such as crankshafts or gears prior to their use in service[151,152].

Thus, plasma nitriding may be preferred to gas or salt bath processes for the following reasons:

1) Ability to depassivate stainless steels and chromium tool steels prior to nitriding.
2) Possible use of low temperatures to minimise tempering.
3) Low distortion on difficult components.
4) Generation of compressive residual stresses in the surface, which increases the fatigue strength of the material.
5) Ease of selective nitriding

### 5.6.2 Wear Resistance

Nitriding confers good wear resistance; this is reflected by its wide application in the automotive industry. However, the corrosion resistance of nitrided steels is also of interest.

### 5.6.3 Corrosion Resistance

It is generally accepted that nitriding results in a moderate increase in the corrosion resistance compared to non nitrided steel. Preliminary work on plasma nitrided EN31 would seem to support this, as shown in Table 6.

Table 6 Corrosion current density of plasma nitrided EN31 bearing steel

| Material | Corrosion current density determined by linear polarisation (nA / $cm^2$) |
|---|---|
| EN31 hardened & tempered | $2.857 \times 10^5$ |
| Plasma nitrided EN31 at 460°C for 4 hours | $7.1612 \times 10^4$ |

Recently, much interest has been shown in the plasma nitriding of stainless steels, primarily because they can be depassivated, in-situ, prior to nitriding.

In general, nitriding of stainless steels improves wear characteristics but impairs corrosion resistance. The reduced corrosion of stainless steels after nitriding is associated chiefly with the loss of chromium from the matrix, due to the formation of chromium nitrides[152]. Ramchandani[153] and Zang et al[152] suggest the use of low temperature plasma nitriding (380 - 400°C) to reduce the formation of chromium nitrides. However, Falex wear test on samples treated at the above temperatures exhibited poor wear resistance; primarily due to the lower case hardness[153].

## 5.7 Thermal Spraying

### 5.7.1 Introduction

Thermal spraying covers a wide range of processes and so only the following will be considered here:

1) Powder spraying
2) Plasma spraying
3) Jet-kote process
4) Detonation or D-Gun process.

It is not proposed to give details of equipment or processes as this is discussed elsewhere[154-156]. However, it should be noted that the above processes have three common stages:

1) The material to be sprayed is heated so that it is substantially molten.
2) The molten material is projected onto the substrate.
3) The projected material adheres to the substrate to give the required coating.

The important differences between the above processes are illustrated in Table 7.

Table 7 Properties of characteristics of deposit produced by various thermal spraying methods[156].

| | POWDER | PLASMA | JET-KOTE | D-GUN |
|---|---|---|---|---|
| Gas temperature (K) | 3000 | 15000 | 2000 | 4000 |
| Velocity of particles (M/s) | 35 | 300 | 1000 | 800 |
| Bond strength ($N/mm^2$) | 45 | 45-120 | 75-150 | 145-360 |
| Total porosity (%) | 10-20 | 2 | 1-2 | 1/2-1 |
| Cost of equipment (£) | 3600 | 30000 | 70000 | Not Sold |

### 5.7.2 Properties of Thermally Sprayed Deposits

Critically, the two most important properties of thermal sprayed deposits are their adhesion and porosity.

Adhesion of sprayed deposits to substrate is primarily by virtue of mechanical keying[156]. Generally, surfaces are grit blasted, to enhance the mechanical keying, prior to spraying. However, according to Malik[157], this may be inadvisable when the sprayed component is subject to a fatigue regime, in which case shot peening should be used. In general, the greater the velocity of the impinging particles, the higher the adhesion strength. Sprayed coatings consist of a heterogeneous mixture of sprayed material, oxides and pores. Shrinkage and degassing after deposition are the principal cause of the porosity.

From a corrosion viewpoint, the porosity of a deposit is particularly important. Although the knowledge of total porosity is useful it is the degree of interconnecting porosity which governs the ease with which corrosive agents can reach the substrate.

Table 7 shows that powder deposits are limited by low bond strength and higher porosity compared to the rest of the processes. However, nickel-chromium-boron powder sprayed deposits can be post fused to give pore free and metallurgically bonded deposits. These deposits are claimed to have good resistance to sliding wear and being fully dense, confer excellent corrosion resistance. The primary disadvantage in this process is that post fusing ($\approx$ 1000°C) may cause thermal distortion of coated

components.

Plasma sprayed deposits are characterised by their better adhesion and reduced porosity, compared to a powder sprayed deposit. Furthermore, due to the high temperatures in the plasma, this permits deposition of high melting point materials. Chromium oxide can be deposited by plasma spraying and is characterised by its high hardness (1300 Hv). For corrosive application, the deposits have to be sealed by sealant, prior to final finishing.

Jet-kote, which is high energy plasma, and D-Gun processes produce deposits which are better bonded, much denser and less porous, compared to deposits from previously discussed processes. As a consequence of the above, these two processes are in direct competition. However, two major factors favour the selection of the Jet-kote process:

5.7.3. Commercial availability:

Union Carbide is the sole operator of the D-Gun process and no commercial units are sold. In contrast, the Jet-kote process is available at several commercial installations in the U.K. Moreover, the price charged for D-Gun is approximately double compared to Jet-kote coatings.

5.7.4. Control of microstructure:

Usually WC-Co alloys are produced by the powder metallurgy route and possess a high resistance to wear. These alloys can also be deposited by Jet-kote and D-Gun processes. As these alloys are dispersion hardened by WC particles, the decomposition

during spraying of these particles should be minimised, as it may impair the mechanical properties of the deposit. It has been reported[158] that approximately 50% of the WC decomposes to $W_2C$ and Co-W compounds in D-Gun deposits. Various workers[159,160], on the basis of x-ray diffraction studies of deposits, claim that Jet-kote deposits exhibit much less decomposition.

Summary of the properties of surface coatings and surface is given in Table 8.

Table 8 Summary of various properties of surface coatings and surface treatments

| Treatment | Suitable Substrate Material | Description of Treatment | Typical Hardness | Major Characteristics | Porosity | Thermal Distortion | Residual Stress | Adhesion | Corrosion Resistance |
|---|---|---|---|---|---|---|---|---|---|
| Boriding | Low C, Med.C & Low alloy steels | Boron diffuses into steel to form $Fe_2B$, at temperatures 900-1000°C. | 1800-2100 | Excellent sliding wear resistance | Slightly porous | Yes, on complex shaped components | Compressive | Metallurgically bonded | Moderate |
| Toyota Diffusion | Tool steels M2, D2, etc. | Salt bath process at 975-1050°C. Various carbides can be formed, $V_4C$, NbC etc. | 3000-3500 | High hardness and resistance to wear | Pore free | As above | Compressive | Metallurgically bonded | Good |
| Electroless Nickel | Most ferrous and non-ferrous metals | Electroless deposition of Ni-P alloys. Deposits can be age hardened | 1000-1100 | Good wear and corrosion | Pore free | No | Tensile | Good | Good |
| Plasma Nitriding | Nitriding steels, tool steel, stabilised stainless steels | Diffusion of nitrogen to form compound layers (Iron Nitrides) and diffusion layer (Alloy Nitrides) carried out at 460°C-550°C | 900-1300 | Good wear Resistance, retention of hardness at elevated temperatures | Pore free | No | Compressive | N/A | Moderate |

Table 8 (continued)

| Treatment | Suitable Substrate Material | Description of Treatment | Typical Hardness | Major Characteristics | Porosity | Thermal Distortion | Residual Stress | Adhesion | Corrosion Resistance |
|---|---|---|---|---|---|---|---|---|---|
| Ni-Cr-B (Post fused) | Ferrous metals | Powder spray followed by post fusing (at 1000°C) | 700-800 | Good resistance to wear and corrosion | Pore free | May be, Due to post fusing | Tensile | Metallurg-ically bonded | Good |
| Chromium Oxide (98%) | Almost all metals | Plasma spraying substrate temp. (< 200°C) | 1300 | Good resistance to wear | Porous (1-2%) | No | Tensile | Less than of hard chromium | As Deposits are porous, Must be sealed |
| 25% WC 5% Ni & W-Cr Carbides | Almost all metals | Jet-kote process substrate temp. (< 200°C) | 1000-1200 | Excellent wear resistance at high temps. Improved corrosion resistance compared to WC-Co alloys | < 1% | No | Tensile | Good as hard chromium | Must be sealed for corrosive application |
| Titanium Nitride (TiN) (P.V.D.) | Tool steels (Hardened & tempered) | Ion plating process (300-400°C) | 2000-2500 | High hardness and wear resistance combined with attractive appearance | May be porous | No | Not known | Good | Good chemical inertness |

# CHAPTER VI

## 6.0 EXPERIMENTAL PROCEDURE

### 6.1 Introduction

From the literature review, it is apparent that wear resistance of surface coatings / treatments has been evaluated by various types of tests. However, as a consequence of the latter, it is difficult to correlate the published wear rates, primarily because the loading, contact geometry, sliding velocity and duration of tests are not comparable. Hence, it was important to evaluate the wear resistance of the previously reviewed surface coatings / treatments, under identical experimental conditions.

Similarly, corrosion data of these surface coatings / treatments tends to be qualitative and therefore, it is difficult to ascertain which one confers best corrosion resistance and why it does so. Hence, electrochemical techniques were used to quantify corrosion resistance, thus making the selection procedure easier. Moreover, these techniques indicate how fast corrosion proceeds and whether or not coatings / treatments exhibit active-passive transitions.

To summarise, evaluation of the wear and corrosion properties was an important phase in the research, whereby the wide range of surface coatings / treatments was tested and failure mechanisms examined in detail using the techniques discussed later in Section 7.2.1., 7.4.5. and 7.6.1

## 6.2 Materials

### 6.2.1 Wear testing

The wear pins were made from EN8 steel bar (6.35mm diameter) in the bright drawn condition. The bar was centreless ground (to 5.94mm) and cut into small pins approximately 55mm long. The ends of the pins were turned on a lathe to give a nominal 50mm length. However, D2 tool steel was used as the substrate material for Toyota Diffusion layer specimens. The main reason for this was that D2 tool steel shows much better response to this process and is more amenable to the post hardening treatment than EN8 steel. The as received discs were made from EN31 steel in the hardened and tempered condition

The pin ends and the surface of the discs were ground flat to a surface finish of 0.1-0.3μm. The pins and discs were demagnetised and cleaned ultrasonically in 'microcleaner' and acetone respectively, then stored in a desiccator for subsequent use.

Table 9. Chemical composition of steels used for wear testing

| | % ELEMENTS | | | | | | |
|---|---|---|---|---|---|---|---|
| | C | Si | Mn | S | P | Cr | Mo |
| EN8 | 0.35-0.45 | 0.05-0.35 | 0.60-1.00 | 0.06max | 0.06max | - | - |
| EN31 | 0.90-1.20 | 0.10-0.35 | 0.30-0.75 | 0.05max | 0.05max | 1.00-1.60 | - |
| D2 | 1.50 | - | - | - | - | 12.00 | 1.00 |

### 6.2.2 . Corrosion Testing

Small cylindrical corrosion samples nominally 1.5cm diameter by 1.8cm long were made from bars (1.6mm diameter) of EN8 steel and austenitic stainless steel. The as-received bars were polished by using 200 and 400 grit wet and dry papers on a lathe.

Specimens 2.0cm long were cut from these bars using a mechanised hack-saw. The cylinders were then turned to the final dimensions on a lathe. A hole was drilled (6mm diameter) in the centre of each cylinder to provide location for an electrical contact for corrosion tests. Austenitic stainless steel (316 grade) was used primarily to study the effect of plasma nitriding and boriding on the corrosion properties. The chemical composition of 316 stainless steel is given below:

| | % Cr | % Ni | % Mo | % C | Mn | Si |
|---|---|---|---|---|---|---|
| 316 grade | 16.0-18.0 | 10.0-14.0 | 2.0-3.0 | 0.05max | 2.0max | 1.0max |

### 6.2.3 Seal Rig Tests

The type of seal, seal ring materials and test parameters were selected, by consultation with Flexibox Ltd., after the evaluation of wear and corrosion properties of the surface coatings / treatments had been carried out. The seal test rig was designed and built by Flexibox Ltd. and the Flexibox Cartridge seal (Type F.F.E.T. ) was used to evaluate the sealing characteristics of the surface coatings / treatments.

6.2.3.1. Seal Ring Materials

6.2.3.1.1 Rotary Sealing Rings

The substrate materials chosen were martensitic (431S29) and austenitic (316S11) grades of stainless steel. The seal faces were lapped to within two light bands and the flatness checked by an optical interference method. The chemical composition of these steels are given below .

| | Cr | Ni | Mo | Cu | C | Fe |
|---|---|---|---|---|---|---|
| 431S29 % | 13 | 1.0 | / | / | 0.2 | Bal |
| 316S11 % | 17 | 13 | 2.2 | / | 0.03 | Bal |

6.2.3.1.2 Stationary Sealing Ring

The counterface material selected was a carbon 304 (FH 8225 grade).

6.2.3.1.3. Stationary Seal Ring Body

This was constructed from a Ferralium alloy 255-3SF, which is a duplex stainless steel whose chemical composition is similar to the conventional 329 stainless steel.

Chemical composition:

| | Cr | Ni | Mo | Cu | N | C | Fe |
|---|---|---|---|---|---|---|---|
| % | 25 | 6 | 3 | 1.8 | 0.18 | 0.04max | Balance |

### 6.2.5 Surface Coatings / Treatments

The surface coatings / treatments investigated in this research and their commercial availability are given below:

(1) Electroless nickel (NiFOSS 3000) supplied by W.Canning Materials..

(2) Electroless nickel co-deposited with silicon carbide particles - Bristol Aerojets Ltd.

(3) Boriding - T.E.E. Heat Treatment Ltd.

(4) Plasma nitriding - Birchfield Extrusions Ltd.

The stainless steels were plasma nitrided at 520°C for 20 hours.

(5) Nickel-chromium-boron and chromium oxide deposits via Plasma Spraying - Metallisation Ltd.

| Ni-Cr-B composition | C% | Cr% | B% | Si% | Fe% | Ni |
|---|---|---|---|---|---|---|
| (alloy code 14670) | 0.6 | 16 | 3.5 | 4.2 | 3.5 | Balance |

Chromium oxide, typical composition as per (S.F.E.C.O.R.D.) technical data sheet:

$Al_2O_3$ : 34%

$TiO_2$ : 6 %

$SiO_2$ : 10%

$Cr_2O_3$ : balance

(6) Toyota Diffusion process - British Metal Treatments Ltd.

A vanadium carbide layer was formed on D2 tool steel samples at a temperature of

1000°C for 3 hours. The samples were then quenched into oil and subsequently double tempered at 145°C.

(7) WC (25%) + Ni (5%) + W-Cr carbides (Balance) deposited by Jet-kote process - Bristol Aerojects Ltd.

(8) Titanium nitride, deposited via ion plating process (400°C for 1 hour) - Tec Vac Ltd., D.G. Teer Ltd.

## 6.3 Electroless Nickel Plating

### 6.3.1 Sample Preparation

The samples were tied tightly with thin copper wire so that they could be jigged in the pre-treatment and plating solution. Superficial dirt and grease was removed from the sample by wiping them with cotton wool soaked in acetone.

### 6.3.2. Solution Preparation

The plating solution used was a commercial formulation, NiFOSS 3000, supplied by W. Canning Materials Ltd. Two litres of plating solution were prepared by mixing 200ml of base solution, 400ml of initial solution and 1400ml of distilled water. Fresh solutions were used for each plating batch and the solution maintained during plating, in accordance with the manufacturers instruction sheet. A beaker containing the plating solution was placed in a thermostatically controlled water bath. A thermometer was placed in the beaker to monitor the temperature of the plating solution, and the mouth of

the beaker covered by a watch glass, to minimise evaporative losses. The pH of the plating solution was checked using a calibrated pH meter.

### 6.3.3. Pretreatments

Thorough pretreatment is essential to remove any contaminants such as dirt, grease and rust, to ensure activation of the surface and good adhesion of plate.

The pretreatment sequence was as follows:

(1) Anodic clean in 'Activax' (5 minutes at 4 Amp/$dm^2$) at 60°C

(2) Rinse thoroughly in water

(3) Acid pickle (50% HCl) for 30 seconds

(4) Rinse thoroughly in water

(5) Anodic clean in 'Klenewell' (2 minutes at 4 Amp/$dm^2$) at room temperature

(6) Rinse thoroughly in water

Thereafter, the samples were transferred to the plating solution immediately.

Heat Treatment:

The electroless nickel was heat treated at the following two temperatures:

(1) At 400°C for one hour (carried out in an air circulating furnace).

(2) At 600°C for one hour (in an air circulating and vacuum furnace).

The wear pins were heat treated as per (1), whereas for the corrosion samples, all three variations in the heat treatment were investigated.

6.3.4 Plating

The samples were jigged carefully so that they did not touch each other. The pH of the solution was checked every 15 minutes and any imbalance in the pH was corrected with additions of dilute sulphuric or 50/50 ammonia, as appropriate. The components were plated at the following plating parameters:

Table 10. Electroless nickel plating parameters

| ARTICLE | PLATING SOLUTION | | |
|---|---|---|---|
| | pH | TEMPERATURE (°C) | PLATING TIME (hrs) |
| Wear Pins | 5.0 | 95 | 1 |
| Corrosion Cylinders | 5.0 | 95 | 1 |
| | 4.5 | 88 | 2 |
| | 4.0 | 85 | 3 |
| Seal Rings | 5.0 | 95 | 1 |
| Stationary Seal Ring Body | 5.0 | 95 | 1 |

The pretreatment sequence for the stainless steel seal components included a nickel

strike, prior to electroless nickel plating. The chloride based strike solution was used and the formulation and pretreatment sequence is given below:

Nickel chloride strike to stainless steel

Solution composition

| | | |
|---|---|---|
| Nickel chloride | | 240 g/l |
| Hydrochloric acid (conc.) | | 86 $cm^3/l$ |
| Distilled water | to | 1 litre |

6.4 Electrolytic Nickel Plating

Corrosion samples were plated with Watts nickel and bright nickel in order to compare their corrosion resistance with that of electroless nickel deposits.

6.4.1 Watts Nickel Plating

Four litres of Watts nickel solution were prepared to the following formulation:

| | |
|---|---|
| Nickel sulphate | 260 g/l |
| Nickel chloride | 55 g/l |
| Boric acid | 30 g/l |

The pH of the solution was adjusted to 4.5 and given a peroxide treatment by adding 2ml per litre of 130 vol hydrogen peroxide. Thereafter, addition of 5g per litre of activated carbon was made and the solution heated to 60°C. Air was bubbled through the solution for 4 hours and then it was filtered and purified by electrolysis, using a corrugated steel cathode, for 10 Amp hour per litre. The pretreatments of samples prior to Watts nickel plating were the same as described for electroless nickel plating.

The operating conditions for plating were as follows:

Operating conditions

| | | |
|---|---|---|
| pH | - | 4.5 |
| Temperature | - | 55°C |
| Plating time | - | 60 minutes |
| Current density | - | 3 A/dm$^2$ |
| Agitation | - | Air |

6.4.2 Bright Nickel Plating

A proprietary bright nickel solution, Gemini Bright Nickel, was used and was made up as follows:

| | | |
|---|---|---|
| High Sulphate Bright Nickel solution (N21201) | - | 4 litres |
| Gemini Rack Initial Brightener (N25277) | - | 10 ml/litre |

The base solution (N21202) had the following formulation:

| | | |
|---|---|---|
| Nickel sulphate | - | 265 g/l |
| Nickel chloride | - | 55 g/l |
| Boric acid | - | 40 g/l |

The operating conditions were as follows:

Operating conditions

| | | |
|---|---|---|
| Pretreatment | - | as for electroless nickel |
| pH | - | 4.5 |
| Temperature | - | 55°C |
| Current density | - | 4 A/dm$^2$ |
| Agitation | - | Air |

## 6.5 Wear Testing

Mechanical seals are essentially a pair of flat surfaces in mutual rubbing contact. If hydrodynamic lubrication of seal faces is prevalent, then one could argue that no wear should occur. However, predominantly adhesive wear conditions occur, in the absence of fluid film lubrication, as discussed in the literature review. Hence, wear tests were conducted unlubricated, as the wear of seal faces tends towards a maximum during dry running. The Pin-on-Disc wear tester was used to evaluate the wear resistance of surface coatings / treatments. In this test, a flat loaded pin is in rubbing contact with a flat rotating disc; thus the contact geometry is similar to mechanical seals. Furthermore, the diameter of the wear pin is of similar magnitude to the width of the F.F.E.T. seal rings.

### 6.5.1 Pin-on-Disc Wear Tester

The wear tester is essentially a lever system and can be schematically represented as shown in Figure 21.

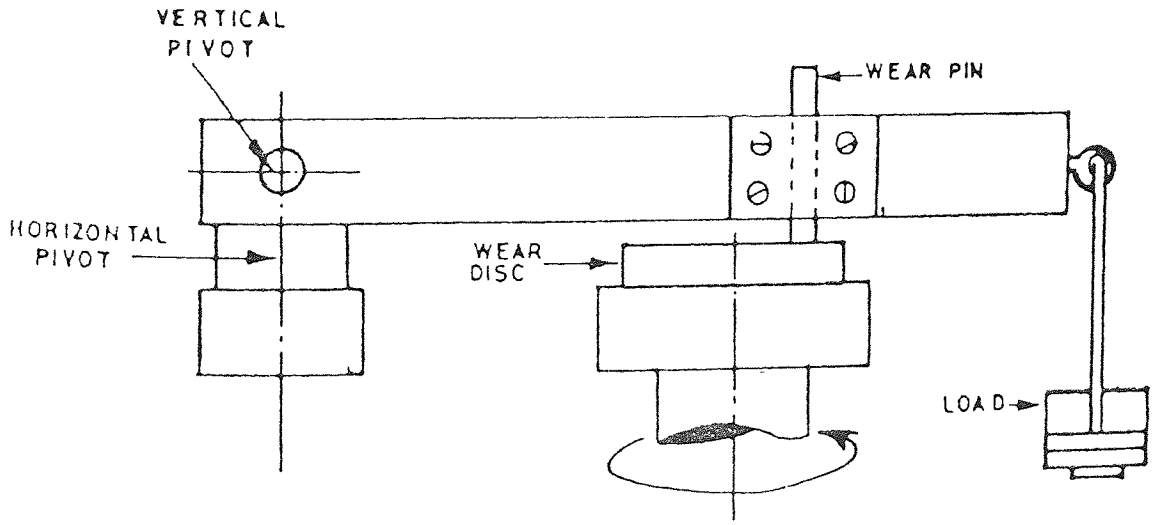


Figure 21 Schematic representation of the Pin-on-Disc wear tester

The wear pin was pushed through a hole in the brass nut and located with a 6.25mm collet. An accurately machined block (13.13mm) was placed between the end of the loading arm and the platform to ensure that the pin was perpendicular to the disc. The brass nut was tightened, which gripped the collet, thus preventing the rotation of the pin during the test. The stop screw was tightened to prevent vertical movement of the pin.

6.5.1.1. Procedure for Wear Testing

(1) The pins were ultrasonically degreased in acetone and then weighed accurately to five decimal places.

(2) The loading arm was adjusted, by means of four bolts, to achieve the desired wear track diameter on the disc. Three wear track diameters per disc were chosen, these being at 9.4, 8.0 and 6.5cm diameters respectively. A sliding speed of $0.5ms^{-1}$ was maintained at each of the wear track diameters, by altering the r.p.m. (revolutions per minute) of the motor; in accordance with the following equation.

$$\text{sliding velocity} = \frac{\{\text{r.p.m.} \times \prod \times D\}}{60}$$

where, D is the diameter of the wear track (cms).

3) Transducers strategically placed on the wear tester, as shown in Figure 22, monitored the wear and torque during the test.

(4) After the test, the pin was re-weighed as per step (1).

(5) The surface finishes on pins and discs were measured after the test, using a Talysurf (model 4).

(6) A minimum of four wear tests were conducted per surface coating / treatment.

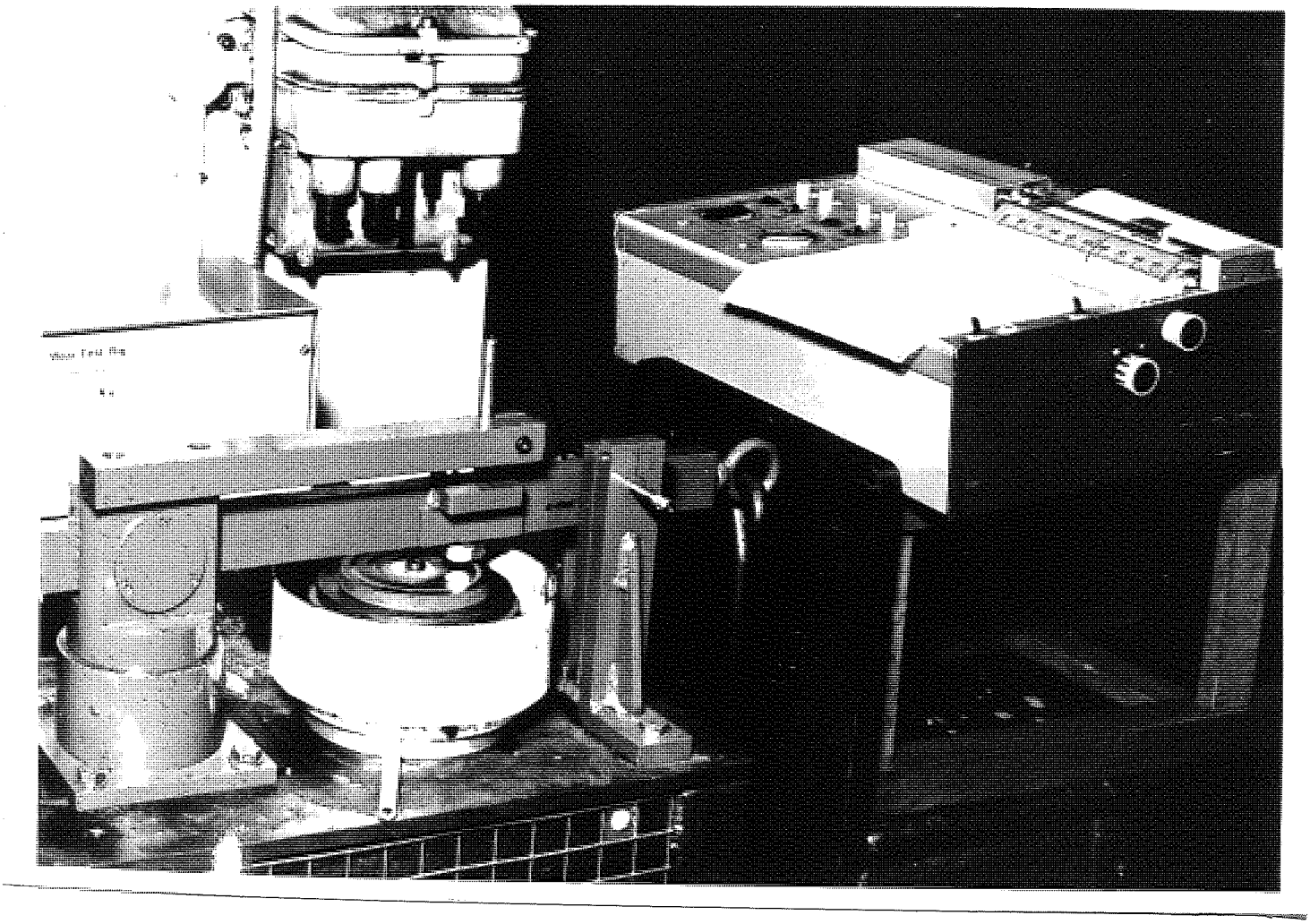

Figure 22. Pin on Disc Wear Tester

The operating parameters for the wear tests are given in Table 11 .

Table 11. Operating parameters for the Pin-on-Disc wear tester

| Load (kg) | Sliding Velocity ($ms^{-1}$) | Test Duration (hrs) |
|---|---|---|
| 4 | 0.5 | 1.5 |
| 8 | 0.5 | 5 minutes running at 4kg before applying 8kg for up to 1.5 hrs. |

## 6.6 Electrochemical Corrosion Testing

Corrosion evaluation of the surface treatments / coatings was undertaken using the Princeton Applied Research Corrosion Measurement Console (model 380-1), which is a microprocessor controlled potentiostat.

### 6.6.1 Sample Preparation

An insulated copper wire (20cm long) was soldered onto the top surface of each cylindrical sample. The samples were then cleaned ultrasonically with microcleaner and acetone to remove any flux residues. Finally, the soldered area and any exposed copper wire were sealed with plating lacquer; this was applied twice. Once the lacquer was thoroughly dried, P.T.F.E. tape was wrapped around the lacquered area to provide

extra sealing action. The total surface area of the exposed surface coating was determined accurately and noted.

6.6.2 Test Solution (A.S.T.M. B287)

A 5% sodium chloride solution acidified with acetic acid (A.S.S.) was used. The pH of the test solution was adjusted to 3.1-3.2 using glacial acetic acid and checked by a calibrated pH meter.

6.6.3 Electrochemical Cell

The electrochemical cell used consisted of four important components; these are shown schematically in Figure 23 .

(1) Working electrode - sample under investigation

(2) Counter electrode - platinum metal

(3) Salt bridge

(4) Saturated Calomel Electrode (S.C.E.)

The end of the salt bridge was placed approximately 1mm from the working electrode.

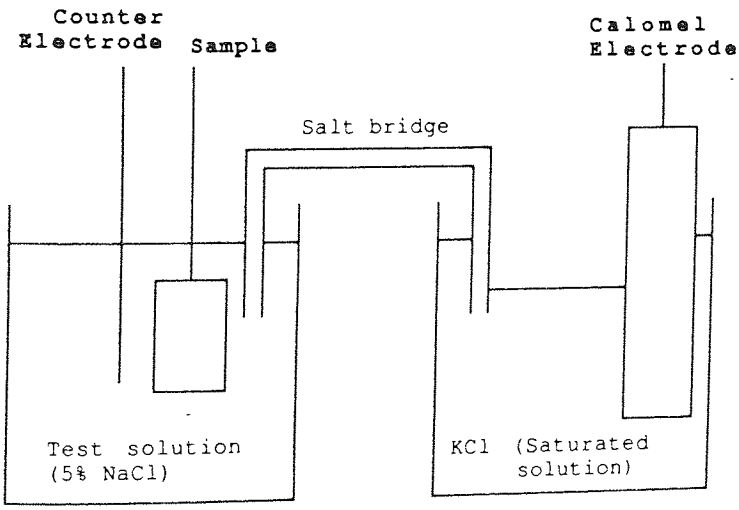


Figure 23. Electrochemical cell for corrosion studies.

For both linear polarisation and potentiodynamic scans, tests were carried out in duplicate.

### 6.6.4 Electrochemical Corrosion Tests

The following test were carried out :

(1) Linear polarisation

(2) Potentiodynamic scan

#### 6.6.4.1 Linear Polarisation

Samples were immersed in the test solution, as described above, and the instantaneous corrosion rate determined weekly for a period of two months. The parameters used to determine the linear polarisation curve, as as follows:

| | | | |
|---|---|---|---|
| Initial potential | - | -10 mV | relative to the corrosion potential |
| Final potential | - | +10 mV | |
| Scan rate | - | 0.166 mV/sec | |

In the presence of oxygen, as in the case of the test solution, the cathodic reaction of $O_2$ was considered to be diffusion controlled and the modified Stern-Geary equation (161) was used :

$$I_{corr} = B_A / 2.3. R_p \qquad (15)$$

#### 6.6.4.2 Potentiodynamic Scan

In this test, the specimen potential was scanned slowly from a cathodic potential to the

corrosion potential and then in the anodic direction, as follows:

| | | |
|---|---|---|
| Initial potential | - 250 mV | relative to corrosion potential |
| Final potential | +1000 mV | |
| Scan rate | 0.166 mV/sec | |

6.6.4.3 Pretreatment Prior to Electrochemical Testing

Pure nickel foil was used to investigate the effect of prior cleaning on the shape of an anodic polarisation curve. The following methods were investigated:

(1) Degrease in acetone

(2) Plating pretreatment, consisting of:

   a) Cathodic clean in 'Activax' (5 minutes at 4 Amps/$dm^2$, 60°C)

   b) Rinse in water

   c) Acid pickle (50% HCl) for 30 seconds

   d) Rinse in water

   e) Transfer to electrochemical cell.

(3) Clean with pure magnesium oxide paste, rinse in distilled water.

(4) Hold specimen in the immune region (-0.960V S.C.E.) for 10 minutes, in the electrochemical cell.

(5) Methods (3) together (4) respectively.

From a procedural viewpoint, it is suffice to say that method (5) was the most satisfactory. Details of the anodic polarisation curves are given later on in the text.

### 6.6.5 Corrosion Evaluation by Atomic Absorption Spectrophotometry (A.A.)

To compare corrosion rates (via linear polarisation), the dissolution rates of nickel and iron from electroless nickel samples were determined using a Perkin-Elmer model 560 (double beam) atomic absorption spectrophotometer. The procedure was as follows:

(1) A measuring flask was used to measure accurately 250ml of A.S.S. solution, which was poured into a beaker. The sample was immersed in the beaker and the level of the solution marked accurately, so that additions could be made after analysis and to allow for evaporative losses.

(2) Analytical glassware was immersed for 24 hours in dilute nitric, prior to use.

(3) Fresh standards (0 and 5ppm) of nickel and iron were prepared before each analysis. These were used to calibrate the A.A., and the absorption checked as per Perkin-Elmer's manual.

(4) A small quantity (0.1-0.9ml) of solution was pipetted from a beaker and diluted in a 5ml measuring flask; such that the metal ion concentration was within the linear range (0-5ppm) of the atomic absorption spectrophotometers. The solution was aspirated in a lean oxyacetylene flame and the concentration was based on an average of five determinations. The analysis was carried out every week, for up to a month, on clear solutions only . In cases where the solution contained corrosion products, the test was terminated. The corrosion products were dissolved in nitric acid and diluted to appropriate volumes for an end analysis.

## 6.7 Metallography

A Buehler cut-off machine with a ceramic bonded cutting wheel was used to prepare cross-sections of surface coatings / treatments, which were subsequently mounted in conductive bakelite. The mounted specimens were polished on a polishing wheel using several grades of wet and dry papers, starting with 120 to 1200 grit size, followed by diamond wheel polishing on 6 and 1 micron pads, respectively. Microhardness indentations were carried out on a Vickers microhardness tester using a 100 gram load with in indentation time of 30 seconds. A series of hardness profiles of the plasma nitrided stainless steel samples were conducted to evaluate the case hardness.

### 6.7.1 Electron Microscopy

A Cambridge Scanning Electron Microscope (model 120) equipped with an energy dispersive analyser was used extensively to study the surface topography of surface treated/coated worn pins, seals and corroded samples. Analysis of the wear debris and corrosion products was made, in duplicate. In addition, a Cambridge Electron Probe (Microscan V) microanalyser was used to study accurately the changes in composition of electroless nickel samples, after corrosion. The composition was measured across the coating using the point counting technique. The data was corrected for atomic number differences, absorption and fluorescence effects using the ZAF correction program run on the Link System. Auger electron spectroscopy was used to examine oxide glazes and changes in surface composition due to heat treatment of electroless nickel deposits in air and vacuum, respectively; by an elemental depth profiling technique. The role of surface oxides has been mentioned in the literature review; from

a wear and corrosion viewpoint, surface oxides prevent asperity microwelding and in some cases, as for austenitic stainless steels, confer chemical passivity respectively.

## 6.8. Seal Rig Tests

### 6.8.1 Introduction

The Flexibox F.F.E.T. cartridge seal was used to evaluate the sealing characteristics of surface coated / treated seals. This is a general purpose seal and widely used for rotating machinery in the process industries. The principal seal components are illustrated schematically in Figure 24 . The rotating seal face and the sliding diameter, on the stationary seal ring body, were surface coated / treated to study the seal face wear and fretting wear of the sliding diameter, respectively.

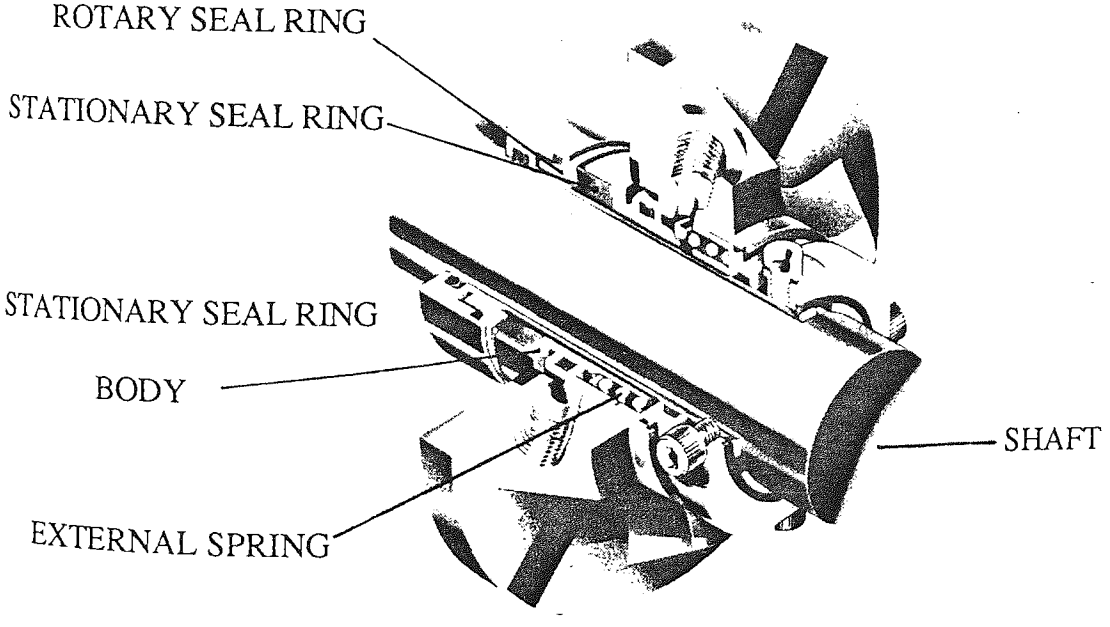


Figure 24. Schematic representation of the F.F.E.T. type Mechanical Cartridge Seal (13)

6.8.2 Rotating Seal Ring

The substrate materials for the rotating seal ring have been previously discussed in Section . The dimensions of the ring and the area to surface coated / treated are shown in Figure 25 .

6.8.3 Stationary Seal Ring Body

The material specification for this component has been given in Section6.2.3, the dimensions and the critical area to be surface coated/treated are illustrated in Figure 25.

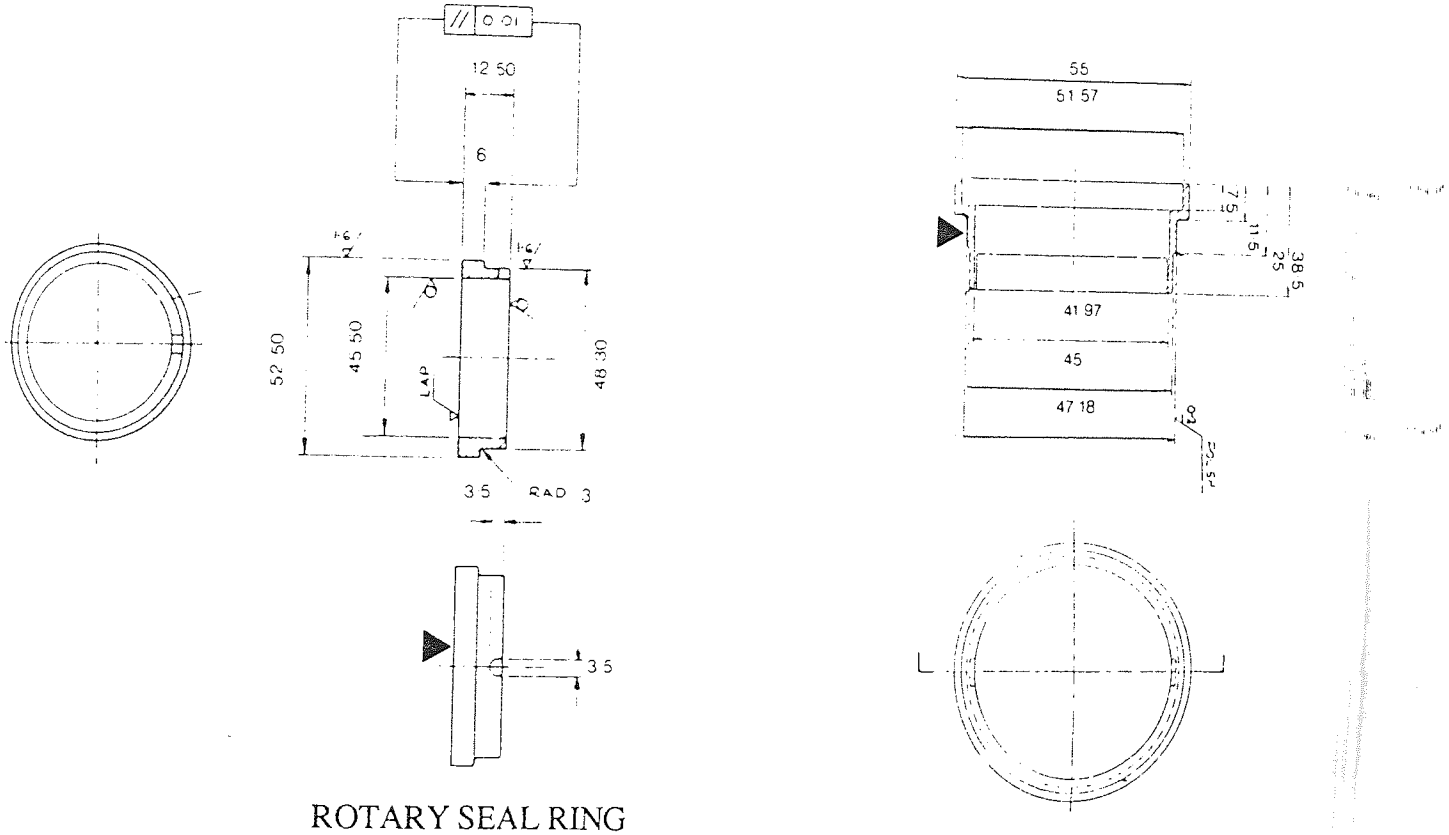


ROTARY SEAL RING

STATIONARY SEAL RING BODY

AREA TO BE SURFACE COATED/TREATED

INDICATED BY " ▶ " SIGN

ALL DIMENSIONS IN MILLIMETRES

Figure 25 .Rotary seal ring and stationary seal ring body(13).

### 6.8.4. F.F.E.T. Seal Test Rig

The F.F.E.T. seal test rig consisted of a closed test chamber in which two F.F.E.T. cartridges were arranged on opposite sides of a rotating shaft, which was driven by a motor. A circulation and an air pump were used to provide the required flow and pressure of the sealed fluid, which was tap water. The test rig is illustrated schematically in Figure 26 .

### 6.8.2.3 Test Parameters

The seals were tested at a pV factor of 85 bar $ms^{-1}$, corresponding to the working limit of a stellite / carbon combination. This equated to a fluid pressure and motor speed of 15 bar and 3000r.p.m., respectively.

### 6.8.5 Seal Face Tests

The surface coated / treated seals were tested at the above parameters for 200 hours duration, tests were conducted in duplicate. The surface finish was measured on the rotating and stationary seal rings before and after the test. The wear rate of the stationary carbon was evaluated by measuring accurately, using a micrometer, the change in the carbon 'nose' height after the test. The fluid leaking from both F.F.E.T. seals was collected separately and measured accurately.

### 6.8.6 Fretting Seal Tests

A rotating silicon carbide and stationary carbon combination were used for the fretting tests. The oscillatory movement was produced by offsetting the rotating seal, by the use of a radially tapered washer, the dimensions of the latter are shown in Figure 27

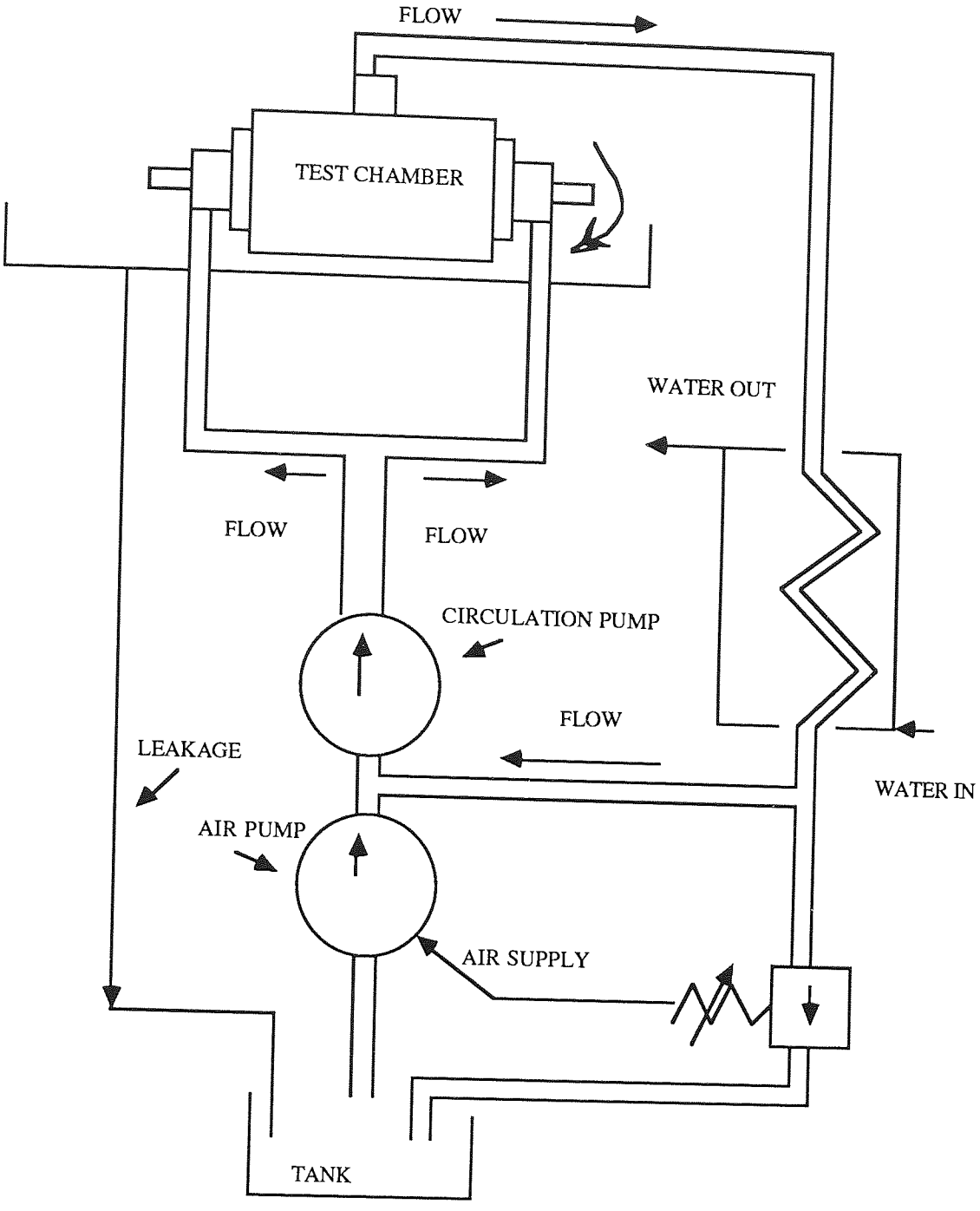


Figure 26 .Schematic representation of the F.F.E.T. type cartridge mechanical seal

The fretting action was accelerated by using a glass filled P.T.F.E. 'O' ring on the sliding diameter. The fretting tests were conducted under the same conditions as the seal face tests. The fretted area and 'O' ring were examined in detail, using a scanning electron microscope. The fretting damage on the sliding diameter was assessed by measuring the surface profile across the fretted area, using a Talysurf (model 4).

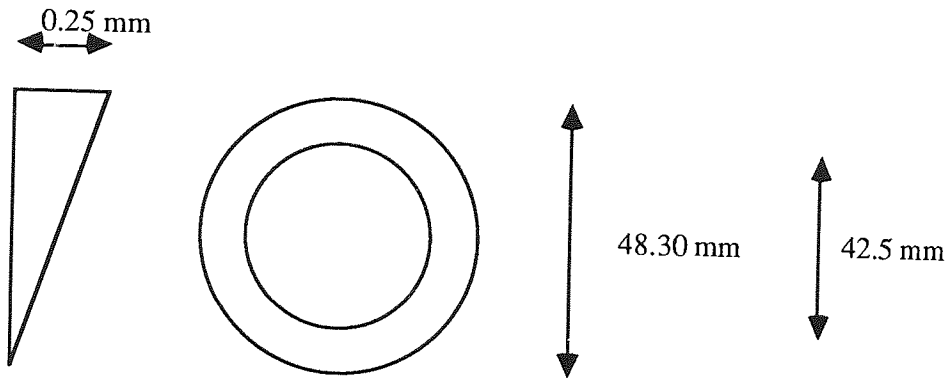


(not to scale)

Figure 27. Diagram showing the geometry and dimensions of radially tapered washer

# CHAPTER VII

## 7.0 EXPERIMENTAL RESULTS

### 7.1 Microhardness and Coating thickness measurements.

The microhardness and coating thickness of surface coatings/treatments investigated in this research are given in Table 12. For the plasma nitrided 316S11 and 431S29 stainless steels, the quoted microhardnesses refer to the peak hardness in the diffusion layers. The microhardness profiles for these plasma nitrided stainless steels are given in Figure 28. It was not possible to measure the microhardness of the vanadium carbide and titanium nitride layers with the available microhardness tester because these coatings were too thin to a valid test.

Table 12. Microhardness and coating thickness measurements for various surface coatings/ treatments.

| | Microhardness $H_V$(100g) | Coating thickness(microns) |
|---|---|---|
| Electroless Nickel (7% P) heat treated at 400 $^oC$ | 1010 | 25 |
| Electroless Nickel Silcon Carbide composite coating heat treated at 400 $^o$ C | 1189 | 40 |

Table 12 continued.

| | Microhardness $H_V$(100g) | Coating thickness(microns) |
|---|---|---|
| Jet-Kote deposit -(Wc/Ni/W-Cr carbides) | 1172 | 150 |
| Borided En 8 Steel | 1402 | 25 |
| Nickel/Chromium/Boron (post fused) | 942 | 100 |
| Chromium Oxide (plasma sprayed) | 1097 | 100 |
| Plasma nitrded 316S11 stainless steel | 1309 | |
| Plasma nitrided 431S29 stainless steel | 1266 | |
| Electroless Nickel (7% P)as plated | 549 | 25 |
| Electroless Nickel (9 %P)as plated | 592 | 20 |
| Electroless Nickel (12 %P)as plated | 571 | 15 |
| Watts Nickel | 241 | 25 |
| Bright Nickel | 520 | 25 |
| Electroless Nickel/Titanium nitride duplex coating(TecVac &D. Teers L.t.d) : | | |
| Electroless Nickel underlay | 1030 | 25 |
| Titanium Nitride layer | / | 4 |
| Vanadium Carbide layer (T.D. Process) | / | 6 |

Figure 28. Microhardness Vs distance plot for plasma nitrided 316S11 and 431S11 stainless steels.

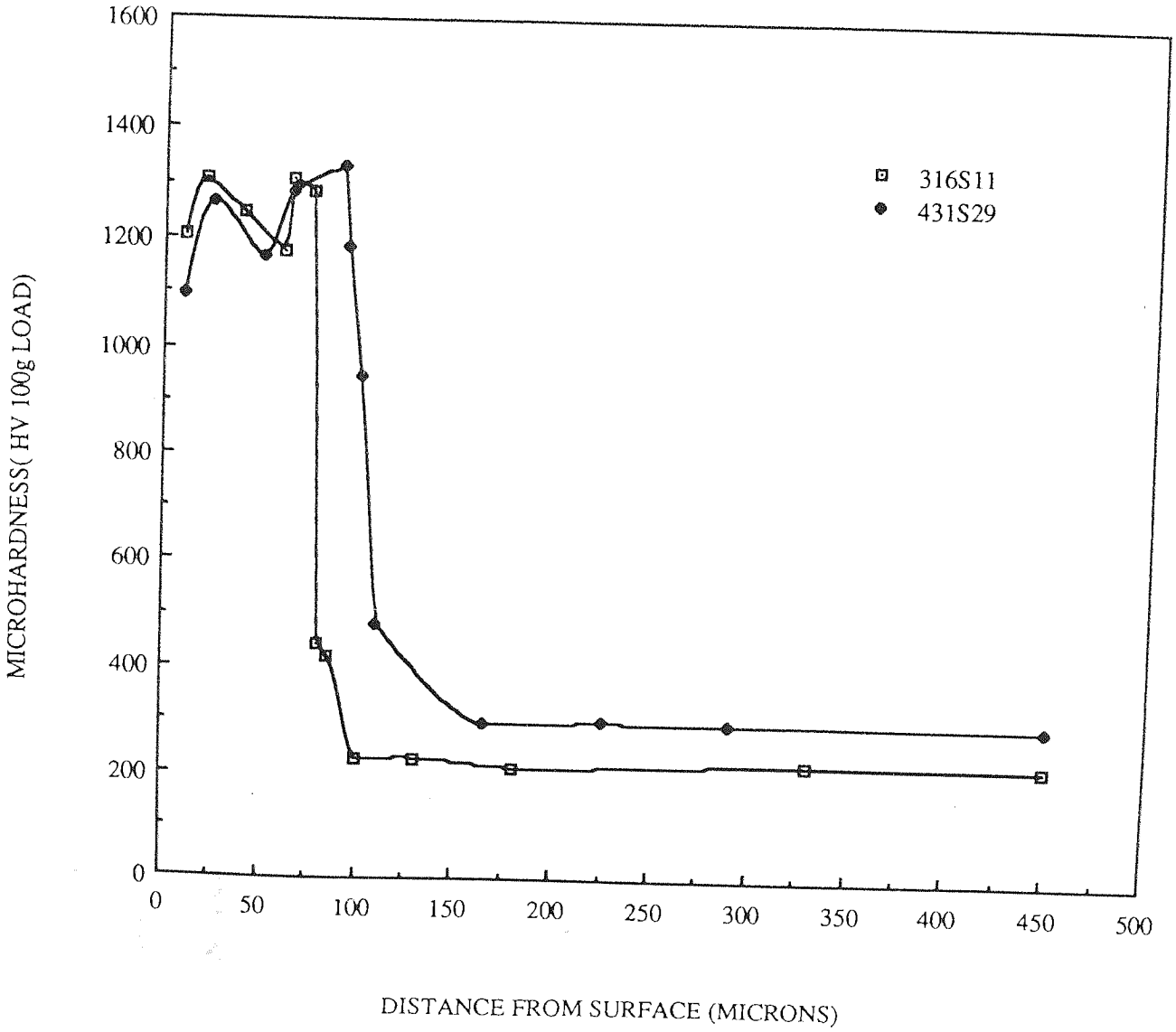

## 7.2 The Wear Rates of Surface Treatments / Coatings

The gravimetric wear rates of the surface treatments / coatings determined at a load of 4 kilograms are given in Table 13. The results are also plotted on a bar chart, as shown in Figure 29. EN8 steel exhibited the highest wear rate, as expected; in contrast, the electroless nickel/titanium nitride (TecVac) duplex coating, the least. The Jet-kote (WC/Ni/W-Cr-C) and vanadium carbide (T.D.layer) deposits exhibited similar wear rates. The wear rate of nickel-chromium-boron (post fused) was slightly higher than that of electroless nickel heat treated at 400°C. The EN8 borided steel exhibited the highest wear rate compared to the other surface coating/treatments.

At the higher load (8 kilograms) only five surface treatments / coatings were tested, primarily because these were the ones applied to mechanical seals. Doubling the load on the pin resulted in a three fold increase in the wear rate for electroless nickel and Jet-kote deposits, but for electroless nickel / titanium nitride (TecVac) duplex coating the wear rate increased by a factor of twelve.

The electroless nickel silicon carbide composite coating (heat treated at 400°C) exhibited a wear rate which was approximately a third of that of conventional heat treated electroless nickel. Thus, it would appear that incorporation of hard silicon carbides

Table 13. The gravimetric wear rates of the surface treatments/ coatings determined using the Pin-on-Disc wear tester

| SURFACE TREATMENTS / COATINGS | GRAVIMETRIC WEAR RATE mg/cm x $10^{-5}$ | |
|---|---|---|
| | 4 kg Load | 8 kg Load |
| EN8 steel | 3.043 | - |
| EN (H.T.400°C) | 0.507 | 1.613 |
| ENSic (Un.Heat) | 0.978 | - |
| ENSic (H.T.400°C) | - | 0.514 |
| Ni-Cr-B | 0.707 | - |
| T.D.Layer | 0.053 | - |
| EN8 Borided | 0.864 | - |
| Chromium Oxide | 0.112 | - |
| Jet-kote | 0.059 | 0.233 |
| EN.TiN(TecVac) | 0.040 | 0.509 |
| EN.TiN(D.Teer) | 0.067 | - |
| Plasma (316) | - | 0.675 |

enhances the wear resistance, however, the abrasive action of these particles on the disc, if any, should also be considered. The wear rates of electroless nickel / titanium nitride (TecVac) duplex coating and plasma nitrided 316 stainless steel were of similar magnitude to that of heat treated electroless nickel silicon carbide composite coating. The Jet-kote deposit exhibited the best wear performance at this load and the wear rate was approximately half of the above surface coatings / treatments, as illustrated in Figure 30.

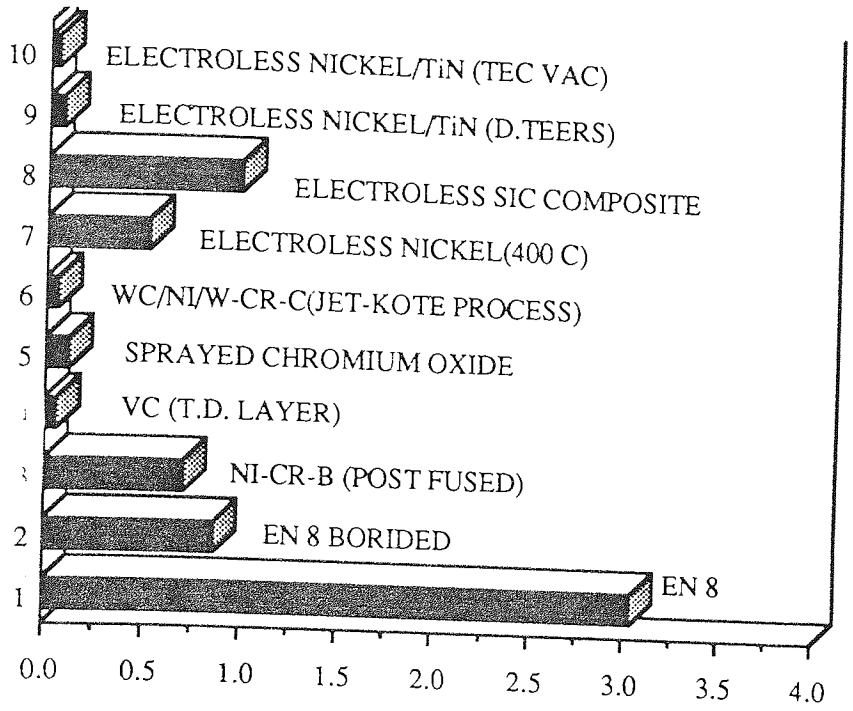


Figure 29. Bar chart illustrating the Gravimetric wear rate determined by the pin on disc wear tester, using a 4 kg load

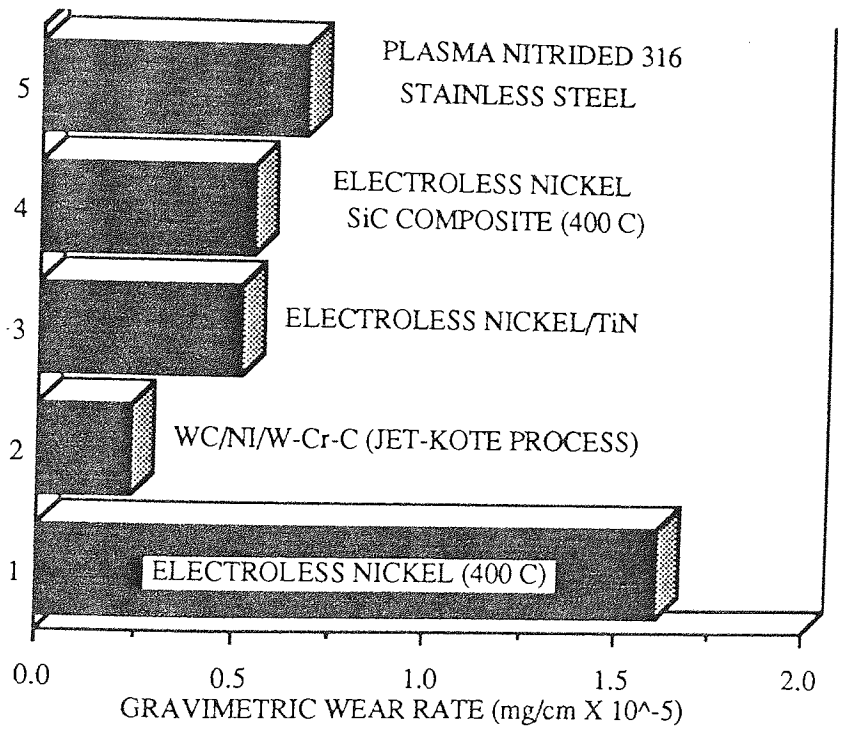


Figure 30. Bar chart illustrating wear rates determined by the pin on disc wear tester, using a 8 kg load

### 7.2.1 Scanning Electron Microscopy of Worn Pin Surfaces

#### 7.2.1.1 EN8 Steel

The EN8 steel worn surfaces are shown in Figure 31. These reveal evidence of ploughing and formation of deep grooves by plastic deformation. The reason for the ploughing is that the EN31 (disc) is much harder than EN8 and therefore, the hard asperites on the former will plough into the EN8 surface

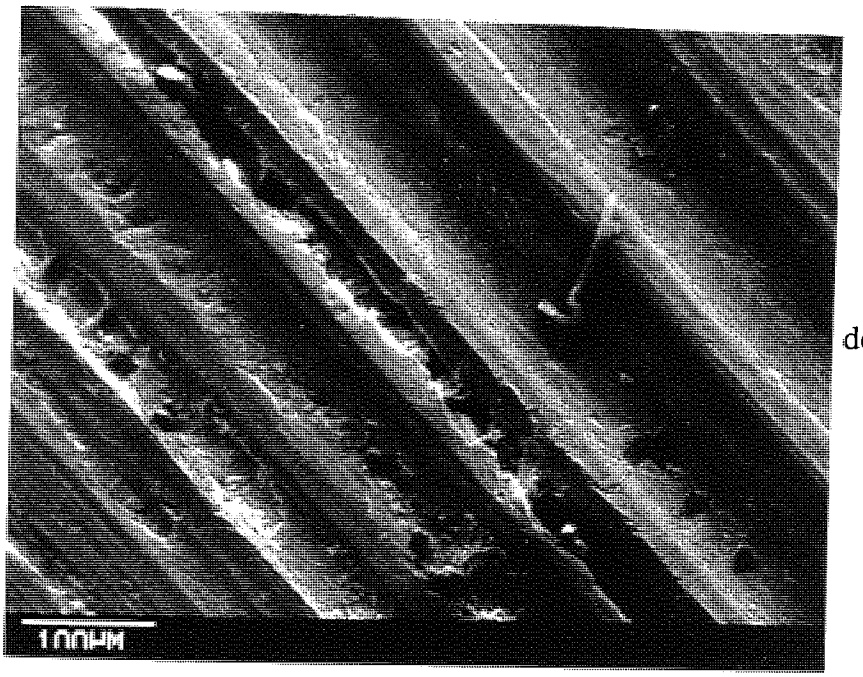


deep ploughing

Figure 31. Worn surface of EN8 steel

7.2.1.2 EN8 Borided Steel

The worn surface of the borided pins exhibited a smooth surface as illustrated in Figure 32. This shows fine ploughing marks in the direction of sliding and a distribution of large and small pores. Some of the pores appear to be elongated in the sliding direction as highlighted in the photomicrograph. It would appear that, as wear proceeds, the size of the pores increase and neighbouring pores may coalesce to form larger ones. If this were to be the mechanism then one would expect small amounts of chromium to be present, as a result of wear debris entrapment. However, analysis of the polished surface and pores was not indicative of this, as shown in Table 14 .

Table 14. E.D.X.A. analysis of the worn EN8 borided surface and wear debris

| | % Si | % Fe | % Mn | % Cr | % S |
|---|---|---|---|---|---|
| Polished Surface | - | 99.71 | 0.24 | 0.05 | - |
| Inside Holes | - | 99.55 | 0.34 | 0.10 | - |
| Adhering Islands | - | 99.12 | 0.51 | 0.36 | - |
| Wear Debris | - | 5.64 | - | 3.22 | 2.64 |

Evidence of adhesive transfer is illustrated in Figure 33. Analysis of the adhering islands indicates a slightly higher chromium content compared to that detected on the polished surface. This trend is apparent when comparing the energy dispersive x-ray spectrum plots from the above areas, as illustrated in Figure (34) and (35) respectively; the former exhibits a pronounced chromium peak. Thus this would support the

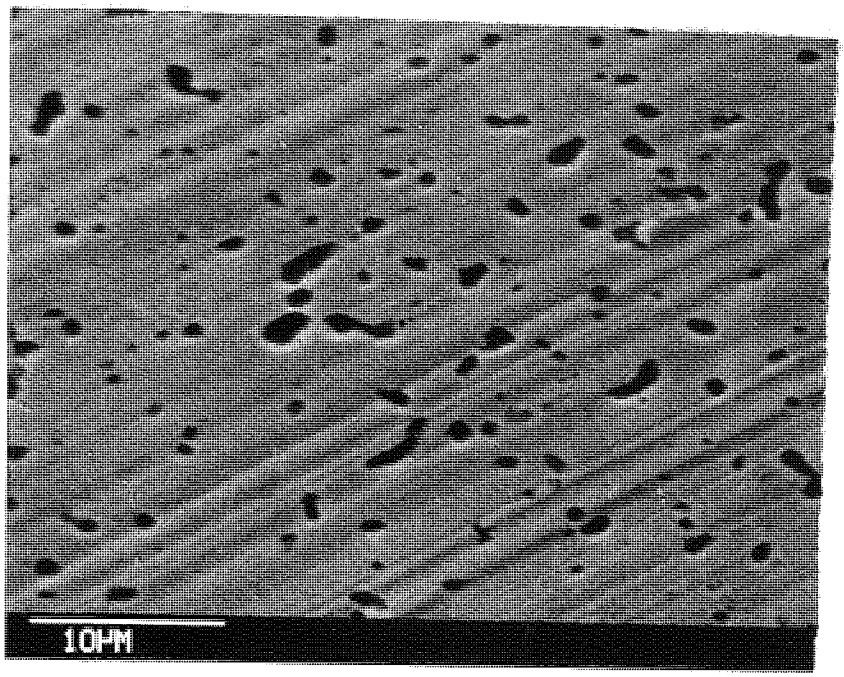


Figure .32. S.E.M. micrograph of worn surface of borided EN8 steel (Load 4 kg)

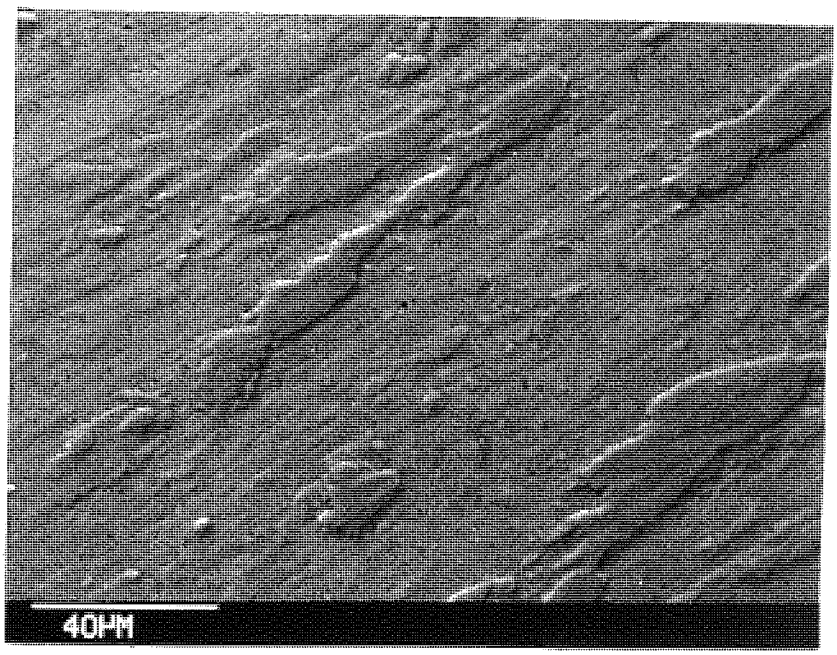


Figure .33 S.E.M. micrograph of worn surface of borided EN8 steel showing adhesive transfer of material (Load 4 kg)

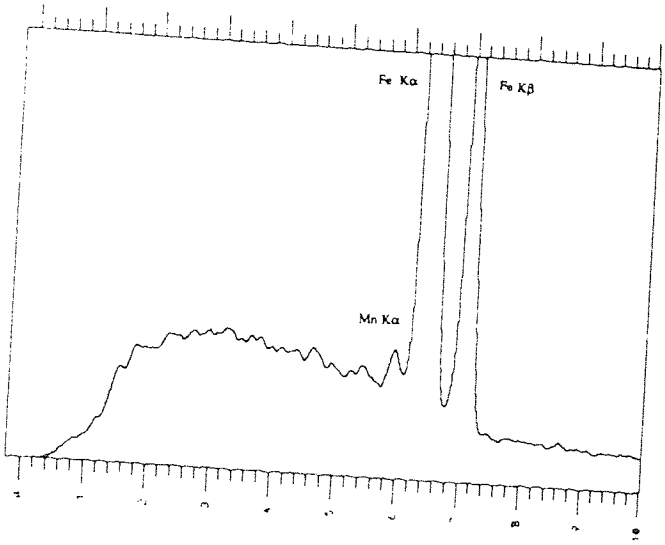


Figure 34. E.D.X.A. spectrum plot of polished worn surface of borided EN8 steel.

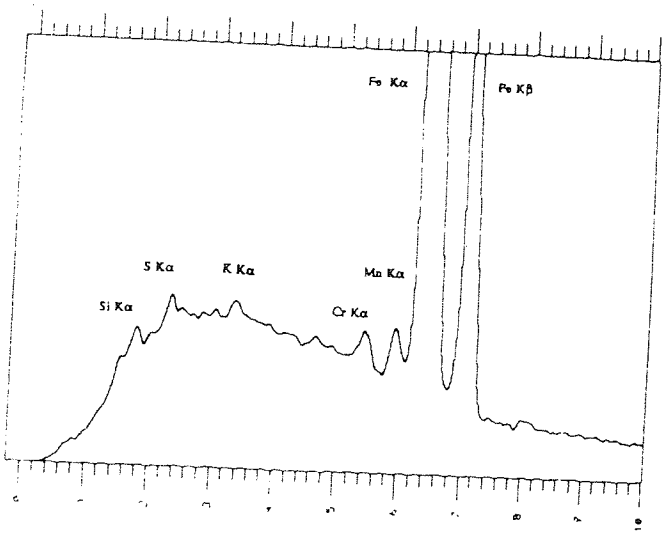


Figure 35. E.D.X.A. spectrum plot of adhesive islands on the worn surface of borided EN8 steel

hypothesis that disc material was transferred by an adhesive wear mechanism.

7.2.1.3 Chromium Oxide (Plasma Sprayed) Deposit

The worn surface of the chromium oxide pins exhibited non-uniform wear and consisted of rough and smooth areas, as illustrated in Figure 36(a). In the smooth areas fine cracks perpendicular to the sliding direction were noted, as shown in Figure 36(b). Using iron and chromium x-ray mapping, it is evident that smooth and rough areas are rich in iron and chromium, respectively, as illustrated in Figure 37. Analysis of the wear debris and worn surface is given below in Table 15 .

Table 15. E.D.X.A. analysis of worn surface of chromium oxide and wear debris.

| | Si | Ti | Cr | Fe | Cu | S |
|---|---|---|---|---|---|---|
| Worn Surface | 2.83 | 7.23 | 29.23 | 58.11 | 2.60 | - |
| Wear Debris | 2.16 | - | 3.03 | 93.78 | 0.60 | 0.37 |

The worn surface analysis confirms that considerable iron (~ 58%) was transferred from the disc. The analysis of wear debris would also suggest that wear is primarily confined to the disc, as small amounts of chromium were detected in the debris. Figure 38 shows another area where cracks have developed and, at a higher magnification (Figure 38(b), a 'V' shaped crack can be seen. It would appear that during sliding wear the chromium oxide spalls off, possibly due to a fatigue mechanism. Material removed in this manner would cause abrasive wear (3 body abrasive wear) of both disc and pin surface. The evidence for the latter is shown in Figure 39, where a deep groove can be seen and fine cracks can be observed running along the groove and therefore, rupture of particles would be an additional mechanism of material removal.

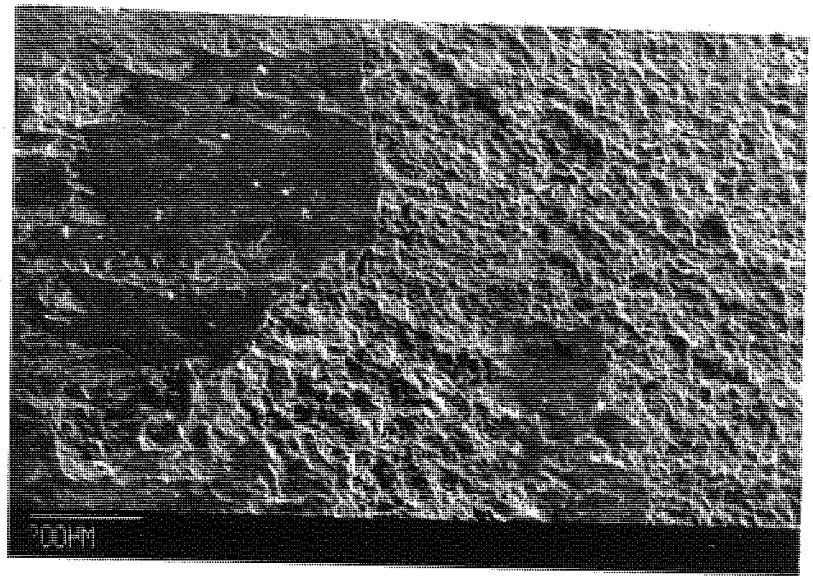

(a) rough and smooth areas

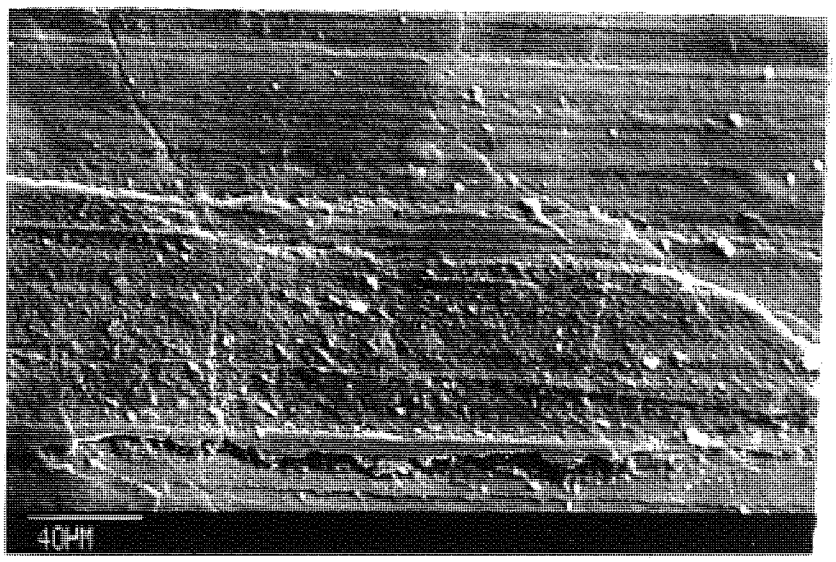

(b) smooth area

Figure 36. S.E.M. micrographs of worn surface of plasma sprayed chromium oxide deposit (Load 4 kg)

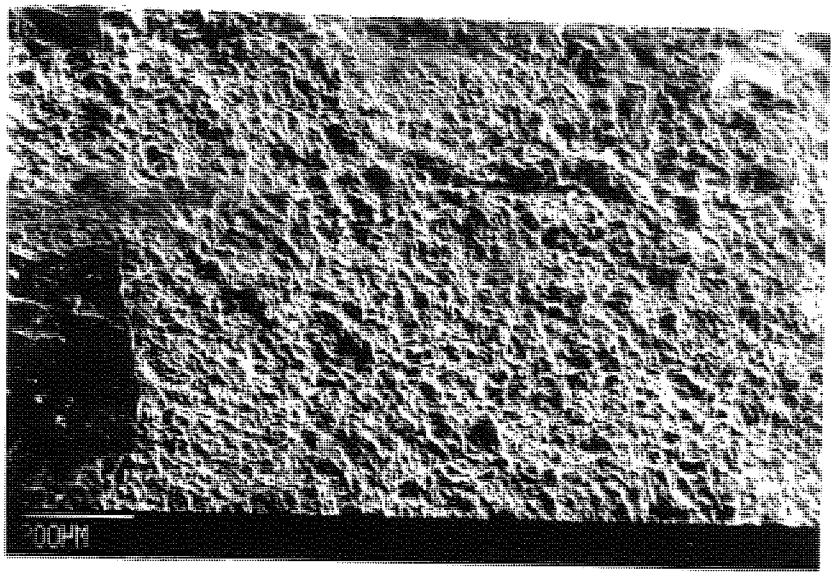

(a) rough and smooth areas


(b) iron x ray mapping

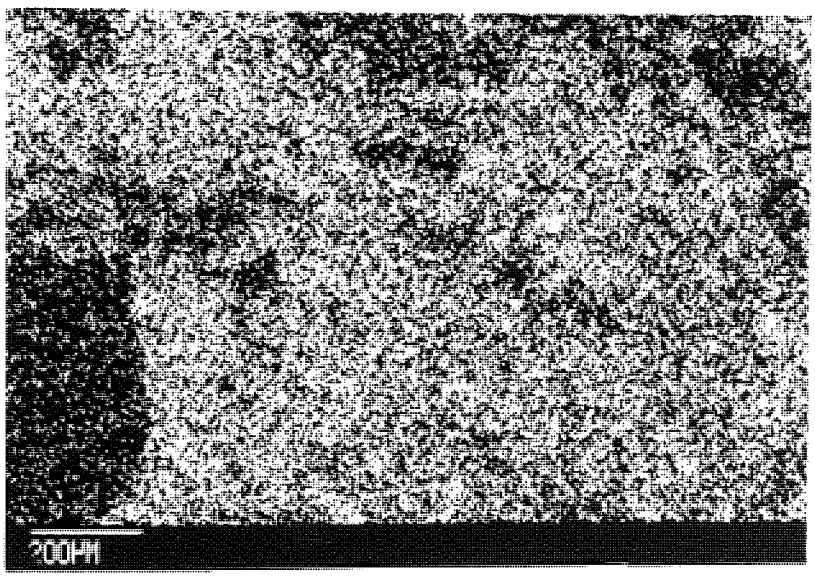


(c) chromium x ray mapping

Figure 37. S.E.M. and x-ray micrographs of worn surface of plasma sprayed chromium oxide deposit (Load 4 kg)

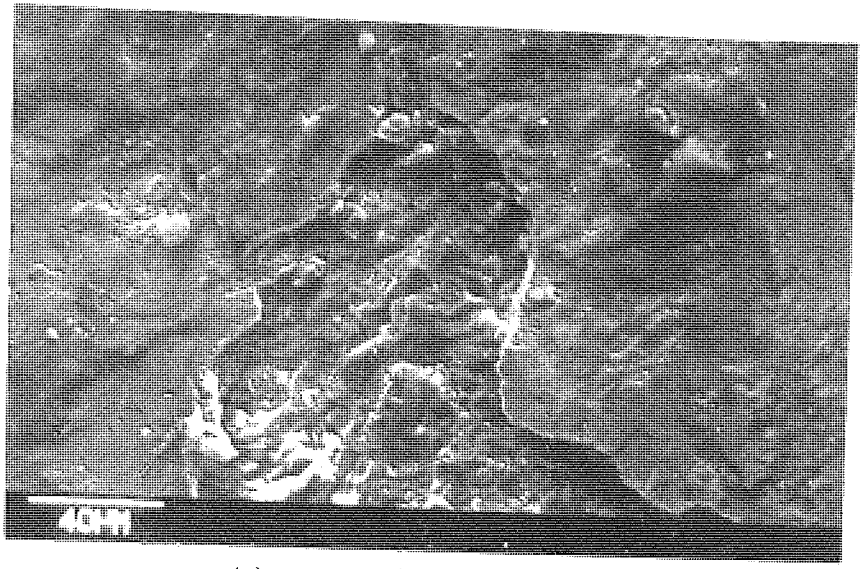


(a) worn surface


(b) higher magnification of cracked area

Figure 38. S.E.M. micrographs of worn surface of plasma sprayed chromium oxide deposit (Load 4 kg)

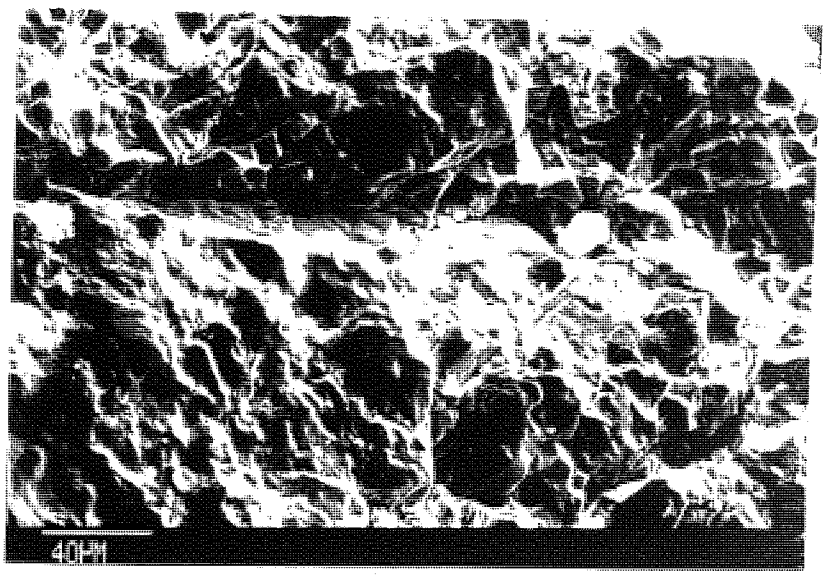


Figure 39. S.E.M. micrograph of worn surface of plasma sprayed chromium oxide showing deep grooving (Load 4 kg)

### 7.2.1.4 Nickel-Chromium-Boron (post fused) Deposit

The worn surfaces of the Ni-Cr-B pins exhibited three typical features:

(1) Ploughing of the surface

(2) Adhesive transfer

(3) Formation of shallow pits.

Figure 40. shows evidence of ploughing and formation of 'tongues' by plastic deformation of surface asperites. The former is probably due to abrasive attack arising from the movement of wear debris between the pin and disc i.e. a three body abrasive wear mechanism.

Figure 41. illustrates an adhesive type of wear, and large islands of material adhering to the surface can be seen. Figure 42 shows a large shallow pit (~ 60μm diameter) formed on the worn surface. It may be that there is a high mutual solubility between Ni-Cr-B and EN31 leading to strong adhesion forces. This would promote microwelding of asperites and wear particles could be formed due to rupture of microwelds. Energy dispersive x-ray analysis (E.D.X.A) of the worn surface and wear debris is given in Table 16.

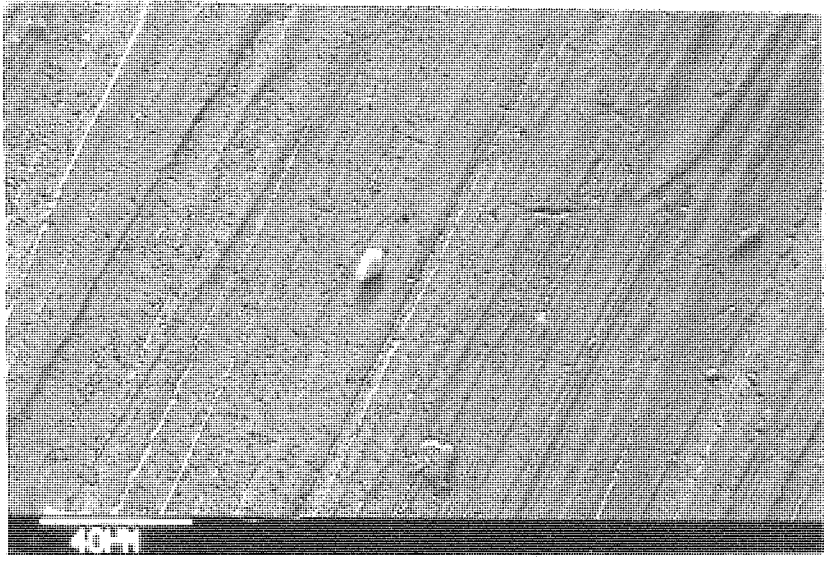

Figure 40. S.E.M. micrographs of worn surface of nickel/chromium/boron deposit showing ploughing and plastic deformation processes. (Load 4 kg)

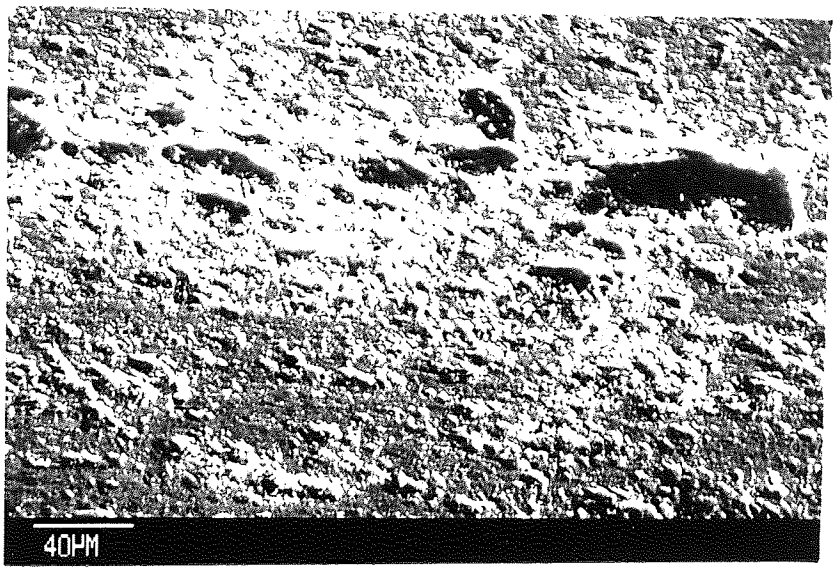


Figure 41. S.E.M. micrograph of worn surface of nickel/chromium/boron showing adhesive transfer of material (Load 4 kg)

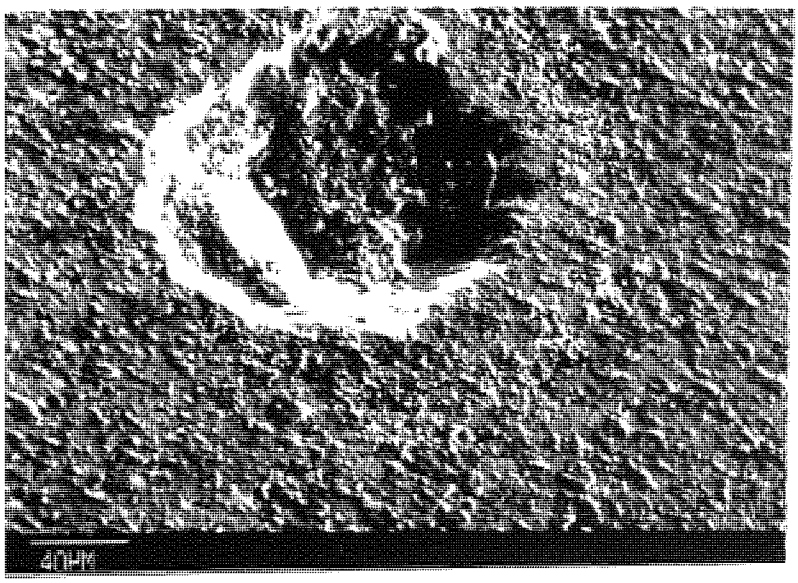

Figure 42. S.E.M. micrograph of worn surface of nickel/chromium/boron showing the formation of shallow pits (Load 4 kg)

Table 16. E.D.X.A. analysis of worn surface of Ni-Cr-B and wear debris.

| | Si% | S% | Cr% | Fe% | Ni% | Mn% |
|---|---|---|---|---|---|---|
| Ni-Cr-B | | | | | | |
| Unworn | 3.34 | 0.02 | 14.95 | 1.58 | 80.10 | - |
| Worn | 3.63 | 0.56 | 9.54 | 47.99 | 38.27 | - |
| Islands | 0.40 | | 4.04 | 92.34 | 2.49 | 0.73 |
| Away from Islands | 2.17 | | 17.92 | 22.84 | 54.95 | 2.14 |
| Debris | 0.92 | 0.13 | 1.91 | 90.38 | 6.66 | - |

From the above analysis, it is evident that a considerable amount of iron (~ 48%) has been transferred to the worn surface. This would suggest that the adhering islands are essentially disc material (EN31 steel). Spot analyses on these islands show higher concentrations of iron and, therefore, would support the above hypothesis. The wear debris consisted of a higher proportion of iron, implying considerable wear on the disc and relatively small amounts of nickel.

7.2.1.5 Vanadium Carbide (Toyota Diffusion) Layer

A typical worn surface is shown in Figure 43(a), and illustrates fine scratching on the surface. Vanadium and iron x-ray mapping showed the transfer of iron to the worn surface, as illustrated in Figures 43(b) and 43(c), respectively. Moreover, the distribution of iron appears to be 'banded' and corresponds to certain areas in the worn surface. The analyses of the worn surface and wear debris are given in Table 17 .

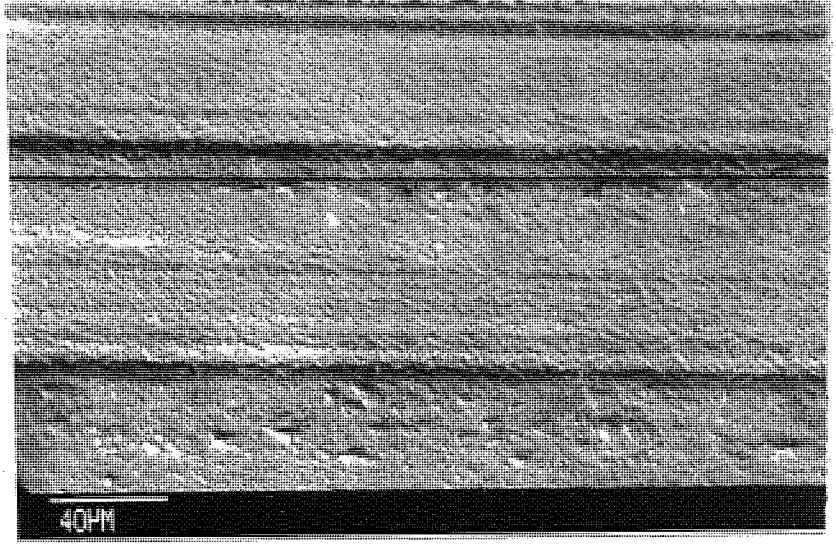


(a) worn surface

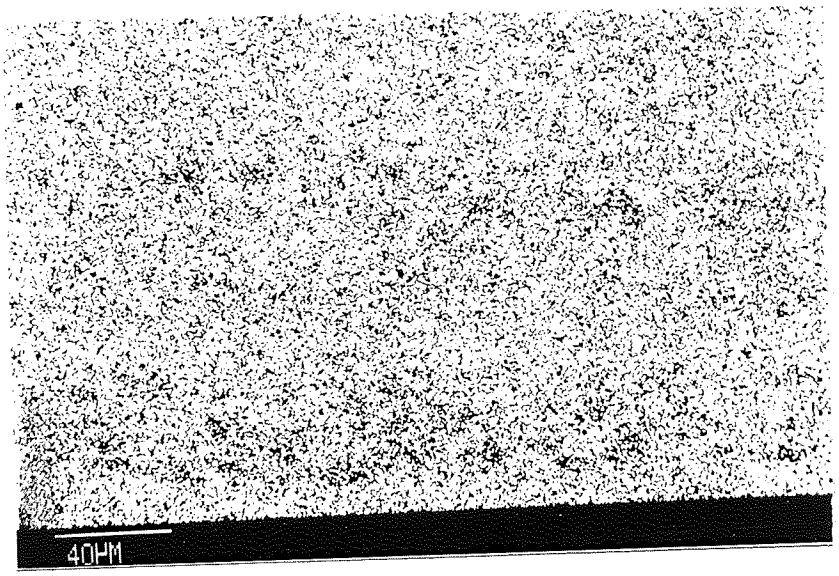


(b) vanadium x ray mapping

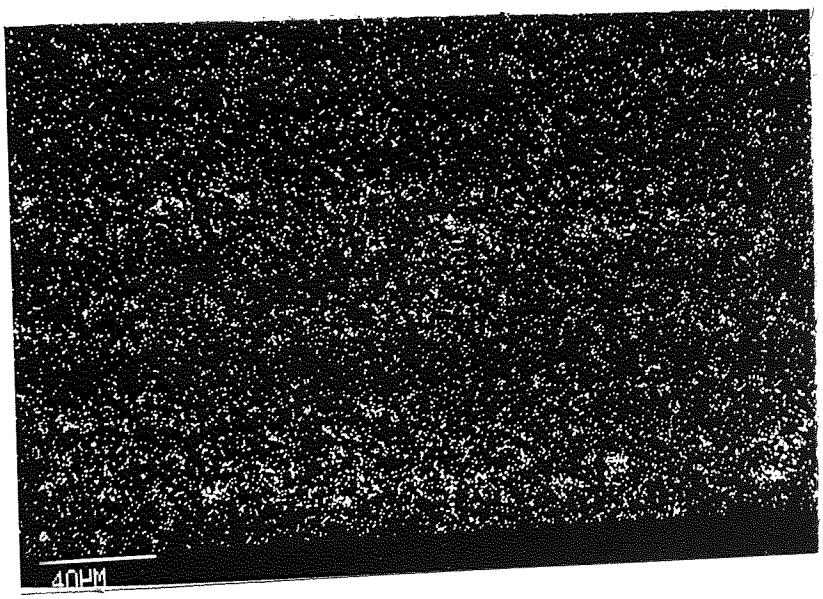


(c) iron x ray mapping

Figure 43. S.E.M. and x-ray micrographs of worn surface of vanadium carbide (Toyota Diffusion Process) layer (Load 4 kg)

Table 17. E.D.X.A analysis or worn surface of vanadium carbide and wear debris

| | Si | S | V | Mn | Fe | Cr |
|---|---|---|---|---|---|---|
| Worn Surface | 0.38 | 0.15 | 93.34 | 0.15 | 6.99 | - |
| Wear Debris | 0.61 | 0.24 | 0.24 | - | 97.90 | 1.01 |

The worn surface analysis shows significant transfer of iron (~ 7%), which would support an adhesive wear mechanism. The analysis of the wear debris would suggest considerable wear on the disc, as evident by the high proportion of iron and very low vanadium percentage.

7.2.1.6 Electroless Nickel

4 Kilogram Load.

The worn surface of the electroless pins exhibited a polished surface as illustrated in Figure 44. This shows fine scratching in the sliding direction and is most probably due to abrasive action by wear debris. Analysis of the worn surface and wear debris is given in Table 18 .

Table 18. E.D.X.A. analysis of worn surface of electroless nickel and wear debris

| Load (Kg) | Ni% | P% | Fe% | Si% | S% | Cr% |
|---|---|---|---|---|---|---|
| Worn Surface | | | | | | |
| 4 | 90.04 | 9.66 | 0.29 | - | - | - |
| 8 | 88.06 | 10.92 | 0.99 | - | - | - |
| Unworn | | | 0.13 | | | |
| Wear Debris | | | | | | |
| 4 | 52.31 | 5.77 | 40.95 | 0.45 | 0.51 | - |
| 8 | 85.12 | 9.55 | 3.58 | 0.79 | 0.84 | 0.12 |

The small amounts of iron detected on the worn surface(4kg) is illustrated by the E.D.X.A. spectrum plot (Figure 45.a). The analysis of the wear debris indicates a high proportion of nickel (52.31%) and this could be interpreted as high wear on the electroless nickel pin. However, very small amounts of wear debris were collected from the latter, whereas a considerable quantity was obtained from other surface treatments and coatings, particularly chromium oxide. The wear debris was not quantified because the majority of it was lost due to rotation of the disc and only that collected by a brush was analysed.

8 Kilogram Load

Worn ends of the pins exhibited a polished appearance similar to that obtained at the lower load. The analysis of the worn surface and wear debris is given above in Table 18. A higher percentage of iron (0.99%) was detected on the worn surface compared with that obtained at the lower load, as illustrated by E.D.X.A. spectrum plot (Figure 45.b). This could further support the adhesive wear mechanism suggested earlier, however it may be argued that the observed trend is due to x-ray fluorescence of steel substrate by high energy nickel x-rays. This was found to be the case, as small amounts or iron (0.13%) were detected on the unworn electroless nickel pin surface, as illustrated in E.D.X.A. spectrum plot (Figure 45.c). However, this still leaves 0.76% Fe, by subtraction, on the worn surface. It may be that there is a transfer of iron on a molecular scale because there was no evidence on the worn surface to suggest adhesive transfer. Analysis of the wear debris would indicate a high wear rate on electroless nickel, as only 3.5% iron was detected. The wear debris exhibited a characteristic plate like morphology as illustrated in Figure 46 . This may be indicative of the delamination theory of wear(65) because it predicts the detachment of plate-like debris during sliding wear.

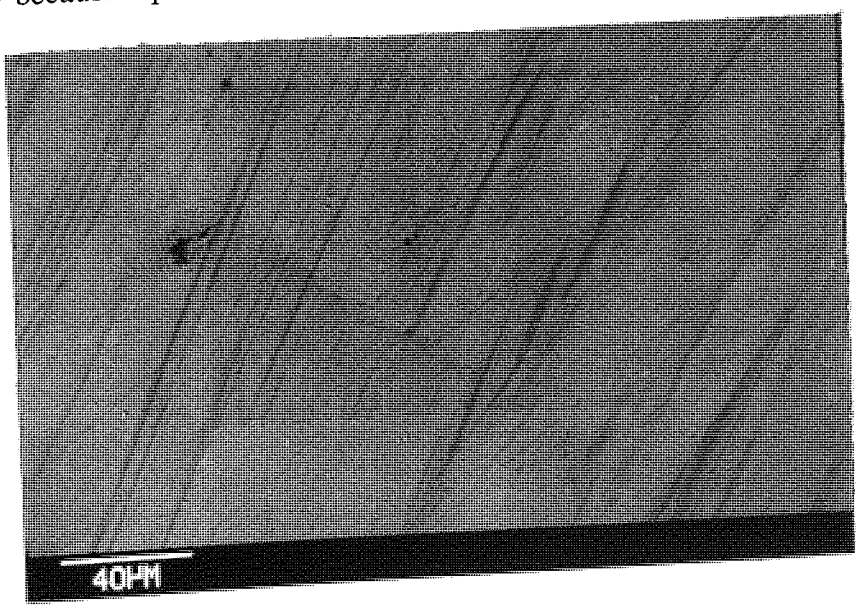


Figure 44. S.E.M. micrograph of worn surface of electroless nickel deposit(4 kg)

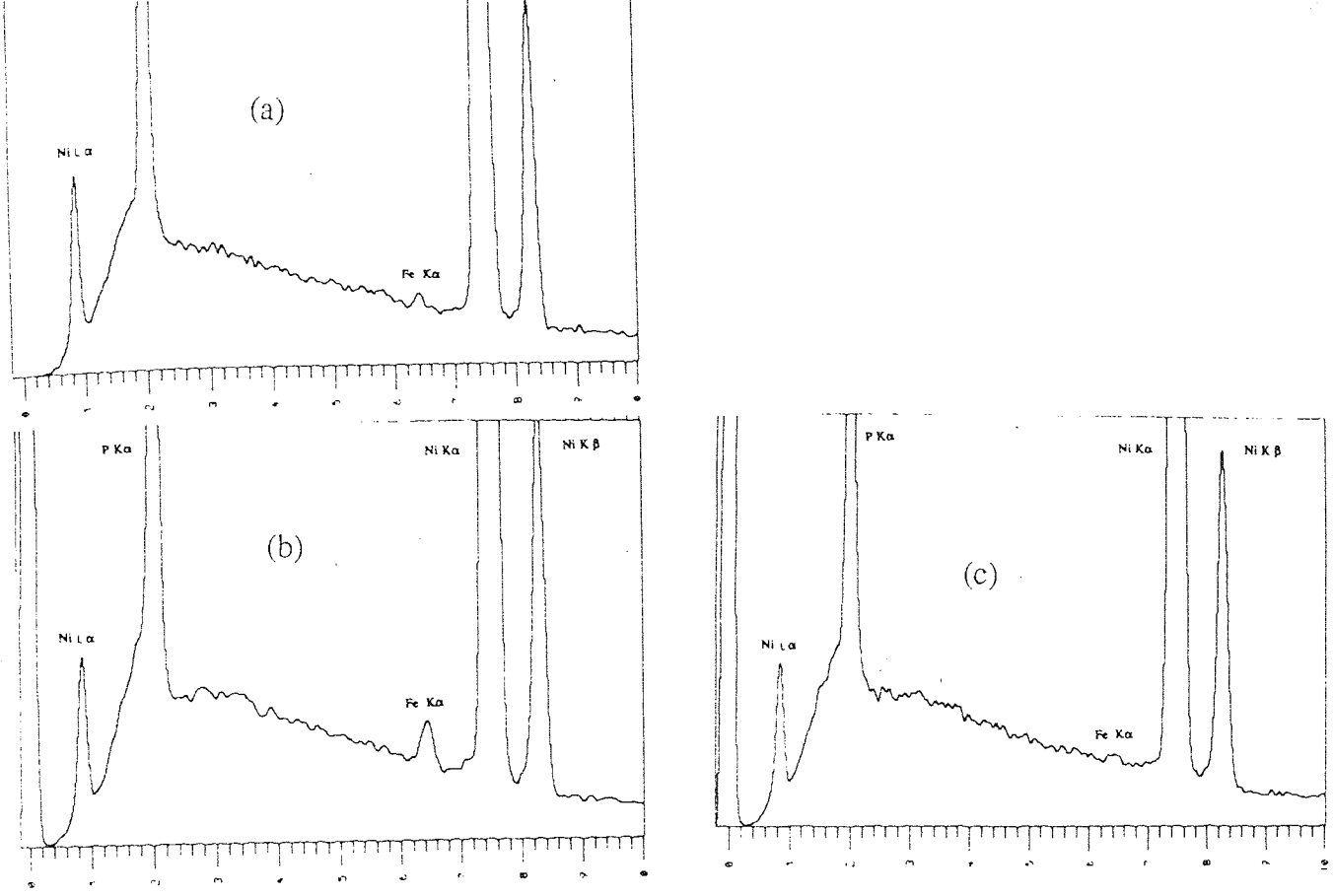


(c) unworn

Figure 45. E.D.X.A. spectrum plots for unworn and worn surfaces of electroless nickel deposits

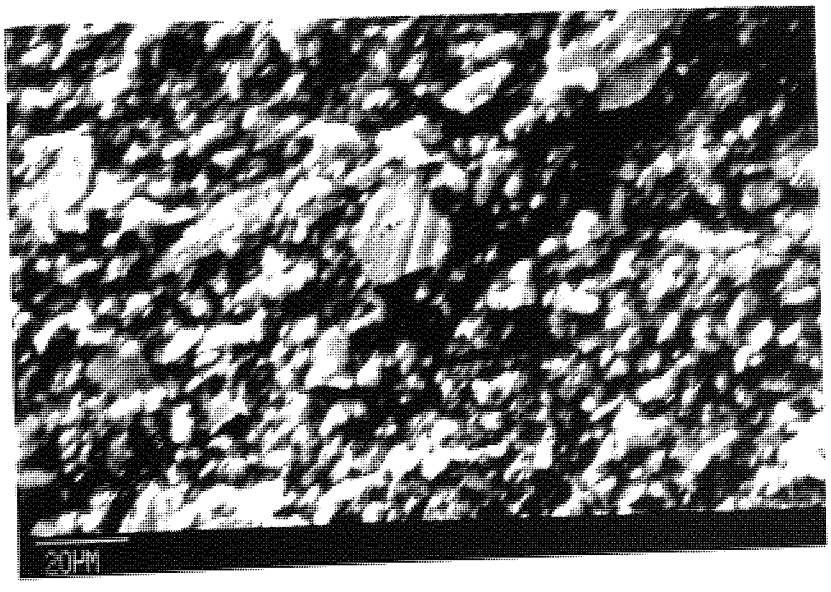

Figure. 46. S.E.M. micrographs of wear debris collected from an electroless nickel / EN 31 disc wear couple.

7.2.1.7 Electroless Nickel Silicon Carbide Composite

4 Kilogram Load

The electroless nickel silicon carbide composite (un-heat treated) exhibited considerable adhesive transfer, as illustrated in Figure 47(a) . Iron, nickel and silicon x-ray mapping confirm the presence of iron in the adhering islands, as evident from Figures 47(b), (c) and (d), respectively. Furthermore, the iron is distributed in areas around the adhering islands, as revealed by iron x-ray mapping. Figure47(e) shows an area at higher magnification, which does not exhibit pronounced adhesive transfer. A crack pattern can be seen which is masked by the raised areas of adhering material. On the bottom left of the photomicrograph it appears that material has been removed, probably by ploughing of the cracked areas. Energy dispersive x-ray analysis of the worn surface and wear debris is given in Table 19.

Table 19. E.D.X.A. analysis of worn surface of electroless nickel silicon carbide composite and wear debris.

| | Load (Kg) | Si | P | Cr | Fe | Ni | S | Mn |
|---|---|---|---|---|---|---|---|---|
| Worn Surface | 4 | 9.02 | 4.69 | 0.18 | 25.65 | 60.48 | - | - |
| Worn Surface | 8 | 8.52 | 7.39 | - | 12.70 | 72.51 | - | - |
| Adhering Material | 4 | 1.07 | 0.72 | 1.04 | 86.76 | 10.12 | - | 0.3 |
| Away From Adhering Material | 4 | 5.08 | 5.15 | 0.11 | 18.83 | 70.83 | - | - |
| Wear Debris | 4 | 0.91 | 0.84 | 0.72 | 91.25 | 6.15 | 0.14 | - |
| Wear Debris | 8 | 4.05 | 1.08 | 1.13 | 83.50 | 7.21 | 3.03 | - |

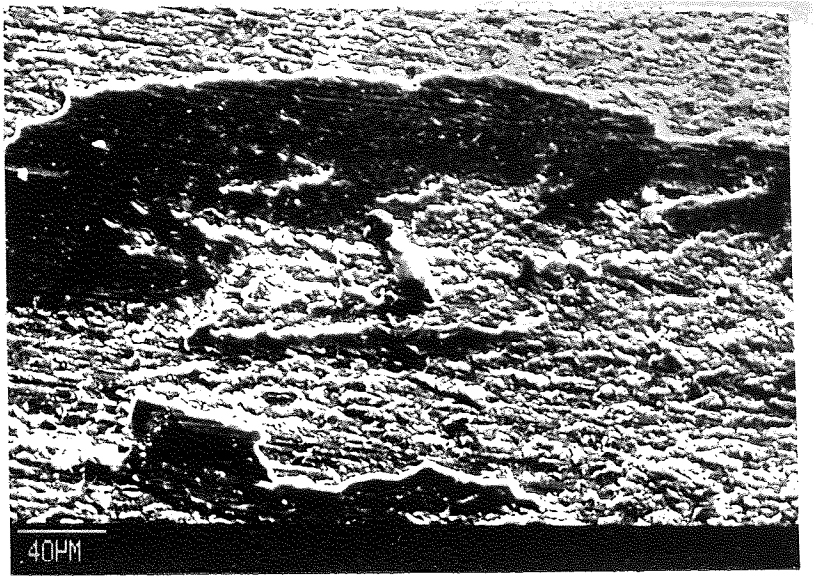


(a) worn surface

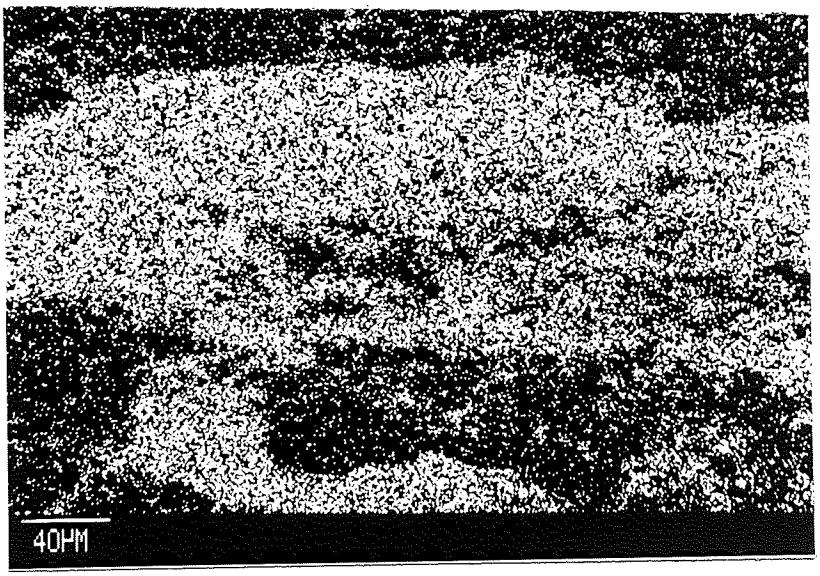


(b) iron x ray mapping

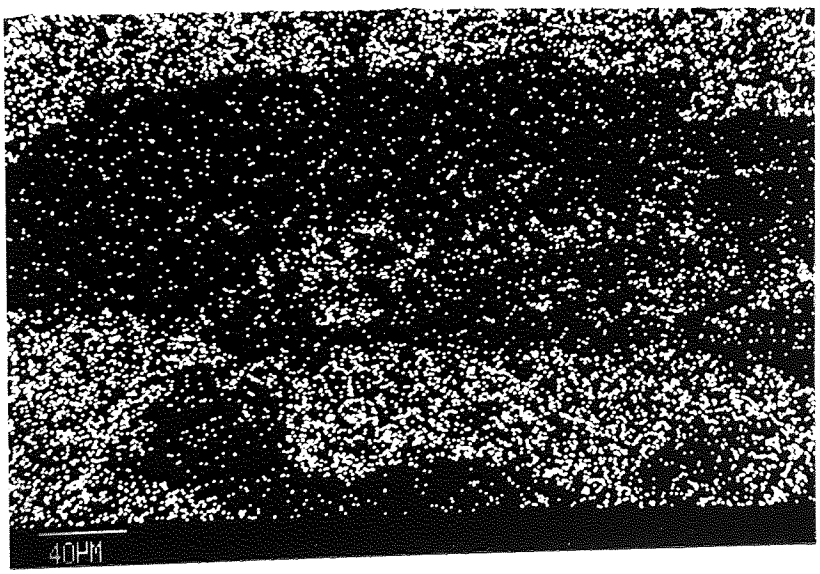


(c) nickel x ray mapping

Figure 47. S.E.M. and x-ray micrographs of worn surface of unheat treated electroless nickel silicon carbide composite coating (Load 4 kg)

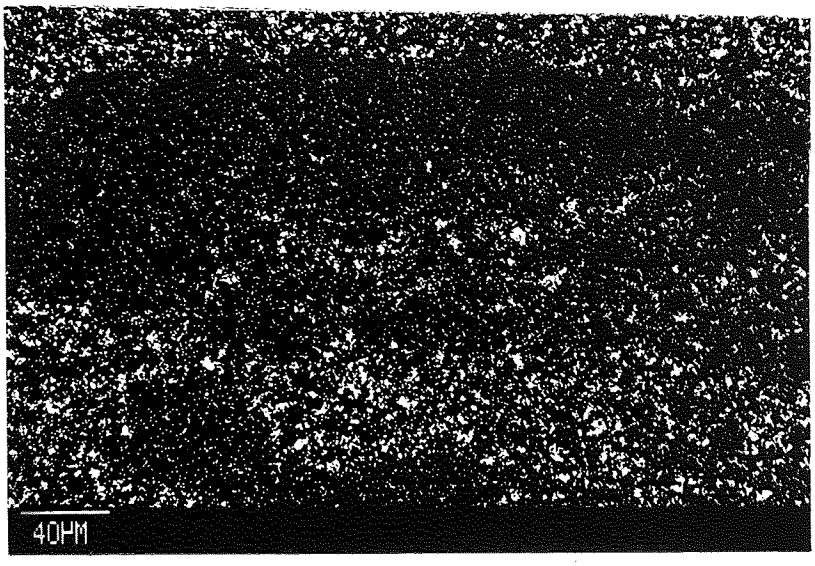


(d) silcon x ray mapping

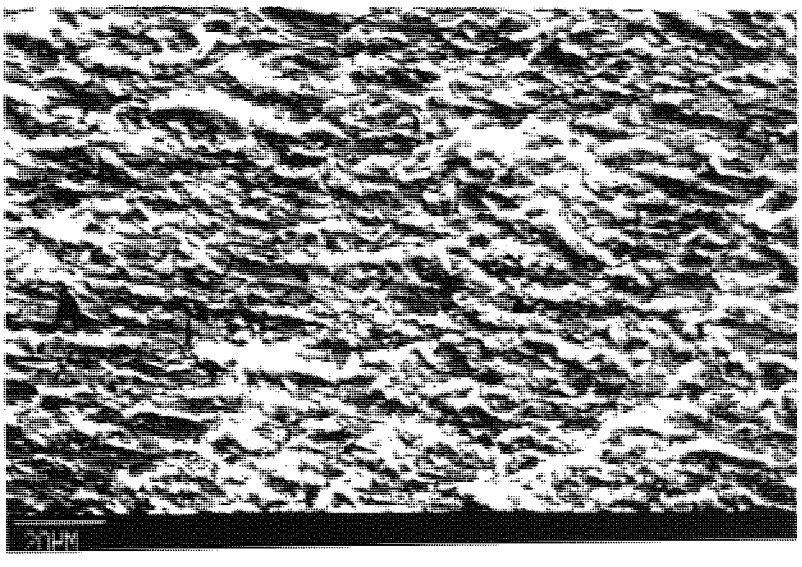

(e) an area showing no adhesive transfer

Figure 47. S.E.M. and x-ray micrographs of worn surface of unheat treated electroless nickel silicon carbide composite coating (Load 4 kg)

Analysis of the adhering material would suggest that it consists principally of iron and small amounts of coating material. In regions away from the adhering material only 20 percent iron was detected, corresponding to the small raised areas (Figure 47(e)).

8 Kilogram Load

The electroless nickel silicon carbide composite (heat treated at 400°C) exhibited similar wear topography. Figure 48(a) illustrates an area showing pronounced adhesive transfer, which was confirmed by iron x-ray mapping. Figure 49(a) shows an area where the transfer of iron is revealed with the aid of iron x-ray mapping. By comparison of Figures 47(e) and 49(a) it can be envisaged that the raised areas are not so pronounced at higher load. This is reflected in the significantly reduced iron (12.70%) compared to that transferred at the lower load. This is probably because the islands of adhering material would tend to fragment at the high loads and evidence for this is illustrated in Figure 48(a) . It is interesting to note that at the 4kg load the ratio of Si : P : Ni is approximately 1 : 1: 6, whereas at the 8kg load it is 4 : 1 : 7; this could imply some pull-out of silicon carbide particles from the electroless nickel matrix during wear.

7.2.1.8 Electroless Nickel / Titanium Nitride Duplex Coating

4 Kilogram Load

The worn surface of electroless nickel / titanium nitride (D.Teer Ltd) duplex coating is shown in Figure 50. From the nickel, titanium and iron x-ray mappings it can be discerned where the TiN has worn away and where ploughing of the electroless nickel

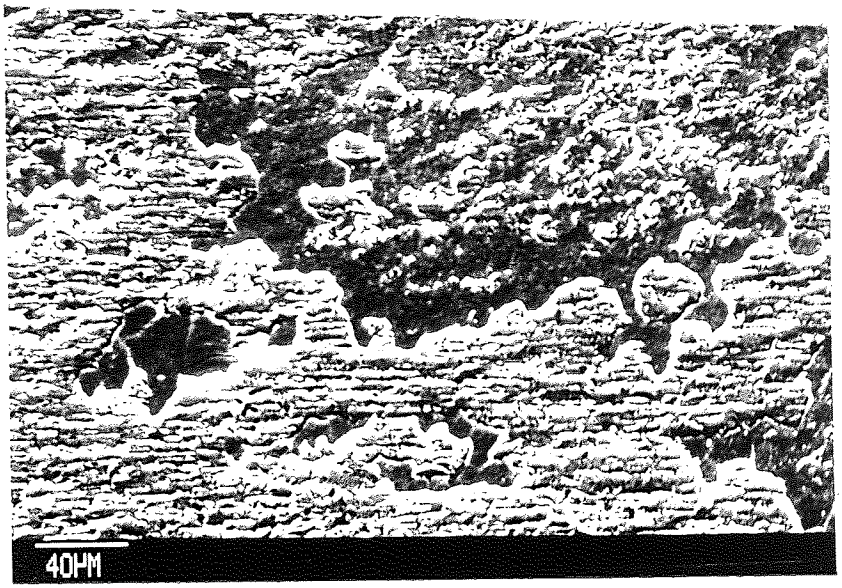


(a) worn surface

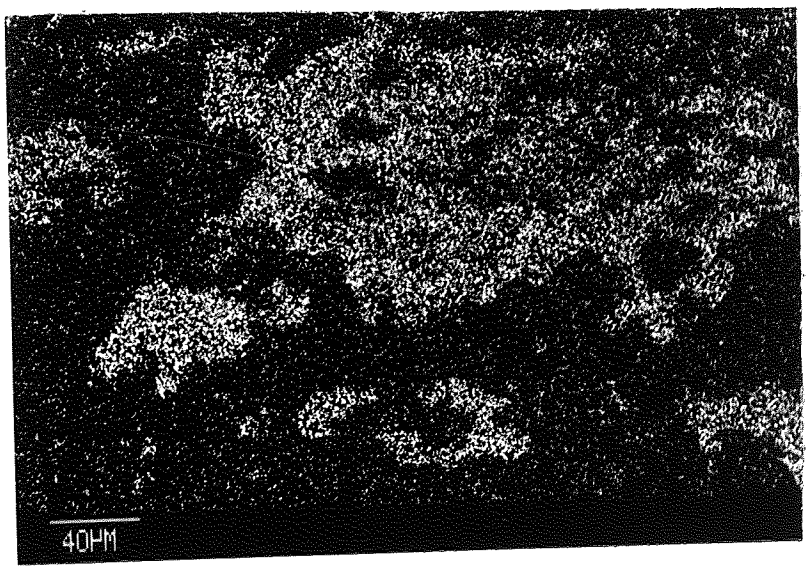


(b) iron x ray mapping

Figure 48. S.E.M. and x-ray micrographs of worn surface of heat treated(400°C) electroless nickel silicon carbide composite coating, showing adhesive transfer(Load 8 kg)

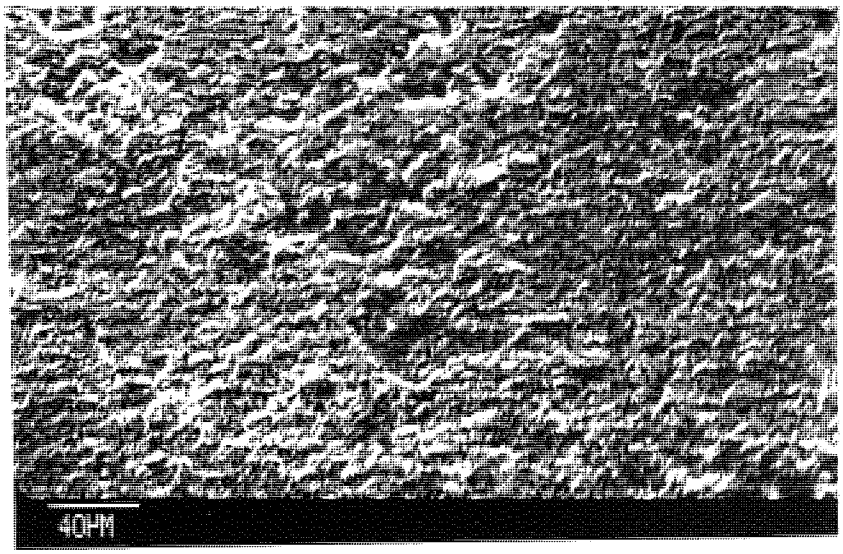


(a) worn surface

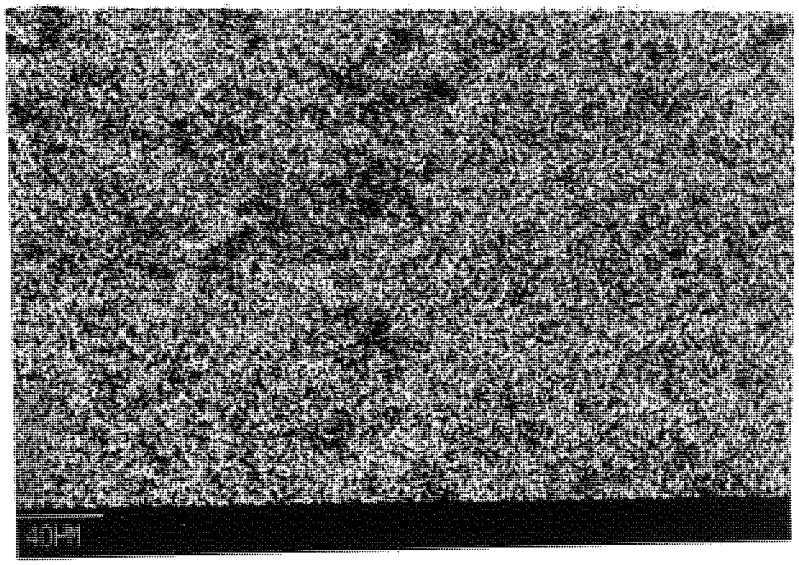

(b) nickel x ray mapping

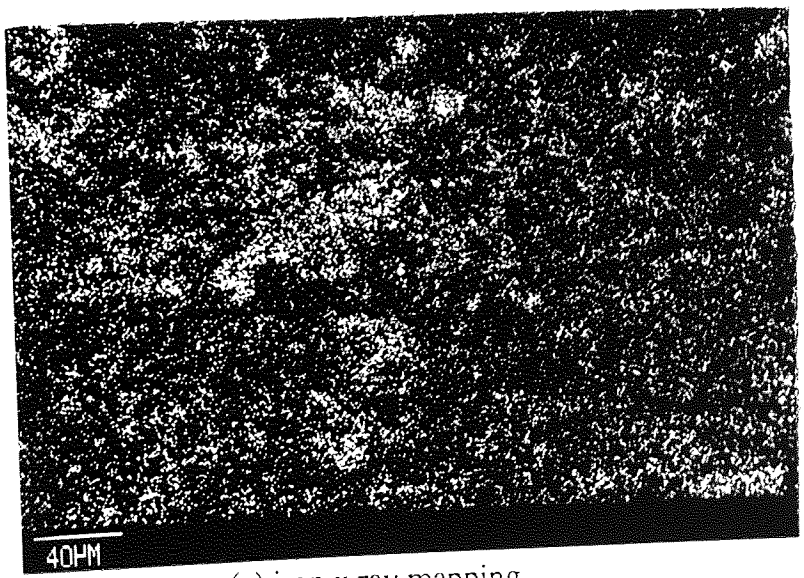


(c) iron x ray mapping

Figure 49. S.E.M. and x ray micrographs of worn surface of heat treated (400 C) electroless nickel silcon carbide composite coating (Load 8 kg)

has occurred. The iron appears to be distributed on both TiN and electroless nickel areas. In contrast, duplex coatings with an overlay of titanium nitride, deposited by TecVac Ltd., exhibited much less removal of the titanium nitride layer, as illustrated in Figure 51. Titanium, nickel and iron x-ray mapping define the areas where the titanium nitride layer has been removed, revealing the electroless nickel underlay and transfer of iron, respectively. A considerable amount of iron has transferred to the titanium nitride layer and very little to the electroless nickel underlay. The latter shows evidence of fine ploughing probably due to abrasive action by wear debris. In both coating systems removal of the titanium nitride layer is probably due to inadequate adhesion to the electroless nickel underlay. The analysis of the worn surface and wear debris is given below in Table 20 .

Table 20. E.D.X.A. of worn surface and wear debris of electroless nickel / titanium nitride duplex coatings (4 kg load)

| Worn Surface | Load (kg) | Si | P | S | Ti | Cr | Fe | Ni |
|---|---|---|---|---|---|---|---|---|
| D. Teer | 4 | 0.32 | 3.94 | - | 41.05 | 0.09 | 13.35 | 41.26 |
| Tec-Vac | 4 | 0.41 | 0.47 | 0.06 | 67.89 | 0.12 | 21.12 | 9.94 |
| Wear Debris | | | | | | | | |
| D. Teer | 4 | 2.77 | 34.23 | 4.67 | - | 0.36 | 2.10 | 55.86 |
| Tec Vac | 4 | 7.78 | - | 0.58 | - | 2.36 | 88.85 | 0.43 |

Analysis of the wear debris (D. Teer) reaffirms that considerable exfoliation of titanium nitride and wear of electroless nickel underlay occurred, as evident from the high

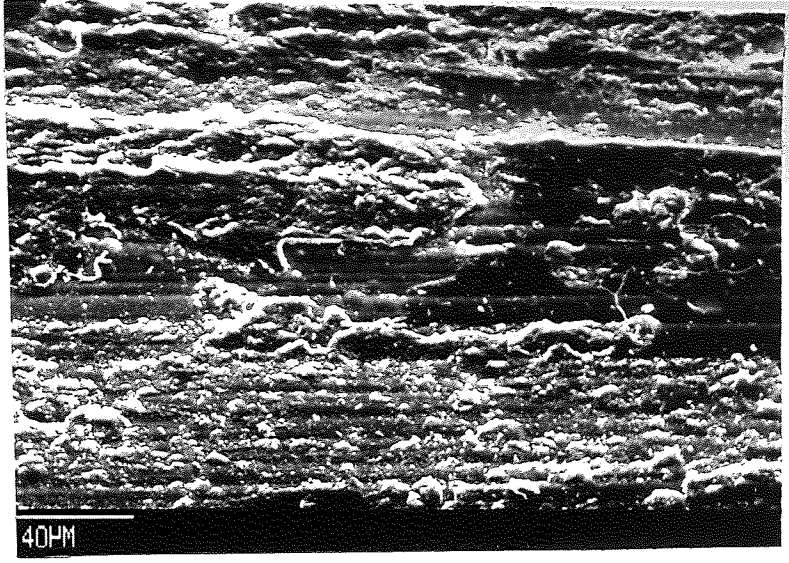


(a) worn surface

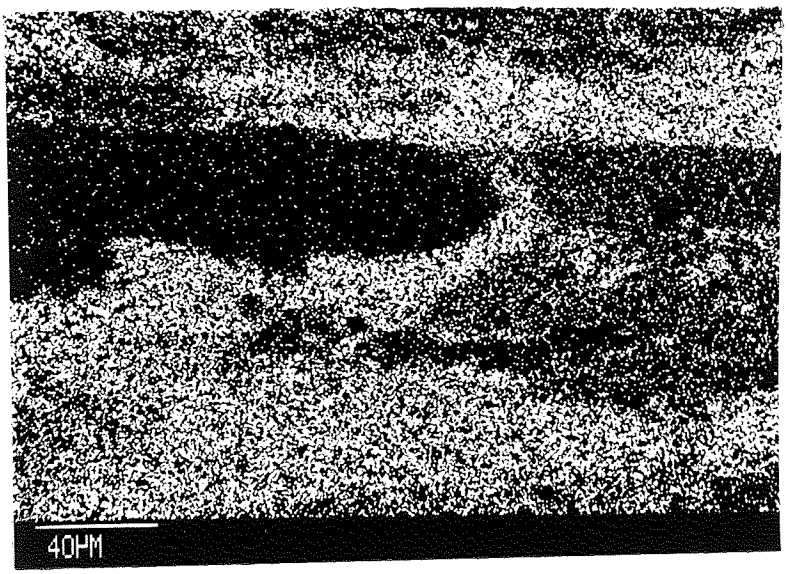


(b) nickel x ray mapping

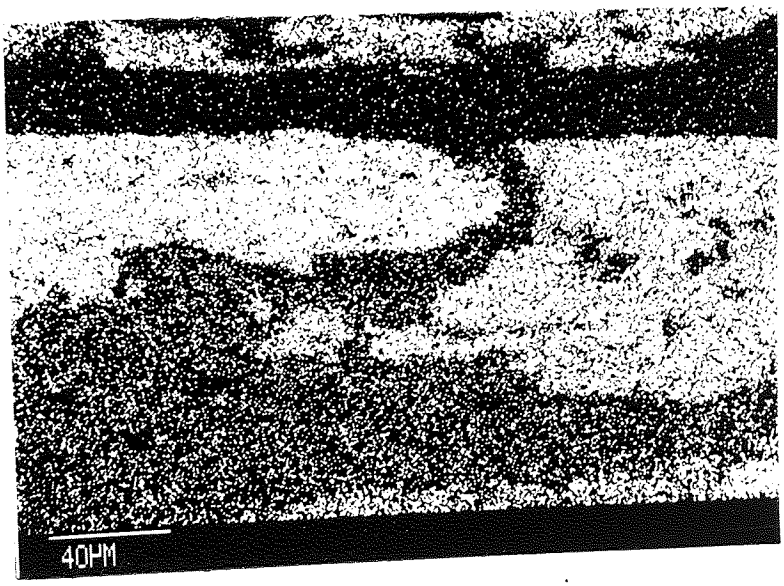


(c) titanium x ray mapping

Figure 50. S.E.M. and x-ray micrographs of worn surface of electroless nickel/titanium nitride duplex coating, D.Teer Ltd. (Load 4 kg)


(d) iron x ray mapping

Figure 50. S.E.M. and x-ray micrographs of worn surface of electroless nickel/titanium nitride duplex coating, D.Teer Ltd. (Load 4 kg)

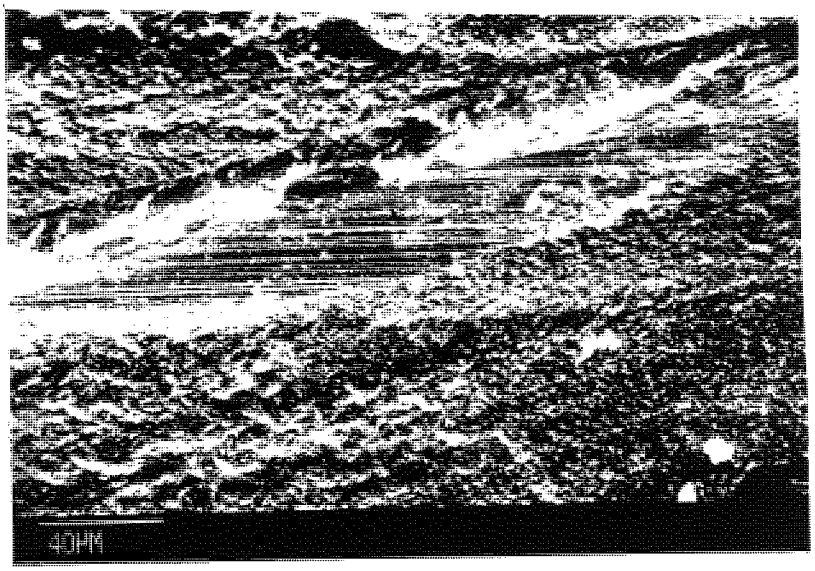


(a) worn surface

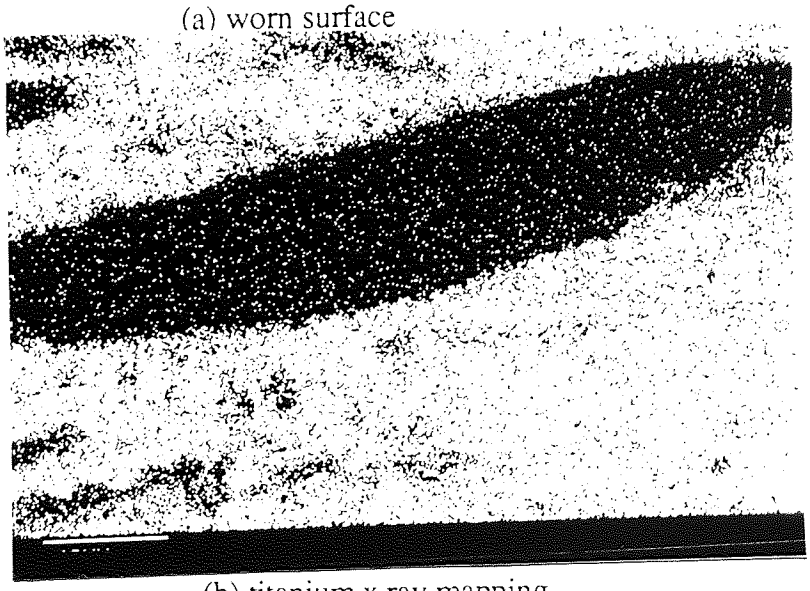

(b) titanium x ray mapping

Figure 51. S.E.M. and x-ray micrographs of worn surface of electroless nickel/titanium nitride duplex coating, Tec Vac Ltd. (Load 4 kg)

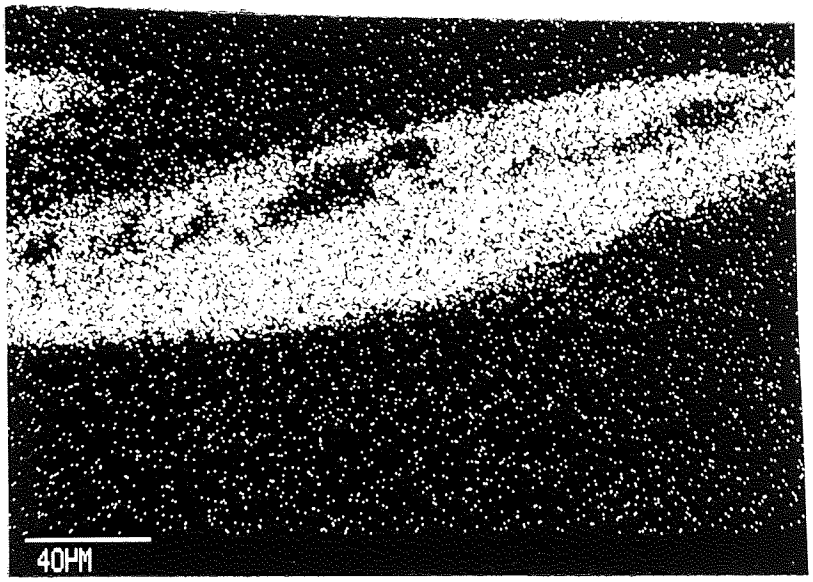


(c) nickel x ray mapping

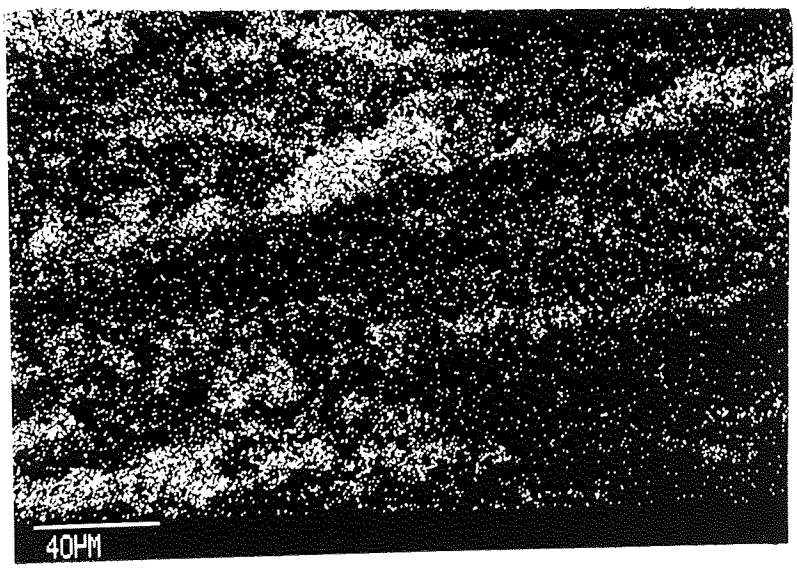


(d) iron x ray mapping

Figure 51. S.E.M. and x-ray micrographs of worn surface of electroless nickel/titanium nitride duplex coating, Tec Vac Ltd. (Load 4 kg)

proportion of nickel in debris. In contrast, Tec-Vac wear debris contained a smaller percentage of nickel .

8 Kilogram Load

From the above results it is apparent that the titanium nitride coatings deposited by D. Teer are inferior to TecVac deposits, hence, at this load only duplex coatings produced by the latter were tested. The worn surface showed four different features:

(1) Complete removal of the titanium nitride layer and gouging of the electroless nickel underlay.

(2) Cracking of the electroless nickel.

(3) Cracking of the titanium nitride layer.

(4) Areas where the titanium nitride layer was still intact.

Figure 52(a) shows an area where the TiN layer had worn away, as evident from the titanium x-ray mapping (Figure 52(d)) and heavy gouging of the electroless nickel. The gouging is probably due to abrasive action by wear debris, evidence for this is illustrated in the iron x-ray mapping (Figure 52(c)). This shows the entrapment of iron (wear debris) within the cracks in the gouged area.

Figure 53(a) illustrates 'plate' like cracking of the electroless nickel and areas of titanium nitride standing proud as evident from nickel and titanium x-ray mapping. The presence of 'plate' like cracking could be suggestive of delamination wear, however, it is most probable that surface shear stresses generated by ploughing action of wear

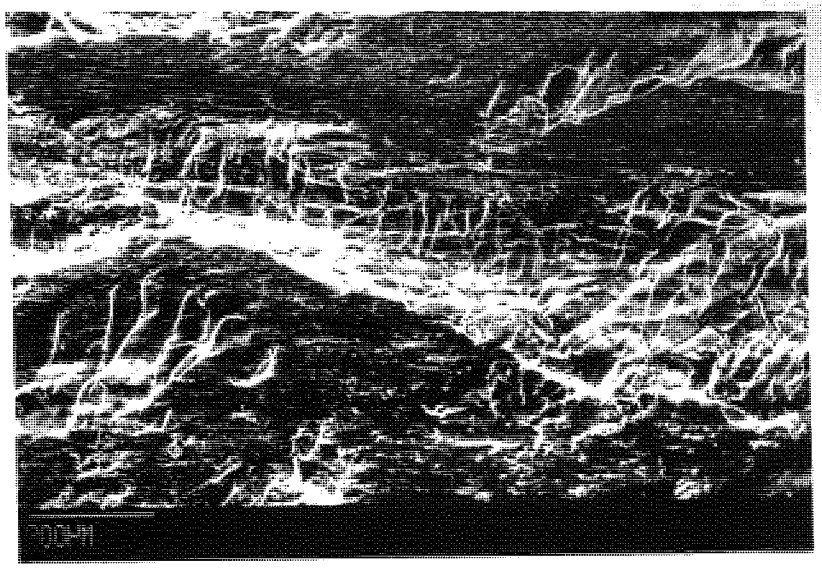

(a) worn surface

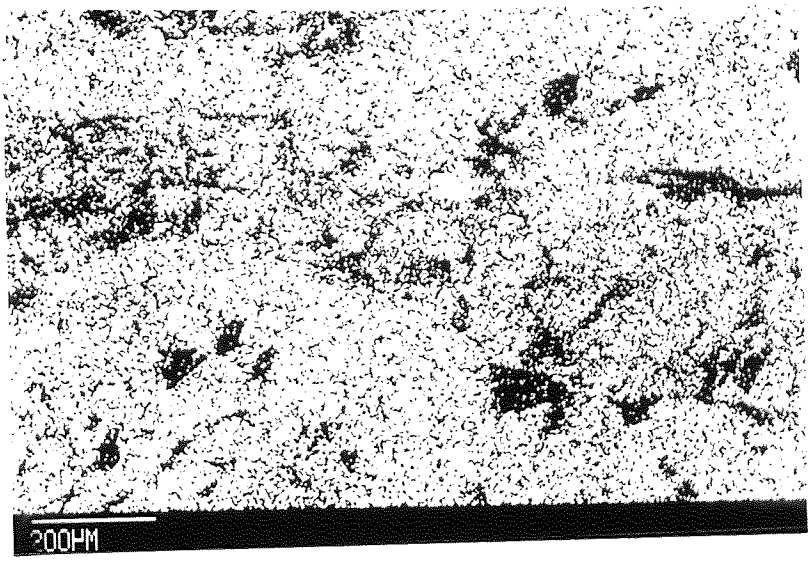


(b) nickel xray mapping

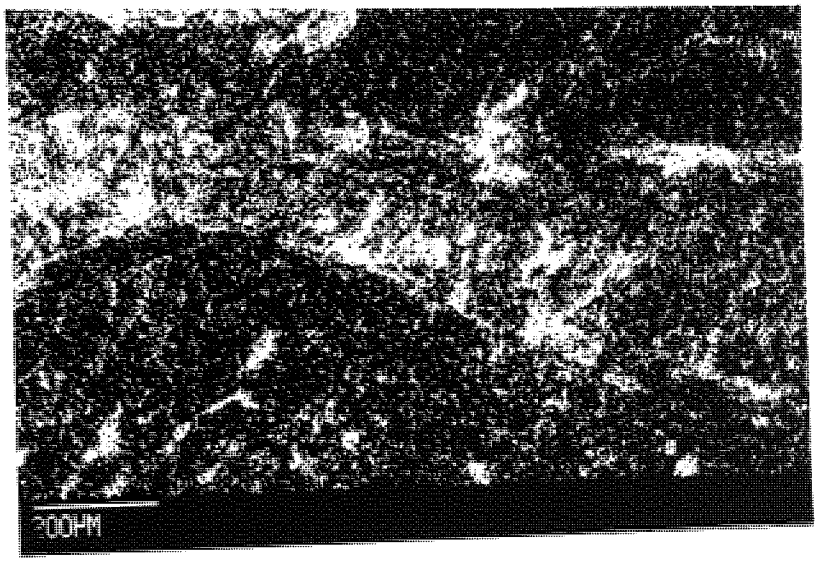


(c) iron x ray mapping

Figure 52. S.E.M. and x-ray micrographs of worn surface of electroless nickel/titanium nitride duplex coating, showing extensive removal of the TiN layer at the 8 kg load

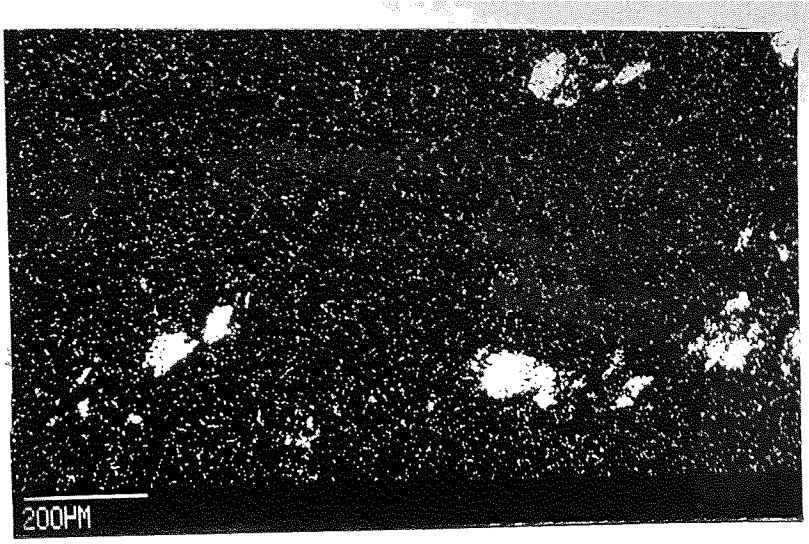


(d) titanium x ray mapping

Figure 52. S.E.M. and x-ray micrographs of worn surface of electroless nickel/titanium nitride duplex coating, showing extensive removal of the TiN layer at the 8 kg load

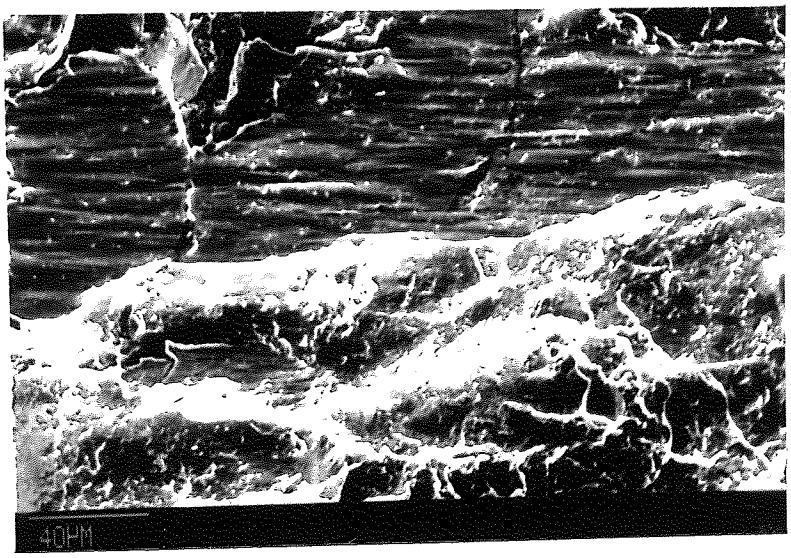


(a) worn surface

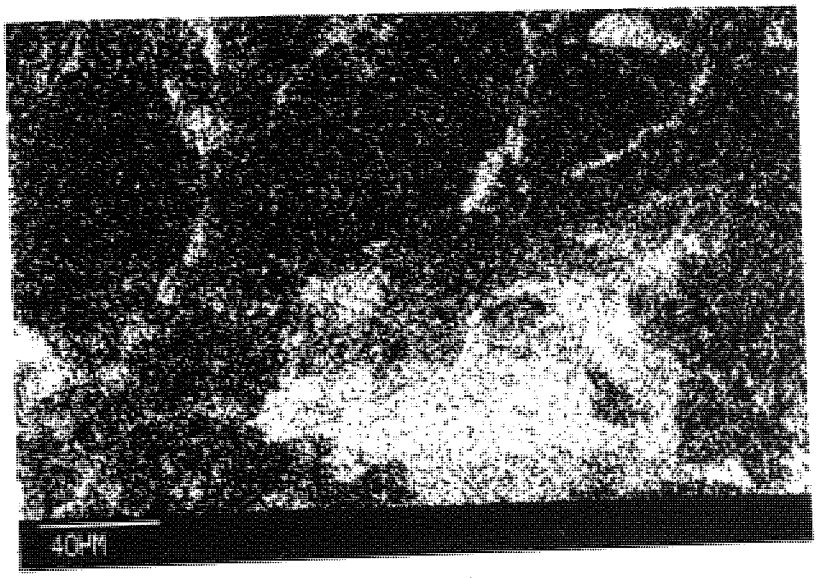


(b) titanium x ray mapping

Figure 53. S.E.M. and x-ray micrographs of worn surface of electroless nickel/titanium nitride duplex coating, showing cracking of the electroless nickel underlay at a load of 8 kg

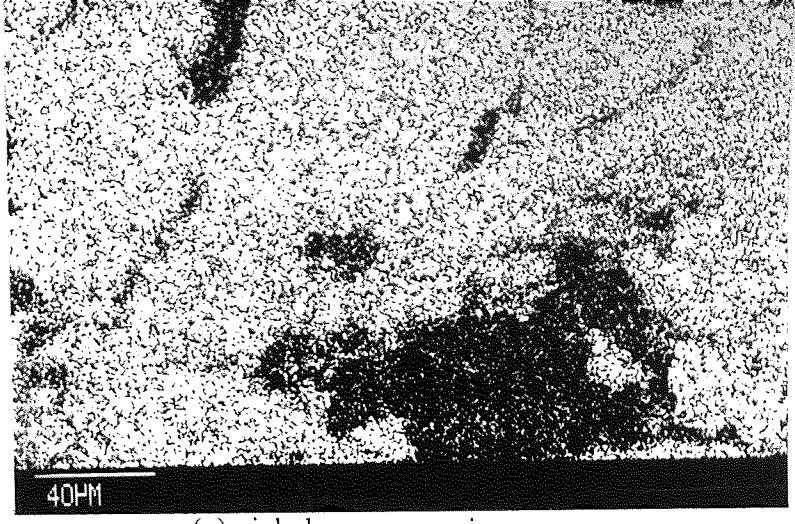


(c) nickel x ray mapping

Figure 53. S.E.M. and x-ray micrographs of worn surface of electroless nickel/titanium nitride duplex coating, showing cracking of the electroless nickel underlay at a load of 8 kg

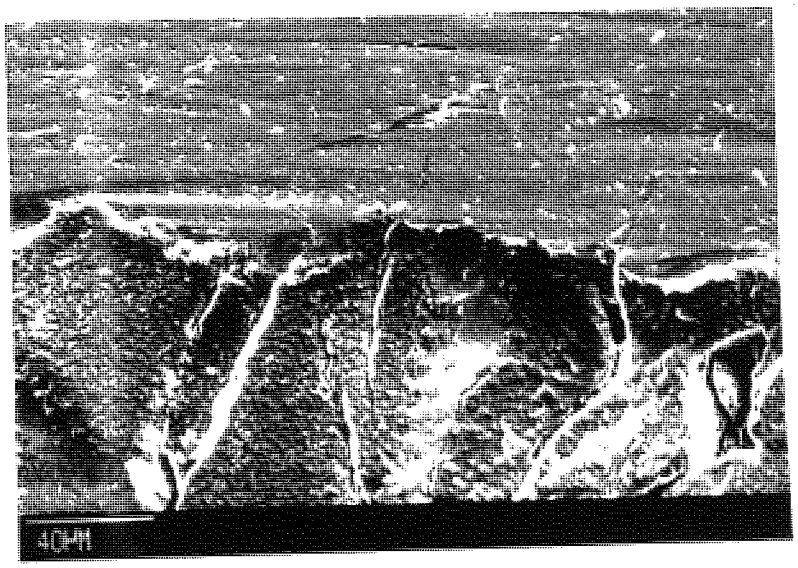


(a) worn surface

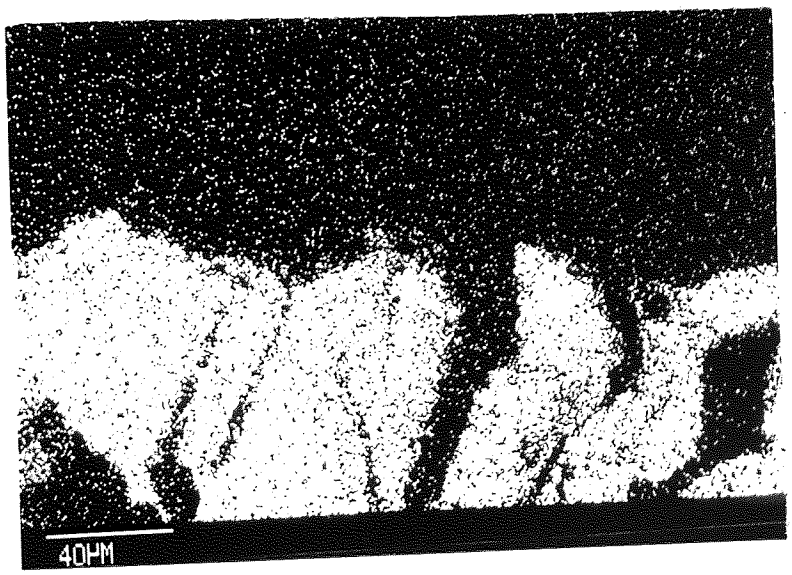


(b) titanium x ray mapping

Figure 54. S.E.M. and x-ray micrographs of worn surface of electroless nickel/titanium nitride duplex coating, showing cracking of the titanium nitride layer (Load 8 kg)

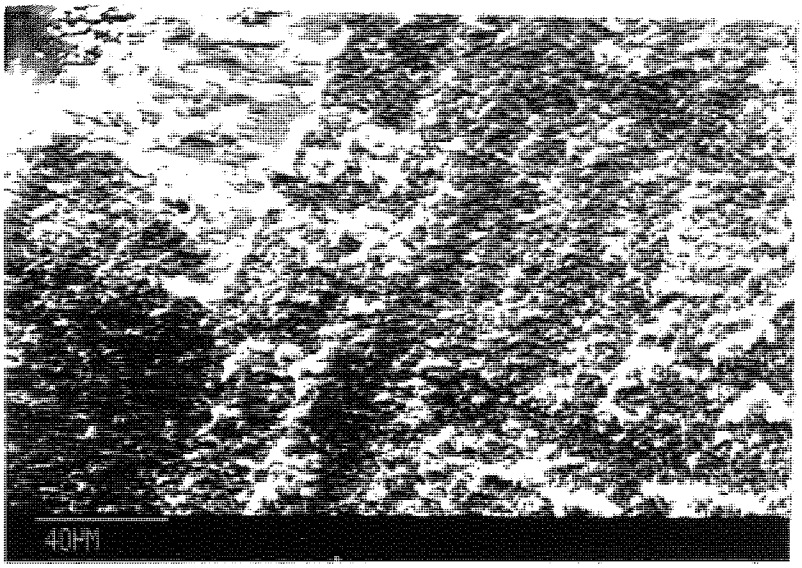

(a) worn surface

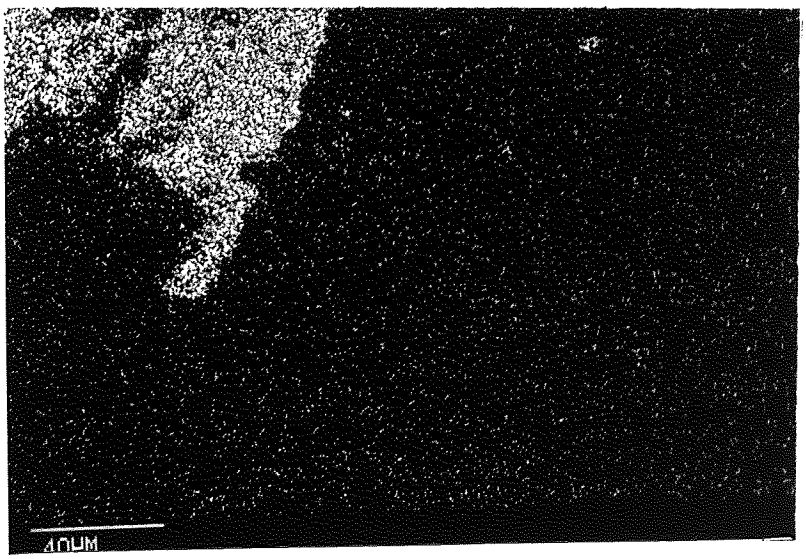

(b) nickel x ray mapping

Figure 55. S.E.M. and x-ray micrographs of worn surface of electroless nickel/titanium nitride duplex coating, showing an area where the titanium nitride layer was still intact (Load 8 kg)

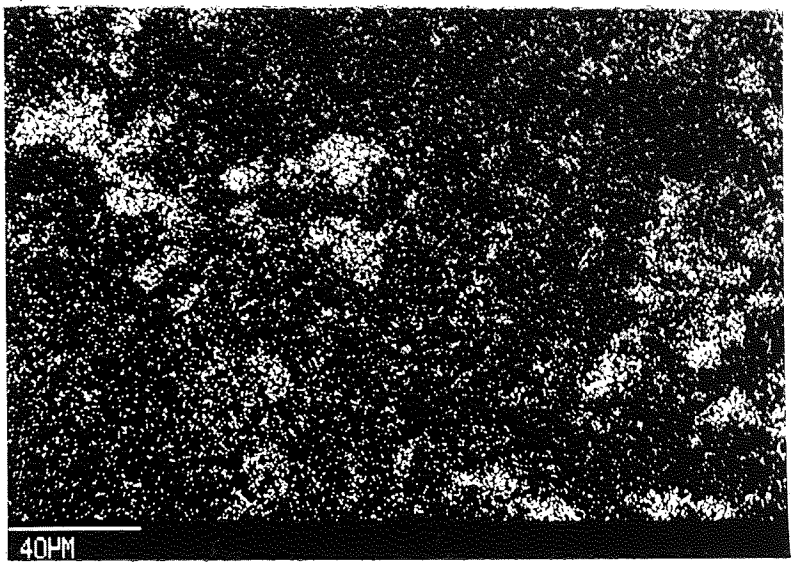


(c) iron x ray mapping

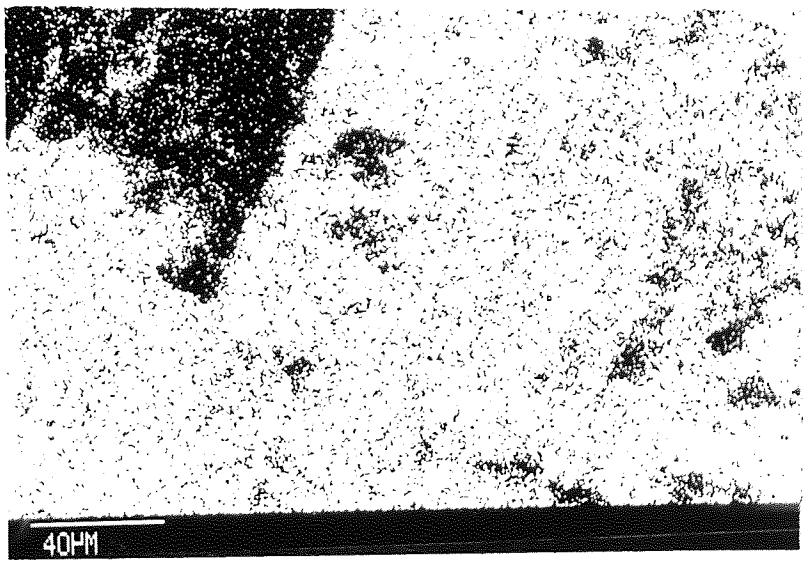


(d) titanium x ray mapping

Figure 55. S.E.M. and x-ray micrographs of worn surface of electroless nickel/titanium nitride duplex coating, showing an area where the titanium nitride layer was still intact (Load 8 kg)

debris initiate cracking. Figure 54(a) illustrates an area where the TiN coating has cracked perpendicular to the sliding direction. It would appear that the TiN layer has been pushed into the electroless nickel underlay, probably by the movement of wear debris across the worn surface. The mechanisms, although exaggerated, may be similar to a hard ball bearing moving across the surface, under a high load. However, it may also be that inadequate adhesion of the titanium nitride layer to the electroless nickel underlay could be a contributing factor which led to cracking of the former. In contrast, Figure 55(a) illustrates an area where the TiN layer is intact and shows transfer of iron, as indicated by iron x-ray mapping. The analysis of worn surface and wear debris is given in Table 21 .

Table 21. E.D.X.A analysis of worn surface of electroless nickel / TiN duplex coating and wear debris (8 kg).

| | Cr | Si | P | S | Ti | Fe | Ni |
|---|---|---|---|---|---|---|---|
| Worn Surface | - | 0.09 | 3.92 | 0.01 | 28.02 | 17.61 | 50.36 |
| Wear Debris | 1.07 | 2.66 | - | 3.18 | - | 92.90 | 0.21 |

From the observation of the worn surfaces it was expected that a high proportion of Ti and Ni would be found in the debris, but the analysis is not indicative of this. It would appear that considerable wear of the disc has taken place as the wear debris contained a high proportion of iron (92.9%) and small amounts of nickel.

7.2.1.8 Wc / Ni / W-Cr-Carbides (Jet-kote deposit)

4 Kilogram Load

The worn surface is illustrated in Figure 56. Very fine scratches can be seen, however, the most noticeable feature is the presence of iron rich areas, as evident from iron x-ray mapping. These areas would appear to be shallow craters filled with wear debris. According to Malik (157) surface grinding of thermally sprayed deposits may result in 'pull out' of particles. Hence, the size of these defects could increase by further loosening of particles, due to abrasive action by wear debris. The entrapment of wear debris as illustrated in Figure 56(a), would be indicative of this.

8 Kilogram Load

The worn surface at this load appeared to be much rougher than at the 4kg load (Figure 56) as illustrated in Figure 57. Iron x-ray mapping shows the transfer of iron at certain areas of the surface. These islands appear to be adhering to the surface, whereas, at the lower load the iron rich areas corresponded to shallow craters filled with wear debris. It is difficult to hypothesise about a wear mechanism for this deposit, as there were no signs of cracking or plastic deformation on the worn surfaces. However, it is most probable that wear at this load is a progression to that obtained at the lower load. Thus, preferential wear may occur on defect areas, such as craters or inadequately bonded particles by abrasive action of wear debris or by asperites on the counterface ploughing the surface. This can be envisaged to occur until the surface is devoid of such defects and produces a surface with better load bearing capacity. The analysis of the worn surface of Wc / Ni / W-Cr-carbides and wear debris is given in Table 22 below.

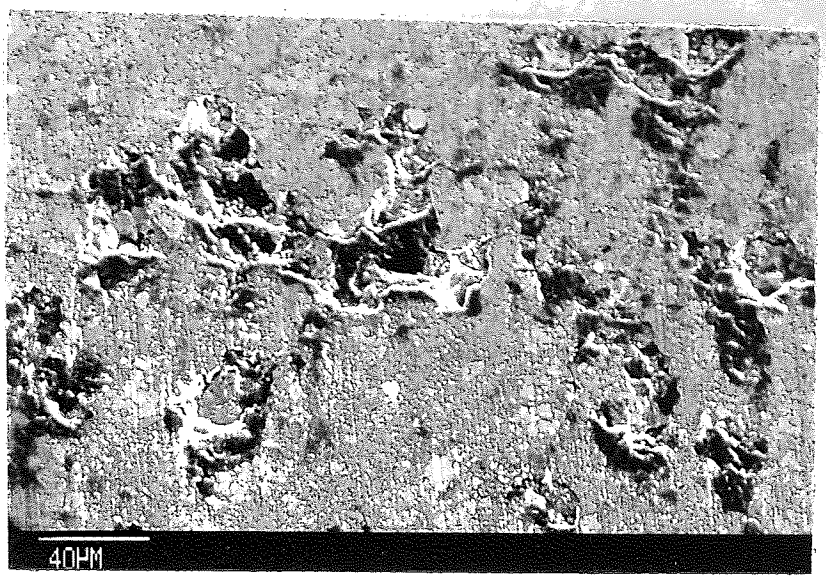


(a) worn surface

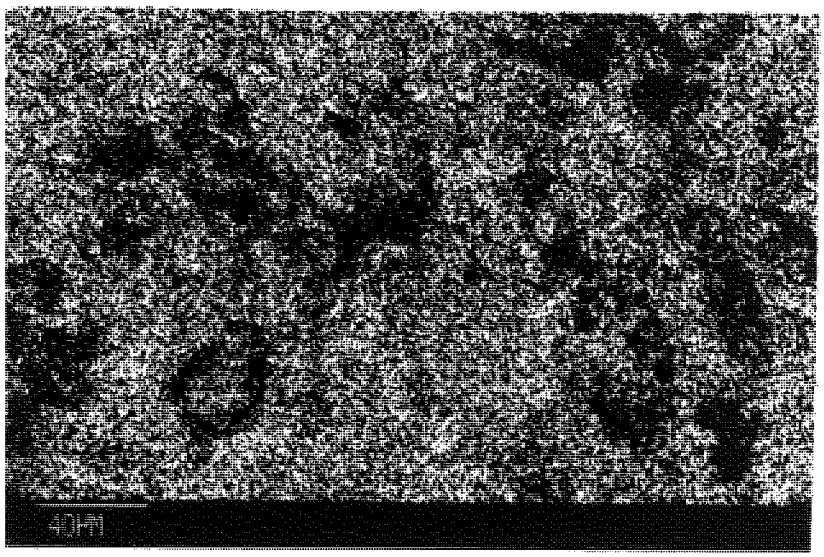


(b) tungsten x ray mapping

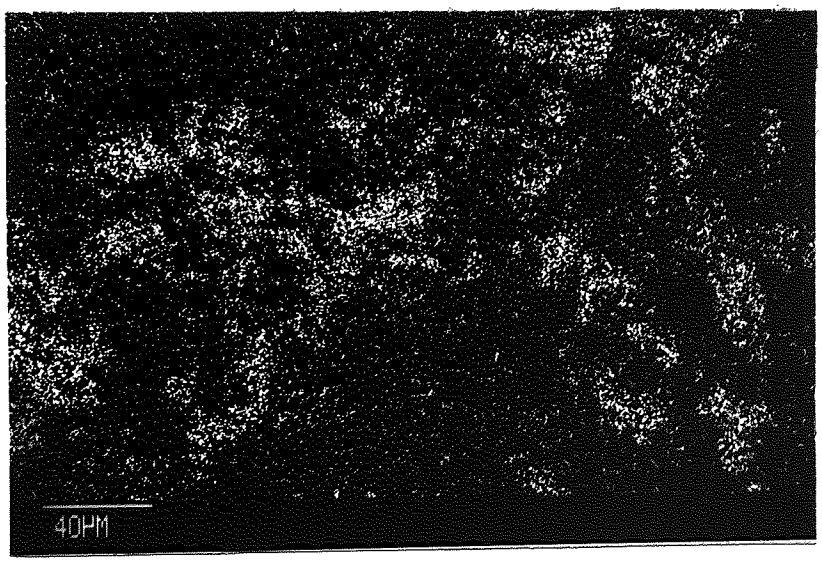


(c) iron x ray mapping

Figure 56. S.E.M. and x-ray micrographs of worn surface of Jet-Kote deposit, showing shallow craters filled with wear debris (Load 4 kg)

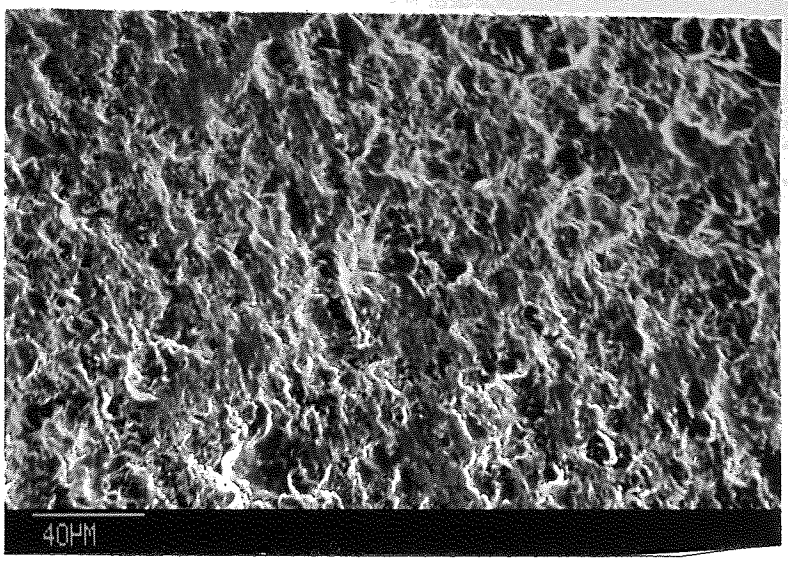


(a) worn surface

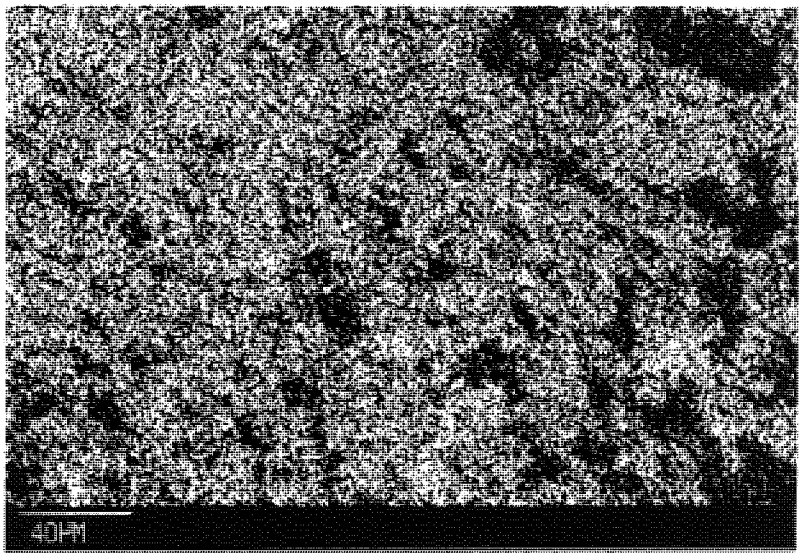


(b) tungsten x ray mapping

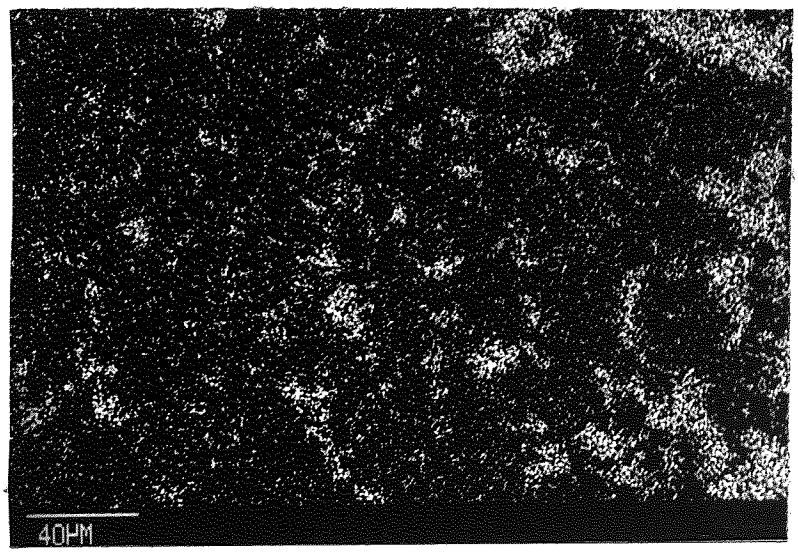


(c) iron x ray mapping

Figure 57. S.E.M. and x-ray micrographs of worn surface of Jet-Kote deposit. (Load 8 kg)

Table 22. E.D.X.A. analysis of worn surface of Wc / Ni / W-Cr-carbide deposit and wear debris

| | Load (kg) | W% | Si% | S% | Cr% | Fe% | Ni% |
|---|---|---|---|---|---|---|---|
| Worn Surface | 4 | 68.39 | - | 0.25 | 12.22 | 10.51 | 8.63 |
| Worn Surface | 8 | 62.05 | - | 0.11 | 13.13 | 13.95 | 9.75 |
| Wear Debris | 4 | - | 0.61 | 0.09 | 1.09 | 98.21 | - |
| Wear Debris | 8 | 5.19 | - | 1.35 | 3.14 | 90.23 | 0.09 |

The analysis of the wear debris (4kg load) did not reveal any tungsten, whereas at the higher load small amounts were detected . The higher chromium and traces of nickel would imply removal of tungsten-chrome carbides and nickel binder from the respective worn surfaces.

7.2.1.9.1 Plasma Nitrided Stainless Steel

8 Kilogram Load

The worn ends of the plasma nitrided stainless steel pins exhibited a polished surface, however in certain instances shallow grooves and fine scratching were seen, as illustrated in Figure 58(a). The chromium x-ray mapping illustrates areas in the groove depleted in chromium, whereas iron is uniformly distributed over the surface. The analysis of the worn surface and wear debris is given below in Table 23 .

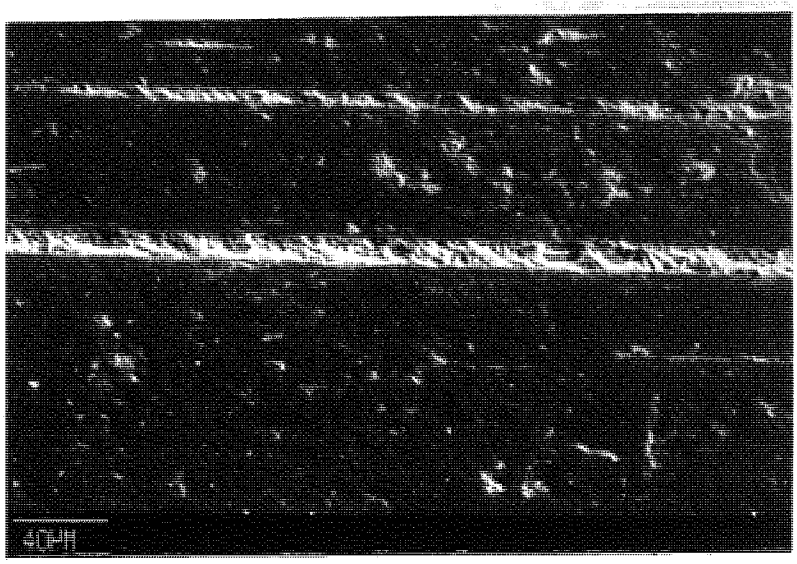

(a) worn surface

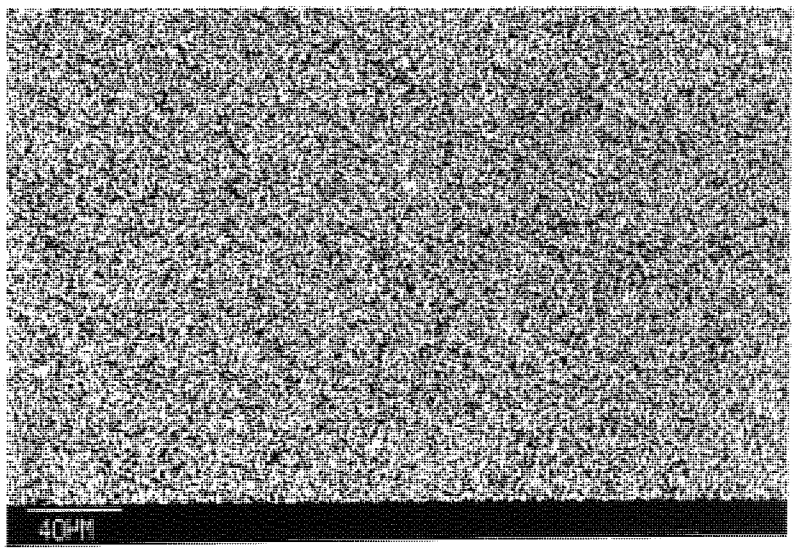

(b) iron x ray mapping

Figure 58. S.E.M. and x-ray micrographs of worn surface of plasma nitrided 316 stainless steel, showing shallow grooving of the surface.

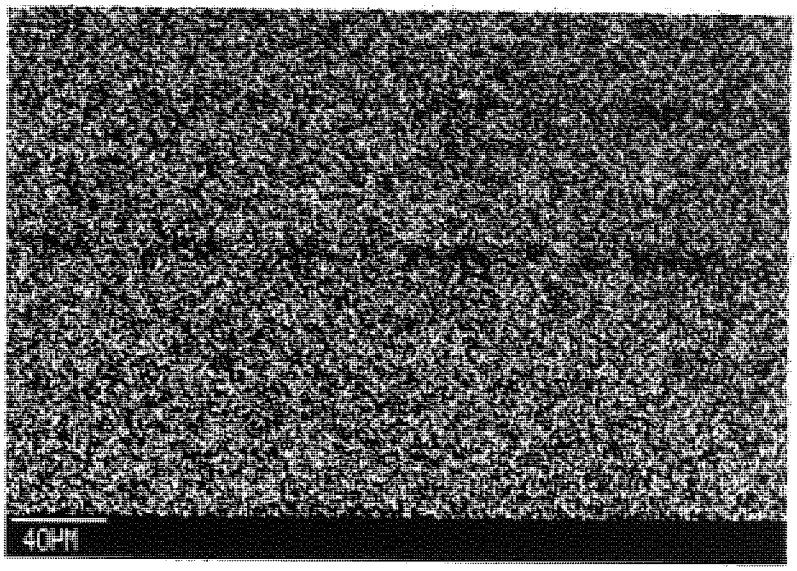


(c) chromium x ray mapping

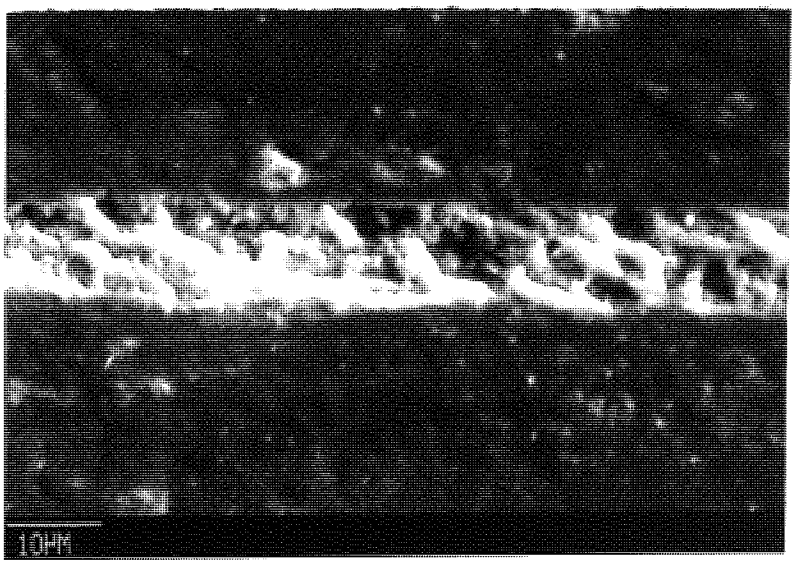


(d) higher magnification

Figure 58. S.E.M. and x-ray micrographs of worn surface of plasma nitrided 316 stainless steel, showing shallow grooving of the surface.

Table 23. E.D.X.A. of worn surface of plasma nitrided stainless steel and wear debris

| | Si | S | Cr | Fe | Ni |
|---|---|---|---|---|---|
| Worn Surface | 0.35 | 0.29 | 17.93 | 71.85 | 9.58 |
| In Groove | 0.35 | 0.28 | 14.06 | 77.78 | 7.54 |
| Wear Debris | 0.96 | 1.56 | 1.29 | 96.19 | - |

The central shallow groove is illustrated at higher magnification in Figure 58(d). It would appear that there is entrapment of debris and this is supported by the fact that there is a higher iron percentage in the grooves than on the worn surface. The analysis of the wear debris indicates considerable wear on the disc because no nickel was detected in debris.

## 7.3 The Coefficients of Friction of the Surface Treatments / Coatings

According to the stick-slip theory of friction (162), the latter may be represented by two components. The static component of friction which is the force required to shear microwelds formed as a result of asperity interaction between moving surfaces. The kinetic component relates to the subsequent slip of the surfaces at a lower force, until once again microwelds are formed (stick). Thus, these forces are directly related to the coefficients of static and dynamic friction. However, this simple theory can be modified to account for ploughing of the surface by hard asperites. In this case:

$$\text{Total frictional force} = S + P \qquad (16)$$

where S, shearing term

P, ploughing term, which relates to frictional resistance due to ploughing by hard asperites.

The ploughing term is particularly important, in view of the considerable ploughing that was observed in some surface coatings / treatments. Finally, before discussing the friction results, it must be stated that the dynamic coefficient was assumed to be half of the static coefficient of friction; the latter was represented by the maximum frictional force, as measured by a transducer set up. In general, the frictional force did not remain constant but varied over a range, this is characteristic of slip-stick motion as illustrated in Figure 59 . The original work by Bowden and Leben [163] assumed that the dynamic coefficient friction occurred at a mid-point between the limits, when microwelds were sheared (static coefficient of friction) and when microwelds start to form, denoted by a minimum value of the coefficient of friction. The mean values of static and dynamic coefficients of the surface coatings / treatments determined at a load of 4 and 8 kilograms are given in Tables 24 and 25, respectively. From the study of the worn surfaces and coefficients of friction, it became apparent that for some surface treatments / coatings the ploughing term of friction was predominant; as evident by the higher values of static coefficient of friction. The surface treatments / coatings which fall into this category are as follows:

(1) EN8 steel

(2) Ni-Cr-B (post fused)

(3) Electroless nickel silicon carbide composite, unheat treated.

(4) Chromium oxide

(5) Jet-kote

Figure 60. shows the variation of the coefficients of friction with sliding distance for EN8 steel. After a sliding distance of approximately 1000m the static coefficient of friction, $\mu_S$, rose to high values ($\approx$1.6). The latter, is probably due to heavy ploughing on the pin surface by hard asperites on the disc or work hardened wear debris (three body abrasive wear). The initial low values of the coefficients of friction prior to higher values of $\mu_S$, probably corresponded to an oxidative wear regime. In which case asperity-asperity contact is minimised by the presence of surface oxides, formed as a result of frictional heating. The change in the wear mechanism after a sliding distance of 1000 metres, may be due to spalling of the oxide layer when it has reached a critical thickness. This type of initial oxidative wear was observed for all the surface treatments / coatings tested and, in some cases, no transitions occurred in coefficients of friction throughout the test.

The nickel-chromium-boron deposit also exhibited high values of $\mu_S$, as illustrated in Figure 61. It is probable that these high values are due to surface ploughing, which was observed on the worn surfaces. However, the ploughing grooves are not as deep as those observed on EN8 steel. Therefore, the high values of $\mu_S$ may be due to a strong mutual solubility between the deposit and disc, which would facilitate the formation of microwelds.

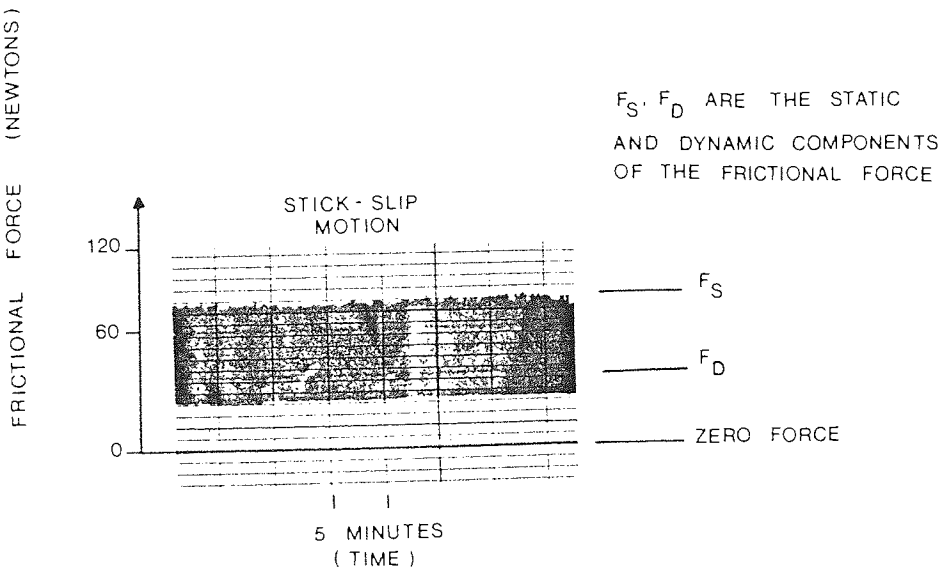


Figure 59. The variation of the frictional force with sliding distance, at load of 4 kg on the pin.

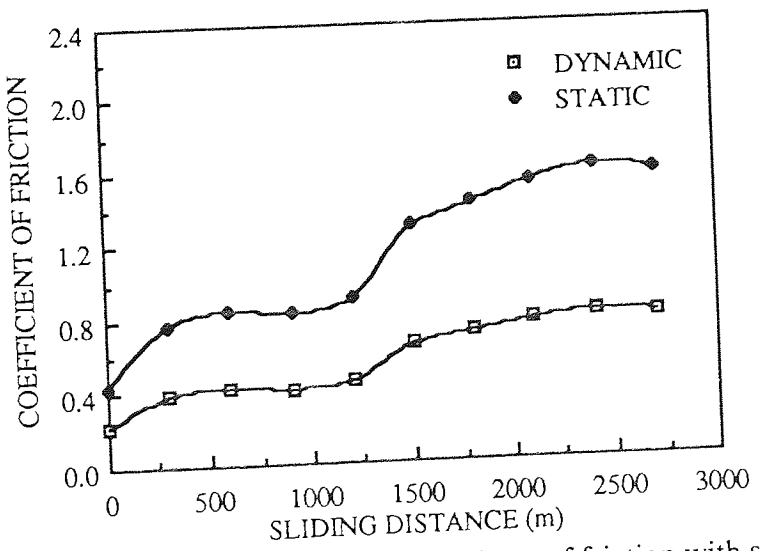


Figure 60. The variation of the coefficients of friction with sliding distance (m) for En 8 steel. Sliding speed 0.5 ms-1, (4kg load)

Table 24. The coefficient of friction determined for various surface treatments / coatings using the Pin-on-Disc wear tester (4 kilogram load)

| Surface Coatings / Treatments | Coefficient of Friction | |
|---|---|---|
| | Dynamic | Static |
| EN8 Steel | 0.56 | 1.12 |
| EN (H.T.400°C) | 0.34 | 0.68 |
| ENSiC (Un-heat) | 0.81 | 1.62 |
| Ni-Cr-B | 0.59 | 1.14 |
| T.D.Layer | 0.37 | 0.75 |
| EN8 Borided | 0.41 | 0.81 |
| Chromium Oxide | 0.49 | 0.98 |
| Jet-kote | 0.59 | 1.17 |
| EN TiN (TecVac) | 0.29 | 0.57 |
| EN TiN (D.Teer) | 0.48 | 0.94 |

Table 25. The coefficient of friction determined for various surface treatments / coatings using the Pin-on-Disc Wear tester (8 kilogram load)

| Surface Coatings / Treatments | Coefficient of Friction | |
|---|---|---|
| | Dynamic | Static |
| EN (H.T.400°C) | 0.34 | 0.68 |
| ENSiC (H.T.400C) | 1.57 | 2.38 |
| Plasma (316) | 0.74 | 1.47 |
| EN. TiN (Tec Vac) | 1.632 | 3.04 |
| Jet-kote | 0.58 | 1.15 |

The variation of the coefficients of friction for unheat treated electroless nickel silicon carbide composite is shown in Figure 62. The values of $\mu_s$ (1.6-2.0) were very high, however, the worn surface did not show evidence of ploughing. The presence of adhering islands on the worn surface would suggest the presence of strong adhesive forces between the latter and the disc. This could have accounted for high values of $\mu_s$, although it is more likely that the silicon carbides in the deposit caused ploughing on the disc; evidence for this is given later in the text.

The variation of the coefficients of friction with a sliding distance for plasma sprayed chromium oxide is shown in Figure 63. The high values of $\mu_s$ (1.2-1.3) could be correlated with either ploughing of the disc by 'rough areas' (Figure 36(a)), or abrasive action by wear debris. For the Jet-kote deposit, high values of $\mu_s$ were also observed, however, no ploughing or degradation of worn surface was noted. This would suggest that the hard asperites on the Jet-kote were ploughing the disc. In contrast to the above surface coatings/treatments, the following exhibited oxidative type of wear, characterised by lower values of $\mu_s$.

(1) Electroless nickel heat treated at 400°C

(2) Vanadium carbide (T.D. layer)

(3) Electroless nickel / titanium nitride duplex coatings

(4) Boriding.

In the above surface coatings / treatments the worn surfaces did not show evidence of deep ploughing. The superior wear performance of the electroless nickel / titanium nitride duplex coating (TecVac) compared to the D.Teer duplex coating was also evident in the lower $\mu_s$ values of the former, as indicated in Table 24. The reason for the

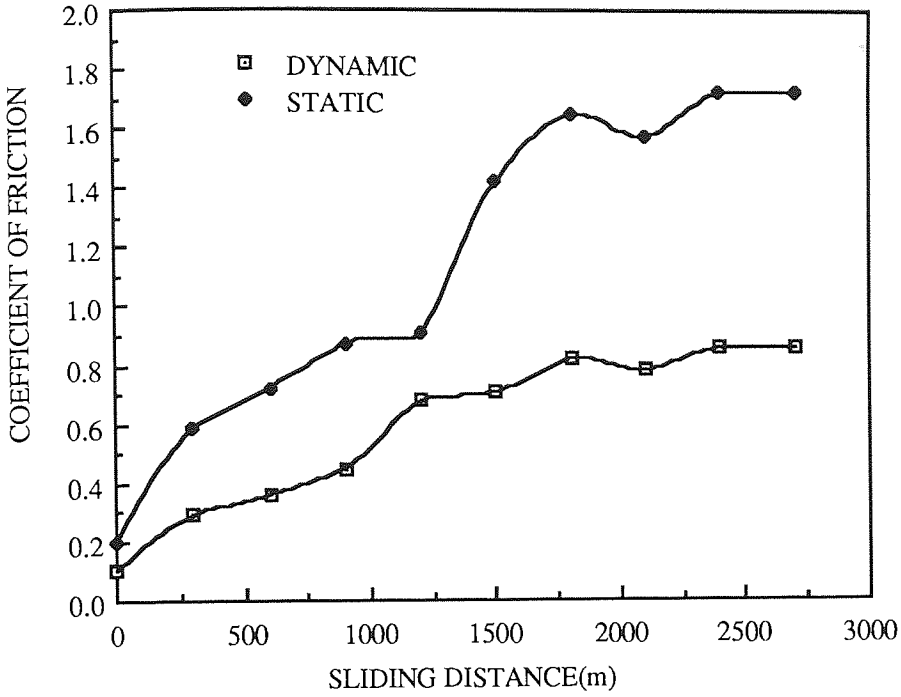


Figure 61. The variation of the coefficients of friction with sliding distance(m) for nickel/chromium/boron(post fused) deposit. Sliding speed 0.5 m/s (4kg load)

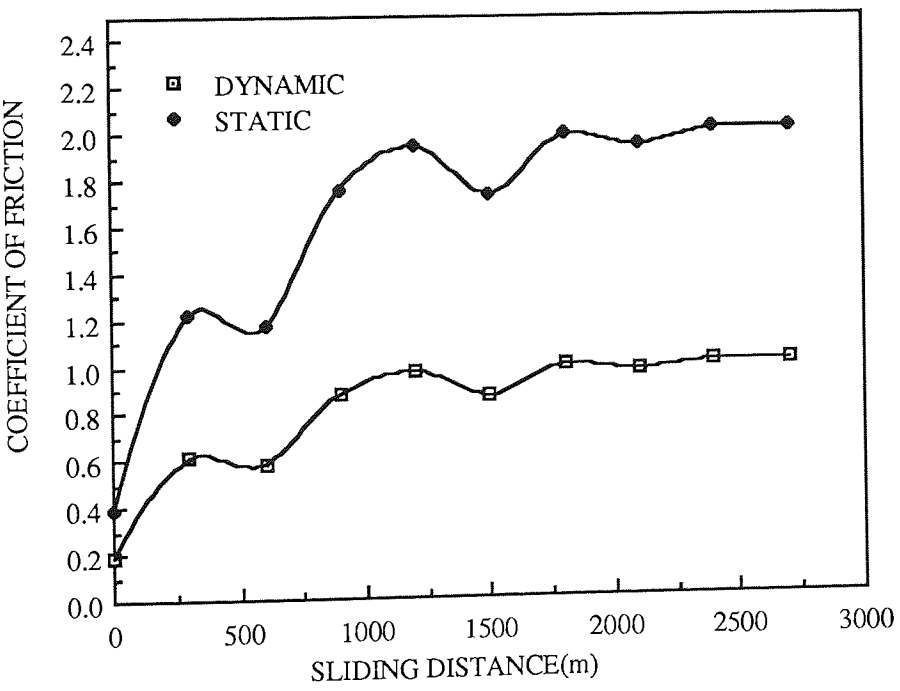


Figure 62. The variation of the coefficients of friction with sliding distance(m) un heat treated electroless nickel silcon carbide composite coating. Sliding speed 0.5 m/s (4kg load)

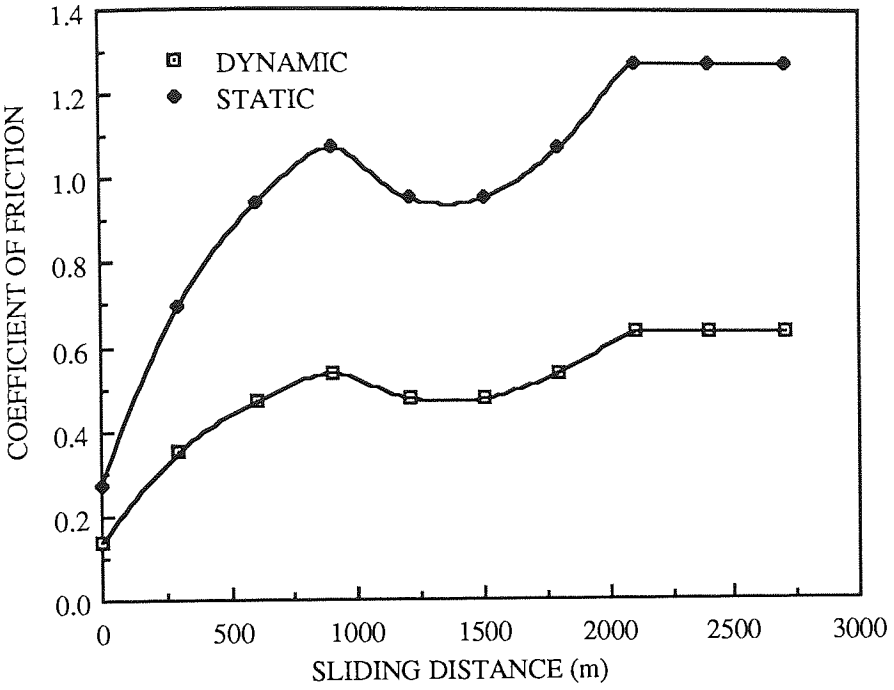


Figure 63. The variation of the coefficients of friction with sliding speed (m) for plasma sprayed chromium oxide. Sliding speed 0.5 m/s (4kg load)

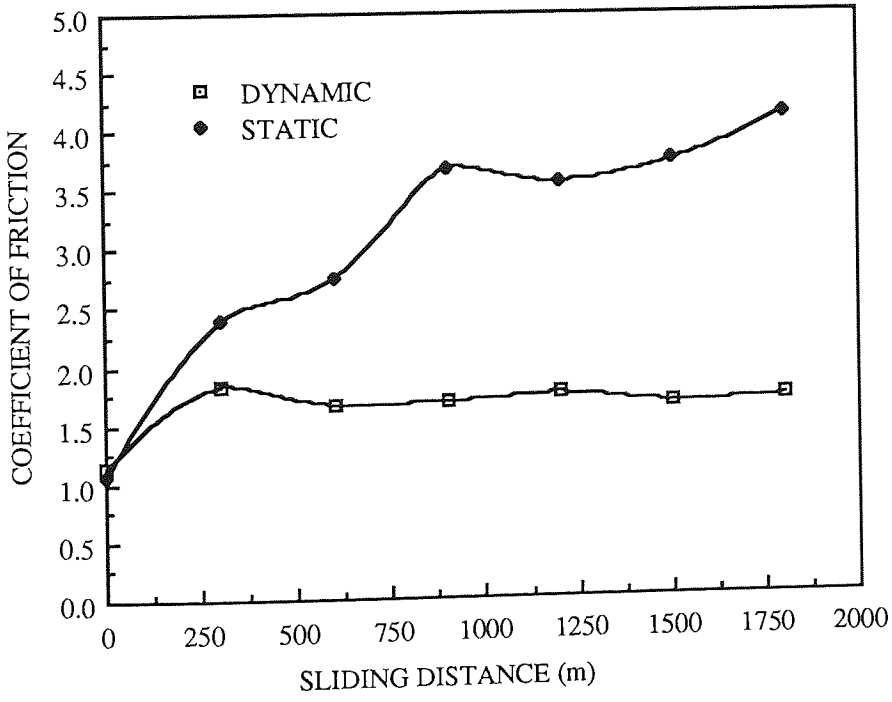


Figure 64. The variation of the coefficients of friction with sliding distance (m) for electroless nickel/titanium nitride duplex coating. Sliding speed 0.5 m/s (8kg load)

difference is that the D.Teer duplex coating exhibited ploughing and exfoliation of the titanium nitride layer, the latter could lead to three body abrasive wear conditions. The worn surfaces of electroless nickel and EN8 borided had smooth surface topography and this was reflected in their low values of static coefficient of friction. In general, for the above surface coatings / treatments the shearing term is predominant and the ploughing contribution is small.

8 Kilogram Load

At this higher load, the electroless nickel heat treated at 400°C exhibited similar values of static friction to that obtained at the 4 kilogram load. A similar trend was observed in the coefficients of friction for the Jet-kote deposit, and this constancy of friction at the two loads supports the first law of friction, e.g. coefficient of friction is independent of the normal force, although the frictional force is proportional to the latter.

Electroless nickel silicon carbide composite coating, plasma nitrided 316 stainless steel and electroless nickel / titanium nitride duplex coating (TecVac) all exhibited high values of $\mu_S$, as indicated in Table 25. For the duplex coating a rapid rise in $\mu_S$ (~ 4.0) was observed, as shown in Figure 64 ; this is indicative of extensive abrasive wear. The variations of the coefficients for plasma nitrided 316 stainless steel are shown in Figure 65. This shows that initially (500 metres) the coefficients of friction were low, which probably corresponded to the wear of the compound layer [151,152]. The latter is often associated with non-galling properties. The subsequent rise in the $\mu_S$ may be associated with the removal of this layer and wear of the alloy nitride diffusion zone. The worn surfaces of the plasma nitrided stainless steel pins had a polished surface similar to that

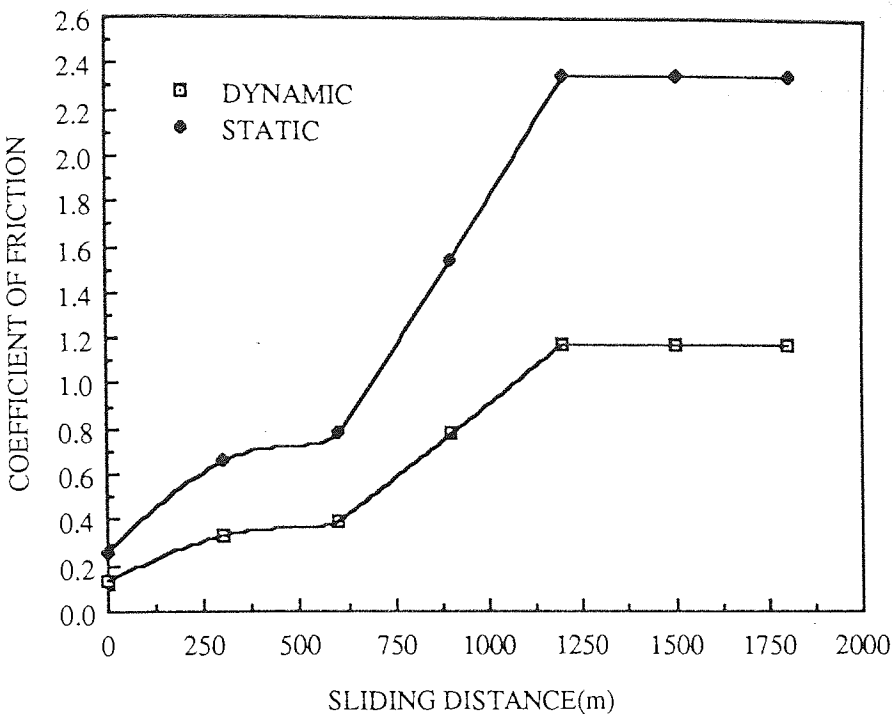


Figure 65. The variation of the coefficients of friction with sliding distance (m) for plasma nitrided stainless steel (316) . Sliding speed 0.5 m/s (8kg load)

obtained by electroless nickel pins. Since there was no evidence of adhesive transfer on the worn surfaces, this would suggest that the high values of $\mu_s$ are indicative of high wear on the disc.

### 7.3.1 Effect of Sliding Wear on the Surface Roughness of Wear Pins

The surface roughness (c.l.a.) of the wear pins, before and after wear testing at 4 kilogram load, are given in Table 26. In general, there was no significant change in surface roughness of the pins after wear, except for the following:

(1) Electroless nickel silicon carbide composite coating (unheat treated)

(2) Electroless nickel heat treated at 400°C

(3) Plasma sprayed chromium oxide.

Electroless nickel pins, after wear, had a polished appearance, as evident by the low c.l.a. (0.04 μm) value. This effect would appear to be a unique feature in the wear

mechanism, which resulted in a surface with a better load bearing capacity and lower coefficients of friction due to reduced ploughing component of friction. Electroless nickel silicon carbide composite coating exhibited a marked reduction in the surface roughness after wear, and probably implies preferential wear of 'high spots' on the original pin surface, until a better load bearing surface was formed. In contrast, chromium oxide deposits exhibit an increase in the surface roughness (15.23 μm) after wear. The high values of $\mu_S$ are probably due to a greater contribution from the ploughing term of friction.

Table 26. The surface finish of wear pins before and after wear testing at 4 kilogram load.

| Surface Coating / Treatments | Surface Finish, C.L.A. (μm) Unworn | Worn | General Effect on Surface Finish |
|---|---|---|---|
| EN8 Steel | 0.25 | 1.60 | ↑ |
| EN (H.T.400°C) | 0.36 | 0.04 | ↓ |
| ENSiC (Un-heat) | 1.30 | 0.28 | ↓ |
| Ni-Cr-B | 0.56 | 0.50 | ↓ |
| T.D.Layer | 0.29 | 0.32 | ↑ |
| EN8 Borided | - | 0.29 | |
| Chromium Oxide | 0.89 | 15.23 | ↑ |
| Jet-Kote | 0.23 | 0.20 | ↓ |
| EN.TiN (TecVac) | 0.43 | 0.56 | ↑ |
| EN.TiN (D.Teer) | 0.48 | 0.48 | |

Table 27 The surface finish of wear pins before and after wear testing at 8 kilogram load.

| Surface Coating / Treatments | Surface Finish, C.L.A. (μm) Unworn | Worn | General Effect on Surface Finish |
|---|---|---|---|
| EN (H.T. 400°C) | 0.36 | 0.09 | ↓ |
| ENSiC (H.T. 400°C) | 1.30 | 0.25 | ↓ |
| Plasma (316) | 0.62 | 0.04 | ↓ |
| EN.TiN (TecVac) | 0.43 | 0.26 | ↓ |
| Jet-Kote | 0.23 | 0.25 | ↑ |

Table 28. The surface finish of the disc after wear testing at 4 and 8 kilogram loads.

| Surface Coating / Treatments | Disc Surface Finish, C.L.A. (μm) | | | |
|---|---|---|---|---|
| | 4 Kilogram Load | | 8 Kilogram Load | |
| | Unworn | Worn | Unworn | Worn |
| EN (H.T. 400°C) | 0.31 | 0.21 | 0.32<br>0.10 | 0.22<br>0.09 |
| ENSiC | 0.31 | 0.13 | 0.65 | 0.41 |
| Plasma (316) | - | - | 0.65 | 0.35 |
| Jet-Kote | 0.31 | 0.27 | 0.65<br>0.10 | 0.21<br>0.15 |
| EN.TiN (TecVac) | 0.31 | 0.22 | 0.65<br>0.10 | 0.27<br>0.18 |
| T.D.Layer | 0.31 | 0.17 | - | - |
| Chromium Oxide | 0.31 | 0.36 | - | - |
| Ni-Cr-B | 0.31 | 0.12 | - | - |

The surface roughness of the wear pins tested at a load of 8 kilograms is given in Table 27. The polishing effect of the worn surfaces of electroless nickel and plasma nitrided stainless steel after wear, was evident in the low values of c.l.a. However, the plasma nitrided stainless steel was characterised by high values of $\mu_s$, which may be due to ploughing of the disc surface. The Jet-kote deposit did not show any significant change in the surface roughness after wear, although the worn surfaces appeared to be rough (S.E.M. examination). In the above discussion the wear on the disc has been speculative and therefore, to consider the overall effect of wear, the wear tracks were studied by surface profilemetry and optical microscopy.

### 7.3.2 The Effect of Sliding Wear on the Surface Topography of the Wear Tracks

The surface roughness of the wear tracks at 4 and 8 kilogram loads are given in Table 28.

4 Kilogram Load

Figure 66(a) illustrates a typical unworn ground finish (0.31 μm c.l.a.), whereas Figure 66(b) shows the surface topography of the wear track in rubbing contact with a chromium oxide pin; this clearly shows abrasive type of wear on the disc. In contrast, the wear tracks for electroless nickel pins showed the presence of the original ground finish, as illustrated in Figure 66(c) . In some areas, there appears to be polishing of the disc, but more importantly, considerable oxidation of the track is evident. The wear tracks for electroless nickel silicon carbide composite coating exhibited low values of c.l.a. (0.13 μm), implying considerable wear of the disc. The wear tracks also showed presence of globular oxides, as illustrated in Figure 66(d). This feature was also noted in the tracks for vanadium carbide, Jet-kote, nickel-chromium-boron and electroless

nickel / titanium nitride duplex coatings.

8 Kilogram Load

In general, at the higher load, there was a decrease in surface roughness of the disc, possibly indicative of high wear on the latter. The wear tracks of electroless nickel silicon carbide composite coating showed considerable gouging marks, probably due to abrasive action by silicon carbide particles, as illustrated in Figure 67(a) . For the Jet-kote and plasma nitrided stainless steel, large patches of adhering oxides were observed on the wear track, as shown in Figure 67(b). The electroless nickel / titanium nitride duplex coating also showed the presence of adhering oxides on the wear track, but not in as great a quantity. A summary of the above results and previous sections are given in Table 29 & 30.

(a) unworn

(b) against chromium oxide pins

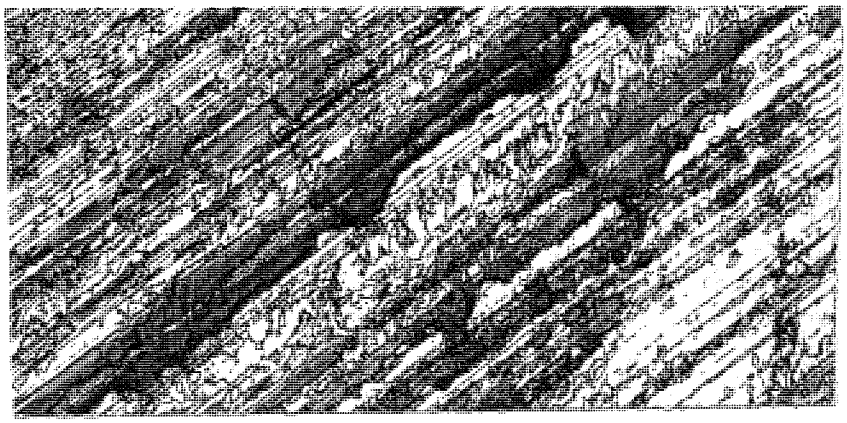

(c) against electroless nickel pins

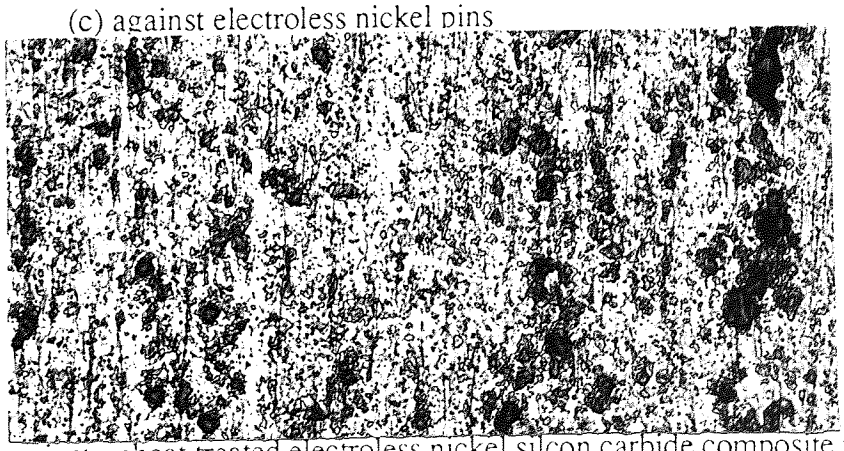

(d) against unheat treated electroless nickel silcon carbide composite pins

Figure 66. Optical photographs of unworn and worn disc wear tracks. Sliding speed 0.5 m/s (4 kg Load)

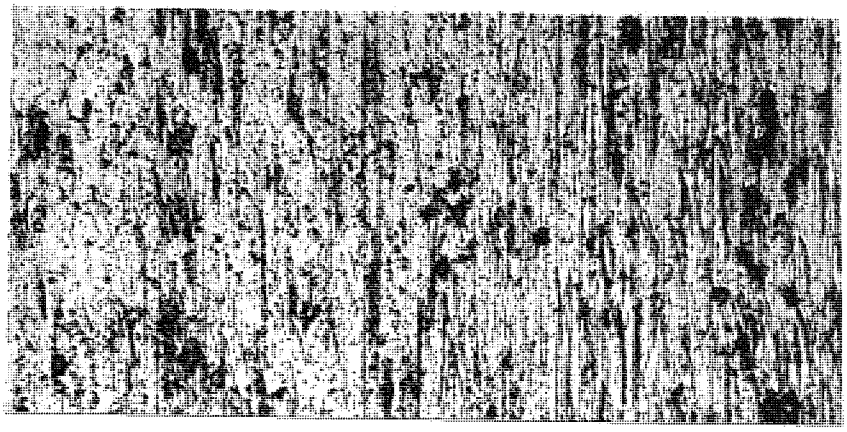

(a) against electroless nickel silcon carbide composite(400 C) pins

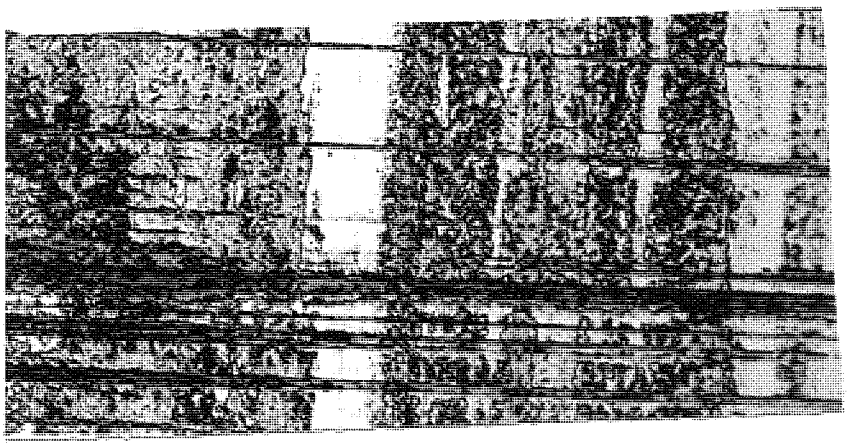

(b) against jet-kote pins

Figure 67. Optical photographs of worn disc wear tracks. Sliding speed 0.5 m/s (8kg Load)

Table 29. General summary of the wear characteristics of surface coatings / treatments tested at a load of 4 kg.

| Materials Surface Coatings / Treatments | Ranking | | Adhesive Transfer on Pin Surface | Iron Transfer to Pin Surface | Wear Debris | General Remarks |
|---|---|---|---|---|---|---|
| | Wear | Friction | | | | |
| EN8 | 10 | 7 | No | | | Extensive ploughing or worn surfaces |
| EN(H.T.400°C) | 6 | 2 | No | Yes, small amounts (0.13%) | 50% deposit material, rest disc material | Worn surfaces highly polished. Low coefficeints of friction |
| EnSiC (Un-heat) | 9 | 10 | Yes | Considerable | 7% deposit, rest disc material | High coefficients of friction and wear on disc |
| Ni-Cr-B | 7 | 8 | Yes | Considerable | 6% deposit, rest disc material | A combination of adhesive and abrasive wear was observed on the worn surfaces |
| T.D.Layer | 2 | 3 | No | Yes, up to 7% | Mainly disc material | Very slight abrasion of worn surfaces was evident |

continued

Table 29 continued

| Materials Surface Coatings / Treatments | Ranking | | Adhesive Transfer on Pin Surface | Iron Transfer to Pin Surface | Wear Debris | General Remarks |
|---|---|---|---|---|---|---|
| | Wear | Friction | | | | |
| EN8 Borided | 8 | 4 | Yes | Difficult to assess because boron concentration could not be evaluated, although small amounts of chromium were detected | Mainly disc material | Preferential wear occurred at porosity in deposit |
| Chromium Oxide | 5 | 6 | No | Considerable | Mainly disc material | Considerable spalling of the coating was observed on the worn surfaces |
| Jet-Kote | 3 | 8 | No | Yes, but due to entrapment of wear debris on worn surfaces | Mainly disc material | No abrasion or spalling of coating was observed, high values of coefficients of friction are probably due to ploughing of the disc |
| En.TiN (Vac) | 1 | 1 | No | Yes, up to 20% | Mainly disc material | Very slight removal of the TiN layer |
| En.TiN (D.Teer) | 4 | 5 | No | Yes, up to 13% | 55% | Considerable exfoliation of the TiN layer occurred. |

Table 30. General summary of the wear characteristic of surface coatings / treatments tested at a load of 8 kg

| Materials Surface Coatings / Treatments | Ranking | | Adhesive Transfer on Pin Surface | Iron Transfer to Pin Surface | Wear Debris | General Remarks |
|---|---|---|---|---|---|---|
| | Wear | Friction | | | | |
| EN (H.T.400°C) | 5 | 1 | No | Yes, small amounts | Mainly deposit material | Worn surfaces highly polished. Low coefficients of friction |
| Plasma (316) | 4 | 3 | No | - | Mainly disc material | Worn surfaces of polished appearance |
| EnSiC (H.T.400°C) | 3 | 4 | Yes | Considerable | 7-8% deposit, rest disc material | Very high coefficients of friction, probably due to abrasive action by silicon carbide particles |
| En.TiN (Tec Vac) | 2 | 5 | No | Yes, in the form of entrapped wear debris | mainly disc material | considerable cracking of the TiN and electroless nickel underlay occurred |
| Jet-Kote | 1 | 2 | Yes, but not as pronounced as for En.SiC (H.T.400°C) | Yes, up to 13% | Small amounts of deposit (5-7%), rest disc material | No abrasion or spalling of coating was observed. The values of coefficients of friction were of similar magnitude to that obtained at lower load. |

## 7.4 Corrosion Behaviour of Surface Coating/ Treatments in Acidified Salt Solution.

### 7.4.1 The Effect of Pretreatments on the anodic behaviour of pure nickel metal.

The effects of the various pretreatments (Section 6.6.4.3.) on the shape of the polarisation curves are illustrated in Figure 68. The onset of passivation as indicated by the critical anodic current density ($I_{crit}$) and primary passivating potential (Epp) are similar for all the pretreatments investigated, except for the plating pretreatment which exhibited higher values of $I_{crit}$ and Epp. Specimens which were acetone degreased, electrochemically cleaned and scrubbed with mgo paste exhibited the lowest residual passivating current density (ip) whereas for the other pretreatments the values were much higher. The 'passive nose' for the acetone degreased was pointed whereas for the cathodic cleaning / mgo paste it was much broader and therefore, the ip was held over a larger potential range.

Electrochemical cleaning and acetone degreasing were both rejected because it was noted that these techniques did not result in satisfactory wetting of the surface. Thus, errors would have occurred in the calculation of surface area of the specimens. Plating pretreatment and mgo paste techniques were rejected because the ip values were much higher than that obtained for electrochemical cleaning / mgo paste; thus, the latter technique was adopted.

Figure 68. Effects of pretreatments on the anodic polarisation behaviour of pure nickel in acidified salt solution

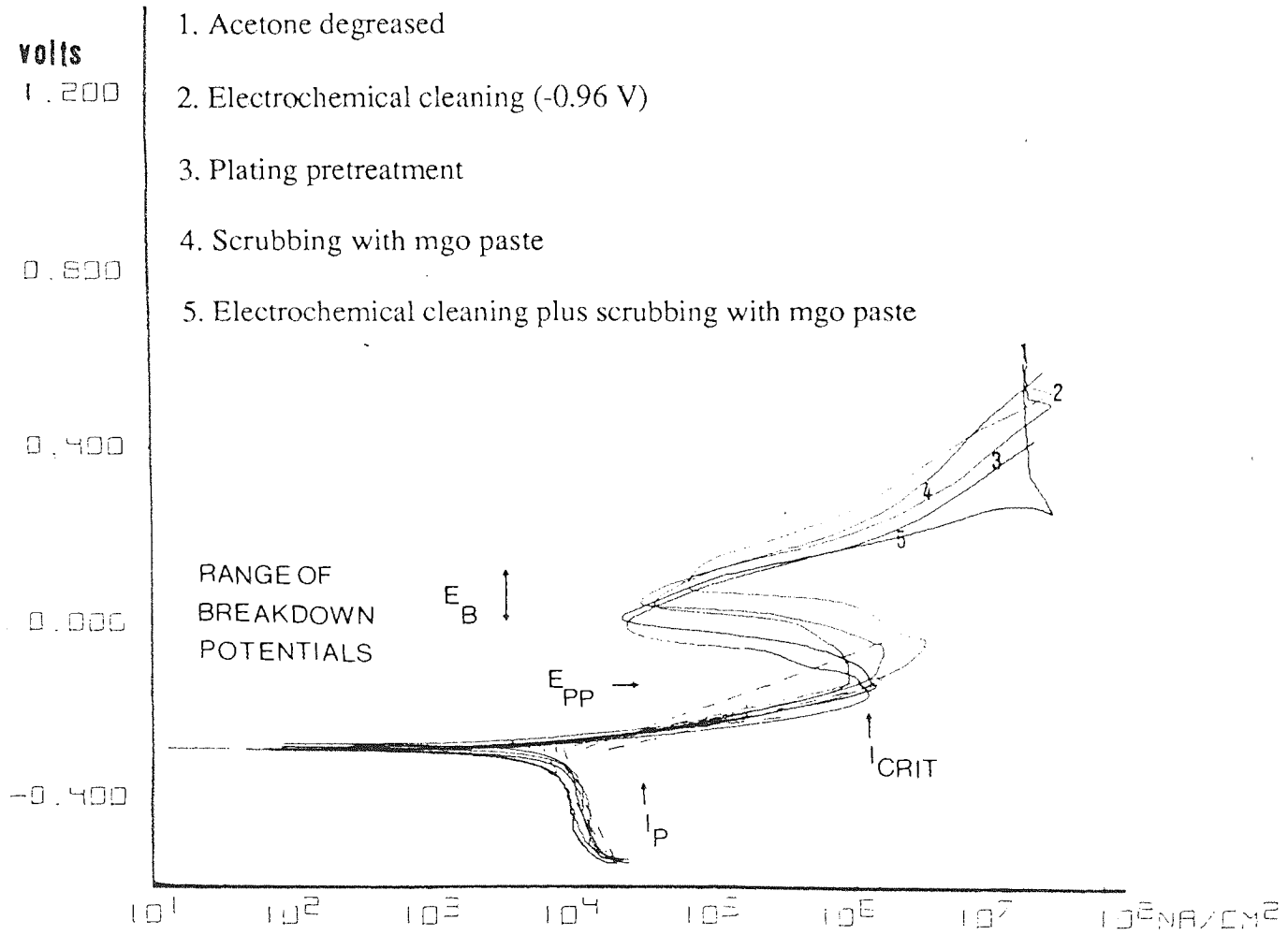

### 7.4.2 Evaluation of the Corrosion Current Density by Tafel Extrapolation

In this section the corrosion behaviour of the surface treatments and coatings was investigated by potentiodynamic cathodic and anodic polarisation respectively. The cathodic polarisation curves showed considerable concentration polarisation and therefore, neither the cathodic Tafel constant nor the corrosion current density could be calculated. However, the anodic curves exhibited a reasonable Tafel behaviour and the Tafel regions extended over 2 to 3 decades of current density. This enabled the determination of the anodic Tafel constant and the corrosion current density by extrapolation. The tendency for the surface coatings / treatments to passivate was also assessed by anodic polarisation to high noble potentials (~ 0.8V S.C.E.). The results of the anodic polarisation are summarised in Table 31.

#### 7.4.2.1 Corrosion Current Density ($I_{corr}$)

EN8 steel exhibited the highest corrosion current density, whereas 316 stainless steel, the least. Plasma nitriding and boriding of 316 stainless steel resulted in a considerable reduction in the corrosion resistance of the latter, as evident from the very high values of corrosion current densities for these surface treatments. Boriding of EN8 steel resulted in a moderate reduction of the corrosion current density and displacement of corrosion potential to less active values than EN8 steel.

An increase in the phosphorus content of electroless nickel deposits was accompanied by an increase in corrosion potential. Thus, implying that the 12% electroless nickel deposits are more corrosion resistant and less active than lower phosphorus deposits, as

Table 31. Corrosion data determined by potentiodynamic anodic polarisation of various surface coatings / treatments in an acidified salt solution.

| Materials and Surface Coatings / Treatments | $E_{corr}$ | Epp | $E_B$ | $I_C$ | $I_{corr}$ | A.T.C. |
|---|---|---|---|---|---|---|
| | | V vs SCE | V vs SCE | nA/cm2 | nA/cm2 | V/decade |
| EN8 | - 0.664 | - | - | - | 8.172E4 | 0.132 |
| EN8 (BO) | - 0.584 | - | - | - | 5.147E4 | 0.160 |
| 316 (BO) | - 0.365 | - | - | - | 2.059E4 | 0.099 |
| 316 stainless | - 0.099 | - | - | - | 0.640E2 | 0.174 |
| Ni-Cr-B | - 0.394 | - | - | - | 2.596E3 | 0.118 |
| VC | - 0.497 | - | - | - | 1.585E4 | 0.161 |
| EN (7%P)A | - 0.317 | - | - | - | 2.371E3 | 0.085 |
| EN (9%P)A | - 0.286 | - | - | - | 2.718E3 | 0.087 |
| EN(12%P)A | - 0.228 | - | - | - | 3.068E3 | 0.200 |
| EN (7%P)H | - 0.284 | - 0.104 | - 0.033 | 1.987E5 | 1.026E4 | 0.142 |
| EN (9%P)H | - 0.261 | - 0.110 | - 0.029 | 1.591E5 | 1.074E4 | 0.153 |
| EN (12%P)H | | - 0.508 | - | - | 6.912E3 | 0.194 |
| EN 600 Air | - 0.246 | - | - | - | 2.195E3 | 0.107 |
| EN 600 Vac | - 0.294 | - 0.119 | - 0.021 | 7.715E5 | 7.475E3 | 0.089 |
| Watts Nickel | - 0.299 | - 0.130 | - 0.013 | 17.985E5 | 1.573E4 | 0.083 |
| Bright Nickel | | - 0.383 | - | - | 1.340E4 | 0.081 |
| Wc/Ni/W-Cr | - 0.472 | - | - | - | 1.936E4 | 0.196 |
| EN/SiC (H) | - 0.292 | - | - | - | 1.571E4 | 0.108 |
| Plasma 316 | - 0.474 | - | - | - | 4.695E3 | 0.049 |
| EN/TiN | - 0.340 | - | - | - | - | - |
| CH-oxide | - 0.392 | - | - | - | - | - |

## KEY TO HEADINGS

| | | |
|---|---|---|
| $E_{corr}$ | : | Corrosion potential |
| Epp | : | Primary passive potential |
| $E_B$ | : | Breakdown potential |
| $I_C$ | : | Critical anodic current density |
| $I_{corr}$ | : | Corrosion current density |
| A.T.C. | : | Anodic Tafel constant |
| E2, E3, E4, E5 | | refer to $10^2$, $10^3$, $10^4$ and $10^5$ respectively |

## KEY TO SURFACE COATINGS / TREATMENTS

| | | |
|---|---|---|
| EN8 (BO) | : | EN8 steel borided |
| 316(BO) | : | 316 stainless steel borided |
| Ni-Cr-B | : | Nickel-chroimum-boron post fused |
| VC | : | Vanadium carbide (T.D.) layer |
| EN (7%P)A | : | As plated electroless nickel (7% P) |
| EN (9%P)A | : | As plated electroless nickel (9% P) |
| EN (12%P)A | : | As plated electroless nickel (12% P) |
| EN (7%P)H | : | Heat treated electroless nickel (7% P) |
| EN (9%P)H | : | Heat treated electroless nickel (9% P) |
| EN (12%P)H | : | Heat treated electroless nickel (12% P) |
| EN600 Air | : | Electroless nickel heat treated at 600°C in air |
| EN600 Vac | : | Electroless nickel heat treated at 600°C in vacuum |
| Wc/Ni/W-Cr | : | Tungsten carbide (25%) / 5% nickel / tungsten-chrome carbides via Jet-kote process |
| EN/SiC (H) | : | Electroless nickel silicon carbide composite coating |
| EN/TiN | : | Electroless nickel / titanium nitride duplex coating |
| CH-oxide | : | Plasma sprayed chromium oxide, sealed with an anaerobic sealant. |

evident from the measured corrosion potentials. Heat treatment of electroless nickel deposits resulted in a four fold increase in the corrosion current density for deposits containing 7% and 9% P, whereas for 12% P deposits, the corrosion current density increased by a factor of two. The reduction in corrosion resistance after heat treatment is often associated with the presence of microcracks in the deposits . However, the type of microcracks referred to by Sadeghi et al (143) were not seen in micro-sections of electroless nickel samples heat treated at 400°C. Thus, to explain the above, an alternative hypothesis is suggested. It may be that phosphorus atoms in as-plated electroless nickel are segregated at the microcrystalline grain boundaries. Thus, heat treatment would result in precipitation of nickel phosphide to form a continuous grain boundary network. Hence, microgalvanic cells may be set up between the nickel matrix and nickel phosphide precipitates and therefore, provide the necessary driving force for corrosion. Whereas, in as plated electroless nickel deposits, the galvanic dissimilarity may be less because these are single phase supersaturated solid solutions of nickel phosphorus alloys. The argument may be further extended to high phosphorus electroless nickel deposits where nickel phosphide would precipitate in a nickel phosphorus matrix. Thus, the galvanic difference between precipitate and matrix might be less and could possibly explain the reason why the heat treated electroless nickel (12% P) exhibited a lower corrosion current density than the lower phosphorus deposits.

Heat treatment in air at 600°C significantly reduced the corrosion current density to a level of similar magnitude to as-plated electroless nickel deposits. As mentioned in the literature review (Section 5.5.2.2) the improved corrosion resistance has been associated with the presence of a protective surface oxides and a Fe-Ni intermetallic

layer; the latter considerably improves the adhesion of deposit to substrate. However, to isolate the relative importance of these features, samples were heat treated in vacuum at 600°C, so that only a Fe-Ni intermetallic layer was obtained. On the basis of the extrapolated corrosion current densities, it would appear that the presence of surface oxide is the predominant factor resulting in the improved corrosion resistance.

The corrosion potential of Watts nickel was similar to that for electroless nickel deposits, however, the corrosion current density was approximately seven times greater than for as-plated electroless nickel and 1.5 times that of heat treated deposits. Bright nickel exhibited a more active potential than Watts nickel, as expected, however, Tafel extrapolation would suggest that the former has a slightly lower corrosion current density than Watts nickel. The latter exhibited a pronounced passivation 'nose' whereas in bright nickel it was absent. The passivation tendency of Watts nickel is discussed in more detail later in the text.

The vanadium carbide (T.D.) layer, nickel-chromium-boron (post fused) and Wc/Ni (binder) / W-Cr-carbides (Jet-kote) deposits exhibited considerably more active corrosion potentials compared to electroless nickel deposits. This would imply that they would corrode at a somewhat faster rate than electroless nickel. Although this suggestion is to some degree supported by the extrapolated $I_{corr}$ values, however, it must be stated that the anodic polarisation curves exhibited considerable non-Tafel behaviour. Figure 69. illustrates the anodic and cathodic Tafel regions for Jet-kote deposit. The curvature of the anodic curve is probably due to a combined dissolution of W, Cr, Ni and/or Fe (substrate), whereas the theory of Tafel is based on a single redox reaction.

7.4.2.2 Summary of the Tafel Extrapolation Results

1. Increasing the phosphorus content of electroless nickel deposits resulted in less active corrosion potentials. However, the extrapolated corrosion current densities for the 12% P electroless deposit were slightly higher than for the lower phosphorus deposits, the discrepancy is most probably due to errors in Tafel extrapolation. The anodic Tafel curves for electroless nickel showed some curvature and, therefore, computer prediction of $I_{corr}$ should be considered with caution. The $I_{corr}$ values of as-plated electroless nickel are less by an order of magnitude compared to heat treated (400°C) electroless nickel deposits. Heat treatment of electroless nickel deposits at 600°C (in vacuum or air) resulted in $I_{corr}$ values of similar magnitude to as-plated deposits.

2. In general, the corrosion potentials of vanadium carbide, Jet-kote, Ni-Cr-B and plasma nitrided 316 stainless steel were considerably more active than those of electroless nickel deposits. From the above, only Ni-Cr-B deposit would appear to have a $I_{corr}$ value of similar magnitude to that of as-plated electroless nickel deposits.

7.4.3 Potentiodynamic : Anodic Polarisation Curves for Surface Coatings / Treatments

Figure 70 illustrates a typical potentiodynamic scan for a 7% P as-plated electroless nickel deposit. It is evident from the shape of the anodic polarisation curve that there was no tendency to passivate in the acidified salt solution. The same trend was observed for as-plated electroless nickel deposits containing 9 and 12% phosphorus.

The portion AB corresponds to the general active corrosion regime, in which nickel and possibly phosphorus dissolution occurs by a complex redox reaction. The portion BC marks the departure from Tafel behaviour and is probably due to concentration polarisation effects. It is unlikely that this region corresponds to oxygen gas evolution because the oxygen evolution potential, based on Ni-$H_2O$ pourbaix diagram at pH 3 is 0.755 volts S.C.E. Thus, this region of limiting current density probably corresponds to a general dissolution (electrolysis) of the electroless nickel deposits because the coating appeared to be stripped off in certain areas. This was also true for 9% P electroless nickel deposits, whereas, the 12% P electroless nickel deposits remained shiny and intact after the test. The potentiodynamic scan for 12% P electroless nickel deposits is illustrated in Figure 71. For the 7% and 9% P electroless nickel deposits the onset of the concentration polarisation region (BC) occurred around +0.150 volts (S.C.E.). In contrast, the anodic polarisation curve for 12% P electroless nickel deposits did not exhibit such a tendency.

The anodic polarisation curves for 7 and 9% P electroless nickel deposits, heat treated at 400°C, exhibited a tendency to passivate, as illustrated in Figure 72. Both deposits had similar primary passivating (Epp) and breakdown ($E_B$) potentials. These denoted the onset of formation and breakdown of a passivating film respectively. However, the critical anodic current density ($I_c$) required to form a passivating film is much greater for 9% P than 7% P electroless nickel deposit. For the latter, the residual passivation current density ($I_p$) is much greater than that measured for 9% P electroless nickel deposits. The 12% P electroless nickel, heat treated at 400°C, did not show any

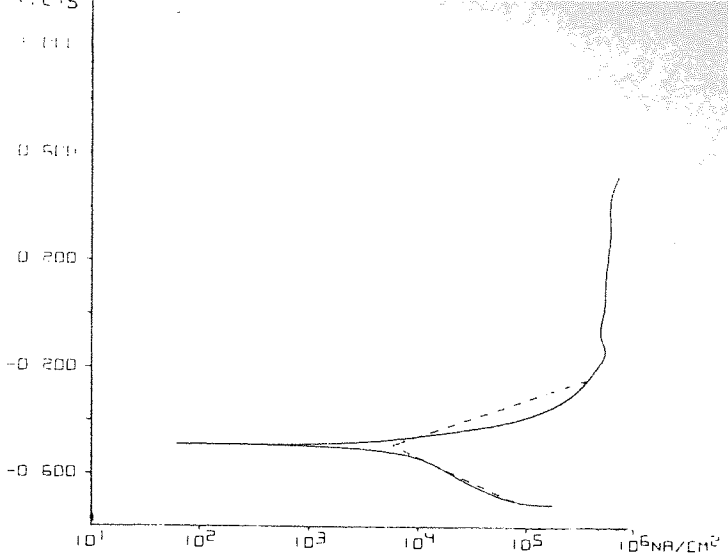


Figure 69. Anodic and cathodic potentiodynamic polarisationn curves for the Jet-Kote deposit in acidified salt solution

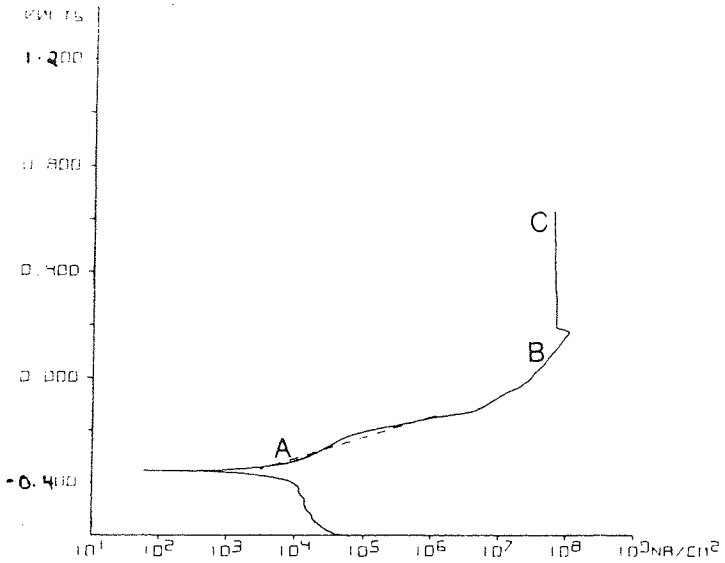


Figure 70. Anodic and cathodic potentiodynamic polarisation curves for 7% P as-plated electroless nickel deposit in acidified salt solution

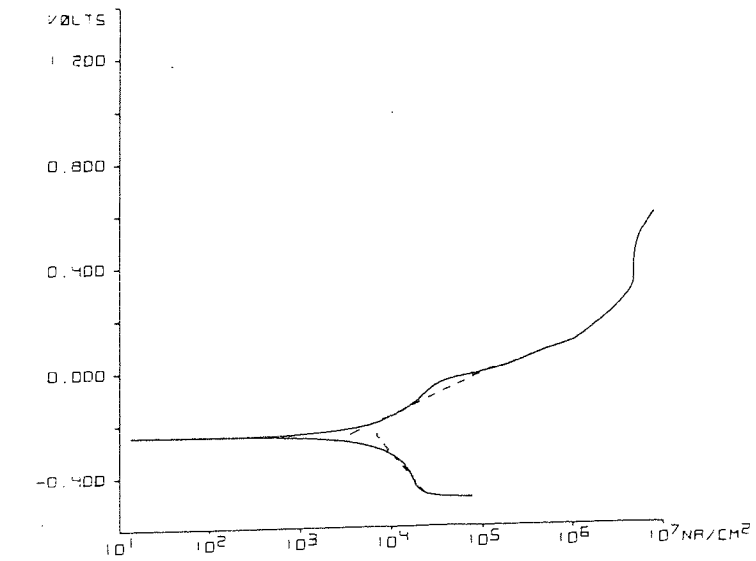


Figure 71. Anodic and cathodic potentiodynamic polarisation curves for 12% P as-plated electroless nickel deposit

tendency to passivate, as illustrated in Figure 73. Electroless nickel (7% P), heat treated in air at 400°C, did not exhibit any tendency to passivate as illustrated in Figure 72. Whereas, deposits heat treated in vacuum at 600°C exhibited a pronounced passivation 'nose', as illustrated in Figure 74. The primary passivation and breakdown potentials were of similar value to those observed for electroless nickel (7 and 9% P) heat treated at 400°C. However, the current density ($I_c$) required to form the passivating film was approximately five times that determined for deposits heat treated at 400°C.

Bright nickel deposits did not show any tendency to form passivating films, whereas Watts nickel exhibited a pronounced passivation 'nose', as illustrated in Figure 75. The anodic polarisation curves for Watts nickel and electroless nickel heat treated at 600°C (vacuum) bear close resemblance and values of Epp and $E_B$ are of a similar order of magnitude. The residual passivating current density is slightly lower for Watts nickel (20.83 $\mu A/cm^2$). However, the critical anodic current density ($I_c$) for the former is approximately double compared to electroless nickel heat treated at 600°C (vacuum). For both coatings the passive region is small and is followed by a localised pitting regime which is accelerated by the presence of chloride ions.

It would appear from the shape of potentiodynamic plots for electroless nickel / titanium nitride duplex coating and 316 stainless steel, that these should passivate spontaneously in acidified salt solution, as illustrated in Figures 76 and 77, respectively. Figure 78 illustrates the theoretical and actual potentiodynamic polarisation plots of active-passive materials. If the cathodic curve intersects the anodic curve in the passive region only, as in Figure 78 a, the material will passivate. Whereas, for electroless nickel deposits the

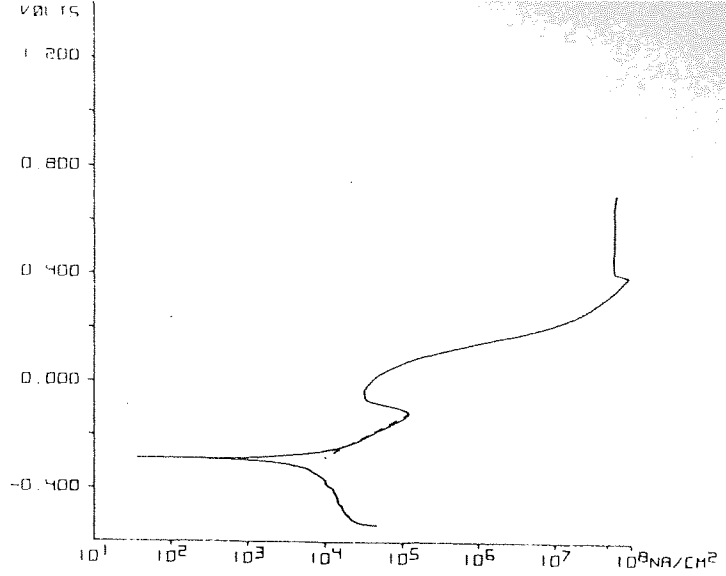


Figure 72. Anodic and cathodic potentiodynamic polarisation curves for 7% P electroless nickel deposit heat treated at 400°C, in acidified salt solution

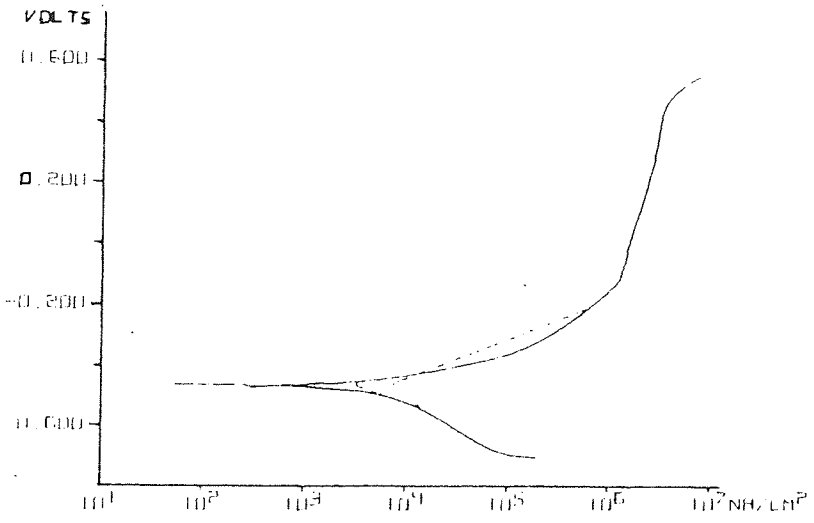


Figure 73. Anodic and cathodic potentiodynamic polarisation curves for 12% P electroless nickel deposit heat treated at 400°C, in acidified salt solution

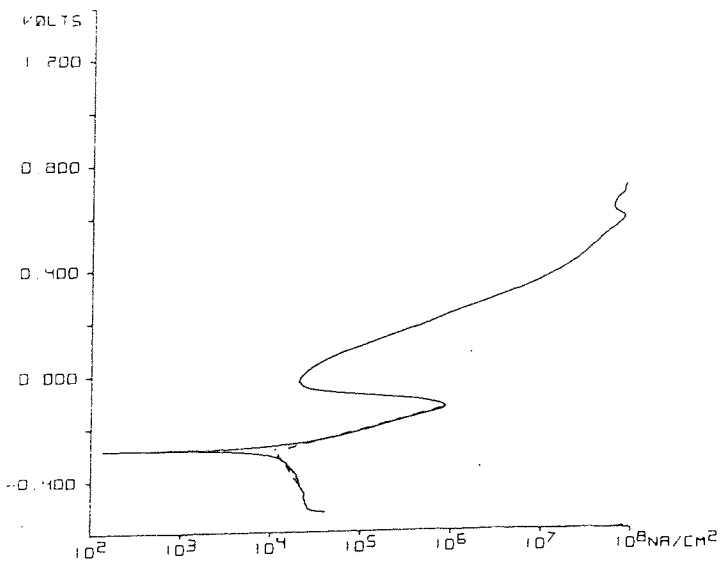


Figure 74. Anodic and cathodic potentiodynamic polarisation curves for 7% P electroless nickel deposit heat treated at 600°C (in vacuum), in acidified salt solution

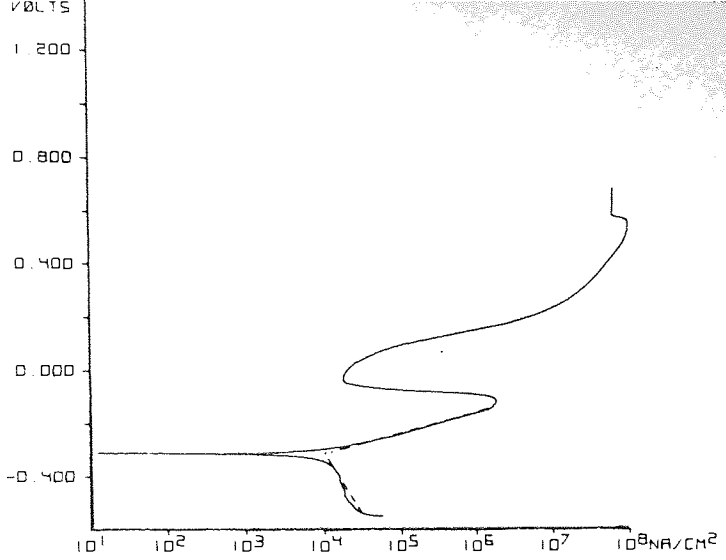


Figure 75. Anodic and cathodic potentiodynamic polarisationm curves for Watts nickel deposit in acidified salt solution

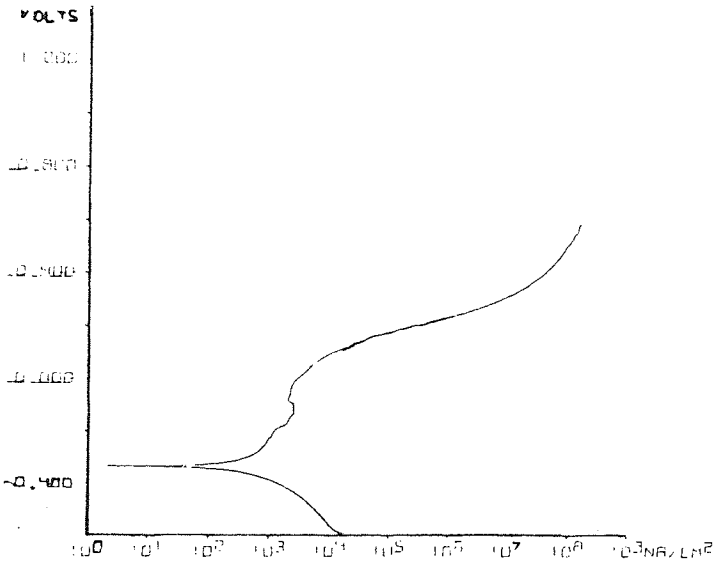


Figure 76. Anodic and cathodic potentiodynamic polarisation curves for 7% P electroless nickel / titanium nitride duplex coating in acidified salt solution

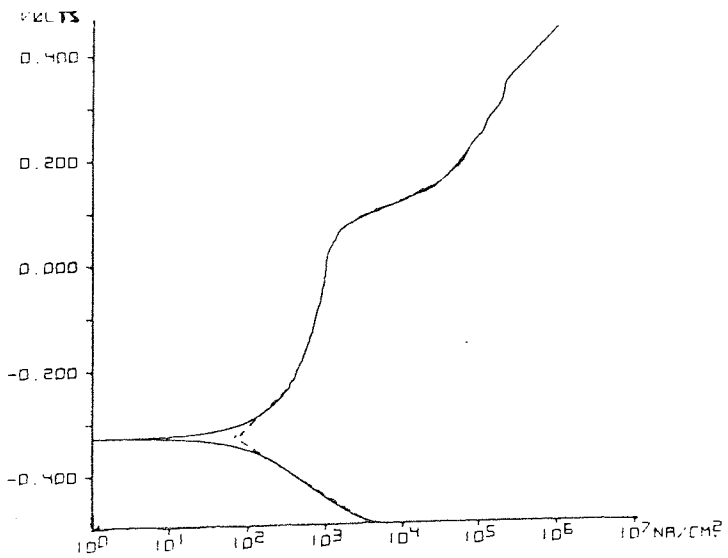


Figure 77. Anodic and cathodic potentiodynamic polarisation curves for 316 stainless steel, in acidified salt solution

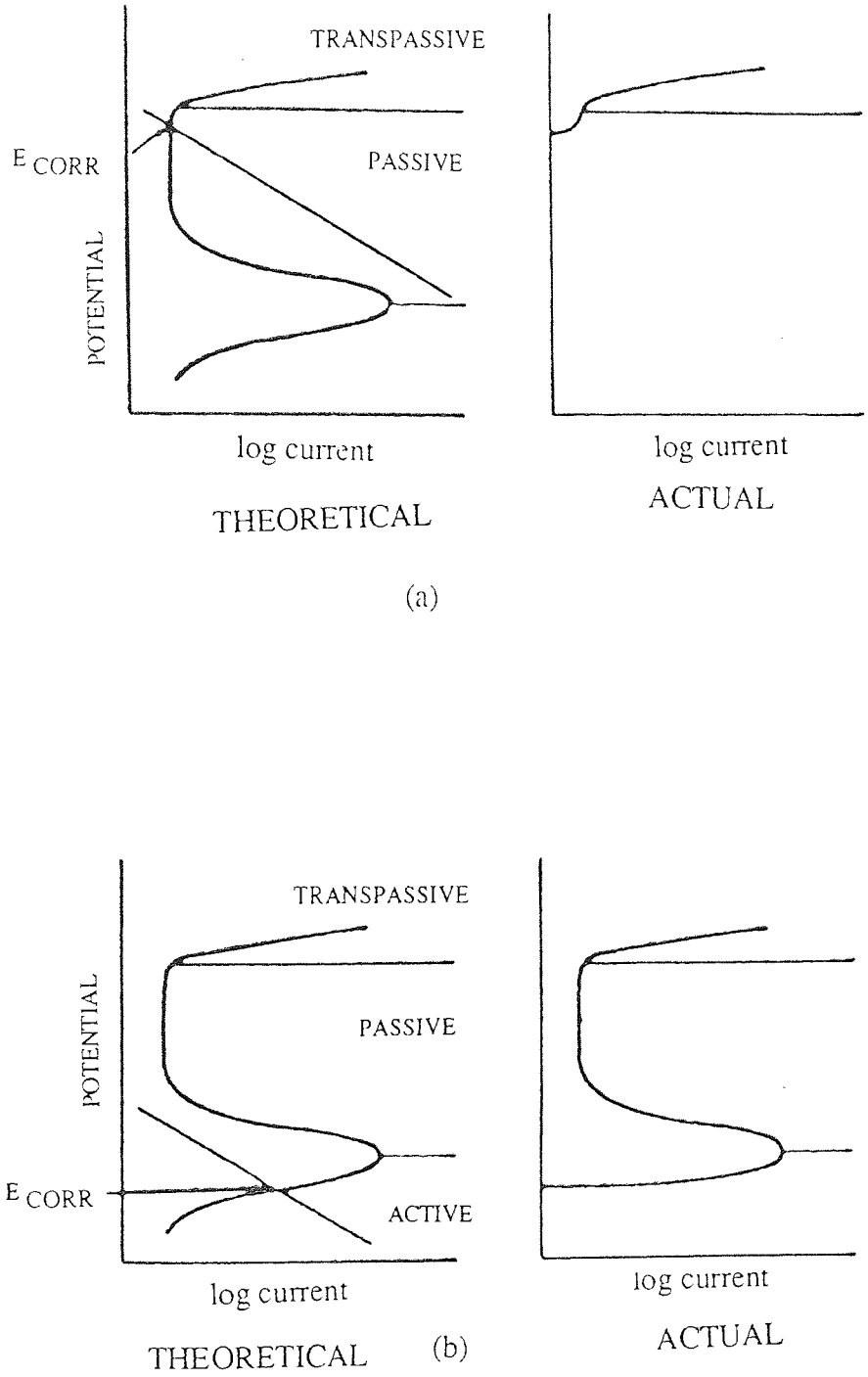


Figure 78. The theoretical and actual potentiodynamic polarisation curves for active-passive metals

cathodic curve would appear to intersect the anodic curve in the active region, as in Figure 78(b). The most interesting phenomenon emerging from the potentiodynamic scans is that, under certain conditions of heat treatment, electroless nickel exhibited a tendency for passivation. The hypothesis proposed to account for this stems from the great similarity between the potentiodynamic curves for electroless nickel (heat treated in vacuum at 600°C) and Watts nickel. It would appear that heat treatment in vacuum at 600°C may cause volatilisation of the phosphorus, leaving a nickel rich surface layer; which, under anodic polarisation , exhibited the passivation tendency. To confirm this hypothesis Auger electron spectroscopy was used to evaluate the nickel, phosphorus and oxygen distributions on as-plated and heat treated electroless nickel deposits. The results of this analysis are given later in the text.

#### 7.4.3.1 Summary of the Results of Potentiodynamic Anodic Polarisation Curves

1. As-plated electroless nickel deposits did not show any tendency to form a passive film, whereas heat treated deposits at 400°C exhibited a slight tendency. A possible explanation for the latter, is that the surface oxide was not effectively removed and therefore, during subsequent anodic polarisation some thickening of the oxide occurred.

2. Electroless nickel heat treated at 600°C in vacuum exhibited a pronounced 'passive nose', very similar to that obtained for Watts nickel. In contrast, electroless nickel heat treated at 600°C in air showed no tendency to passivate; this may be due to the inability to remove the thick surface oxide prior to anodic polarisation.

3. The passivity of Watts nickel compared to bright nickel was clearly demonstrated by the anodic polarisation curves, as evident by a pronounced 'passive nose' in the former.

### 7.4.4 Long Term Corrosion Tests

The long term corrosion performance of surface coatings / treatments was assessed by the following methods:

(1) Monitoring the corrosion potential of samples with time.

(2) Determination of instantaneous corrosion rates via linear polarisation method.

(3) Evaluation of surface coating / treatment dissolution by atomic absorption spectrophotometry.

Table 32 describes the visual appearance of corrosion samples at various stages of immersion in acidified salt solution (A.A.S.S.). All surface coatings / treatments failed within 7 weeks, except for electroless nickel / titanium nitride (duplex coating) and chromium oxide (impregnated with sealer) which did not show signs of rusting. The average corrosion current density determined for the surface treatments / coatings is given in Table 33.

Table 32 The visual appearance of corrosion sample at various stages of immersion in acidified salt solution

| Materials/ Surface Coatings/ Treatments | Week 1 | Week 2 | Week 3 | Week 4 | Week 5 | Week 6 |
|---|---|---|---|---|---|---|
| EN8 | | rusted | FAILED | | | |
| EN8 (BO) | slight rusting | rusted | FAILED | | | |
| Ni-Cr-B | - | tarnished | thin layer of rust | | | as wk. 3 |
| VC | rust spec. on surface | rusted | FAILED | | | |
| EN(7%P)A | tarnished | black | as wk. 2 | as wk. 3 | as wk.4 | rusted |
| EN(9%P)A | tarnished | black | as wk. 2 | as wk. 3 | as wk. 4 | rusted |
| EN(12%P)A | - | thin layer of red rust | rusted | FAILED | | |
| EN(7%P)H | - | slight rusting | rusted | FAILED | | |
| EN(9%P)H | - | - | slight rusting | rusted | FAILED | |
| EN(12%P)H | - | - | - | rusted | FAILED | |
| EN600 Air | - | - | - | - | - | slight rusting |
| EN600 Vac | - | black | as wk. 2 | as wk. 3 | slight rusting | rusted |
| Watts Nickel | - | crevice corrosion at lacquer | as wk. 2 | rust patches | rusted | FAILED |
| Bright nickel | tarnished | black & rusted | as wk. 2 | rusted | FAILED | |
| Wc/Ni/W-Cr | slight rusting | rusted | FAILED | | | |
| EN/SiC(H) | - | slight rusting | as wk. 2 | 50% rusted | rusted | FAILED |
| Plasma 316 | large red spots (0.5 mm) | rusted | FAILED | | | |

table 32. continued.

| | | | | | | |
|---|---|---|---|---|---|---|
| EN/TiN | - | - | - | - | - | - |
| CH-oxide | - | - | - | - | - | - |

Table 33. Comparison of the corrosion current densities determined by linear polaristion and Tafel extrapolation techniques

| Materials, Surface Coatings / Treatments | Corrosion Current Density ($nA/cm^2$) Tafel Extrapolation | Linear Polarisation (Average 7 weeks) |
|---|---|---|
| EN8 Steel | 8.172 E4 | 9.097 E4 |
| 316 Stainless | 0.640 E2 | 1.910 E2 |
| EN8 (BO) | 5.147 E4 | 8.573 E4 |
| VC | 1.585 E4 | 1.391 E4 |
| Ni-Cr-B | 2.596 E3 | 8.710 E3 |
| EN (7% P) A | 2.371 E3 | 1.679 E4 |
| EN (9% P) A | 2.718 E3 | 1.297 E4 |
| EN (12% P) A | 3.068 E3 | 3.862 E4 |
| EN (7% P) H | 1.026 E4 | 1.588 E4 |
| EN (9% P) H | 1.074 E4 | 1.227 E4 |
| EN (12% P) H | 6.912 E3 | 4.174 E4 |
| EN / SiC (H) | 1.571 E4 | 2.468 E4 |
| EN 600 Air | 2.195 E3 | 6.065 E3 |
| EN 600 Vacuum | 7.475 E3 | 1.730 E4 |
| Watts Nickel | 1.573 E3 | 1.067 E4 |
| Bright Nickel | 1.340 E3 | 1.686 E4 |
| Wc/Ni/W-Cr | 1.936 E4 | 5.609 E4 |
| Plasma 316 | 4.649 E3 | 3.605 E4 |

By applying Faraday's law to electrochemical corrosion, it can be shown that:

$$\text{Corrosion Rate (mpy)} = \frac{0.13\, I_{corr}\, (E.W.)}{d} \qquad (17)$$

where

$I_{corr}$ = Corrosion current density ($\mu A / cm^2$)

E.W. = Equivalent weight at the corroding species, g

d = Density of the corroding species, $g/cm^3$.

Thus, the corrosion current density is proportional to the corrosion rate and the above equation assumes general corrosion. For the purpose of discussion of results, the corrosion rate has been expressed as Log $I_{corr}$, so that any significant changes in the corrosion behaviour of surface coatings / treatments can be assessed.

Figures 79 & 80 illustrate the variation of the corrosion potentials and corrosion rates with time, respectively. EN8 borided, chromium oxide, nickel/chromium/boron and vanadium carbide (T.D. layer) all exhibited corrosion potentials in the active regime and this is reflected in their high corrosion rates, with the exception of chromium oxide. From the shape of the linear polarisation curve of the latter, it would appear that the system is under resistance control at the corrosion potential, as illustrated in Figure 81(a). Furthermore, the measured uncompensated resistance ($R_{unc}$) was very high (52480 Ω) which therefore, invalidates the use of the linear polarisation method. In contrast, the $R_{unc}$ was very small for other materials and surface coatings / treatments tested, of the order 0.1-0.4 Ohms. The resistance control in chromium oxide deposits reduced considerably after a four weeks immersion in the test solution, as illustrated in Figure 81(b). This resistance control may be attributed to the sealer used to fill porosity in sprayed

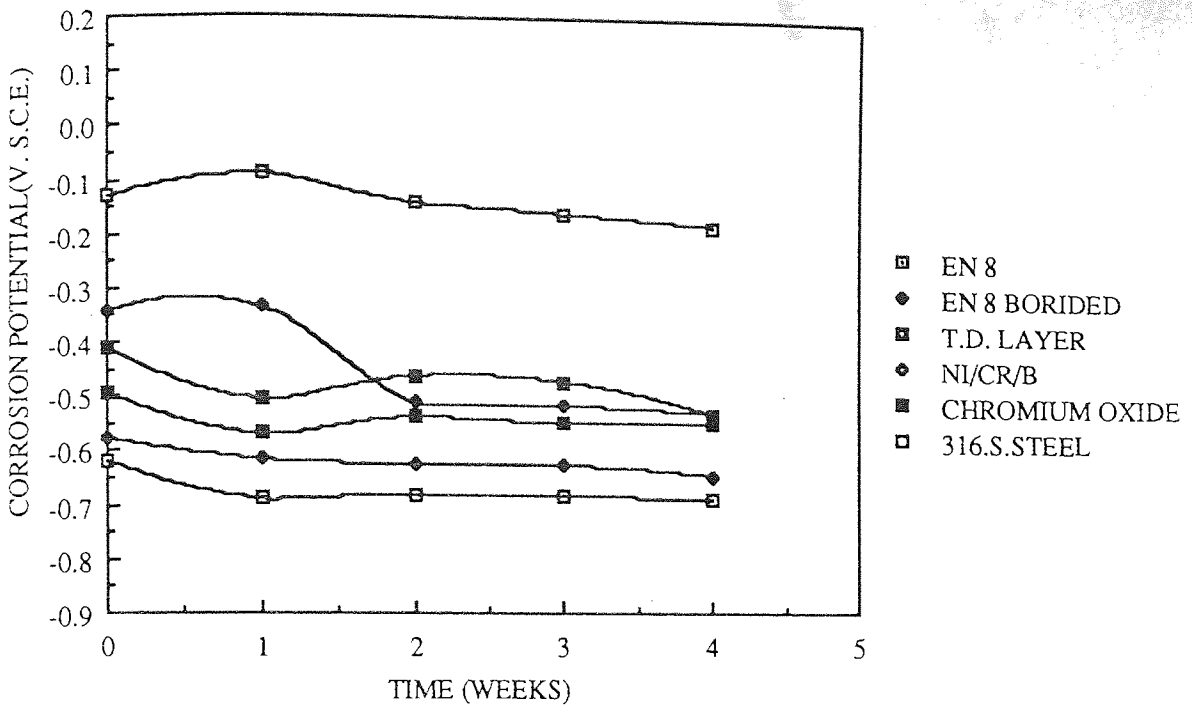


Figure 79. The variation of the corrosion potential(V. S.C.E.) for various materials and surface coatings/treatments with time(weeks)

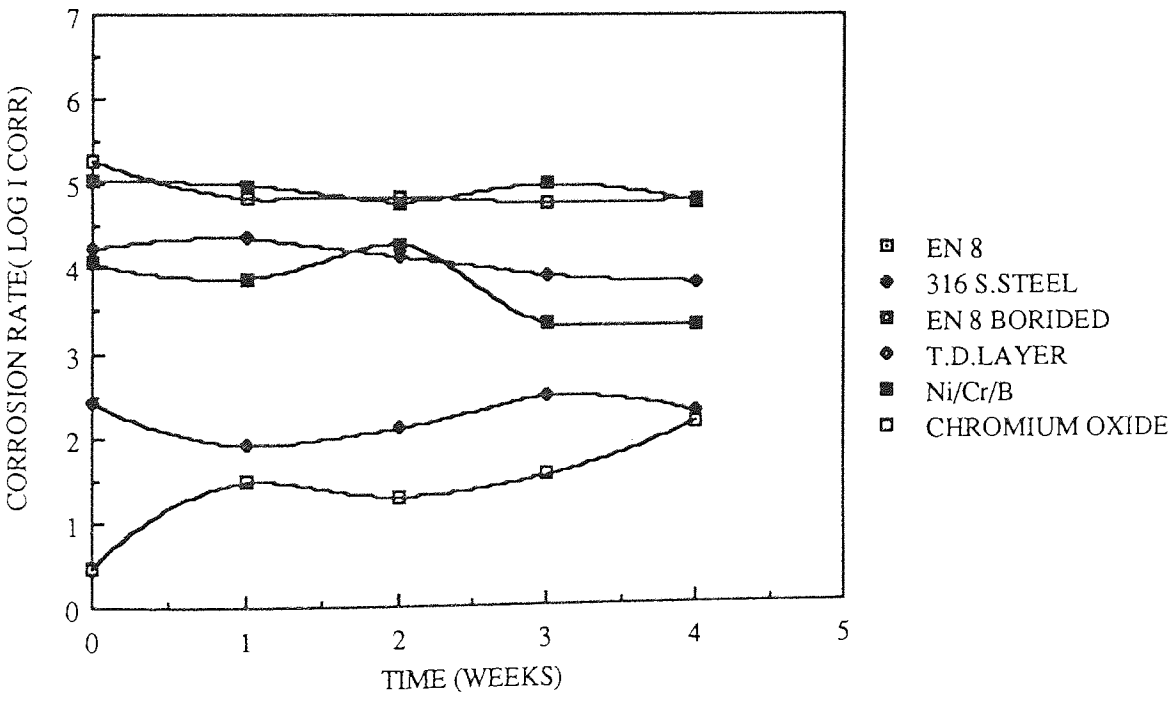


Figure 80. The variation of the corrosion rate for various materials and surface coatings/treatments with time(weeks)

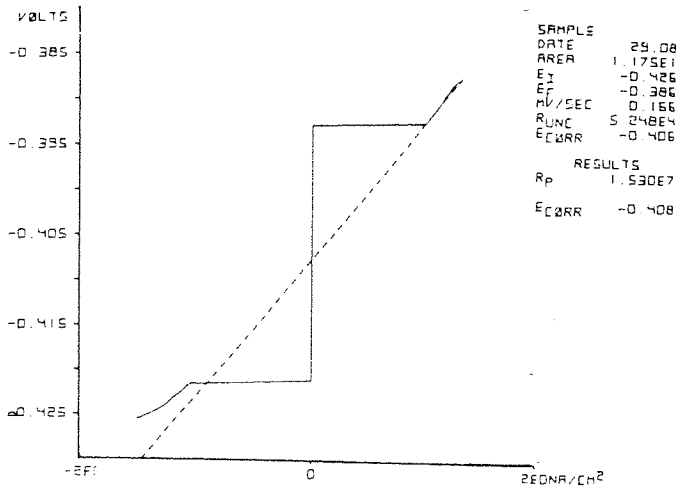


(a) 1 week immersion

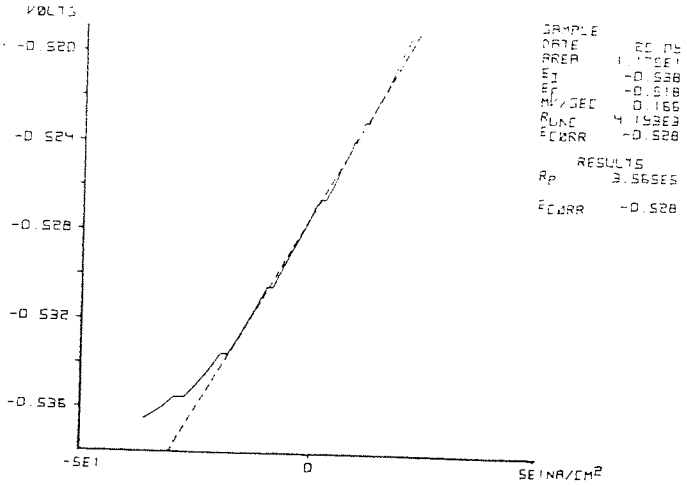


(b) 4 week immersion

Figure 81. Linear polarisation curves for plasma sprayed chromium oxide (sealed) deposit after immersion in acidified salt solution

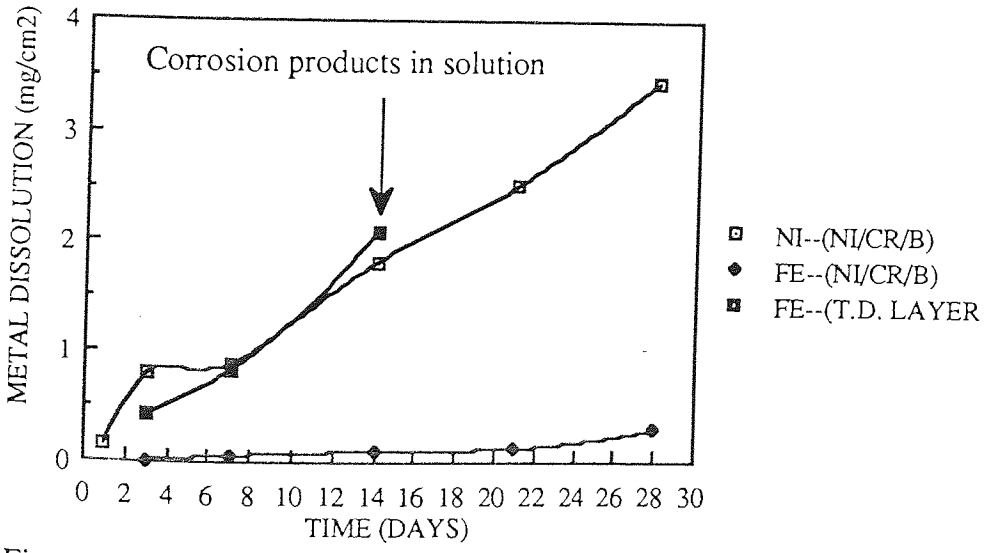


Figure 82. The variation of metal dissolution from nickel/chromium/boron and vanadium carbide(T.D. layer) deposits with time (weeks)

chromium oxide deposits, which is providing an insulating film around the specimen. The "apparent corrosion rate" (Figure 80) for chromium oxide increased with immersion time, this could be interpreted as a reduction in the sealing efficiency of deposit.

The corrosion potential for vanadium carbide became more active after one week, this is probably due to the rapid dissolution of iron from substrate, as illustrated in Figure 82. The corrosion potential of Ni/Cr/B remained essentially constant after one week, but then became more active in the following weeks. This trend is also revealed by analysis of the corroding solution, which showed that during the first week some dissolution of nickel occurred. A period of rapid nickel dissolution followed, as illustrated in Figure 82. There is also a slow and progressive increase in the iron dissolution, probably from the coating as it contains 5% iron. It was evident from the corrosion potential and rates, that EN8 borided steel has poor corrosion resistance properties. The corrosion potential and rates are very similar to those obtained for EN8 steel.

As-plated electroless nickel (7% and 9% P) deposits failed after 6 weeks immersion in acidified salt solution, whereas the 12% P deposit failed after four weeks. However, the latter remained shiny but was covered by a thin layer of rust, whereas, the above coatings exhibited tarnishing and darkening. Thus, it may be stated that the 12% P deposit conferred poor 'corrosion protection' but better corrosion resistance, than the lower phosphorus deposits. As-plated electroless nickel (7, 9 and 12% P) deposits exhibited a significant drop in their corrosion potentials after one week's immersion, as illustrated in Figure 83. This was followed by a period where the potentials tended to

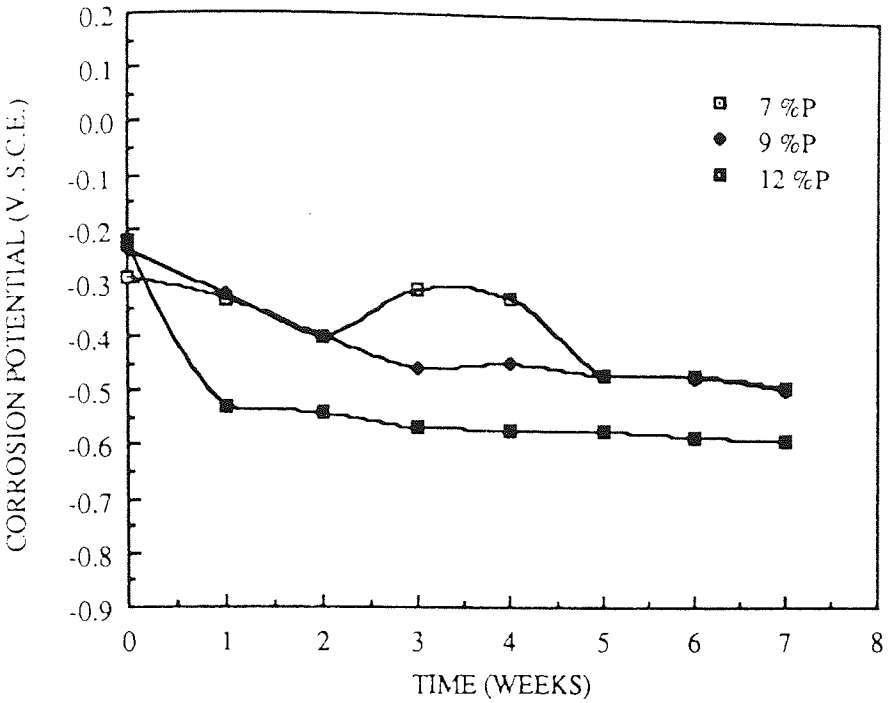


Figure 83. The variation of the corrosion potential(V. S.C.E.) of asplated electroless nickel deposits with time (weeks)

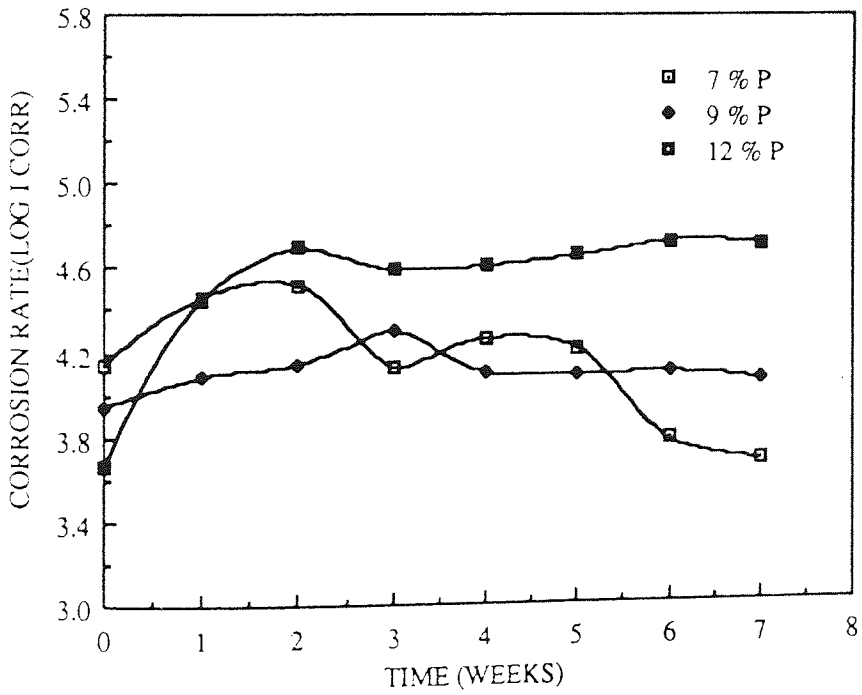


Figure 84. The variation of the corrosion rate for asplated electroless nickel deposits with time (weeks)

stabilise except for the 7% P deposit, which experienced an increase in potential, probably corresponding to the formation of the 'black layer' on the specimen. The drop in corrosion potential (week 1) coincided with an increase in the corrosion rate, as illustrated in Figure 84. Thereafter, the corrosion rates stabilised except for the 7% P deposit, which showed a progressive lowering of the corrosion rate with time. The corrosion rates determined at the start of the experiment (week 0) would support the hypothesis that higher phosphorus deposits confer better corrosion resistance. Analysis of the corroding solutions indicated a higher nickel dissolution for the 7% P than for the 9% P electroless nickel deposits, as illustrated in Figure 85. However, a higher amount of iron dissolution was detected from the 9% P electroless nickel deposit.

The heat treated electroless nickel (7, 9 and 12% P) deposits failed after approximately 4 weeks immersion in acidified salt solution, whereas the as-plated electroless nickel deposits failed after 6 weeks. The profiles of the corrosion potential versus immersion time were similar to those obtained from as-plated deposits, however, the end potentials were more active, as illustrated in Figure 86. The heat treated 12% P electroless nickel deposit exhibited a higher corrosion rate than electroless nickel deposits containing 7% and 9% P, as illustrated in Figure 87. The corrosion potential for heat treated electroless nickel silicon carbide composite was less active than the above heat treated deposits. However, the average corrosion rate was much higher compared to 7% P and 9% P heat treated electroless nickel deposits.

Analysis of the corroding solutions revealed that after 3 days, the iron dissolution was approximately 15 times that detected in as-plated electroless nickel corroding solutions.

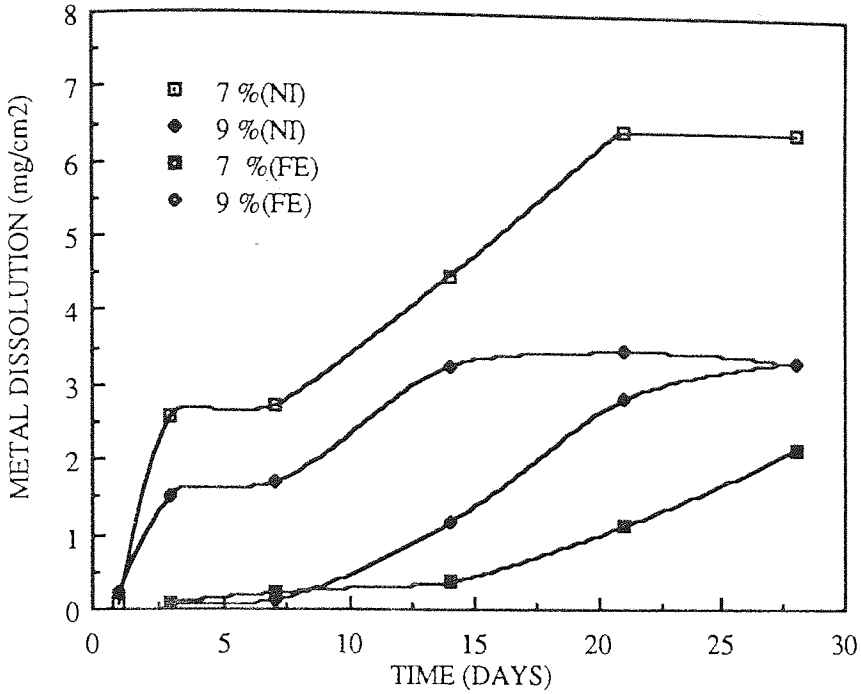


Figure 85. the variation of metal dissolution(mg/cm2) from asplated electroless nickel deposits with time (days)

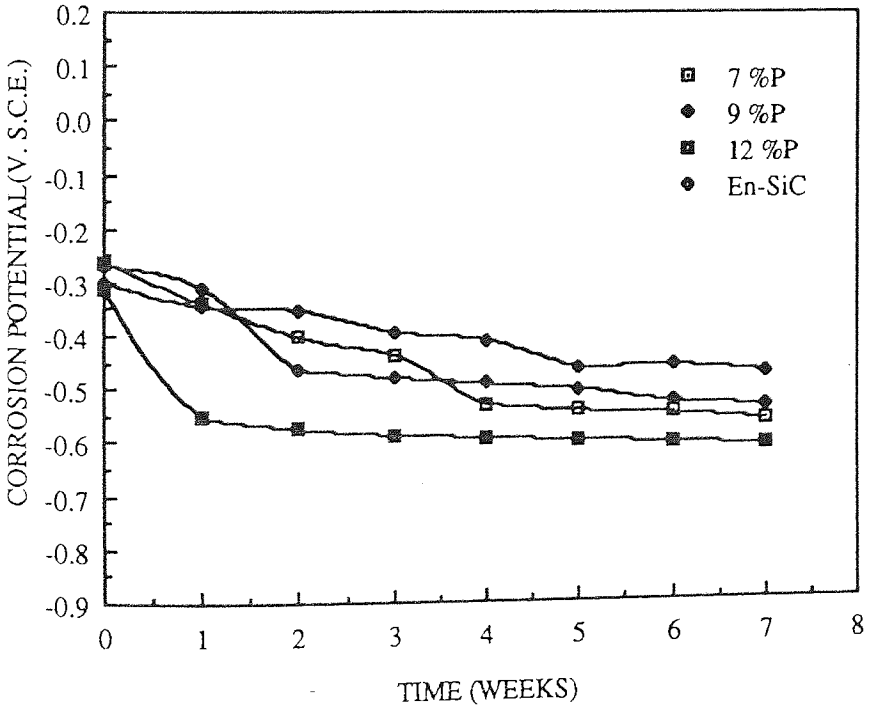


Figure 86. The variation of the corrosion potential (V. S.C.E.) for heat treated (400 C) electroless nickel deposits with time (weeks)

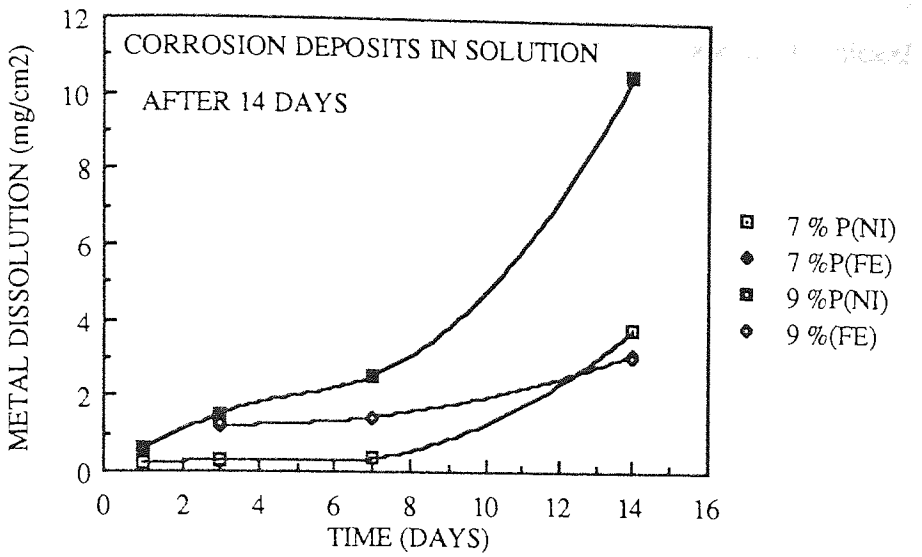


Figure 88. The variation of metal dissolution(mg/cm2) from heat treated (400 C) electroless nickel deposits with time (days)

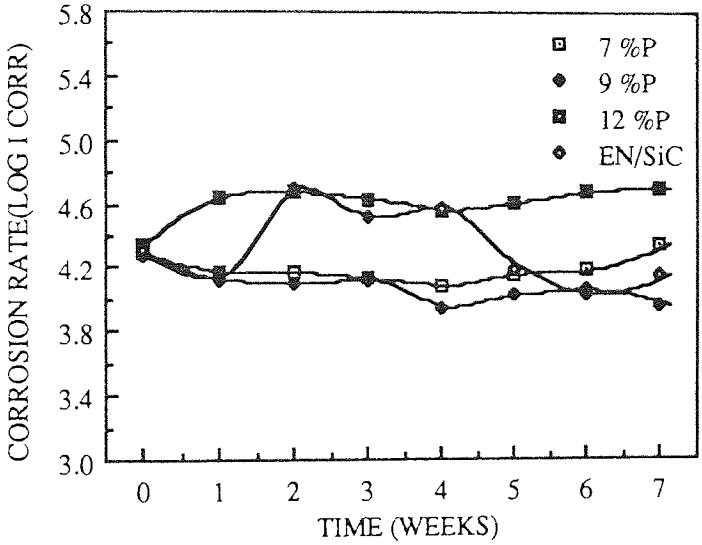


Figure 87. The variation of the corrosion rate for heat treated (400 C) electroless nickel deposits with time (weeks)

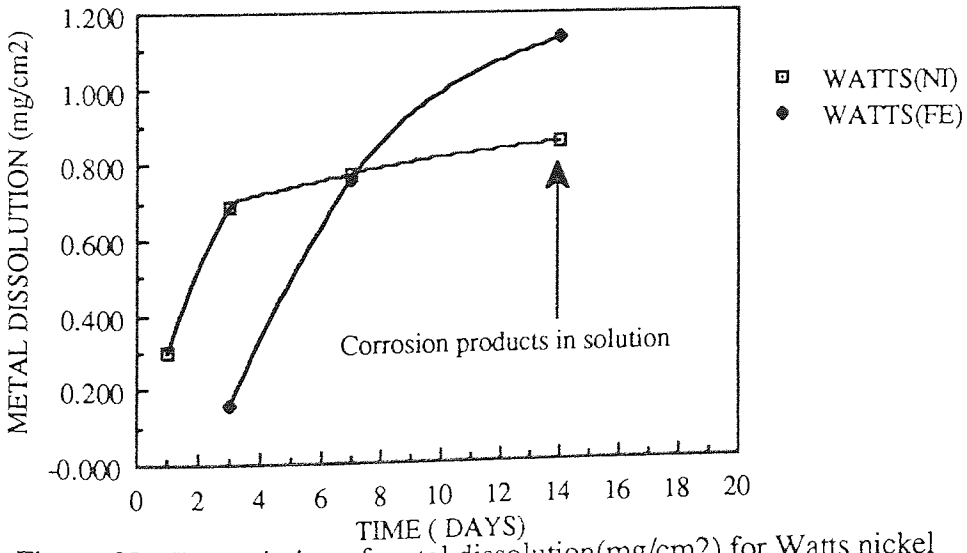


Figure 89. The variation of metal dissolution(mg/cm2) for Watts nickel deposit with time (weeks)

Furthermore, there appears to be a 3 and 8 times increase in the nickel dissolution compared to that obtained for as-plated electroless nickel deposits containing 7% and 9% phosphorus respectively. The variation of the iron and nickel dissolution from heat treated electroless nickel deposits is illustrated in Figure 88. In contrast, the dissolution of nickel and iron from Watts nickel was, in general, much less than for both as-plated or heat treated electroless nickel deposits, as illustrated in Figure 89. This trend is further supported by the lower corrosion current density of Watts nickel compared to electroless nickel deposits, as indicated in Table 33 .

Electroless nickel deposits heat treated at 600°C (air and vacuum) exhibited a better corrosion resistance than those heat treated at 400°C. The latter were rusted after 4 weeks immersion in acidified salt solution, whereas, deposits heat treated at 600°C rusted after approximately 6 weeks. The corrosion potentials for the latter remained essentially constant for up to 4 weeks, whereas the as-plated and heat treated (400°C) were characterised by a rapid drop in the corrosion potential. After this steady corrosion potential period, the vacuum heat treated deposits became slightly more active than those heat treated in air at 600°C. However, the end corrosion potential for both these deposits was similar, as illustrated in Figure 90.

Analysis of the corroding solution revealed that considerable dissolution of the iron occurred for both deposits, as illustrated in Figure 91. Furthermore, a higher nickel dissolution rate was evident in the vacuum heat deposit than from the air heat treated deposit. The source of the iron leaching out may be from the substrate or the Fe-Ni intermetallic layer formed when heat treatment was carried at 600°C.

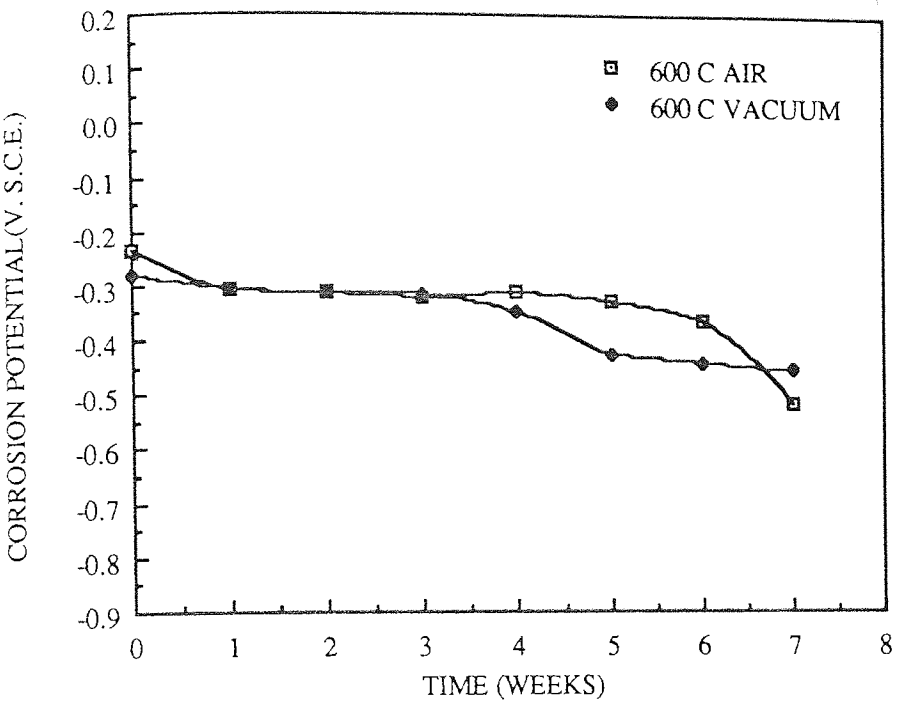


Figure 90. The variation of the corrosion potential(V. S.C.E.) for heat treated(600 C) electroless nickel deposits with time(weeks)

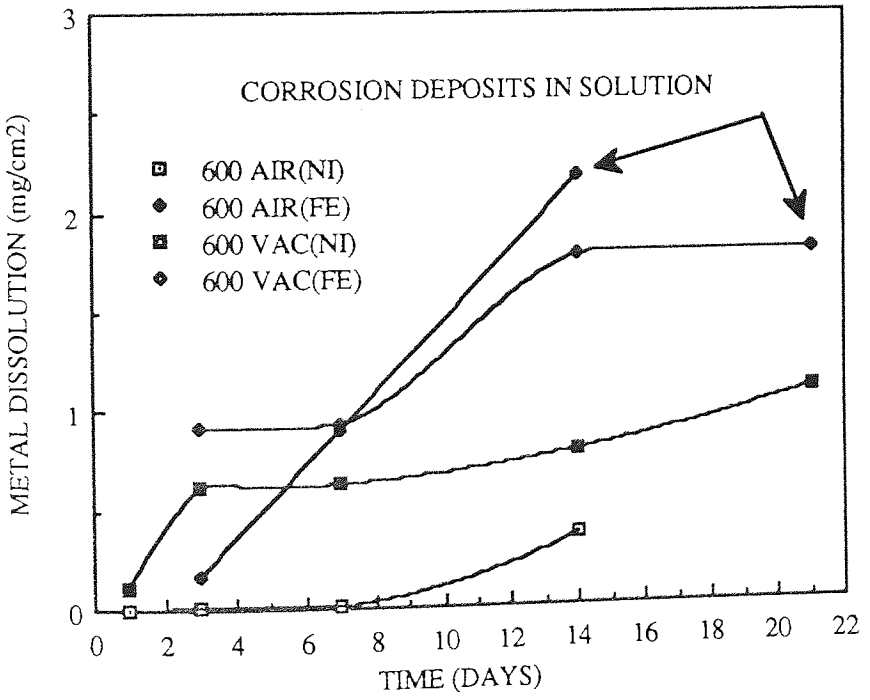


Figure 91. The variation of metal dissolution(mg/cm2) for heat treated(600 C) electroless nickel deposits with time(weeks)

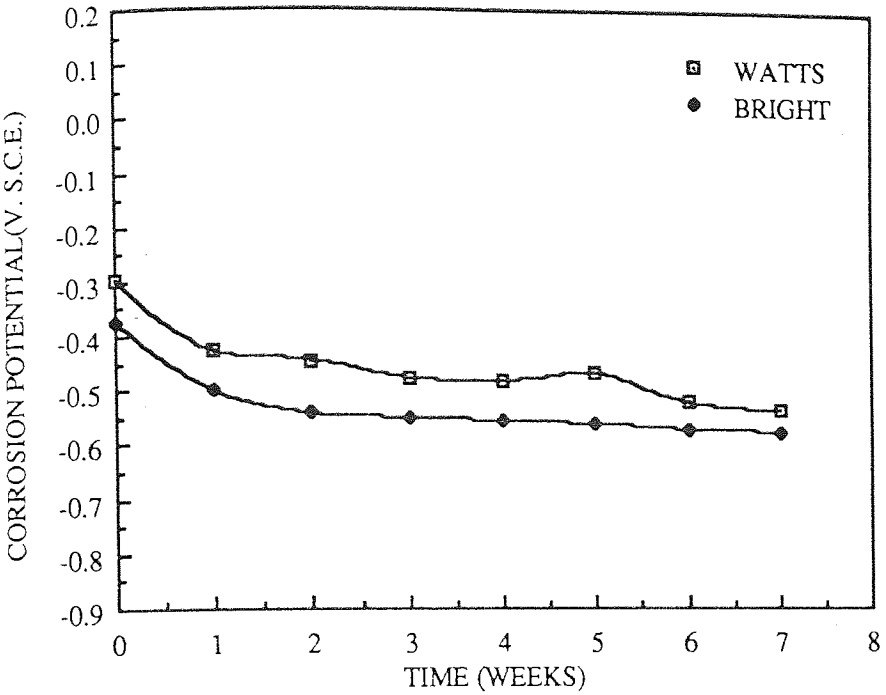


Figure 92. The variation of the corrosion potential(V. S.C.E.) for Watts and bright nickel deposits with time (weeks)

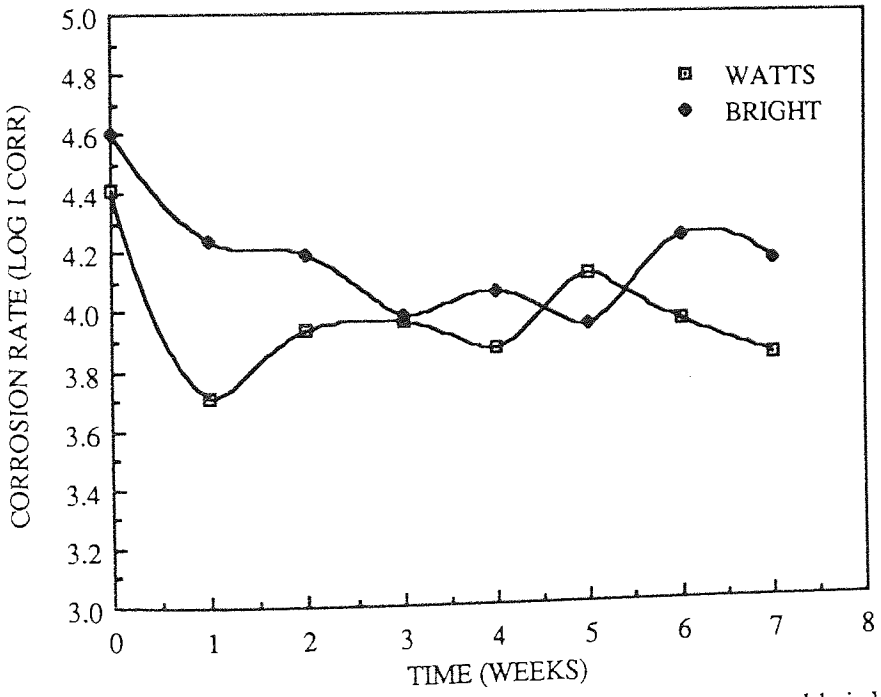


Figure 93. The variation of the corrosion rates for Watts and bright nickel deposits with time (weeks)

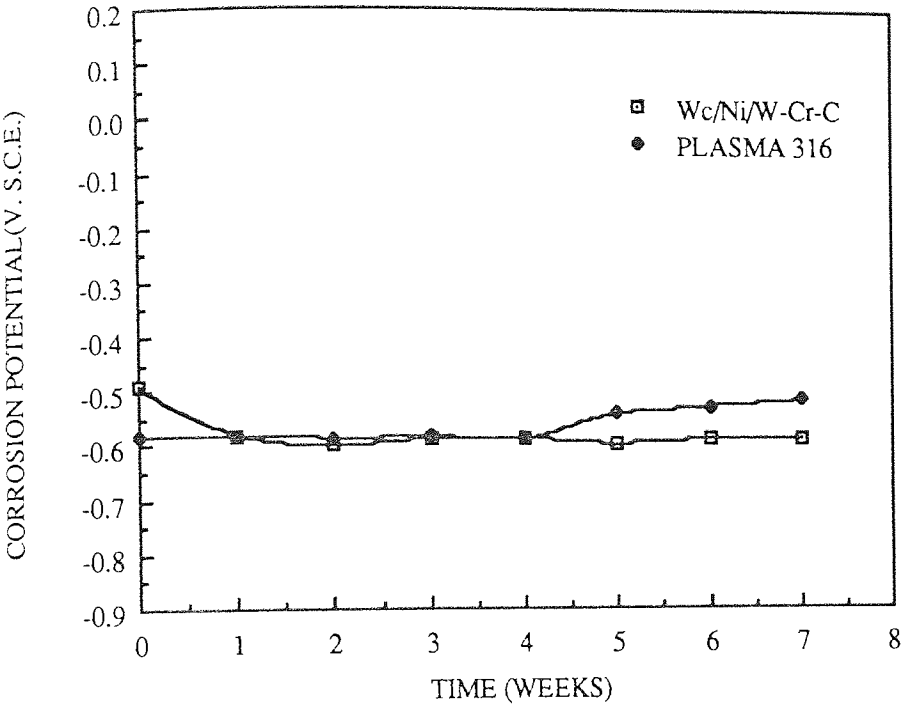


Figure 94. The variation of the corrosion potential (V. S.C.E.) for plasma nitrided 316 stainless steel and Jet-Kote(Wc/Ni/W-Cr-carbides) with time (weeks)

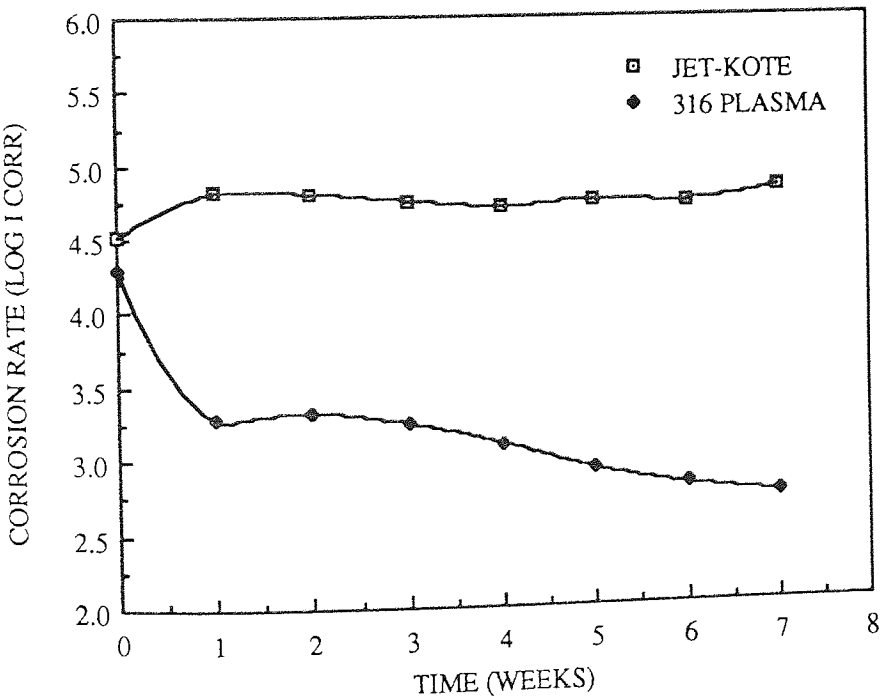


Figure 95. The variation of the corrosion rate for plasma nitrided 316 stainless steel and Jet-Kote (Wc/Ni/W-Cr-carbides) with time (weeks)

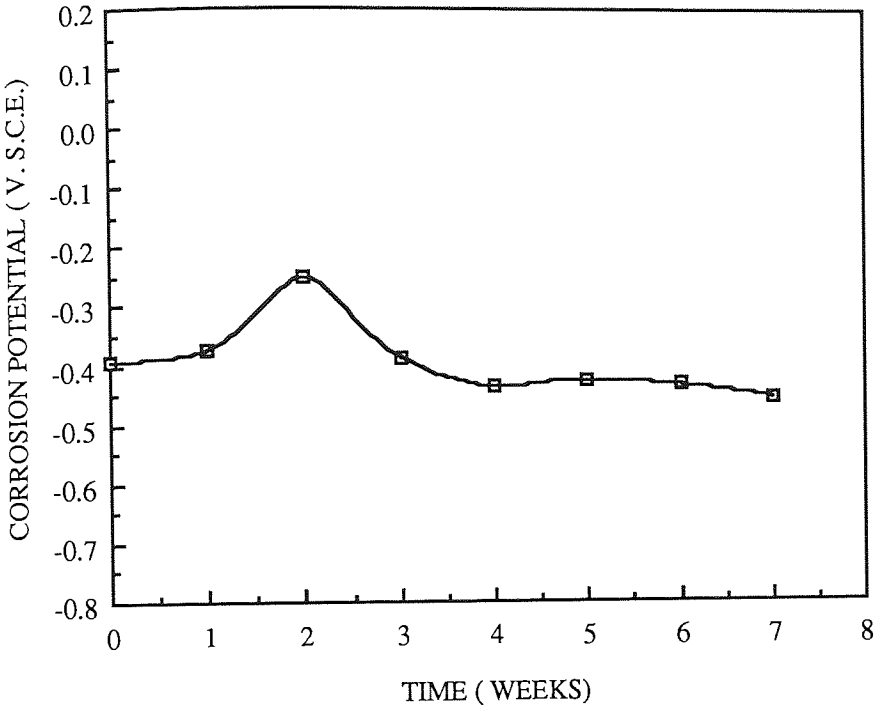


Figure 96. The variation of the corrosion potential (V. S.C.E.) for electroless nickel/ titanium nitride duplex coating with time (weeks)

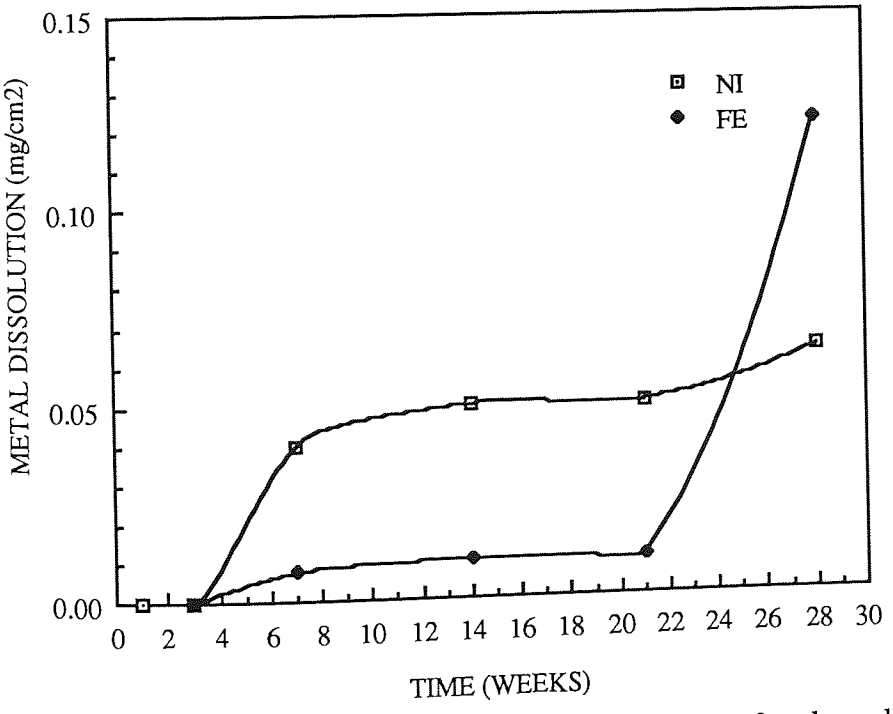


Figure 97. The variation of the metal dissolution(mg/cm2) for electroless nickel/ titanium nitride duplex coating with time (days)

Bright and Watts nickel deposits failed after 5 and 6 weeks immersion in acidified salt solution respectively. The corrosion potentials for these deposits dropped significantly after one week, but stabilised thereafter, as illustrated in Figure 92. The corrosion potentials of Watts and bright nickel were separated by approximately 70 millivolts, the latter being more active. The decrease in corrosion potential was surprisingly accompanied by a decrease in corrosion rate, and this was greater for the Watts nickel deposit, as illustrated in Figure 93. Thereafter, the corrosion rates fluctuated, but on average the Watts nickel exhibited a lower corrosion rate than bright nickel deposits.

Plasma nitrided 316 stainless steel and Jet-kote deposit (Wc/Ni/W-Cr carbides) were heavily rusted after two weeks immersion in acidified salt solution. The corrosion potentials for the above remained fairly active throughout the test, as illustrated in Figure 94. The fact that the Jet-Kote deposit failed so quickly would indicate the presence of inter-connecting porosity in the deposit. The active corrosion potentials exhibited by Jet-kote deposits corresponded to high corrosion rates, however, for plasma nitrided 316 stainless steel a reduction in corrosion rate (Figure 95) was found. This contradiction to visual observations was due to the fact that the linear polarisation curves showed the presence of resistance polarisation, similar to that encountered with sealed chromium oxide deposits. Thus, the high polarisation resistance (Rp) determined led to the misleading $I_{corr}$ values.

The best corrosion performance was exhibited by the duplex coating of electroless nickel / titanium nitride, which showed no signs of rusting after 7 weeks immersion in acidified salt solution. The corrosion potential of the duplex coating was slightly more

active than electroless nickel deposits and became more active with increasing immersion time, as illustrated in Figure 96. Analysis of the corroding solution indicated small amounts of nickel and iron dissolution, as illustrated in Figure 97.

#### 7.4.4.1 Summary of the Long Term Corrosion Tests

1. The best corrosion performances were shown by electroless nickel / titanium nitride duplex coating, nickel-chromium-boron and electroless nickel deposits heat treated at 600°C respectively.

2. EN8 borided and plasma nitrided 316 stainless steel exhibited poor corrosion performance, as evident by their rapid rusting, active corrosion potentials and high corrosion current densities. The failure of Jet-kote deposit was primarily due to its inherent porosity, however, sealing thermally sprayed deposits would appear to be an effective technique to improve corrosion protection, as exemplified by the sealed plasma sprayed chromium oxide deposit.

3. As-plated electroless nickel deposits exhibited a better corrosion performance than heat treated deposits. For the latter, there was marked increase in iron dissolution from the specimens during the first week, possibly indicative of defects in the coating.

### 7.4.5. Scanning Electron Microscopy of Corroded Specimens

The surface morphology of the corroded specimens was examined using the S.E.M., and analyses conducted with the aid of the energy dispersive x-ray analyser (E.D.X.A.). However, only semi-quantitative analysis was carried out because the specimens were curved and therefore, the take off angle for the x-rays cannot be known with precision. Secondly, correction for x-ray fluorescence, absorption and atomic number differences were not conducted and finally, oxygen cannot be detected due to its low atomic number. Therefore, analyses should not be compared between different specimens, however, at high magnification, analyses on different areas are comparable, as the error in the take off angle would be minimal. The effect of corrosion on the composition of electroless nickel deposits was evaluated using electron probe microanalysis. In this technique, a series of spot analyses were carried out on cross sections of deposits, using flat polished mounted specimens.

The corroded surface of as-plated electroless nickel (7% P) deposit is illustrated in Figure 98(a). This showed areas of adherent corrosion products as evident from the iron x-ray mapping, and also a distribution of small and large pits. At higher magnification (Figure98(d)) small pits were observed which had a diameter of approximately 1 micron. A large hemispherical pit is illustrated in Figure 98(e), this is probably a feature of the original surface caused by hydrogen gas evolution during electroless nickel plating. Analysis of the corroded surfaces and corrosion products is given in Table 34.

Table 34 E.D.X.A. of corroded surfaces and corrosion products

| | Ni% | P % | Fe % | Cl % | Si |
|---|---|---|---|---|---|
| As-plated electroless nickel (7% P) | | | | | |
| Corroded surface | 91.41 | 8.27 | 0.31 | - | |
| Corrosion products | 32.63 | 8.80 | 50.14 | 8.80 | |
| As-plated electroless nickel (9% P) | | | | | |
| Corroded surface | 81.53 | 13.11 | 0.33 | 5.02 | |
| Circular region | 82.53 | 16.73 | 0.37 | 0.38 | |
| Corrosion products | 29.08 | 3.68 | 65.19 | 2.06 | |
| Black area | 80.71 | 15.44 | 1.50 | 2.35 | |
| Heat treated electroless nickel (400°C, 7 % P) | | | | | |
| Corroded surface | 85.44 | 11.18 | 3.16 | 0.23 | |
| corrosion products | 6.10 | 0.63 | 92.32 | 0.95 | |
| Asplated electroless nickel (12% P) | | | | | |
| corrosion products | 1.68 | 0.17 | 98.13 | 0.02 | |
| Heat treated electroless nickel (400 C, 12 % P) | | | | | |
| corrosion products | 6.34 | 0.21 | 93.36 | 0.09 | |
| Heat treated electroless nickel (600°C in air) | | | | | |
| Nodular cracked area | 76.73 | 22.34 | 0.44 | 0.48 | |
| Circular shallow crater | 85.13 | 13.42 | 0.92 | 0.24 | |
| Heat treated electroless nickel (600°C in vacuum) | | | | | |
| Position X | 75.36 | 23.48 | 0.91 | 0.25 | |
| Position Y | 70.11 | 23.12 | 6.62 | 0.16 | |

(table 34 continued)

| | Ni % | P % | Fe % | Cl % | Si % |
|---|---|---|---|---|---|
| Watts Nickel | | | | | |
| Grainy area | 97.93 | - | 2.01 | 0.06 | - |
| Corrosion products | 71.83 | - | 27.92 | 0.06 | 0.2 |

Figure 99(a) illustrates the corroded surface of the 9% P as-plated electroless nickel deposit, this showed a central circular region which is darker than the surrounding area. At high magnification the latter revealed small interconnected pits, as illustrated in Figure 99(b). Analysis of the corroded surface detected approximately 5% chlorine, probably in the form of chlorides, whereas the circular region contained only 0.37% Cl. This would suggest the higher pitting density (Figure 99(b)) observed for the 9% P deposit compared to 7% P electroless nickel (Figure 98(d)) is a consequence of the higher chloride content of the former. As mentioned in Table 32, some of the as-plated electroless nickel deposits turned black during the course of testing; such an area is illustrated in Figure 99(c). This photomicrograph shows black areas confined within the cracked adherent corrosion products. The black areas at high magnification, revealed fine striated cracks, as illustrated in Figure 99(d). Both the black areas and corrosion products contained approximately 2.5% chlorine, probably in the form of chlorides. It is unlikely that these black areas are protective because they appear to be cracked and the analysis would suggest that they are complex nickel-phosphorus-chlorides. It was observed that the corrosion potentials did not become less active with the formation of the black layers, except for 7% P as-plated electroless nickel deposit, which exhibited a small transient increase in corrosion potential. The subsequent drop in the corrosion

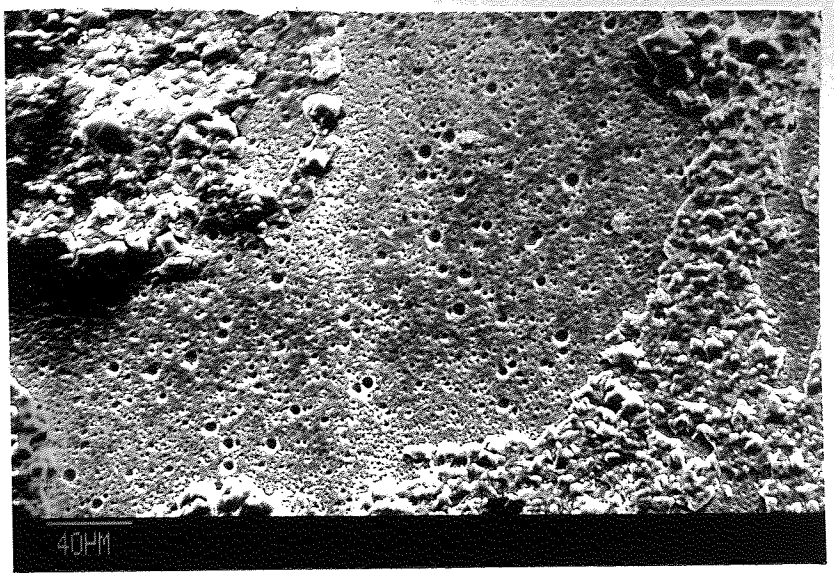


(a) corroded surface

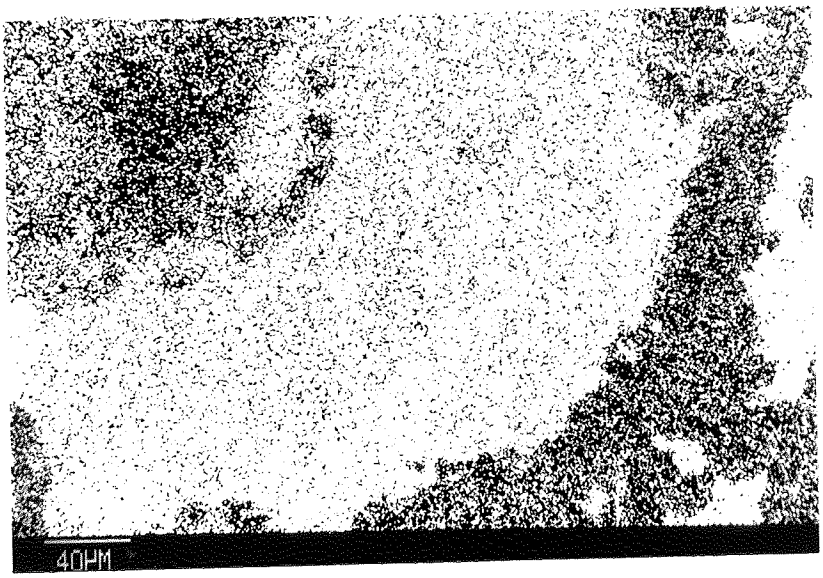


(b) nickel x ray mapping


(c) iron x ray mapping

Figure 98. S.E.M. and x-ray micrographs of corroded surface of 7% P as-plated electroless nickel deposit

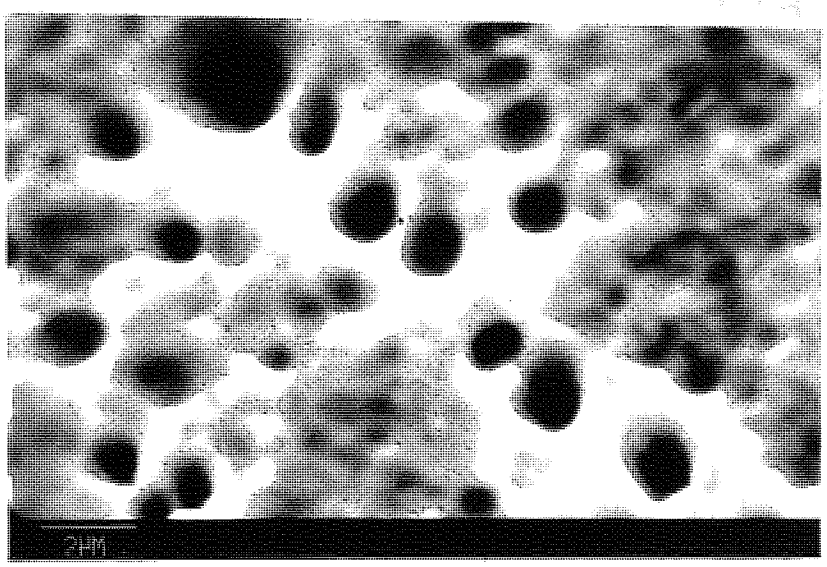

(d) higher magnification of corroded surface

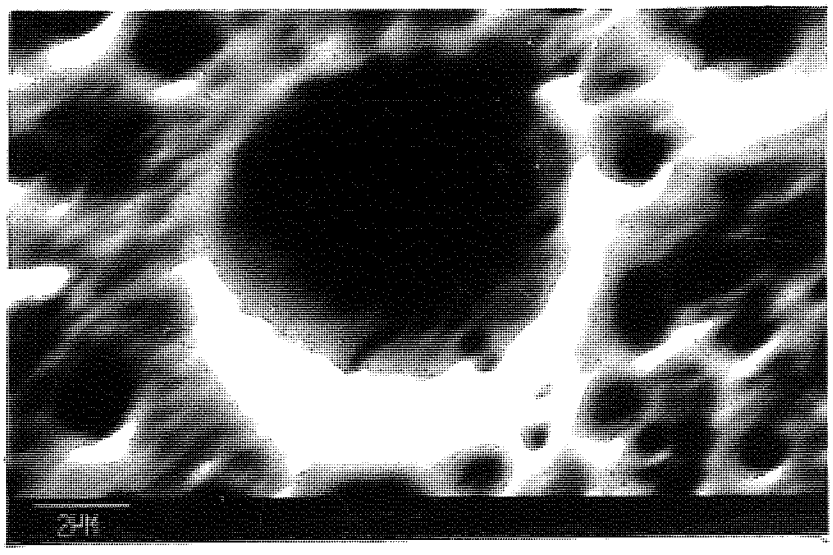

(e) hemispherical pit

Figure 98. S.E.M. and x-ray micrographs of corroded surface of 7% P as-plated electroless nickel deposit

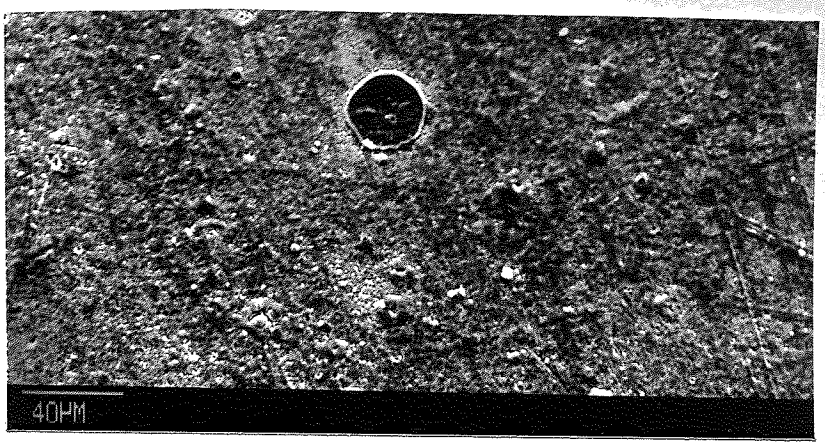


(a) corroded surface

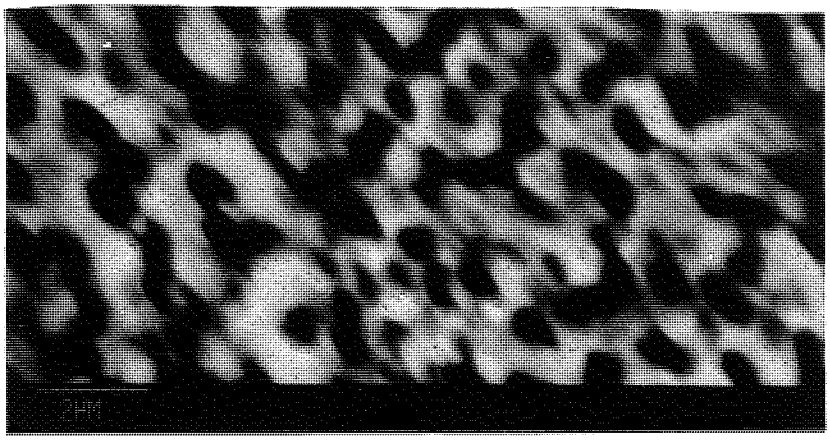

(b) higher magnification of corroded surface

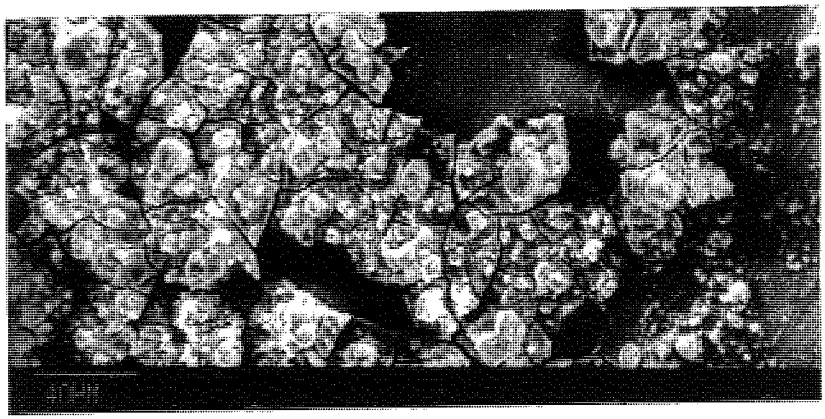

(c) corrosion products

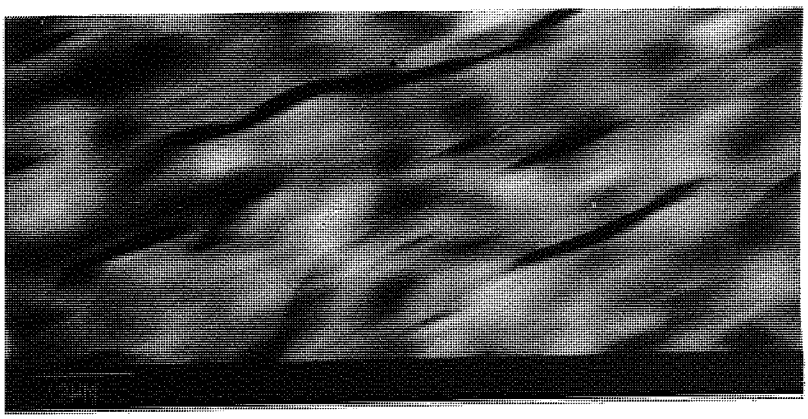

(d) black areas

Figure 99. S.E.M.micrographs of corroded surface of 9% P as-plated electroless nickel deposit

potential is most probably related to the cracked nature of this layer, which provided the necessary pathways for resumption of corrosion.

The corroded surface of the 7% P electroless nickel heat treated at 400°C is illustrated in Figure 100 (a). This photomicrograph showed that pitting appeared to be predominant in certain regions corresponding to 'troughs', whereas, the 'higher' areas appear to be unattacked. Deep pits and adherent nodular shaped corrosion products were also observed on the corroded surface, as illustrated in Figures 100 (b) and (c), respectively. The corrosion products on as-plated (9% P) electroless nickel were adherent cracked islands, whereas, in the above they appeared to be nodular shaped. The latter contained a higher proportion of iron, whereas, corrosion products on as-plated electroless deposits, except for 12% P, contained a significantly higher proportion of nickel and phosphorus. Hence, it would appear that in heat treated electroless nickel deposits pitting results in leaching of higher amounts of iron than nickel and phosphorus, a similar trend was shown in the analysis of the corroding solution. The leaching of iron through the deposit to form nodular shaped corrosion products is illustrated in Figure 101. It would appear that underneath these nodules, fine pits were present, as evident from areas where the nodules are absent.

The corroded surface of electroless nickel heat treated at 600°C (in air) exhibited signs of preferential corrosion on the original surface topography, as illustrated in Figure 102(a). The 'lighter' areas corresponded to regions where corrosion has resulted in greater removal of deposit material than darker regions. Figure 102(b) shows a shallow circular shaped crater where preferential corrosion has taken place, and a nodular area,

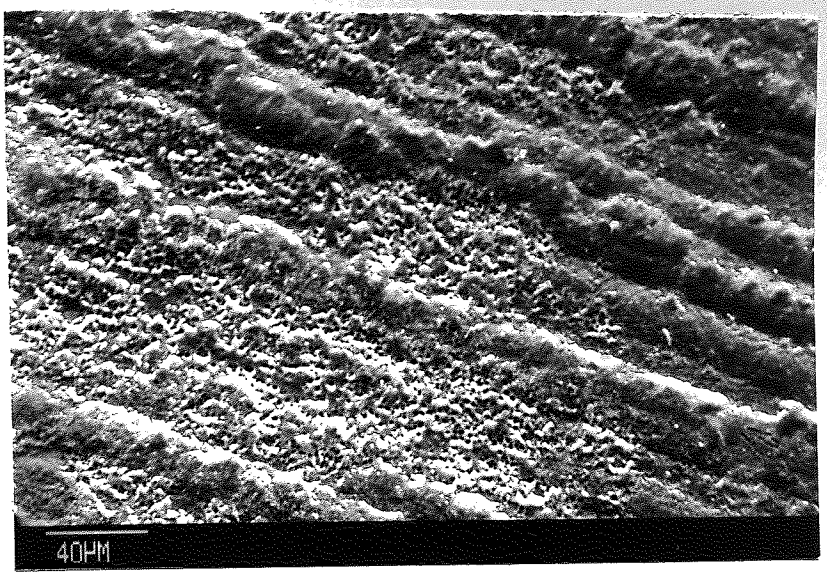


(a) corroded surface

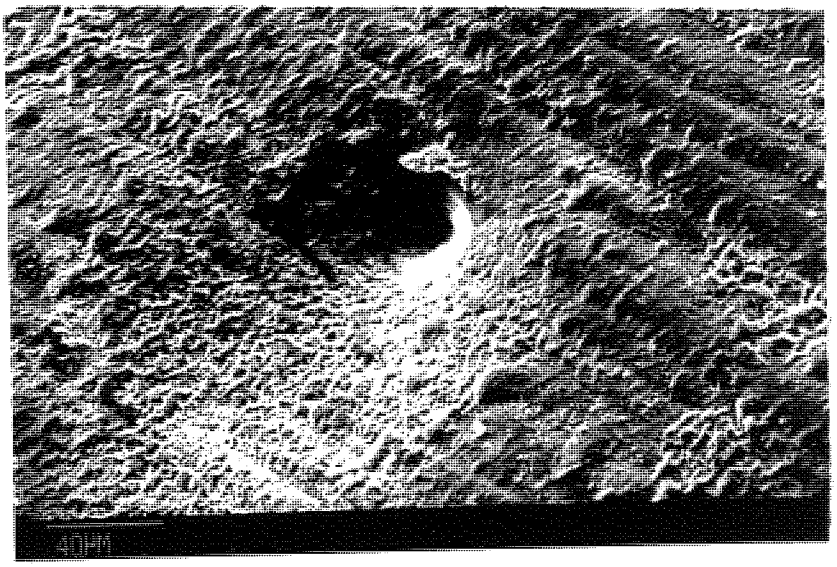

(b) large pit

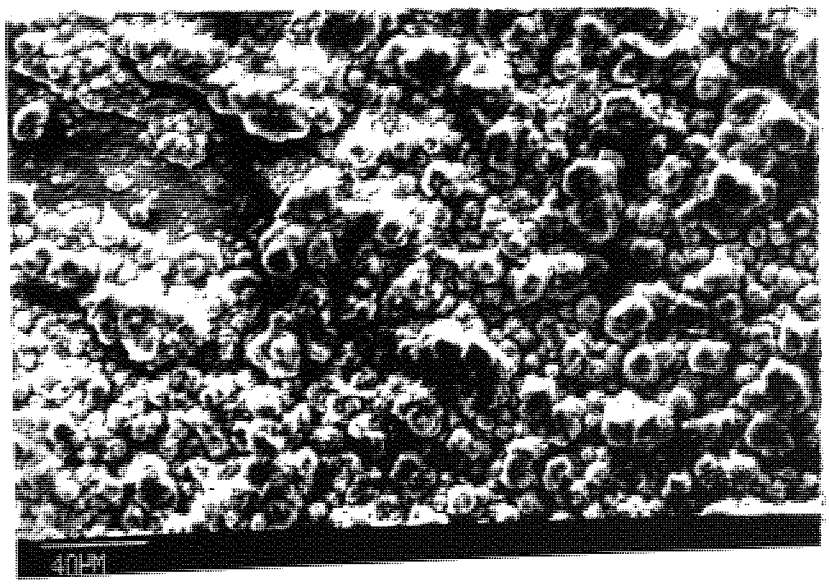

(c) corrosion products

Figure 100. S.E.M. micrographs of corroded surface of 6% P heat treated (400°C) electroless nickel deposit

Figure 101. S.E.M. micrographs of corroded surface of 9% P heat treated (400°C) electroless nickel deposit showing nodular corrosion products

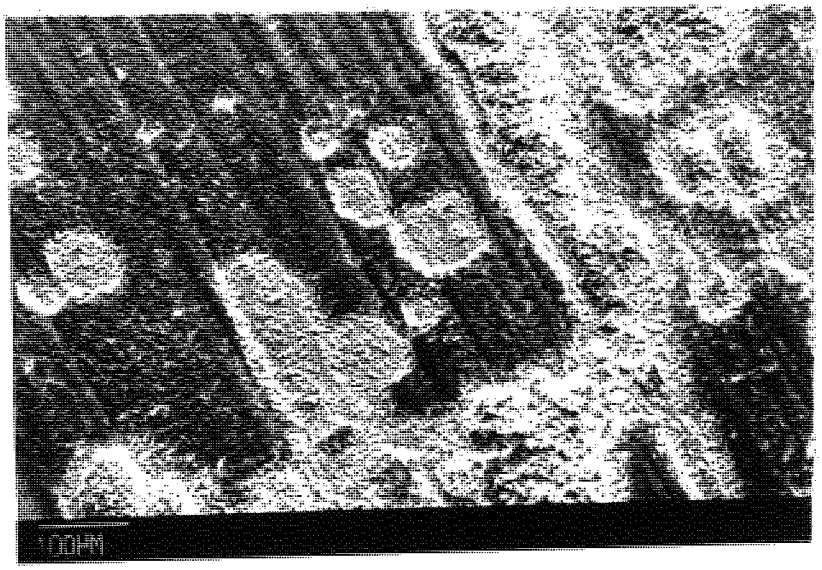

(a) corroded surface

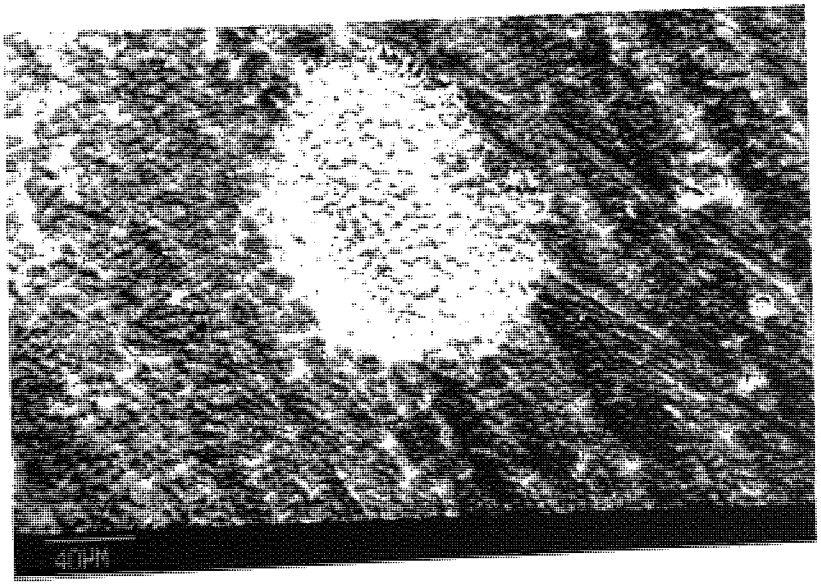

(b) corroded surface

Figure 102. S.E.M. micrograph of corroded surface of 7% P electroless nickel deposit heat treated at 600°C in Air

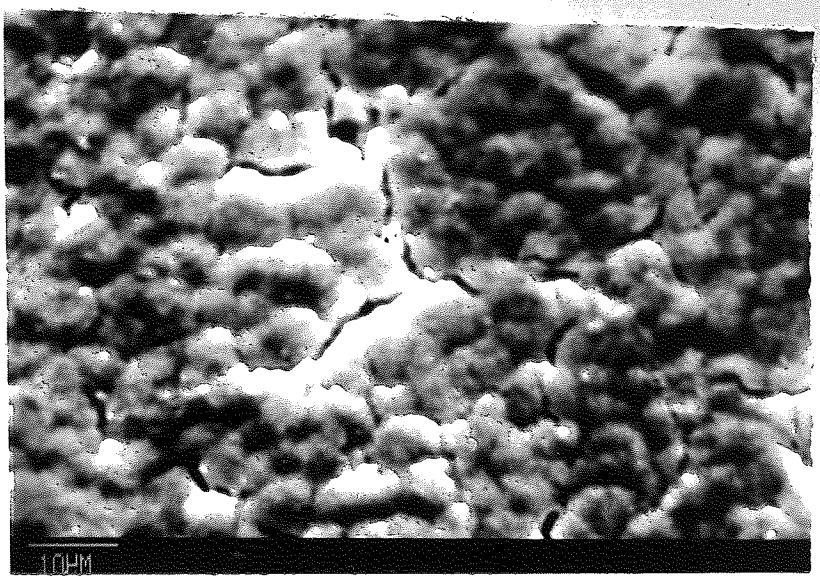

(c) high magnification of corroded surface

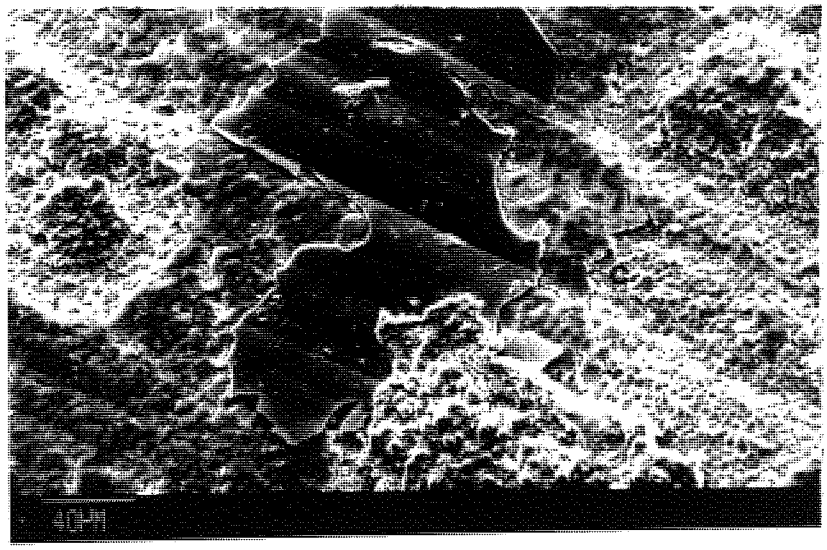

(d) corroded surface showing original surface layers

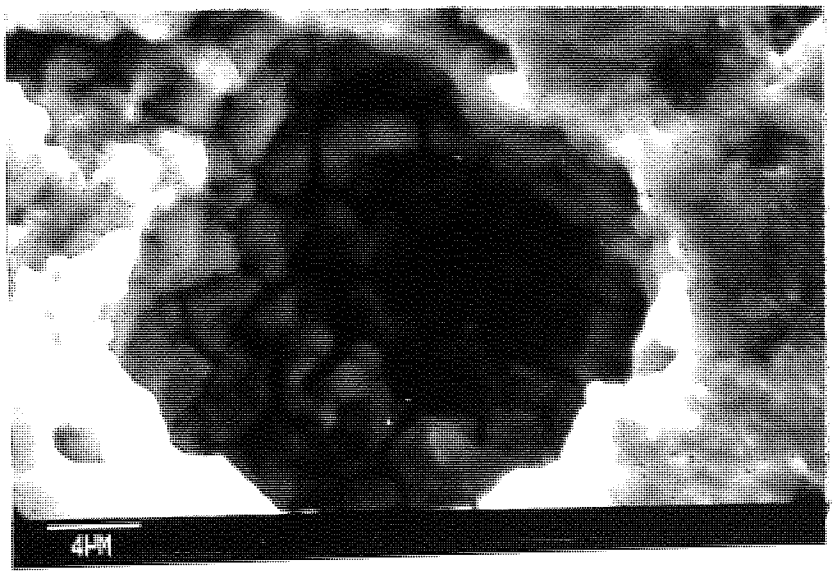

(e) large pit

Figure 102. S.E.M. micrograph of corroded surface of 7% P electroless nickel deposit heat treated at 600°C in Air

which appeared to show evidence of interconnecting cracking. The latter is shown at high magnification in Figure 102(c), this would strongly suggest that the observed cracking was due to coalescence of small pits along the nodular boundaries. Comparison of the analyses at nodular areas and shallow circular shaped craters would suggest preferential dissolution of nickel in the former. The effect of corrosion on the original top surface can be envisaged from Figure 102(d). This photomicrograph shows an island of original tip surface surrounded by the nodular cracked regions. Regions A, B, C illustrate the removal of the top surface, presence of an underlying nodular cracking and extensive exfoliation of the latter, respectively. Large deep pits were also observed and a nodular crack pattern was evident in the bottom of the pit, as illustrated in Figure 102(e).

In contrast, electroless nickel heat treated at 600°C (vacuum) did not exhibit evidence of internodular corrosion, however, the corroded surface showed preferential corrosion on original surface topography, as illustrated in Figure 103 (a). The pitted region is shown at higher magnification in Figure 103 (b), the central pore is approximately 4 microns diameter and the surrounding area is covered by small pits (< 1 micron diameter). Comparison of the analyses at areas X and Y suggest that the only significant change in the composition is the presence of approximately 7% iron at the latter. This may be attributed to the fine pits leaching out iron from the substrate or the Fe-Ni intermetallic layer.

In comparison to the above electroless nickel deposits the corroded surface of Watts nickel exhibited a grainy surface topography with small areas of adherent corrosion

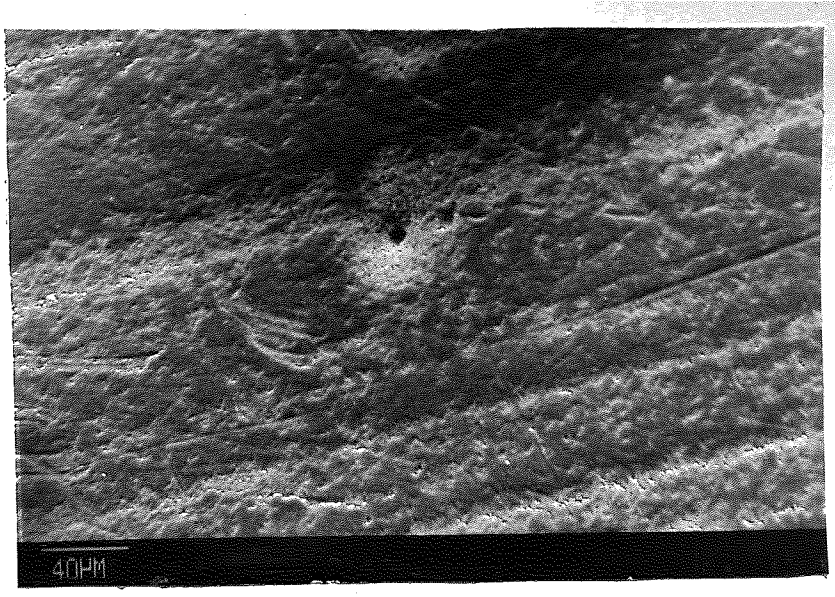

(a) corroded surface

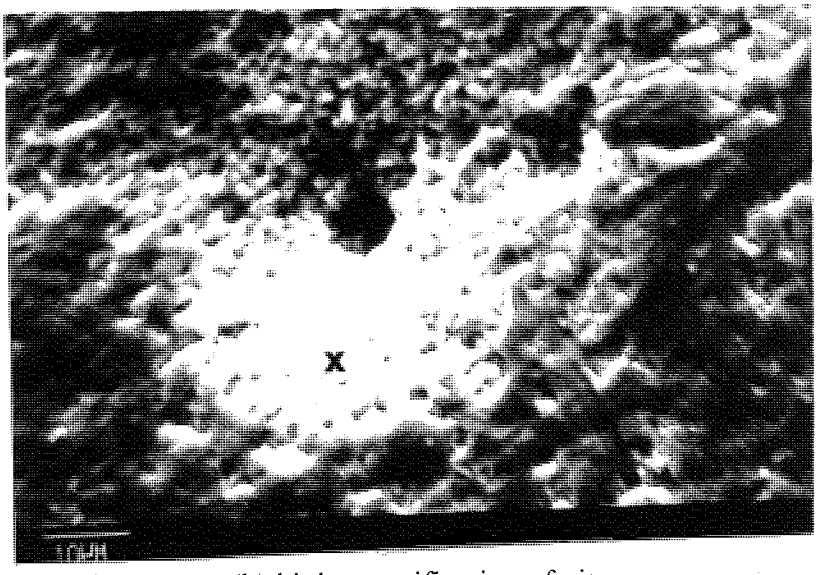

(b) high magnification of pit

Figure 103. S.E.M. micrographs of corroded surface of 7% P electroless nickel deposit heat treated at 600°C in Vacuum

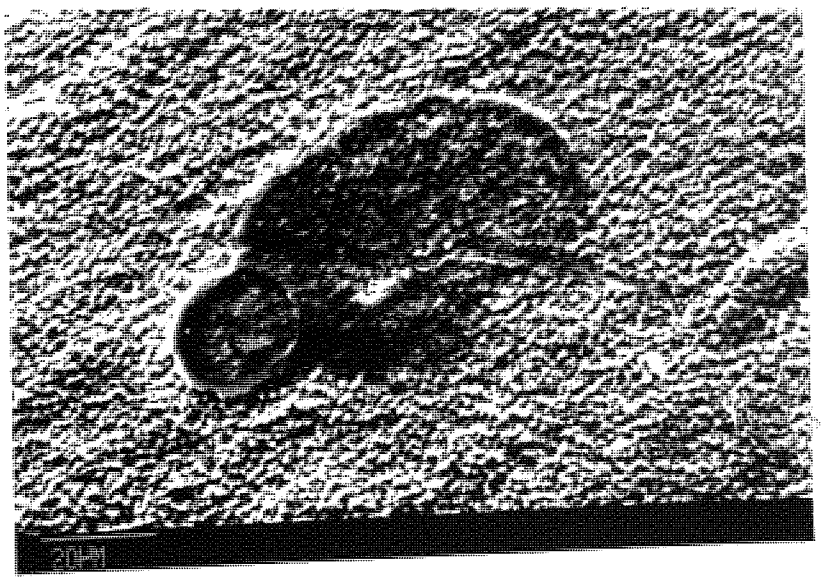

Figure 104. S.E.M. micrograph of corroded surface of Watts nickel deposit

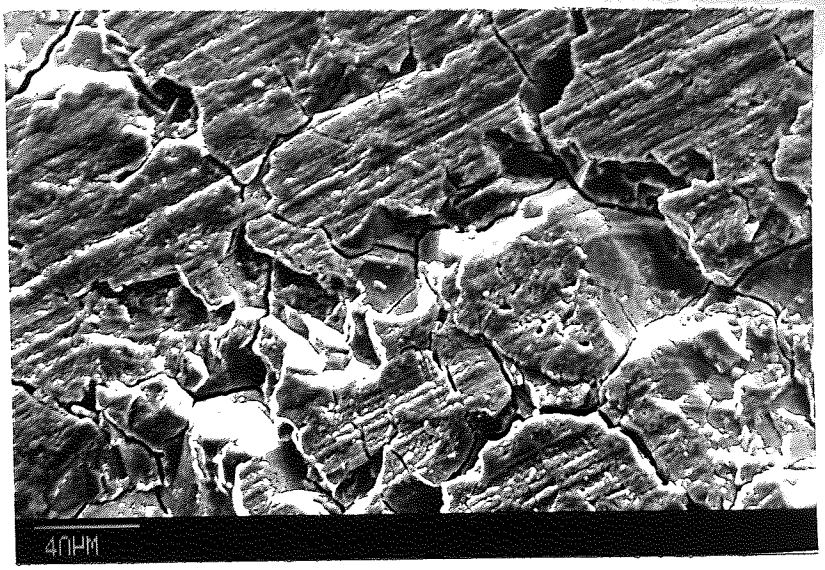

Figure 105. S.E.M. micrograph of corroded surface of 316 plasma nitrided stainless steel, showing evidence of intragranular corrosion

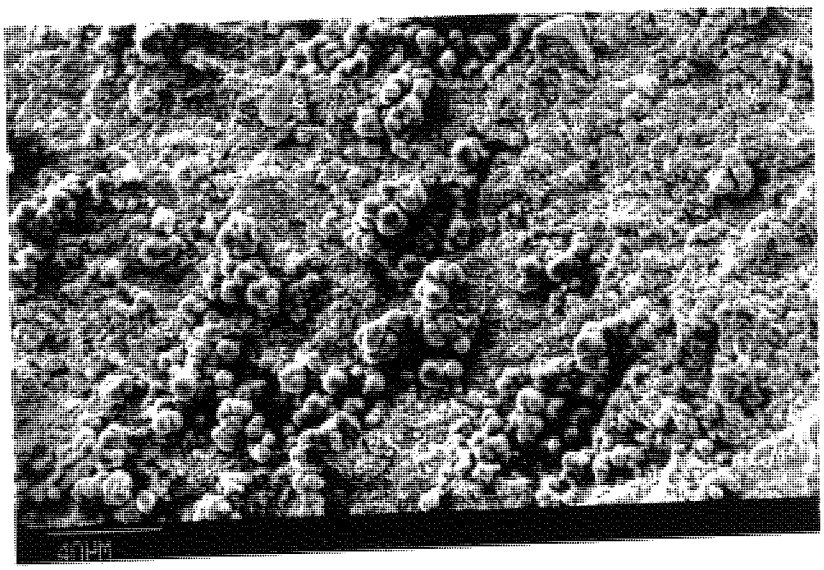

(a) corroded surface

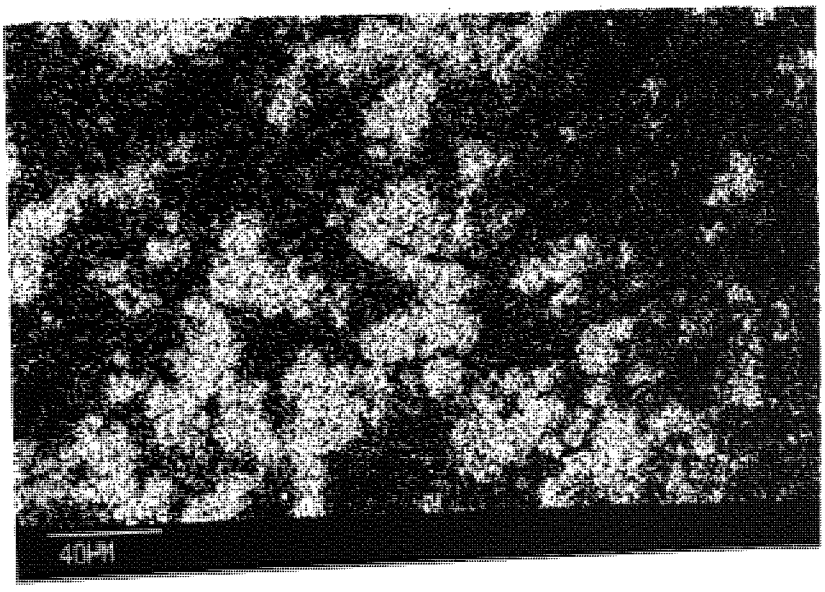

(b) iron x ray mapping

Figure 106. S.E.M. and x-ray micrographs of corroded surface of Jet-Kote deposit, showing the presence of nodular corrosion products.

products, as illustrated in Figure 104. These areas contained iron (27%), and under close examination fine pits can be seen in close proximity. The corroded surface of plasma nitrided stainless steel (316 grade) exhibited evidence of intergranular corrosion as illustrated in Figure 105. It may be that chromium nitrides are precipitated at the grain boundaries and therefore, areas adjacent to grain boundaries are denuded of chromium. Alternatively, precipitation of chromium carbides at the grain boundaries could have occurred during the plasma nitriding treatment (570° for 20 hours). In both cases differences in electrode potential between the grain boundaries and grain would lead to the formation of microgalvanic corrosion cells. The corroded surface of the Jet-kote deposit exhibited nodules of iron rich corrosion products, as evident from the iron x-ray mapping (Figure 106 (a)). Thus, it would appear that it is the presence of interconnecting porosity which provides the necessary pathway for corrosive agents (e.g. chlorides) to attack the substrate.

### 7.4.6. Electron Probe Microanalysis of Corroded Electroless Nickel Deposits

Scanning electron microscopy of cross sections of corroded electroless nickel deposits revealed severe corrosion of the substrate, as illustrated in Figure 107(a). This type of exfoliation was exhibited by all electroless nickel deposits, except those heat treated at 600°C. Electron probe microanalysis may be used to determine accurately the chemical composition across the deposit in the exfoliated areas and, also, where the deposit was intact (good areas). Electron probe microanalyses of corroded electroless nickel deposits, after correction for x-ray fluorescence and absorption effects, are given in Tables 35 to 38. The nickel concentration was determined by difference, and the number of analyses is given in the Tables.

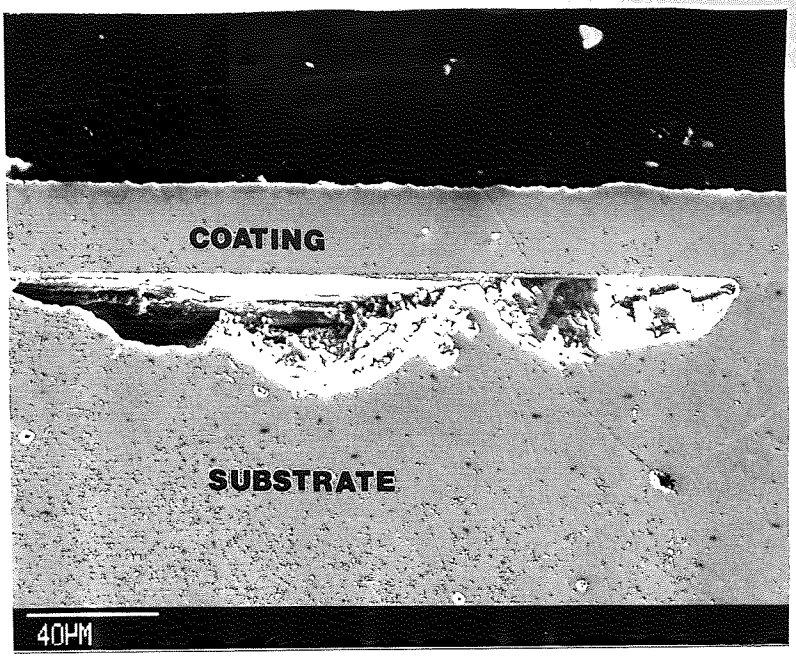


(a) 7 % P electroless nickel deposit heat treated at 400 C

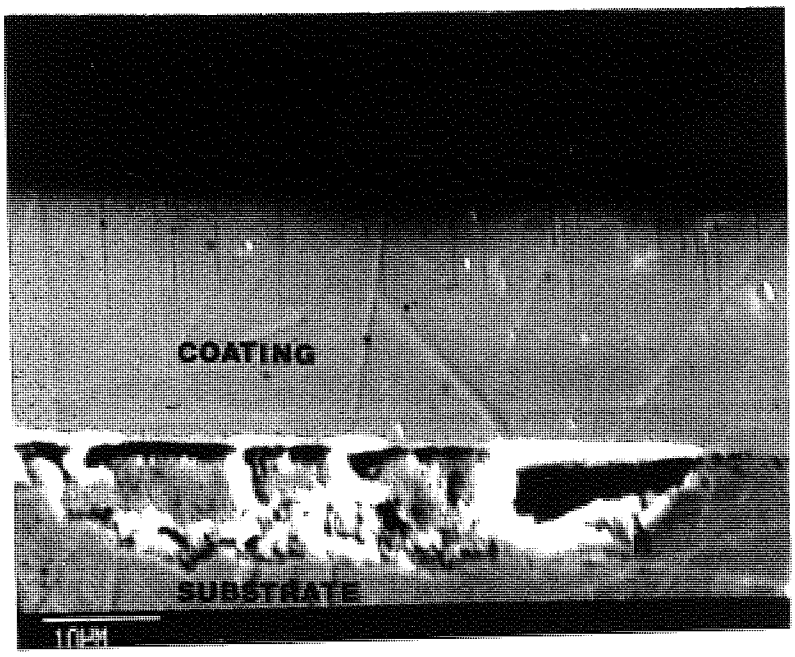


(b) asplated 9 % P electroless nickel deposit

Figure 107. S.E.M. micrographs of corroded electroless nickel deposits, in cross-section, showing exfoliation of the deposit

Table 35. Electron probe microanalysis (after ZAF correction) of 7% P electroless nickel deposits

| Deposit Condition | Ni % | P% ± S.D. | No.of Analyses | t value | t limits (0.001) | Reject or Accept Null Hypothesis | % Cl at Deposit / Substrate Interface |
|---|---|---|---|---|---|---|---|
| As-Plated | 93.047 | 6.963±0.236 | 24 | | | | |
| Corroded, Un-Heat Treated | | | | | | | |
| Good Area | 93.832 | 6.176±0.161 | 8 | 8.231 | +3.646 -3.646 | R | - |
| Good Area | 93.136 | 6.873±0.342 | 8 | 0.833 | " | A | - |
| Exfoliated Area | 93.007 | 7.003±0.333 | 8 | -0.374 | " | A | 1.541 |
| " | 92.938 | 7.072±0.287 | 8 | -1.072 | " | A | 2.228 |
| Corroded, Heat Treated at 400°C | | | | | | | |
| Good Area | 92.512 | 7.499±0.172 | 8 | -5.899 | " | R | - |
| Good Area | 92.206 | 7.806±0.088 | 8 | -9.787 | " | R | - |
| Exfoliated Area | 92.474 | 7.525±0.133 | 8 | -6.361 | " | R | 3.149 |
| " | 93.186 | 6.824±0.088 | 8 | 1.613 | " | A | 0.617 |

KEY

R - Reject

A - Accept

S.D. - Standard deviation

Table 36. Electron Probe microanalysis (after ZAF correction) of 7% electroless nickel deposits heat treated at 600C.

| Deposit Condition | Ni % | P% ± S.D. | No.of Analyses | t value | t limits (0.001) | Reject or Accept Null Hypothesis | % Cl at Deposit / Substrate Interface |
|---|---|---|---|---|---|---|---|
| Heat Treated at 600°C (Air) | 92.097 | 7.915±0.117 | 12 | -13.12 | +3.608<br>-3.608 | R | |
| Heat Treated at 600°C (Vacuum) | 93.645 | 6.365±0.226 | 12 | 7.265 | " | R | |
| Corroded, 600 (Vac) | 92.918 | 7.042±0.134 | 7 | -7.712 | +3.965<br>- 3.965 | R | - |
| | 92.977 | 7.032±0.138 | 7 | -7.032 | " | R | - |
| | 93.474 | 6.535±0.668 | 7 | 0.818 | " | A | - |
| 600 (Air) | 92.275 | 7.737±0.407 | 7 | 1.442 | " | A | - |
| | 92.107 | 7.905±0.289 | 7 | 0.107 | " | A | - |
| | 92.364 | 7.648±0.267 | 7 | 3.040 | " | A | - |

R - Reject

A - Accept

Table 37. Electron probe microanalysis (after ZAF correction) of 9% P electroless nickel deposits

| Deposit Condition | Ni % | P% ± S.D. | No.of Analyses | t value | t limits (0.001) | Reject or Accept Null Hypothesis | % Cl at Deposit / Substrate Interface |
|---|---|---|---|---|---|---|---|
| As-Plated | 90.740 | 9.276±0.551 | 24 | | | | |
| Corroded, Un-Heat Treated | | | | | | | |
| Good Area | 91.545 | 8.468±0.445 | 8 | 3.740 | +3.646 - 3.646 | R | - |
| Good Area | 90.485 | 9.532±0.551 | 8 | -1.138 | " | A | - |
| Exfoliated Area | 90.485 | 9.532±0.495 | 8 | -1.167 | " | A | 0.805 |
| " | 90.397 | 9.620±0.579 | 8 | -1.511 | " | A | 0.647 |
| Corroded, Heat Treated at 400°C | | | | | | | |
| Good Area | 90.603 | 9.414±0.142 | 8 | -0.693 | " | A | - |
| Exfoliated Area | 90.720 | 9.296±0.175 | 7 | 0.033 | +3.659 - 3.659 | A | 9.360 |
| " | 91.516 | 8.498±0.109 | 7 | 3.672 | " | R | 0.306 |

R - Reject

A - Accept

Table 38. Electron probe microanalysis (after ZAF correction) of 12% P electroless nickel deposits

| Deposit Condition | Ni % | P% ± S.D. | No.of Analyses | t value | t limits (0.001) | Reject or Accept Null Hypothesis | % Cl at Deposit / Substrate Interface |
|---|---|---|---|---|---|---|---|
| As-Plated | 88.277 | 11.748±0.199 | 32 | | | | |
| Corroded, Un-Heat Treated | | | | | | | |
| Good Area | 88.064 | 11.961±0.085 | 8 | -2.944 | +3.570 - 3.570 | A | - |
| Exfoliated Area | 88.974 | 11.048±0.276 | 8 | 8.226 | " | R | 0.378 |
| " | 88.451 | 10.570±0.138 | 8 | 15.74 | " | R | 0.304 |
| Corroded, Heat Treated at 400°C | | | | | | | |
| Good Area | 89.568 | 10.452±0.129 | 8 | 17.430 | " | R | - |
| Exfoliated Area | 88.936 | 11.087±0.355 | 8 | 7.096 | " | R | 0.488 |
| | 88.870 | 10.149±0.242 | 8 | 19.486 | " | R | 0.388 |

R - Reject

A - Accept

From inspection of the tables, it would appear that areas which exhibited exfoliation are characterised by the presence of small amounts of chlorine (0.3-2.0% Cl) at the deposit / substrate interface. Whereas, in the 'good areas' no chlorine was detected at the interface. Figure 107(b) illustrates another exfoliated area, where fine pits (< 1μm diameter) can be seen originating from the top surface of deposit. Thus, it would appear that these fine pits provide the necessary pathways for chloride ion to attack the substrate. However, the above figure does not provide conclusive evidence because these pits cannot be seen along the whole of the deposit.

The main theme of the electron probe microanalysis studies was to investigate changes in the electroless nickel deposits after corrosion. To test the significance of the above, the students 't' distribution was applied to the results. The null hypothesis formulated was, that there is no difference in the chemical composition between un-corroded and corroded electroless nickel deposits for a given phosphorus content. The alternative hypothesis was, that there is a real difference in the chemical composition of electroless deposits after corrosion. The results were tested at a significance level of 1% (99% confidence limits). Thus, if the null hypothesis was rejected, this could be interpreted as providing almost conclusive evidence of real difference between the population mean (un-corroded) and sample mean (corroded).

Considering Table 35, it would appear that for un-heat treated (7% P) electroless nickel deposits, there is no evidence to suggest a change in deposit composition, as evident by the acceptance (3 to 1) of the null hypothesis. Whereas, for heat treated (7% P) electroless nickel deposits the null hypothesis was rejected (3 to 1) and this could be interpreted as a preferential dissolution of nickel during corrosion. From Table 36, it would appear that heat treatment of 7 % P deposits at 600°C significantly changes the deposit composition, as evident by the rejection of the null hypothesis. Heat treatment at

600°C in air would appear to increase the phosphorus content of the deposit, whereas, in vacuum the reverse was observed. The corroded electroless nickel deposits (600°C vacuum) exhibited a higher phosphorus content after corrosion, as evident by the rejection of the null hypothesis (2 to 1), whereas, for deposits heat treated at 600°C in air no trend was apparent.

For the 9% P electroless nickel deposits (Table 37) there was no evidence to suggest a change in composition after corrosion, as evident by acceptance of the null hypothesis for un-heat treated (3 to 1) and heat treated (2. to 1) deposits. However, for the 12% P electroless nickel deposits, there appears to be strong evidence to suggest that the phosphorus content of these deposits decreases after corrosion. The null hypothesis was rejected for un-heat treated deposits (2 to 1), and more convincingly for the heat treated deposits, as indicated in Table 38.

#### 7.4.4.4 Summary of the S.E.M. and Electron Probe Microanalysis of Electroless Nickel Deposits

1. Fine pits (1-2μm) diameter were observed on the corroded surfaces of as-plated and heat treated electroless nickel deposits. These pits would appear to penetrate the deposit and allow the migration of chloride ions to attack the substrate, leading to exfoliation of the deposit.
2. On the basis of electron probe microanalysis of corroded electroless nickel deposits, the following showed an increase in the phosphorus content, possibly due to preferential dissolution of nickel in the deposit.

   (a) 7% P heat treated at 400°C

   (b) 7% P heat treated at 600°C Vacuum.

In contrast, both 12% P as-plated and heat treated deposits exhibited a decrease in the phosphorus content.

## 7.5 Auger Electron spectroscopy

A study was conducted on the characterisation of the surface composition of as-plated and heat treated electroless nickel deposits, using the depth profiling technique. The depth profiles for the 7% P as-plated electroless nickel deposit are illustrated in Figure 108. The initial surface analysis indicated the presence of 55% Ni, 35% O and 10% P (atomic percentage), this would suggest a mixture of nickel and phosphorus oxides. The oxygen concentration line falls rapidly to zero after sputtering off 15nm and therefore, could be interpreted as a measure of the thickness of the oxide layer.

Heat treatment at 400°C in air significantly increases the thickness of the oxide layer (~0.18 μm), as illustrated in Figure 109. This showed the oxygen concentration profile (~38% At.) extended up to about 0.18μm and then dropped rapidly. The latter was accompanied by an increase in the nickel and phosphorus concentrations, which stabilised after about 0.27μm. It would appear that nickel oxide was the predominant oxide because the phosphorus concentration is only 4% Atomic throughout the oxide layer.

The depth profiles for electroless nickel heat treated at 600°C in air are illustrated in Figure 110, the oxygen concentration profile (~ 38% At.) extended to approximately 0.8μm from the surface. The latter represented the thickness of the oxide layer, which was approximately four times as thick as that obtained at 400°C in air. Since the phosphorus concentration in the oxide layer is very small, it would appear that nickel oxide was the predominant oxide. Sadeghi et al (143) found that electroless nickel deposits heat treated at these temperatures conferred better corrosion resistance, which was attributed to the presence of a tenacious surface oxide

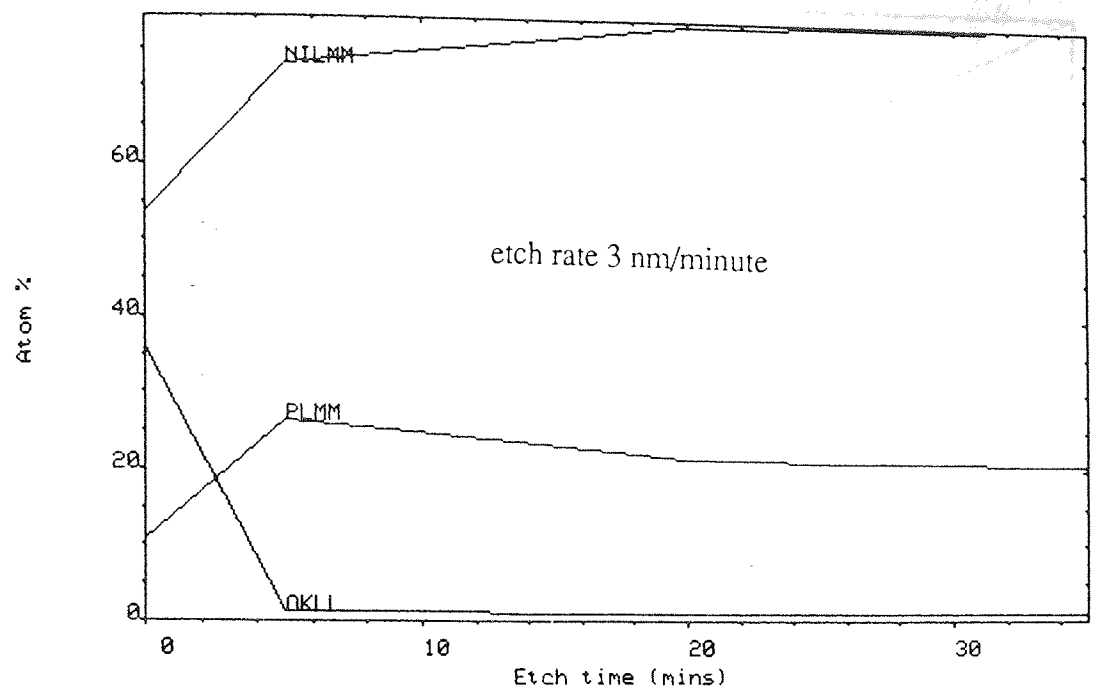


Figure 108. Depth concentration profiles for 7% P as-plated electroless nickel deposit

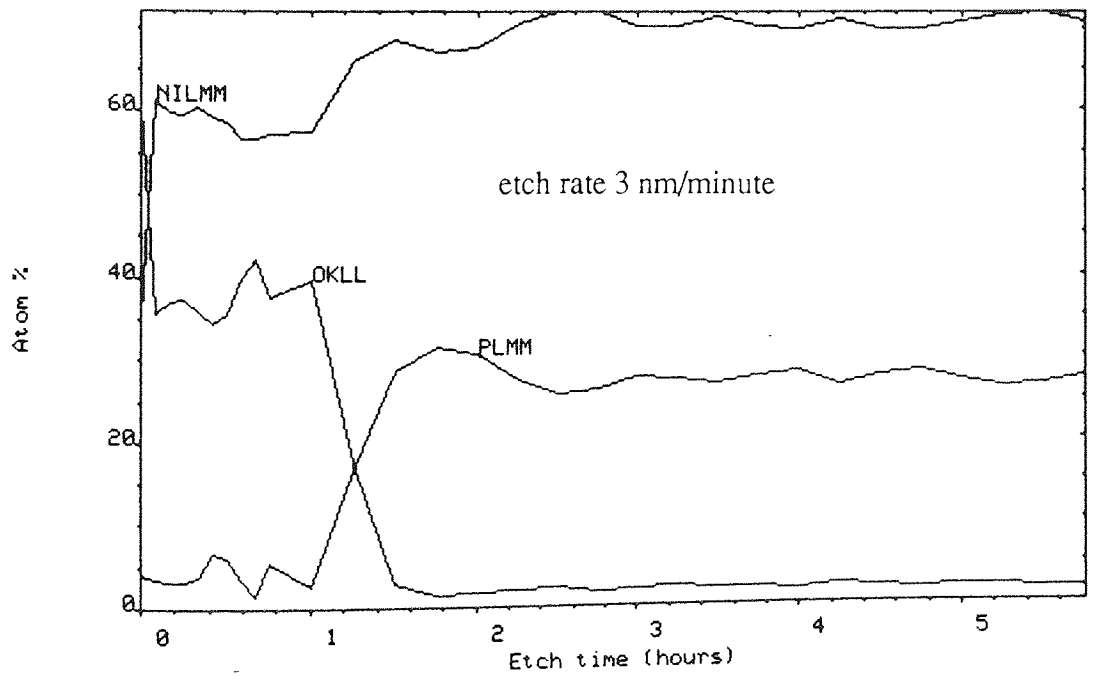


Figure 109. Depth concentration profiles for 7% P electroless nickel deposit heat treated at 400°C in air

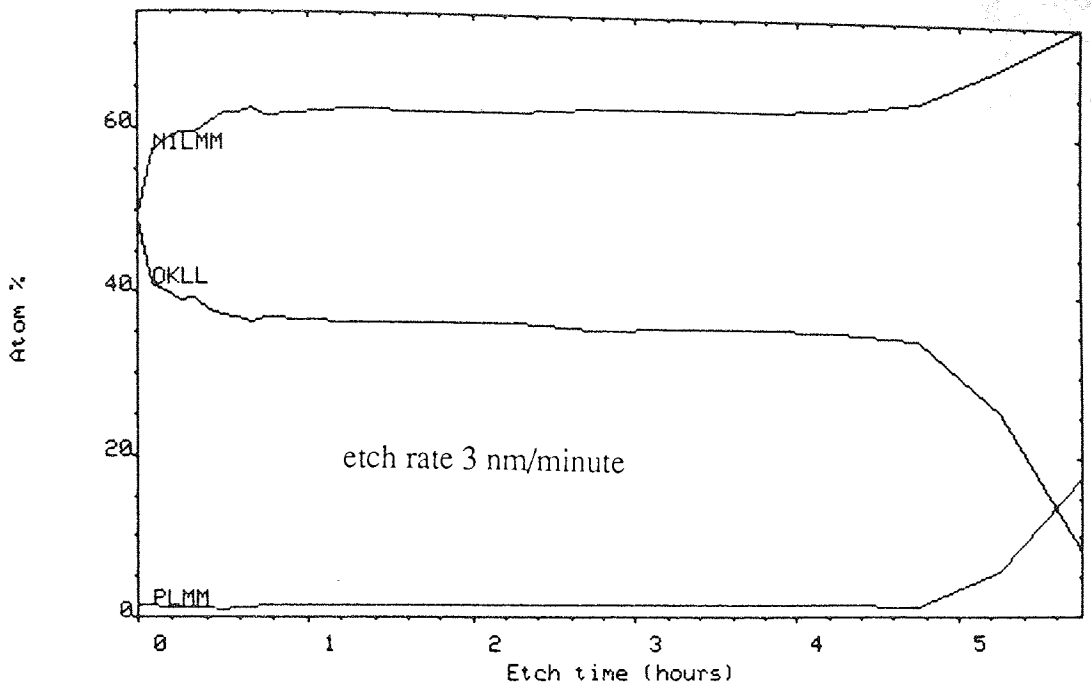


Figure 110. Depth concentration profiles for 7% P electroless nickel deposit heat treated at 600°C in air

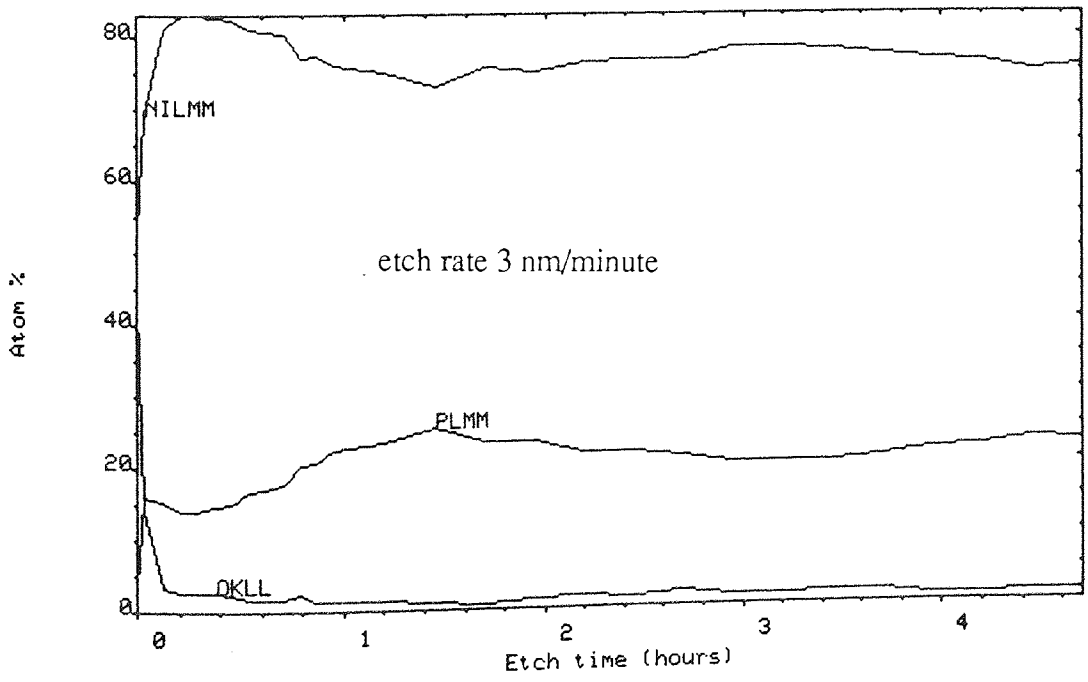


Figure 111. Depth concentration proflie for 7% electroless nickel deposit heat treated at 600 C in vacuum.

and an iron-nickel intermetallic layer. However, they did not evaluate the chemistry of the surface oxides, neither did they speculate on the nature of the oxide.

The depth profiles for electroless nickel heat treated at 600°C in vacuum are illustrated in Figure 111., these indicate the presence of a thin oxide layer; as evident by the high oxygen concentration (~ 40% At.) prior to depth profiling. However, the oxygen concentration falls rapidly, this was accompanied by an increase in the nickel concentration. The latter rose to a maximum of 82.5% Atomic at a depth of 0.036μm, whereas, the nickel concentration at the same depth for as-plated electroless nickel, heat treated at 400°C and 600°C in air was 75%, 60% and 60% respectively. These results would appear to support the hypothesis stated in Section 7.4.3 , that heat treatment of electroless nickel deposits at 600°C in vacuum conditions may result in the enrichment of nickel at it surface, due to volatisation of the phosphorus from the deposit.

## 7.6 Seal Rig Tests

The results of the seal rig tests are given in Table 39 , which lists the surface coating / treatments applied to the rotary seal rings and a description of seal faces after the test. A common failure mechanism of the seal faces was by abrasion, which was manifested in the form of heavy circumferential grooving of the seal face . It is probable that detached wear debris from the rotary seal face embedded into the soft carbon seal counterface, thereby causing abrasive attack of the rotary face. However, the carbon seal rings were re-lapped and checked for surface flatness and used for subsequent tests. The circumferential grooving of the seal faces was characterised by an increase in surface roughness and high carbon wear rates, as indicated in Table 40 . The following seals failed in this respect.

(1) 316 S11 (Austenitic stainless steel)

(2) EN 151 (Electroless nickel-substrate 431529 martensitic stainless steel)

(3) EN/TiN 137 and 151 (Electroless nickel / titanium nitride duplex coating on 316511 and 431S29 substrates respectively).

The plasma nitrided seals did not show signs of severe abrasion, as above, but were characterised by high leakage rates, which can also be interpreted as seal failure. Micro-hardness close to the worn surfaces, in cross section, of plasma nitrided 137 and 157 seal rings gave values of 220 and 310 HV respectively. This would strongly suggest that the plasma nitrided layer had been completely worn away. However, it must be stated that as-received plasma nitrided seals had a poor surface finish, characterised by uneven nitriding and small pits. This necessitated post lapping of the seals, which most likely removed the important compound layer. The latter is associated with maximum hardness and non-galling properties.

The only seals that performed satisfactorily were as follows:

(1) 431 S29

(2) EN 137 (Electroless nickel - substrate 316S11)

(3) ENSiC 137 and 151

(4) Jet-kote 137 and 151

The 431529 seal exhibited evidence of light circumferential scoring, whereas, the electroless nickel coated seal (EN 137) showed no signs of abrasion of the seal face. Surprisingly, the oxide glaze formed during heat treatment was still evident after the test, this would suggest that seal faces were separated by a thin hydrodynamic film. In contrast, the electroless nickel (EN 151) seal exhibited heavy circumferential grooving of seal face. The only major difference between the above coated seals, apart from the difference in substrate hardness, was the pretreatment prior to electroless nickel plating. For the martensitic stainless steel (431S29) a chloride based nickel strike solution was

used, however, this caused severe pitting of the austenitic stainless steel (316S11). Therefore, for the latter a sulphate based strike solution was adopted. Hence, it may be poor adhesion of the electroless nickel deposit to the martensitic substrate that was responsible for the seal failure. The best performance was achieved by the Jet-kote and electroless nickel silicon carbide composite coated seals, neither of these showed any leakage of the pumped fluid or abrasion of the seal faces. However, the latter caused some wear of the carbon seal rings as indicated in Table 40 . In contrast, seals coated with Jet-kote deposit showed no measurable wear on the carbon seal rings.

*type cartridge mechanical seals after operating at a pV factor of 85 bar.m.s$^{-1}$ for 200 hours*

| Test Number | Rotary Seal Ring | Stationary Seal Ring | Visual Appearance of Seal Faces After 200 Hours Testing | Leakage |
|---|---|---|---|---|
| 1 | 316511 (137) austenitic stainless steel | 304 Carbon | Heavy grooving across both rotary and stationary seal faces. The former had carbon deposits in the bore, indicative of high carbon wear rates. | Initial leakage of 1.7cm$^3$/hr which reduced to zero after 50 hours. |
| 2 | 431529 (151) martensitic stainless steel | 304 carbon | Light circumferential grooving on both rotary and stationery seal faces. In general, both seal faces were in good condition. | Initial leakage 0.05cm$^3$/hr which reduced to zero after 50 hours. |
| 3 | Plasma (137) nitrided 316511 steel | 304 carbon | Light circumferential scoring on both stationary and rotary seal faces. | High leakage 0.11 cm$^3$/hr |
| 4 | Plasma (151) nitrided 431529 steel | 304 carbon | Carbon deposits on inner and outer edges of rotary seal face. Carbon seal face showed light circumferential scoring. | As above. |
| 5 | EN/TiN (137) Electroless nickel/ titanium nitride duplex coating | 304 carbon | TiN layer partially worn away, circumferential grooving and carbon deposits in rotary seal ring bore. Carbon seal face showed heavy circumferential grooving and deposits in the bore. | No leakage. |
| 6 | EN/TiN (151) Electroless nickel/ titanium nitride duplex coating | 304 carbon | TiN layer completely worn away, heavy grooving and carbon deposits in rotary seal ring bore. Carbon seal face showed circumferential grooving | No leakage. |

continued

Table. 39. continued

| Test Number | Rotary Seal Ring | Stationary Seal Ring | Visual Appearance of Seal Faces After 200 Hours Testing | Leakage |
|---|---|---|---|---|
| 7 | EN (137) Electroless nickel on 316511 steel | 304 carbon | Rotary seal face exhibited the blue/purple oxide glaze formed during prior heat treatment (400°C in air). Therefore, indicating no apparent wear on the seal face. The carbon seal showed fine scoring on the face. | High, 0.15 $cm^3/hr$ |
| 8 | EN (151) Electroless nickel on 431529 steel | 304 carbon | Heavy circumferential grooving of both stationary and rotary seal faces. Carbon deposits were evident in the bores of the seals. | Low, 0.09 $cm^3/hr$ |
| 9 | ENSiC (137) electroless nickel + SiC composite on 316511 steel | 304 carbon | Slight circumferential scoring on rotary seal but in good condition. No apparent abrasion on carbon seal face was evident. | No leakage |
| 10 | EnSiC (151) | 304 carbon | As above | No leakage |
| 11 | Jet-kote 137 Wc/Ni/W-Cr-carbides on 316511 steel | 304 carbon | Rotary seal face in good condition and no abrasion of rotary or stationary face was evident. Although very slight carbon deposition was noted in the rotary seal ring bore. | No leakage |
| 12 | Jet-kote 151 Wc/Ni/W-Cr-carbides on 431529 steel. | 304 carbon | As above | No leakage |

Table 40 . The surface finish and carbon nose wear rates (μm/h) of surface coated / treated F.F.E.T. type mechanicals seals after operating at a pV factor of 85 bar.m.s$^{-1}$ for 200 hours

| Test Number | Materials or Surface coatings/ Treatments | Surface Finish of Seal Rings (μm) Before | After | Carbon Nose Wear Rate (μm/hr) | Predicted Life (over 2.5mm) of Carbon Seal (hrs) |
|---|---|---|---|---|---|
| 1 | 316511 | 0.05 | 1.50 | - | |
| | 304 carbon | 0.13 | 1.78 | 0.275 | 9,091 |
| 2 | 431529 | 0.06 | 0.08 | - | |
| | 304 carbon | 0.14 | 0.25 | - | - |
| 3 | Plasma 137 | 0.05 | 0.34 | - | |
| | 304 carbon | 0.25 | 0.82 | 0.035 | 71,428 |
| 4 | Plasma 151 | 0.05 | 0.07 | | |
| | 304 carbon | 0.15 | 0.23 | 0.050 | 50,000 |
| 5 | EN/TiN 137 | 0.03 | locally damaged | - | |
| | 304 carbon | 0.14 | 1.63 | 0.288 | 8,695 |
| 6 | EN/TiN 151 | 0.03 | 2.13 | - | |
| | 304 carbon | 017 | 1.95 | 0.475 | 5,263 |
| 7 | EN 137 | 0.05 | 0.05 | - | |
| | 304 carbon | 0.24 | 0.15 | - | - |
| 8 | EN 151 | 0.10 | 2.25 | | |
| | 304 carbon | 0.21 | 2.30 | 0.075 | 33,333 |
| 9 | ENSiC 137 | 0.028 | 0.06 | | |
| | 304 carbon | 0.230 | 0.10 | 0.075 | 33,333 |
| 10 | ENSiC 151 | 0.028 | 0.11 | | |
| | 304 carbon | 0.110 | 0.30 | 0.075 | 33,333 |
| 11 | Jet-kote 137 | 0.030 | 0.08 | | |
| | 304 carbon | 0.120 | 0.10 | - | - |
| 12 | Jet-kote 151 | 0.020 | 0.13 | | |
| | 304 carbon | 0.150 | 0.13 | - | - |

| | |
|---|---|
| Test Duration | 200 hours |
| Fluid Pressure | 15 bar. (1.5mn/m$^2$) |
| Flow Rate | 15 litres/minute |
| Seal Balance | 65% |
| Pump Speed | 3000 r.p.m. |

### 7.6.1 Scanning Electron Microscopy of Worn Seal Faces

Abrasion of 316S11 (austenitic stainless steel) seal face was evident by deep parallel grooves, as shown in Figure 112. In contrast, the 431S29 (martensitic stainless steel) exhibited fine random scratchings of the seal face, as shown in Figure 113(a). These are probably lapping marks and unlikely to be due to seal wear, in which case parallel marks would have been expected. Near the bore of the seal extensive adhesive transfer of the carbon seal material occurred, as shown in Figure 113(b). In this region boundary lubrication seems to be predominant, due to convergence of seal faces, resulting in intimate contact and prevention of leakage.

The plasma nitrided (Plasma 137) seal face exhibited light abrasion, evident by fine parallel gouging marks, as shown in Figure 114(a). In the centre of the photomicrograph is an area where much deeper gouging had occurred, as shown at higher magnification in Figure 114(a). Material removed in this manner, would tend to embed into the softer carbon counterface seal, possibly resulting in further abrasive action. The wear topography of the plasma nitrided (Plasma 151) seal face was very similar to the above.

The worn surface of the electroless nickel coated seal (EN 151) exhibited considerable gouging of the seal face, as shown in Figure 115(a). The nickel x-ray mapping identifies the areas where the deposit had been partially removed. Further below this region, deeper and wider gouging channels were observed, as shown in Figure 115(c). These channels would appear to contain wear debris, which was probably responsible for the abrasive action. In contrast, the electroless nickel coated seal (EN 137), did not show any evidence of abrasive wear, in fact, the seal face appeared to be unworn, as illustrated by the presence of surface oxides formed during heat treatment. The high leakage rate observed for this seal, would suggest that the seal faces were separated by


Figure 112. S.E.M. micrograph of worn seal face of austenitic stainless steel (316S11) rotary seal ring

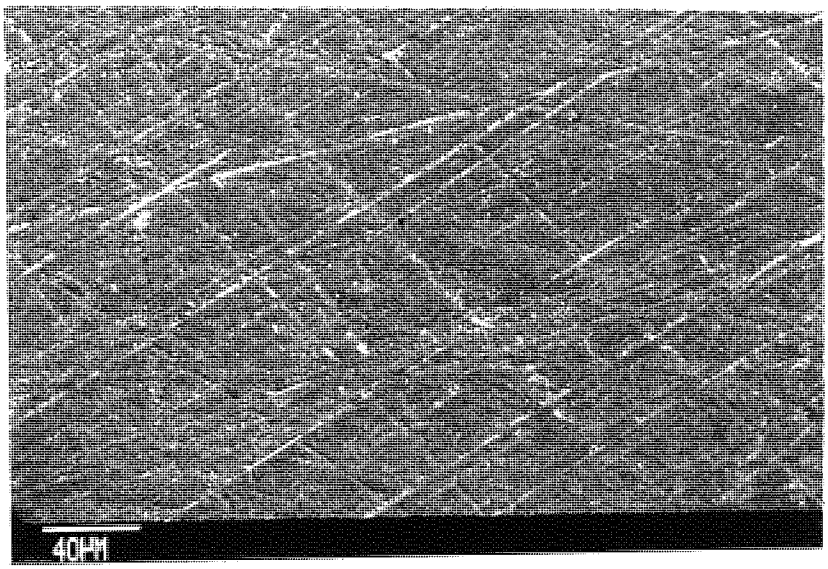


(a) worn seal face

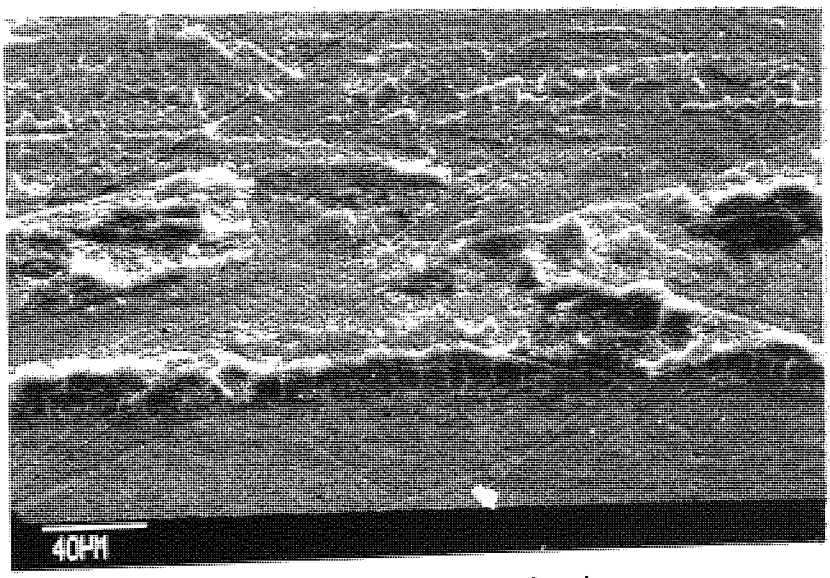


(b) adhesive transfer of carbon

Figure 113. S.E.M. micrographs of worn seal face of martensitic stainless steel (431S29) rotary seal ring

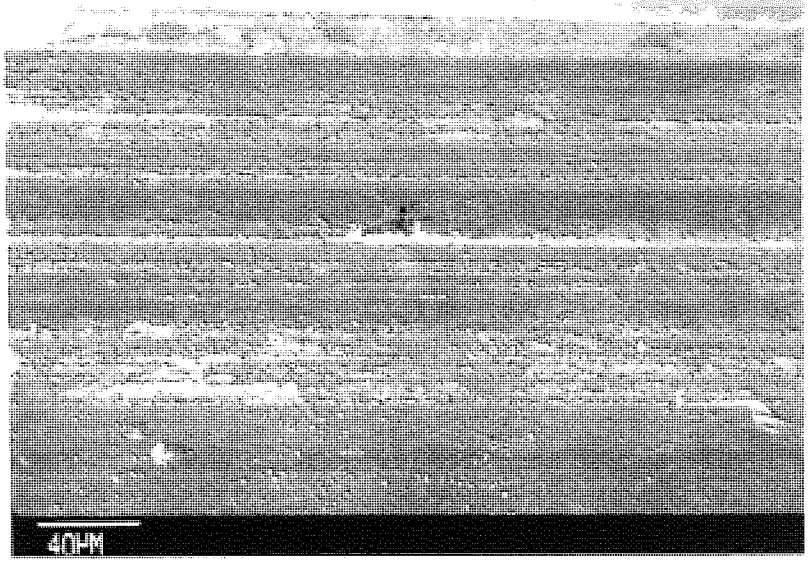


(a) worn seal face

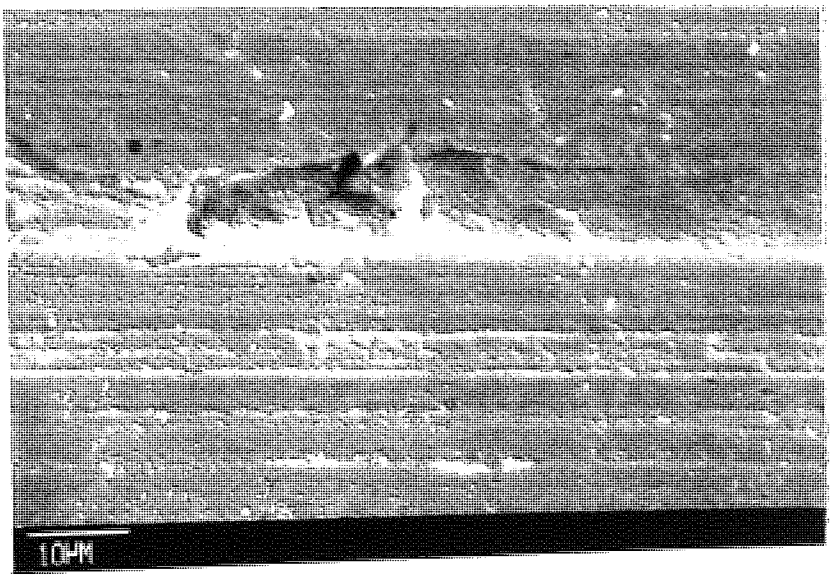


(b) higher magnification

Figure 114. S.E.M. micrograph of worn seal face of plasma nitrided austenitic stainless steel (316S11) rotary seal ring

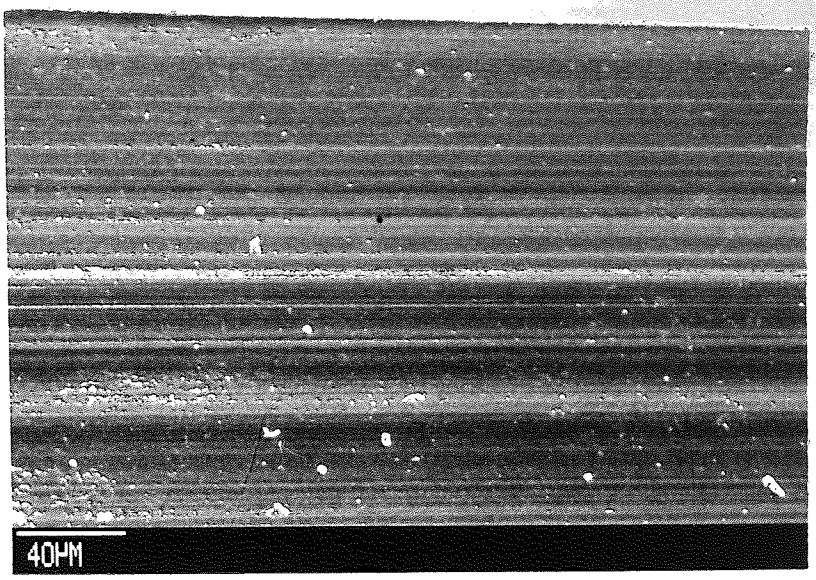


(a) worn seal face

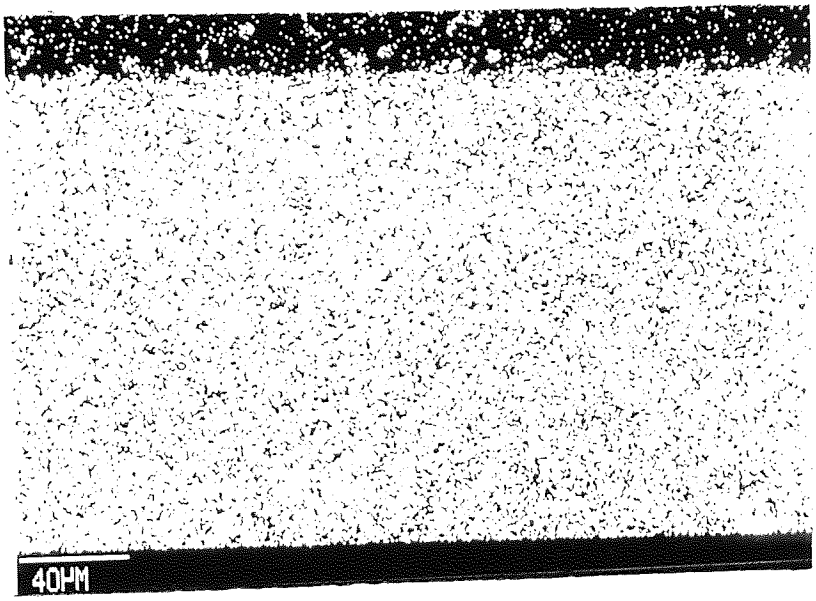


(b) nickel x ray mapping

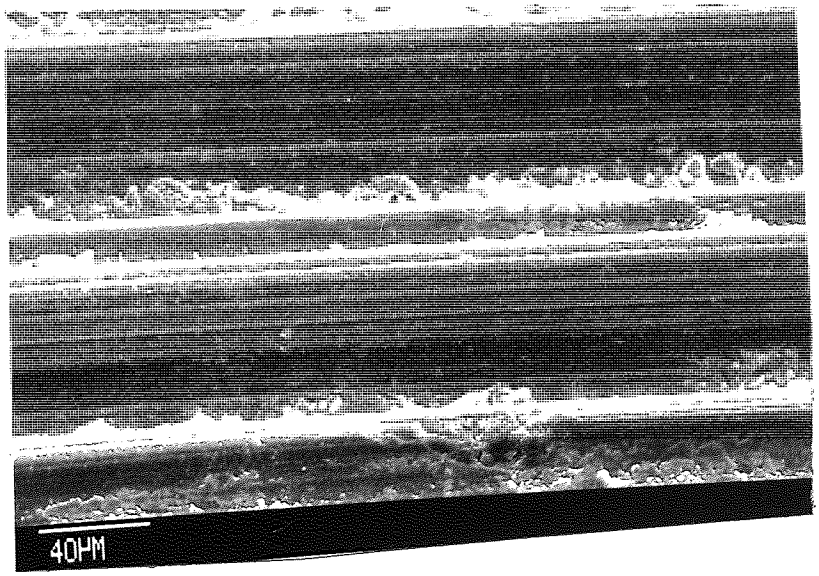


(c) ploughing of seal face

Figure 115. S.E.M. and x-ray micrographs of worn seal face of electroless nickel coated martensitic stainless steel ring

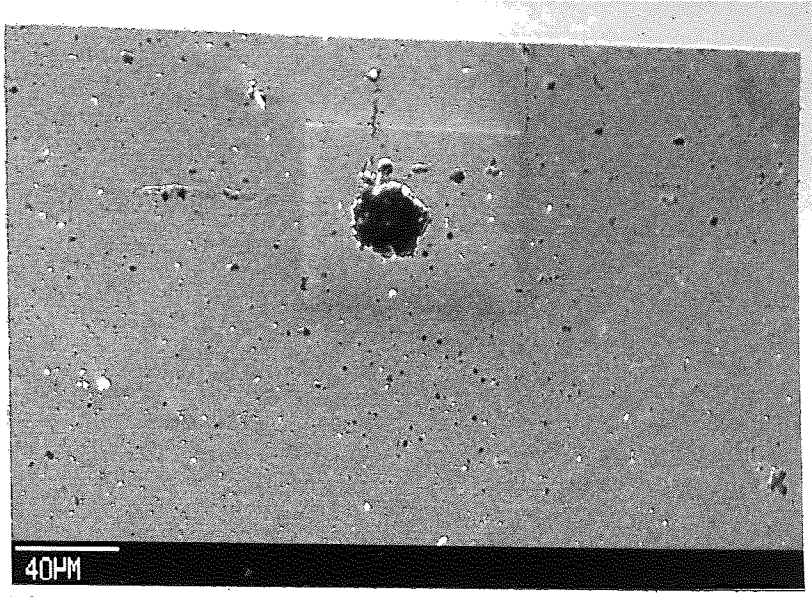


Figure 116. S.E.M. micrograph of worn seal face of electroless nickel coated austenitic stainless steel ring

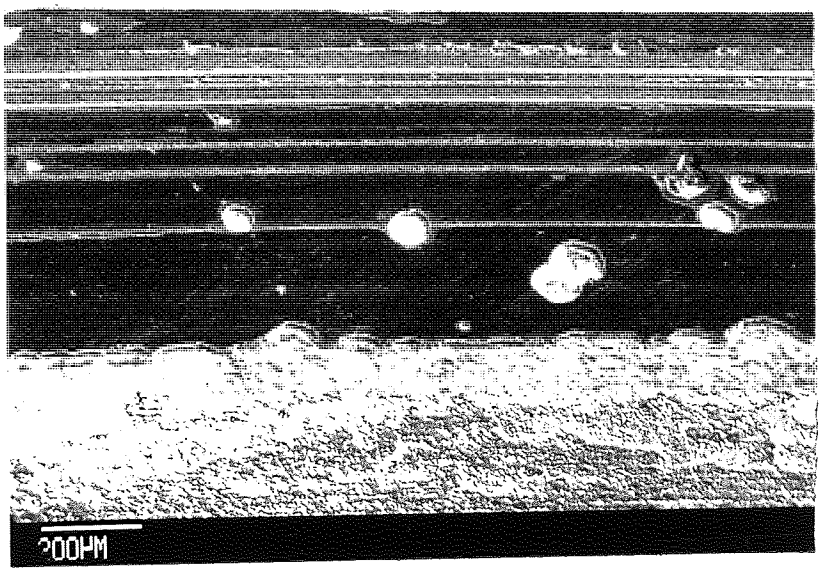


(a) worn seal face

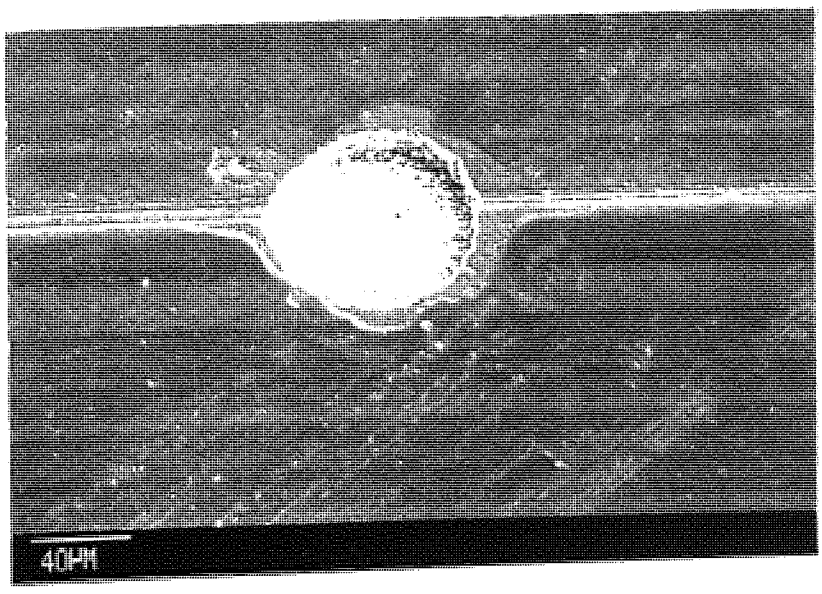


(b) higher magnification of worn seal face

Figure 117. S.E.M. and x-ray micrographs of worn seal face of electroless nickel / titanium nitride duplex coated austenitic stainless steel seal ring.

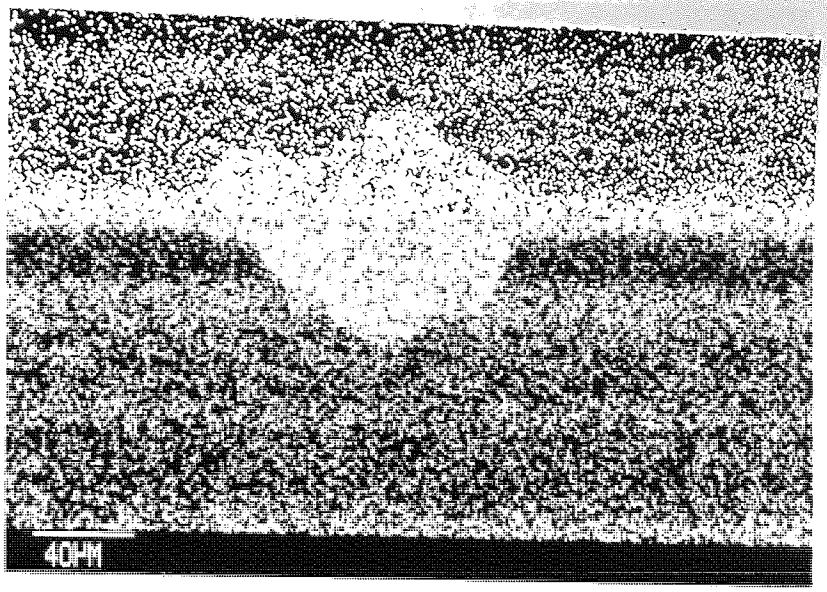


(c) nickel x ray mapping

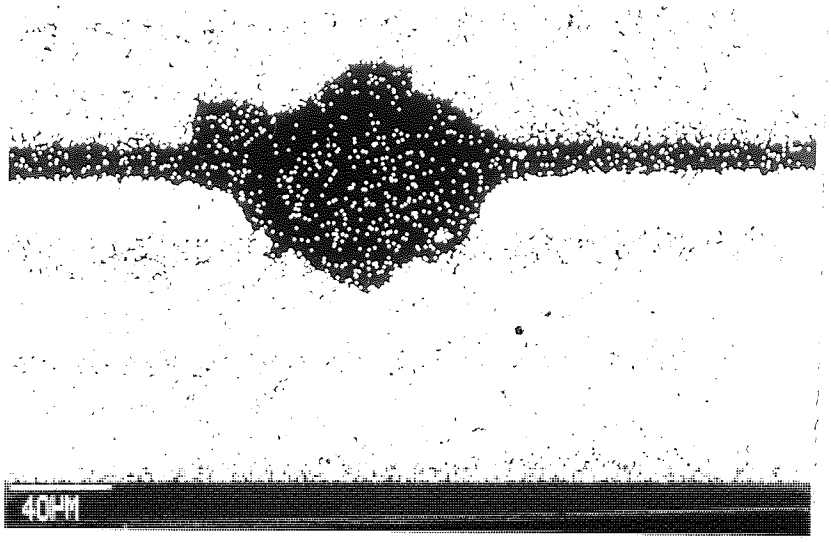


(d) titanium x ray mapping

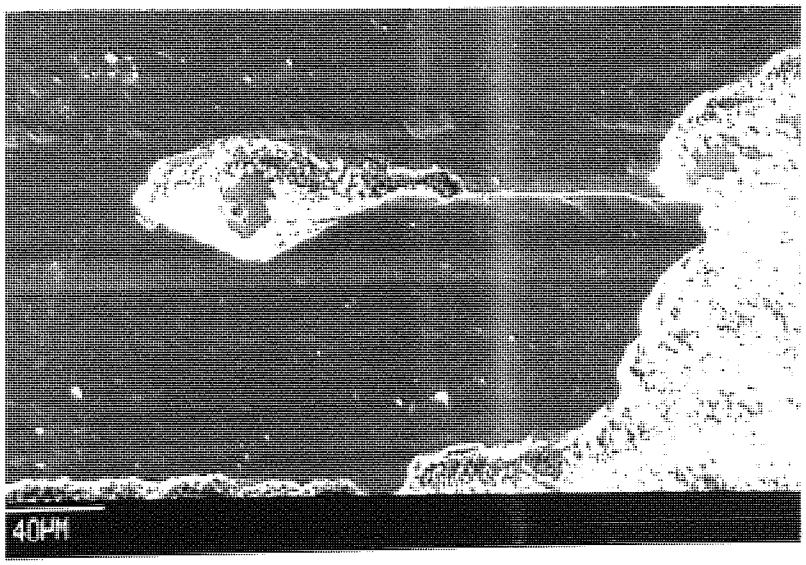


(e) cohesive failure of electroless deposit

Figure 117. S.E.M. and x-ray micrographs of worn seal face of electroless nickel / titanium nitride duplex coated austenitic stainless steel seal ring.

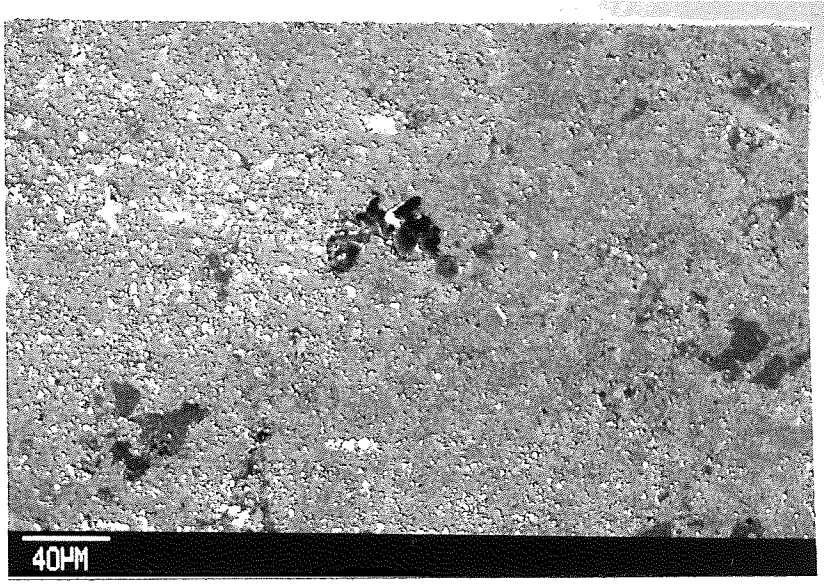


(a) worn seal face

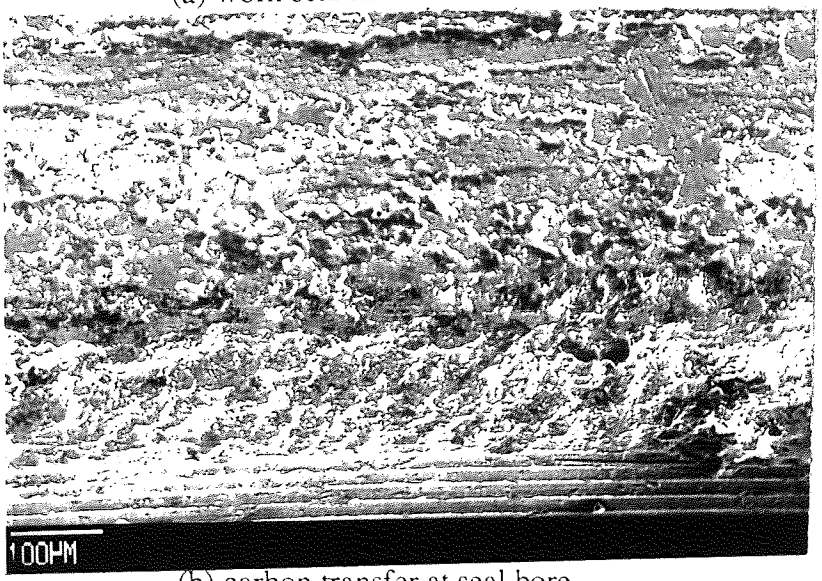


(b) carbon transfer at seal bore

Figure 118. S.E.M. micrographs of worn seal faces of Jet-Kote coated austenitic stainless steel seal ring

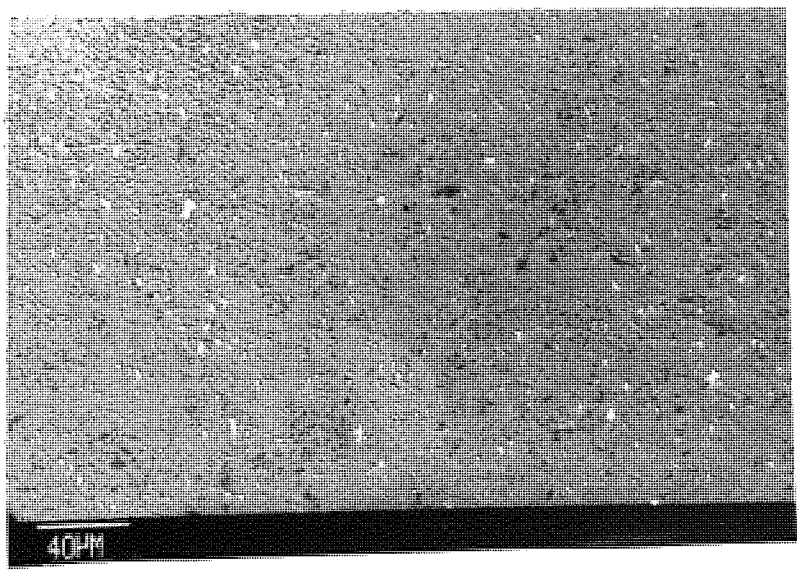


Figure 119. S.E.M. micrograph of worn seal face of electroless nickel silicon carbide composite coated martensitic stainless steel seal ring.

a thick lubricant film. The only interesting feature on the seal face was the presence of numerous pits, as shown in Figure 116. The large central pit appeared to be filled in by carbon seal material. The directionality of the smaller pits above the large central pit, suggest that their origin may be related to the surface topography and pre-treatment sequence prior to electroless nickel plating.

The electroless nickel / titanium nitride coated seal (EN / TiN 137) face exhibited partial removal of the titanium nitride layer, as shown in Figure 117(a). The important feature on this photomicrograph was the intersection of the gouging marks with a large circular crater, as shown at higher magnification in Figure 117(b). Titanium and nickel x-ray mapping showed that the gouging marks leading towards the crater, corresponded to the removal of the titanium nitride layer. The crater had a rough appearance which suggests cohesive fracture of the electroless nickel deposit. The removal of deposit material would certainly lead to further abrasive wear; particularly if it embeds into the softer counterface. However, the cause of the localised rupture of the deposit seems unclear. Examination of other craters revealed small pits in the substrate, as shown in Figure 117(e). This would suggest that poor adhesion of deposit, coupled with shear stresses generated at the coating-substrate, could lead to exfoliation of the deposit. The cause of the pitting may be related to the pre-treatment sequence prior to electroless nickel plating.

The Jet-kote coated seals (JET-KOTE 137 and 151) did not show any signs of abrasion of the seal faces, although small craters filled with carbon seal material were observed, as shown in Figure 118(a). Near the bore of the seal considerable carbon seal material transfer (Figure 118(b)) had occurred, which presumably provided the necessary intimate contact to prevent leakage of the pumped fluid. The electroless nickel silicon carbide composite coated seals (ENSiC 137 & 151) showed no evidence of abrasion of

the seal face, as shown in Figure 119. However, it must be stated that prior to composite plating, the seal faces were grit blasted and therefore, the better performance of the composite coated seals compared to the conventional electroless nickel may be due to better adhesion in the former case.

### 7.6.2 Summary of Seal Rig Tests

The best seal performances were exhibited by Jet-kote and electroless nickel silicon carbide coated seals. The failure of the electroless nickel and electroless nickel / titanium nitride duplex coated seals was probably due to inadequate adhesion of the deposits to the substrate. Abrasion of the seal faces was the principal wear mechanism.

# CHAPTER VIII

## 8.0. DISCUSSION

The main factors which affect the performance of mechanical seals are the wear and corrosion of seal faces. On the basis of the literature search, certain surface coatings / treatments were selected as possible candidates for mechanical seal application. The main objectives of the research was to evaluate their wear and corrosion behaviour, using the pin-on-disc wear tester and electrochemical corrosion studies respectively.

### 8.1. Wear Behaviour of Surface Coatings / Treatments

The wear rates, coefficients of friction and wear mechanisms have been discussed in the previous chapter. However, collective consideration of the tribological properties of the surface coatings / treatments with parameters such as surface finish and hardness revealed little correlation, as shown in Table 41 . The coefficient of linear regression, $\tau$, was calculated using experimental results in tables 12, 13, 24, 25, 26, 27. The values of the coefficient of correlation, $\tau$, is always between -1 and +1. Considering two variables x and y, a value of '$\tau$' equal to -1 indicates a prefect linear relationship between sample values of x and y, with the value of y decreasing as the value of x increases. If there is no relationship between sample values of x and y, then '$\tau$' will have a value near zero, as exemplified by the relationship between $\mu$ and suface roughness at 4 kg load. A strong connection between the two variables would be indicated by values of '$\tau$' in the range 0.8 - 0.95, however, the determined coefficients of correlation were much lower, as indicated in Table 41.

Table 41. The coefficient of correlation for various tribological relationships

| Relationships | Coefficient of Correlation 'τ' Load on Pin | |
|---|---|---|
| | 4kg | 8kg |
| μ Vs Surface Roughness | $4.48 \times 10^{-8}$ | 0.631 |
| μ Vs Hardness | - 0.675 | 0.657 |
| μ Vs Wear Rate | 0.5093 | - 0.498 |
| Wear Rate Vs Hardness | - 0.6197 | - 0.318 |

Where, μ refers to the coefficient of dynamic friction.

Thus, no trends can be inferred from the above relationships. The main reasons for the lack of agreement between the various parameters is due to the complexity of wear and friction. In this section, an attempt is made to explain why there is a disparity in the observed wear mechanisms. The tribological performance of the surface coatings / treatments is affected by the following factors:

(1) Flash temperatures generated at surface asperites

(2) Mutual solubility

(3) Tribo-oxidation products

(4) Microstructure.

High transient temperatures may be generated at asperites, due to dissipation of

frictional energy during sliding wear. The temperatures may be high enough to cause the following effects:

(a) Martensitic phase formation, as reported by Welsh[62], but this effect is irrelevant to the surface coatings / treatments investigated.

(b) Production of surface oxides (tribo-oxidation products) which prevent intermetallic adhesion and therefore, reduce wear and friction. It is interesting to compare the wear behaviour of electroless nickel and the electroless nickel silicon carbide composite coating at 8kg load. The worn surface of the former was highly polished, whereas in the case of the composite coating, considerable adhesive transfer of disc material was evident. The silicon carbide particles in the electroless nickel matrix caused ploughing of the disc, which was reflected in the high values of the static coefficient of friction. High temperatures may be generated at the silicon carbide particles, which could rapidly oxidise the ploughed disc material, due to its large surface area to volume ratio. The presence of adhesive islands on the composite coatings must be directly related to the presence of silicon carbide particles, since no such features were observed on the conventional electroless nickel worn surface. The lower wear rate of the composite coating may be due to its ability to promote oxidational wear of the disc, thereby minimising the wear of electroless nickel matrix. The nickel content of the wear debris from the composite and conventional deposit was 7.21 and 85.12% Ni respectively; this would support the above mechanism.

(c) Heat generated at the sliding surfaces may result in thermal gradients being set up if it is not efficiently conducted away. This may lead to differential thermal expansion

and therefore, cracking of the surface coating. This effect is particularly relevant to mechanical seals, and the susceptibility of surface coatings / treatments to thermal cracking is considered in more detail later on.

The main concept of adhesive wear theory, is the formation of microwelds due to elastic-plastic asperity interactions. The tendency to form strong welds is greater, if there is high mutual solubility between the two components of the wear couple(66). In general, ceramic based materials, such as titanium nitride, tungsten carbide and chromium oxide have low mutual solubility with iron because these compounds have lower surface energies compared to their respective parent metals. It is also important to mention that the contact area is inversely proportional to the hardness, thus, a combination of small and weak microwelds would be a primary mechanism of protection against wear. Iron x-ray mapping revealed the transfer of iron to the worn surfaces, for example on titanium nitride and vanadium carbide deposits. It is likely that the iron pick-up corresponds to a thin iron oxide layer, which is scraped off by ploughing action of asperites, consequently, fresh transfer of iron could occur which rapidly oxidises. The removal of the oxide would be accompanied by some loss of coating material, but the overall effect is to reduce wear by contamination of the rubbing surfaces by surface oxides.

The microstructure can have a profound effect on the wear behaviour of materials. Guang-Xi-Lu et al (164) studied the wear resistance of hypereutectic electroless nickel deposits, and showed that heat treatment at 600°C conferred better wear resistance than deposits heat treated at 400°C. This was attributed to a greater volume fraction of ductile nickel phase formed at 600°C, resulting in higher fracture toughness : hardness ratio

compared to deposits heat treated at 400°C. In contrast, Gawne and Ma (165) have attached considerable significance to the role of nickel phosphide precipitates, which are thought to prevent adhesive type wear because of their low mutual solubility with iron. The worn surfaces of electroless nickel pins were highly polished and showed no evidence of adhesive transfer, which supports Gawne and Ma's proposition. Whereas, for the post fused nickel-chromium-boron sprayed deposit, considerable adhesive transfer was evident on the worn surfaces, presumably due to its higher mutual solubility with iron.

In thermally sprayed deposits, such as chromium oxide and Jet-kote, interparticle bonding is an important factor affecting their wear resistance. The presence of oxidised, unmelted and/or porosity are potential sites for crack initiation. The wear of the chromium oxide is primarily due to intergranular failure of the deposit. The cause of this is due to the combination of the following factors:

(a) Sprayed chromium oxide deposits are susceptible to heat checking which could explain the observed surface cracks (Figure 36).

(b) Repeated loading and unloading of asperites during sliding may lead to a fatigue cycle and eventual brittle fracture of asperites.

(c) Evans and Wilshaw (166) have shown that when a hard sharp asperity slides over an elastic glassy material, cracks can propagate from the asperity tip radially, laterally and axially. Thus, particles of chromium oxide removed by (a) and/or (b) could plough the surface and enhance the propagation of cracks (Figure 39).

The Jet-kote worn surface also exhibited evidence of brittle fracture of deposit (Figure 57). However, it is difficult to assess whether failure is intragranular or transgranular

due to the fine dispersion of tungsten and chromium carbides. The better wear performance of Jet-kote compared to the chromium oxide deposit may be due to the higher fracture toughness : hardness ratio of the former. The binder phase in chromium oxide deposits is a hard brittle vitreous phase which is unlikely to prevent crack propagation. Whereas, in the Jet-kote deposit, the presence of a ductile nickel binder may inhibit crack propagation by a plastic blunting process.

In summary, the tribological performance of surface coatings / treatments is affected by the degree of mutual solubility with disc material, formation of surface oxides, microstructure and, in the case of hard brittle deposits, their susceptibility to cracking should be considered.

## 8.2. Corrosion Behaviour of Surface Coatings / Treatments in Acidified Salt Solution

The corrosion performance of the surface coatings / treatments was assessed by determination of the corrosion current density ($I_{corr}$) by Tafel extrapolation and by linear polarisation techniques. These results are discussed in Chapter 7. In general, the following surface coatings / treatments exhibited poor corrosion performance:

(1) EN8 borided steel

(2) Toyota diffusion process (vanadium carbide layer)

(3) Plasma nitrided 316 austenitic stainless steel

(4) Jet-kote deposit (Wc/Ni/W-Cr-carbides).

The failure of the EN8 borided and Jet-kote deposit can be attributed to the presence of

inherent deposit porosity, which provided the necessary pathways for corrosive agents(e.g. chloride ions) to attack the substrate. Boriding of steels results in the formation of an acicular deposit consisting of columnar crystals of iron boride ($Fe_2B$). Porosity in the deposit is due to the presence of intercolumnar voids, these are clearly shown on the worn surfaces (Figure 34). Porosity in high velocity thermally sprayed deposits, such as Jet-kote, is primarily due to shrinkage and degassing after deposition(156). The total porosity may vary from 0.5 to 1% depending on the spraying technique used. Isolated porosity in the deposit is unlikely to be deleterious from a corrosion viewpoint, however, interconnected porosity would expose the substrate to corrosive attack. Vacuum impregnation of thermally sprayed deposits with an anaerobic sealer would appear to be an effective method of filling deposit porosity, as evidenced by the better corrosion performance of sealed plasma sprayed chromium oxide deposit. The failure of the vanadium carbide layer and the plasma nitrided 316 stainless steel specimens was primarily due to localised pitting attack.

The rapid pitting of the vanadium carbide layer was evident in the detection of iron dissolution from the substrate (Figure 82) during the first week of immersion. Since the vanadium carbide layer was cathodic (-0.497 V) to the steel substrate (-0.664 V) low anode/cathode area ratios provided the necessary driving force for localised pitting.

The corrosion potentials for as-plated and heat treated (400°C) electroless nickel deposits became considerably active during the first two weeks of immersion in acidified salt solution (Figures 83 & 86). However, deposits heat treated at 600°C (vacuum and air) remained at essentially constant corrosion potential for up to four weeks (Figure 90). Analysis of the corroding solution for heat treated deposits at 400°C

(Figure 88) revealed that considerable dissolution of iron had occurred after 3 days immersion in the test solution; this could be indicative of either through thickness defects or rapid localised pitting. To explain the above, it is necessary to consider whether electroless nickel deposits are slightly porous or pore free.

Recent studies by Tomlinson [167] suggested that porosity in electroless nickel deposit is due to hydrogen evolution at converging nodular growth boundaries. They also suggested that non-metallic inclusions in the substrate did not initiate porosity. Whereas, Beer [168] stresses that sulphide inclusions in a substrate may locally poison the autocatalytic reaction and therefore, result in porosity. Studies by Brown [169] suggest that inadequate rinsing of hydrochloric acid during the pre-treatment sequence leads to voids in the initial deposited layers of electroless nickel, which might be precursors for subsequent through thickness porosity. Thus, the above evidence suggests that electroless nickel deposits are likely to be slightly porous. Hence, the observed drop in the corrosion potentials for as-plated and heat treated (400°C) electroless nickel are probably due to penetration of the deposit due to inherent porosity by corrosive agents (e.g. chloride ions), together with active metal dissolution (Figures 83 & 86), as revealed by atomic absorption analysis of the corroding solution. Since the deposits heat treated at 600°C (air and vacuum) did not exhibit such a drastic drop in the corrosion potential (Figure 90), it would appear that the Fe-Ni intermetallic layer formed at the coating / substrate interface prevented attack of the substrate.

The poor corrosion performance of heat treated electroless nickel at 400°C is often associated with microcracking of the deposit, which exposes the substrate to corrosion and therefore, results in poor corrosion protection. However, further consideration should be given to whether as-plated or heat treated (400°C) have different corrosion

rates. Heat treatment of electroless nickel at 400°C results in the precipitation of nickel phosphides from a supersaturated solid solution of phosphorus in a microcrystalline nickel matrix. Assuming that the electrode potential for the nickel matrix to be -0.299V S.C.E., i.e. similar to that of Watts nickel, and the nickel phosphides -0.228V S.C.E. represented by the 12% P as-plated electroless nickel deposit, it would appear that the matrix is anodic to the nickel phosphides. Since as-plated deposits are single phase solid solutions, microgalvanic cells could be formed by virtue of local segregation of phosphorus or due to grain boundaries. If the matrix dissolution is the predominant anodic reaction, then a higher nickel dissolution and corrosion rate should be expected for heat treated than for as-plated deposits because the former should contain less phosphorus in the matrix.

Evidence for the above hypothesis is given below:

1) The corrosion current densities determined by Tafel extrapolation for heat treated (400°C) electroless nickel were greater by an order of magnitude compared to as-plated deposits, as indicated in Table 31. However, the anodic Tafel constants, which are a measure of the resistance to anodic dissolution, were higher for heat treated at 400°C than as-plated deposits. This contradiction is probably due to the fact that surface oxides on heat treated specimens were not removed effectively prior to electrochemical testing. The linear polarisation technique was unable to show any differences in the corrosion current densities between as-plated and heat treated electroless nickel deposit; this was again primarily due to the presence of surface oxide and rust on the latter, generating higher values of Rp, resistance polarisation parameter.

2) Electron probe microanalysis of cross-sections of corroded electroless nickel deposits, heat treated at 400°C, exhibited an approximately 0.5% increase in the bulk phosphorus content compared to as-plated deposits (Table 35). This change in composition is probably related to fine pits observed on the corroded surface which penetrate through the deposit to the substrate. However, no such trend was apparent for the 9% electroless nickel deposit.

3) Analysis of the corroding solution showed that the initial period of immersion for heat treated deposits was accompanied by a higher rate of nickel dissolution compared to that observed for as-plated deposits. With time, only the 9% P heat treated deposit exhibited a higher nickel dissolution compared to the corresponding as-plated deposit.

In general, electroless nickel deposits with high phosphorus content (11-13%) are thought to confer better corrosion resistance than those containing lower levels of phosphorus. Hence, an increase in the phosphorus content of the deposit, should be accompanied by a decrease in the corrosion current density ($I_{corr}$). However, $I_{corr}$ determinations for 7, 9 and 12% as-plated deposits, using Tafel extrapolation method, did not reveal such a trend. This contradiction is due to the inaccuracies in the technique, as evident by the curvature in the anodic Tafel regions (Figures 70 & 71). However, it is important to note that the 12% P deposits remained shiny and intact after anodic polarisation to 1 volt, with respect to the corrosion potential, whereas, the 7 and 9% P deposits were essentially stripped off. Futhermore, from the above mentioned figures, it can be seen that for a given overpotential with respect to the rest potential, the rate of anodic dissolution of the 12 % P deposits is less than by an order of magnitude compared to 7 % P deposits. This suggests that for 12 % P deposits a greater activation

energy is required for anodic dissolution than for 7 % P deposits.

In the long term tests, there was a discrepancy between the determined $I_{corr}$ values by linear polarisation and the visual appearance of the specimens. After 7 weeks immersion in acidified salt solution the appearance of the 7 and 9% as-plated deposits was characterised by their loss of lustre and the presence of adherent 'reddish' corrosion products, whereas, the corroded surface of the 12% P deposit was shiny and covered with non-adherent 'reddish' corrosion products. The above disagreement may be explained as follows:

1) The 12% P deposit was thinner (~15μm) compared to the 7% and 9% P (20-25μm) and therefore, there is greater probability of through-thickness porosity in the former. This could account for the rapid drop in the corrosion potential after one week's immersion in test solution; refer to Figure 83.

2) The corrosion products formed on the specimens can lead to misleading Rp, resistance polarisation parameters and therefore, the $I_{corr}$ values, this would invalidate the use of linear polarisation in such circumstances.

In the original work on linear polarisation by Skold and Larson [90], it was suggested that the corrosion rate is proportional to the reciprocal of Rp. Thus, consideration of the average Rp, prior to the appearance of surface corrosion products, would indicate a lower corrosion rate for 12% P than for the 7% and 9% as-plated electroless nickel deposits, as shown in Table 42 below.

Table 42. The Rp determinations for as-plated electroless nickel deposits

| Phosphorus content % | Resistance polarisation parameter, Rp $n\ \Omega / cm^2$ |
|---|---|
| 7 | $1.970 \times 10^3$ |
| 9 | $2.990 \times 10^3$ |
| 12 | $1.6740 \times 10^4$ |

Flis and Duquette[170] have suggested that the better corrosion performance of high phosphorus (11-13% P) electroless nickel deposits is due to their ability to form phosphates, which act as inhibitors in solution, or to the formation of insoluble phosphate compounds on the surface. Electron probe microanalysis of cross-sections of corroded 12% P as-plated and heat treated coatings confirms the preferential dissolution of phosphorus from the deposit, as indicated in Table 34. E.D.X.A. of the corrosion products revealed small amounts of nickel, phosphorus and iron being the major constituent. This suggests that the phosphates were in solution. However, it is most probable that these phosphates act as anodic inhibitors. In which case, if the concentration of the inhibitor is not sufficient to cover all the anodic sites, a situation may occur leading to low anode/cathode area ratios, resulting in localised pitting. Since the laboratory tests were conducted in a solution of finite volume, then concentration of phosphates could be expected to build up with increased anodic dissolution. However, in an industrial situation where the solution volume may be very large or solution may flow across a coated component, then the inhibition effect by phosphates would be minimal.

8.2.1. Potentiodynamic Anodic Polarisation Curves

As-plated (7%, 9% and 12% P) electroless nickel deposits did not exhibit any tendency to passivate in the test solution. In contrast, the heat treated deposits at 400°C apparently showed a slight tendency to passivate, however, these spurious results were due to inadequate removal of the thick oxide film prior to testing. Heat treatment at 600°C in vacuum produced a pronounced passivation 'nose' similar to that observed for Watts nickel. The effect of heat treatment on the surface composition of electroless nickel deposits was assessed by Auger electron spectroscopy. This revealed that at a depth of 0.036 μm from the surface, the specimens heat treated at 600°C (in vacuum) were 8-10 Atomic % richer in nickel than as-plated deposits. It is surprising that a small change in surface composition resulted in a significant change in passivation tendency. However, the explanation might be related to the nature of the oxide formed on electroless nickel deposits.

Pai and Marton [171] suggested, on the basis of electron diffraction studies, that surface oxide on electroless nickel deposits consists of NiO and $P_2O_5$; the latter are crystallites dispersed in the NiO matrix. A.E.S. studies of as-plated and heat treated electroless nickel deposits confirm the presence of phosphorus in the oxide layers. Thus, the decomposition of $P_2O_5$ might result in defects in the oxide layer and therefore, could explain why the air formed and heat treatment oxides confer a limited protection.

It is difficult to explain the reasons for the passivation tendency of the vacuum heat treated (600°C) deposit, however, the loss of phosphorus at the surface might reduce

the likelihood of $P_2O_5$ forming in the passive film. At 600°C, considerable grain growth and coarsening of precipitated nickel phosphides occur in electroless nickel deposits. Therefore, dissociation of nickel phosphide precipitates could occur in vacuum conditions as follows:

$$\underset{\text{vacuum}}{Ni_3P} \xrightarrow{600^\circ C} 3Ni_{(s)} + P_{(g)} \qquad (18)$$

This could result in a distribution of small areas of nickel in previous precipitate positions, which might facilitate passive film formation. It is difficult to prove whether the above reaction is thermodynamically feasible because published values of standard entropy of formation of nickel phosphide are not available and therefore, the change in free energy cannot be evaluated.

The passivity of titanium nitride layers has been demonstrated by various workers using potentiodynamic polarisation in various test solutions [172,173]. However, in salt spray tests, titanium nitride coated steel failed rapidly in a neutral salt spray solution [174]. This was attributed to porosity in the titanium layer, since the latter is cathodic to the steel, porosity results in low anode/cathode area ratios resulting in rapid localised corrosion. However, in long term immersion tests, no attack of the electroless nickel / titanium nitride duplex coating was apparent. Assuming the electrode potential of a titanium nitride layer to be (-340 mV) and that of the electroless nickel underlay (-284 mV), then the latter would be cathodic to the titanium layer. Thus, any porosity should be passivated by a cathodic reaction due to high anode / cathode area ratio.

So far in the discussion both wear and corrosion of surface coatings / treatments have

been considered in isolation. It is difficult to predict the synergistic effect of wear and corrosion because of the complexity of each of the processes. When mechanical seal faces are separated by a thin hydrodynamic film, then corrosion may be predominant, however, under discontinuous seal operation, i.e. start-stop, such film formation is unlikely to occur, in which case wear of seal faces would be expected to predominate. Furthermore, a situation could arise where the corrosion of seal faces occurs during steady state operation, but if the pump is switched off and restarted, wear of the corroded faces would occur, until hydrodynamic lubrication were again prevalent. Therefore, some inferences can be made on the effects of corrosion on a worn surface or conversely, wear on a corroded surface.

The presence of adhesive transfer and plastic deformation on the worn surfaces of Ni-Cr-B deposits would probably lead to a higher corrosion rate due to greater structural and compositional heterogeneity. In contrast, the worn surfaces of electroless nickel pins were highly polished and no evidence of adhesive transfer or cracking of the deposit was apparent. Therefore, any subsequent corrosion should proceed at similar rates to those determined in static laboratory tests. However, corrosion of electroless nickel deposits, manifested in the form of fine pits penetrating through the deposit to the substrate, resulted in loss of adhesion. Such a surface is likely to fail rapidly when subjected to sliding wear. In mechanical seals the surface finish of seal faces during service is very important, because if, as a consequence of wear, the surface roughness of the faces increases, disruption of the thin hydrodynamic film would occur. In this respect, the observed polishing effect on the worn surfaces of electroless nickel and plasma nitrided 316 stainless steel pin is of significance.

In the case of thermally sprayed deposits, the question arises as to whether the efficiency of the sealing, using anaerobic sealers, is lowered by the effects of wear. The surface cracks observed on chromium oxide deposits may extend to the subsurface, for reasons discussed in previous sections, and therefore, lower corrosion protection, even if the deposit were to be sealed. In the case of the Jet-kote deposit, no such cracking was observed, even at the higher pin load, and therefore, sealing should be beneficial in improving the corrosion protection. However, de-bonding of the sealer within the deposit could occur due to the effects of subsurface shear stresses. A possible solution, is to use a Watts nickel underlay, which would significantly protect the substrate from corrosion.

A major factor affecting corrosion behaviour of mechanical seals is the degree of galvanic dissimilarity between the rotary and stationary seal faces. Galvanic corrosion of the surface coatings / treatments will be favoured by the following factors:

1) The greater electrochemical nobility of carbon-graphite stationary seal rings, compared with the investigated coatings / treatments, would result in the formation of macro cathodes and anodes respectively.

2) Physical contact of seal faces when the pump is switched off, due to a net closing force on the seal rings, provided by the spring drive.

3) Electrically conductive pumped fluid, for example, sea water.

The net effect of the galvanic coupling with the surface coatings / treatments, would be to raise their electrode potentials and therefore, increase the corrosion rate. This type of behaviour can be related to the anodic potentiodynamic curves (Section 7.4.3), which showed that none of the surface coatings / treatments exhibited passivity, except for the electroless nickel / titanium nitride duplex coating. Since the rotary and stationary seal faces have similar areas, the effect of anode : cathode area ratios should be minimal. Hence, galvanic coupling with the duplex coating and carbon-graphite stationary ring could lead to low corrosion rates, providing the electrode potential of the former remains in the passive region. In lower chloride and/or higher pH solutions, the passivity is likely to extend over a larger potential range and therefore, allow a greater margin of safety.

## 8.3. Surface Treatments / Coatings Selection for Mechanical Seal Application

In general, good wear and corrosion resistance of seal faces are the primary material requirements, however, the wear resistance is more important, since it relates to the functional requirement of seal faces. The coefficients of friction are also important, as they influence the torque requirements for mechanical seals. However, other physical properties of surface treatment / coatings should also be considered, for example:

1) Internal stress of coating / treatments.
2) Adhesion of coating / treatments to substrate.
3) Coefficient of linear expansion.
4) Coefficient of thermal conductivity.
5) Degree of porosity.

Compressive internal stresses in surface coatings / treatments are desirable, because they reduce the likelihood of fatigue crack propagation during sliding wear. Furthermore, their role may be beneficial in reducing thermocracking of seal faces. The resistance to thermocracking may be expressed using the Thermal Shock Parameter (T.S.P.)[33].

$$T.S.P. = \frac{T.C \times U.T.S}{L.E \times Y.MOD} \qquad (5)$$

Where

T.C = Coefficient of thermal conductivity

U.T.S = Ultimate tensile strength

L.E = Coefficient of linear expansion

Y.MOD = Young's modulus

The higher the T.S.P value, the greater the resistance to thermocracking. A high T.S.P value is attained by materials with the following mechanical / thermal properties.

1) High coefficient of thermal conductivity
2) Low coefficient of linear expansion
3) High ultimate tensile strength
4) Low Young's modulus

However, very little is published on the tensile strength and Young's modulus of surface coatings / treatments and therefore, only thermal properties will be considered. Finally, the surface coating / treatments should have good adhesion to substrate and a low porosity. The evaluated wear and corrosion data, together with published values of the above properties, were used collectively in a material selection analysis.

In this approach material requirements and material properties were analysed

systematically and assigned weighting factors (methodology is given in Appendix VI) $\alpha$ and $\beta$ respectively. Each $\beta$ value was multiplied by the appropriate $\alpha$ value, the product is termed the $\gamma$ value. The products were then summed, the material having the highest ($\Sigma\ \gamma$) value is the preferred material. Tables 43,44 and45 illustrate the determination of $\alpha$, $\beta$ and $\gamma$ values, respectively. The surface coatings / treatments may be ranked (highest ($\Sigma\ \gamma$) as follows:

1. Electroless nickel / titanium nitride duplex coating

2. Toyota diffusion process, vanadium carbide layer

3. Nickel-chromium-boron (post fused)

4. EN8 borided steel

5. Jet-kote deposit (not sealed)

6. Plasma sprayed chromium oxide deposit (sealed with an anaerobic sealer

7. Electroless nickel heat treated at 400°C.

| | DECISIONS | | | | | | | | | | | | | | | | | | | | | | | | | | | SUM | α VALUE |
|---|---|---|---|---|---|---|---|---|---|---|---|---|---|---|---|---|---|---|---|---|---|---|---|---|---|---|---|---|---|
| | 1 | 2 | 3 | 4 | 5 | 6 | 7 | 8 | 9 | 10 | 11 | 12 | 13 | 14 | 15 | 16 | 17 | 18 | 19 | 20 | 21 | 22 | 23 | 24 | 25 | 26 | 27 | 28 | | |
| Wear | 10 | 10 | 10 | 10 | 10 | 10 | 10 | | | | | | | | | | | | | | | | | | | | | | 70 | 0.184 |
| Corrosion | 8 | | | | | | | 8 | 8 | 8 | 8 | 8 | 8 | | | | | | | | | | | | | | | | 56 | 0.147 |
| Internal Stress | | 4 | | | | | | 4 | | | | | | 5 | 5 | 5 | 5 | 5 | | | | | | | | | | | 33 | 0.087 |
| Adhesion | | | 7 | | | | | | 7 | | | | | 8 | | | | | 8 | 8 | 8 | 8 | | | | | | | 54 | 0.142 |
| Linear Expansion | | | | 5 | | | | | | 5 | | | | | 5 | | | | 5 | | | | 5 | 5 | 5 | | | | 35 | 0.092 |
| Thermal Conductivity | | | | | 5 | | | | | | 5 | | | | | 5 | | | | 5 | | | 5 | | | 5 | 5 | | 35 | 0.092 |
| Porosity | | | | | | 7 | | | | | | 8 | | | | | 7 | | | | 6 | | | 6 | | 6 | | 5 | 45 | 0.118 |
| Friction | | | | | | | 9 | | | | | | 8 | | | | | 8 | | | | 7 | | | 7 | | 7 | 7 | 53 | 0.139 |

GRADING : 10 - Best : 1 - Worst

Table 44. Determination of Beta (β) Values

| | Wear Rate (mg/cm x $10^{-5}$) | Corrosion Rate, Linear Polarisation ($nA/cm^2 x 10^4$) | Internal Stress | Adhesion ($MN/m^2$) | Coefficient of Linear Expansion ($x10^{-6} K^{-1}$) | Coefficient of Thermal Conductivity ($Wm^{-1} K^{-1}$) | Porosity (%) | Coefficient of Friction (μ) |
|---|---|---|---|---|---|---|---|---|
| Electroless nickel | 0.507 | 1.58 | Tensile | 420 | 13 | 5.024 | 0 | 0.34 |
| β Value | 7.88 | 49.36 | 66.6 | 61.76 | 47.69 | 9.13 | 100 | 85.29 |
| Chromium Oxide | 0.112 | - | Tensile | 20.0 | 6.2 | 2.30 | 6 | 0.49 |
| β Value | 35.71 | 100 | 66.6 | 2.94 | 100 | 4.18 | 94 | 59.18 |
| EN8 Borided | 0.864 | 8.73 | Compressive | metall. bonded | 8 | 25.0 | 0 | 0.41 |
| β Value | 4.63 | 8.97 | 100 | 100 | 77.5 | 45.45 | 100 | 70.73 |
| Ni-Cr-B | 0.707 | 0.87 | Tensile | metall. bonded | 12.6 | 12.0 | 0 | 0.59 |
| β Value | 5.65 | 90.0 | 66.6 | 100 | 49.20 | 21.82 | 100 | 49.15 |
| Toyota Diffusion | 0.053 | 1.39 | Compressive | metall. bonded | 7.2 | 35 | 0 | 0.37 |
| β Value | 75.47 | 56.35 | 100 | 100 | 86.11 | 63.63 | 100 | 78.37 |
| Jet-Kote | 0.059 | 5.61 | Tensile | 75 | 8.28 | 55 | 0.5 | 0.59 |
| β Value | 67.79 | 13.97 | 66.6 | 11.03 | 74.87 | 100 | 99.5 | 49.15 |
| Electroless nickel/ titanium nitride duplex coating | 0.040 | - | Compressive | 680 | 9.35 | 29 | 0 | 0.29 |
| β Value | 100 | 100 | 100 | 66 | 66.31 | 52.72 | 100 | 100 |

Table 45. Determination of Gamma (γ) Values

| | Wear Rate | Corrosion Rate, Linear Polarisation | Internal Stress | Adhesion | Coefficient of Linear Expansion | Coefficient of Thermal Conductivity | Porosity | Coefficient of Friction | Σγ |
|---|---|---|---|---|---|---|---|---|---|
| Electroless nickel | 1.45 | 7.25 | 5.79 | 8.76 | 4.38 | 0.83 | 11.8 | 11.85 | 52.11 |
| Chromium Oxide | 6.57 | 14.7 | 5.79 | 0.42 | 9.2 | 0.38 | 11.09 | 8.23 | 56.38 |
| EN8 Borided | 0.851 | 1.32 | 8.70 | 14.2 | 7.13 | 4.18 | 11.8 | 9.83 | 58.01 |
| Ni-Cr-B | 1.04 | 13.23 | 5.79 | 14.2 | 4.52 | 2.0 | 11/8 | 6.83 | 59.41 |
| Totota Diffusion | 13.89 | 8.28 | 8.70 | 14.2 | 7.92 | 5.85 | 11.8 | 10.89 | 81.53 |
| Jet-Kote | 12.47 | 2.05 | 5.79 | 1.57 | 6.88 | 9.2 | 11.74 | 6.83 | 56.53 |
| Electroless nickel/ titanium nitride duplex coating | 18.40 | 14.70 | 8.70 | 9.37 | 6.10 | 4.85 | 11.80 | 13.9 | 87.82 |

The above analysis suggests that the most suitable surface treatment / coating is electroless nickel / titanium nitride duplex coating. In the above analysis, a 'β' value of 100 was assigned to the corrosion properties of electroless nickel / titanium nitride duplex coating and chromium oxide deposit because the corrosion current density could not be determined due to effects of passivation and resistance polarisation, respectively. Furthermore, these deposits conferred good corrosion protection, as evidenced by the absence of rusting on the specimens in the long term immersion tests. However, if the Jet-kote deposit was sealed, its corrosion protection would be similar to that of the chromium oxide deposit and, therefore, a higher ranking than listed above could be expected. The final short list was affected by certain practical factors. Initially, D2 tool steel was considered as a suitable substrate material for the seal rings, however, the collaborating body suggested that austenitic (316S11) and martensitic (431S29) stainless steel should be used. As a consequence of this, the Toyota diffusion process and Ni-Cr-B deposit were rejected because there is insufficient carbon in these steels to produce a carbide layer, and the likelihood of cracking of the 431S29 steel during post fusing of the Ni-Cr-B deposit, respectively. Mechanical seal rings are optically flat and therefore, high temperature processes such as boriding and, again, Toyota diffusion process were rejected due to the possibility of thermal distortion of seal rings.

At this stage other surface coating / treatments were considered, such as, electroless nickel silicon carbide composite coating and plasma nitriding. The latter process is particularly important, as it can depassivate stainless steels in the reaction chamber, prior to nitriding. The wear resistance of the above surface coating / treatments was considerably better than that of conventional electroless nickel. Consequently, the

following surface coatings / treatments were chosen to be applied to mechanical seals, which were then tested on an industrial seal testing rig:

1) Electroless nickel
2) Electroless nickel silicon carbide composite coating
3) Jet-kote deposit
4) Electroless nickel / titanium nitride duplex coating
5) Plasma nitriding.

## 8.4. Seal Rig Tests

A F.F.E.T type cartridge mechanical seal was used to evaluate the sealing performance of surface coated / treated seals, which were tested at a pV factor of 85 bar.m.s$^{-1}$. This corresponds to the operating limits for stellite faced balanced seals. The results of the seal rig tests and S.E.M. examinations of the worn seals have been discussed in Chapter 7.

### 8.4.1. Plasma Nitrided Seals

These exhibited poor sealing performance, as characterised by their high leakage rates. Microhardnesses in cross-section below the surface, suggested complete removal of the compound and diffusion layer in the case of both 431S29 and 316S11 plasma nitrided seals. The surface finish of these seals after plasma nitriding was poor, characterised by numerous pits and uneven nitriding, this necessitated post lapping which presumably removed a considerable proportion of the diffusion layer. Therefore, the performance of these seals is not representative of the wear resistance of the hard iron and alloy nitrides formed during plasma nitriding.

### 8.4.2. Electroless Nickel Coated Seals

The failure of the electroless nickel and electroless nickel / titanium nitride duplex coated seals was due to abrasive wear of the seal faces. The inadequate adhesion of the electroless nickel, coupled with shear stresses generated at sliding surfaces, resulted in adhesion failure of the deposit. Hence, coating material removed in this manner, became embedded into the softer counterface and therefore, accelerated the wear of the coated seals. This resulted in an increase in the surface roughness of the latter, and consequently led to high carbon wear rates, as indicated in Table 40.

The better performance of the electroless nickel silicon carbide composite coated seals is primarily due to the better level of coating adhesion compared to the above mentioned seals. Prior to composite plating, the seal faces were grit blasted and therefore, the improved adhesion is due to mechanical keying of the deposit. Whereas, the conventional electroless nickel and duplex coatings were applied to a lapped seal ring.

### 8.4.3. Jet-Kote (Wc/Ni/W-Cr-Carbides) Coated Seals

The Jet-kote coated seals exhibited the best seal performance, characterised by no measurable leakage or carbon nose wear. S.E.M. examination of the worn seals showed no evidence of abrasion, but small craters filled with carbon-graphite material were observed. These features are not due to seal wear, but are a consequence of surface grinding and lapping of seal faces. In general, thermally sprayed deposits are rough (1-2 μm c.l.a.) and therefore, surface grinding can lead to pull-out of deposit material (157).

It was intended to test the Jet-kote and composite coated seals at much higher pV limits, but this was not possible due to a constraint of time. The pV limits for plasma sprayed chromium oxide is 400 bar.m.s$^{-1}$ and, since the wear rate of the Jet-kote, determined by pin-on-disc, is less than that of the former, it may be inferred that Jet-kote coated seals could be used at much higher pV limits than chromium oxide sprayed seals. Furthermore, the worn pin surfaces of the latter, were characterised by extensive cracking and spalling of deposit. In contrast, no such features were observed on the worn Jet-kote surface, even at the higher pin load.

In the above seal tests, the pumped fluid was water and therefore, corrosion of seal faces would be minimal. Hence, consideration should be given to the possible performance of these surface coated / treated seals in an environment similar to the experimental system (acidified salt solution), for example, injection pumps are extensively used to assist oil recovery in North Sea oilfields. Although sea water is a potentially corrosive media, the performance of mechanical seals would probably be governed by the wear resistance of the seal faces, because of the following factors:

(1) Presence of sand and grit in sea water would lead to abrasion of seal faces.

(2) Sea water is a poor hydrodynamic lubricant.

Therefore, from a wear resistance viewpoint, the obvious choice would be the Jet-Kote deposit because it exhibited the least wear at the high load (8 kg) in the Pin-on-Disc tests. However, the electroless nickel / titanium nitride duplex coating would also be worthy of consideration because of the passivity of the titanium nitride layer in acidified salt solution. However, it must be rejected because of its lower load bearing capacity,

compared to the Jet-Kote deposit, as evidenced by cracking and spalling of the titanium nitride layer on the worn pin surfaces. Plasma nitrided seals would also be unsuitable for sea water application, in this case due to poor corrosion resistance of the iron and alloy nitrides. In electroless nickel and electroless nickel silicon carbide composite coated seals, the most likely problem would be pitting of the deposit leading ultimately to exfoilation. Although the latter effect could arise in the Jet-Kote deposits, due to the presence of interconnecting porosity, this could be minimised by the use of anaerobic sealers, and so the Jet-Kote deposit would appear to be the best compromise for sea water application.

The other aspect investigated in the seal rig tests, was the fretting wear of the sliding diameter on the stationary seal ring body. In the F.F.E.T. type mechanical seal, the rotary seal is at a fixed position on the shaft and intimate contact of the rubbing seal faces is maintained by axial movement of the stationary seal ring body. However, if this movement is prevented, as a result of fretting action of the 'O' ring on the sliding diameter, shaft 'hang-up' occurs leading to excessive leakage. Axial oscillatory movement of the stationary seal ring body was achieved by slightly offsetting the rotary seal, as described in Chapter 6. The fretting action was accelerated by using a glass filled / P.T.F.E. 'O' ring.

The uncoated stationary seal ring body exhibited a characteristic oxidised fretting scar on the sliding diameter. Similar, but non-oxidised scars were observed on electroless nickel and electroless nickel / titanium nitride duplex coated sliding diameters; in the latter case, the titanium nitride layer appeared to be worn away. Inadequate surface grinding of the sliding diameter of Jet-Kote coated component resulted in an

unsatisfactory surface finish, this led to shaft 'hang-up' and excessive leakage at the operating pressure (15 bar). The fluid pressure was reduced to 4 bar to minimise leakage, however, it is questionable whether axial oscillatory movement of the stationary seal ring body was attained. A similar problem was encountered with the electroless nickel silicon carbide composite coated stationary body. This is surprising since no problems were evident in the tests using electroless nickel coated components. Clearly, these tests need to be repeated so that meaningful results can be obtained. It has been reported in the literature that various workers[75,76,85] have suggested the use of solid lubricants to minimise fretting wear. Hence, electroless nickel / P.T.F.E. composite coatings could be applied to the stationary seal ring body to reduce fretting wear of the sliding diameter. However, due to a limited number of available components and constraint of time, it was not possible to investigate this proposition.

# CHAPTER IX

## 9.0 CONCLUSIONS AND FURTHER WORK

### 9.1 Conclusions

1. Various surface treatments / coatings were evaluated for wear resistance using the Pin-on-Disc wear test. At a load of 4 kg on the pin, the best wear resistance was exhibited by electroless nickel / titanium nitride duplex coating, whereas, at a load of 8 kg, the Jet-kote deposit conferred the best wear resistance.

2. At 4 kg load, moderate coefficients of friction were exhibited by electroless nickel / titanium nitride duplex coating, electroless nickel, Toyota diffusion layer and borided EN8 steel, the first named being the best. At 8 kg load, high coefficients of friction were observed for electroless nickel / silicon carbide composite coating, electroless nickel / titanium nitride duplex coating and plasma nitrided 316 stainless steel. The magnitude of the coefficients of friction are affected considerably by ploughing action of surface asperities and wear debris.

3. In general, no correlation was found between hardness and wear resistance of surface finish and friction.

4. In long-term immersion tests in acidified salt solution, the best corrosion performances were exhibited by electroless nickel / titanium nitride duplex coating,

nickel-chromium-boron post fused and electroless nickel deposits heat treated at 600°C. In contrast, poor corrosion performances were shown by borided EN8 steel, Toyota diffusion layer, plasma nitrided 316 stainless steel and Jet-kote deposit.

5. Under conditions of anodic potentiodynamic polarisation, electroless nickel, both as-plated and heat treated at 400°C, did not exhibit any tendency to passivate, whereas, deposits heat treated at 600°C in vacuum exhibited pronounced passivation, similar to that observed for Watts nickel deposits. Passivity was also demonstrated by the electroless nickel / titanium nitride duplex coating.

6. Auger electron spectroscopy of electroless nickel deposits heat treated at 600°C in vacuum, showed nickel enrichment of the surface, which has been correlated with the observed passivation tendency in anodic potentiodynamic tests. In contrast, deposits heat treated at 600°C in air, form thick nickel surface oxides which improve the corrosion protection afforded by the deposits.

7. The surface coating / treatments were ranked using a systematic method, involving the use of weighting factors for primary seal face requirements and physical / chemical properties of surface coating / treatments.

8. The best seal performances were exhibited by the Jet-kote and electroless silicon carbide composite coated seals. Abrasion of the seal faces was the principal wear mechanism.

## 9.2 Further work

Further work could be divided into the following two areas: (1) improvement of the wear and corrosion properties of electroless nickel deposits and (2) seal rig tests.

There is some evidence in the literature[139,164] that electroless nickel deposits heat treated at 600°C confer better wear resistance than deposits heat treated at 400°C. A possible application of this would be to heat treat electroless nickel silicon carbide composite coatings at 600°C, so that the Fe-Ni intermetallic layer formed at the substrate / coating interface would improve adhesion and corrosion resistance. The reduction in hardness due to over-aging may be offset, to some degree, by the presence of hard silicon carbide particles and therefore, optimum wear and corrosion properties may be attained.

The electroless nickel / titanium nitride duplex coating has considerable potential for application in chloride environments, however, its tribological performance is affected by the adhesion of the titanium nitride layer to the electroless nickel underlay. A possible solution would be to conduct the ion plating at much higher temperatures (550-600°C), this would promote thermal diffusion between the titanium nitride layer and electroless nickel, thereby improving adhesion. Furthermore, at these temperatures the formation of the Fe-Ni intermetallic layer would improve the adhesion of the electroless nickel underlay to the substrate. The PVD TiN evaluated in the present work was deposited by an electron beam evaporation technique. It would be worth evaluating TiN

coatings produced by other methods that are now available commercially, e.g. arc process or hollow cathode techniques.

Further work is required to determine the operating PV limits for Jet-Kote and electroless nickel silicon carbide coated seals, and also to compare their performances with sintered silicon carbide seals. The sealing behaviour of these coated seals should be assessed by field trials in more aggressive environments than those employed in this investigation.

## 9.3 REFERENCES


1. Nau, B.S. Mechanical seal failures on process plants - what can be done about them? Process Engineering, October, 1972, 102-108

2. Buck, G.S. A methodology for design and application of mechanical seals. A.S.L.E. Transactions, 1980, **23**, 3, 244-252

3. Summers-Smith, J.D. Performance of mechanical seals in centrifugal process pumps. 9th Int. Conf. on Fluid Sealing, Paper H1, B.H.R.A., 1981

4. Nau, B.S. Tribology in the process industry: Seals. BHRA report EX 201, 1975

5. Flitney, R.K. Reduce the risk of shaft seal failure. Machinery and Production Engineering, 1978, **132**, 29-31

6. Nau, B.S. Seal survey sorts out the source of leaks. Process Engineering, February, 1977, 59-62

7. Nau, B.S. Rotary mechanical seal in process duties: an assessment of the state of the art. Proc. Instn. Mech. Engrs., 1985, **199**, No.A1, 17-31

8. Nau, B.S. Mechanical seals: service experience. Tribology Int., 1986, **19**, No.4, 184-186

9. Buchter, H.H. Industrial Sealing Technology. A Wiley-Interscience publication

10. Mayer, A. Mechanical seals ( 2nd edition). I.L.F.F.E. Books.

11. Flitney, R.K. Factors affecting mechanical seal design and application. Trib.Int., 1977, **10**, 267-272.

12. Lymer, A Mechanical seals. Trib.Int., 1973, **6**, 57-61

13. Flexibox L.t.d. Seal users guide 1987. Nash road, Trafford Park, Manchester.

14. Denny, D.F. Some measurements of fluid pressure between plane parallel thrust surface with special references to the balancing of radial face seals. Wear, 1961, **4**, 1, 64-83

15. Batch, B.A. and Iny,E.H. Pressure generation in radial face seals. 2nd Int.Conf. on Fluid Sealing, B.H.R.A., paper **F4**, 1964

16. Nau, B.S. Hydrodynamics of face seals. 2nd Int.Conf. on Fluid Sealing, B.H.R.A., paper **F5**, 1964

17. Schoenherr, K. Materials in end-face mechanical seals. Mach. Des., 1964, **36**, 130-137

18. Field, G.F. Seals that survive heat. Mach. Des., 1975, **47**, 76-79

19. Bayliss, N. Material Performances for seals and packings. World Pumps, 1987, 195-196

20. Whateley, K. Mechanical seals: some development in face materials. Trib. Int., 1986, **19**, 4, 198-203

21. Piehn, L.D. The application of tungsten carbide for mechanical seal faces. Lub. Eng., 1965, **21**, 9, 381-385

22. Echtenkamp, A.L. Combating corrosion / wear with hard carbide alloys. Lub. Eng., 1979, **35**, 10, 577-582

23. Lashway, R.W. Slicon carbide for mechanical shaft seals. 9 th Int.Conf.on Fluid Sealing, B.H.R.A., paper **A4**, 1981.

24. Lashway, R.W. Various forms of silcon carbide and their effects on seal performance. Lub.Eng., 1984, **40**, 6, 356-363.

25. Neale, M.J. Tribology Handbook, Butterworths

26. Austin, R.M. Dynamic seal failures. C.M.E., 1978, **25**, 81-85

27. Strugala, E.W. The nature and causes of seal carbon blistering. Lub. Eng., 1972, **28**, 9, 333-339

28. Merrick, E.A. and Brooks, C.R. Interface war reactions in nickel - nickel simulated face seals. Wear, 1974, **29**, 195-207

29. Merrick, E.A. and Brooks, C.R. Interface wear reactions between ordered and disordered nickel - 20 At.% molybdenum alloys in a simulated face seal. Wear, 1975, **33**, 129-139

30. Roan, Y.F. and Brooks, C.R. The new behaviour of Hastelloy B against graphite in a simulated face seal . Wear, 1975, **35**, 211-232

31. Sibley, L.B. A study of refractory materials for seals and bearing, application in aircraft accessory units and rocket motor. PB 151 483, Battelle Memorial Institute, Oct., 1958.

32. Abar, J.W. Rubbing contact materials for face type mechanical seals. Lub. Eng., 1964, **20**, 10, 381-386

33. Lohou, J. Mechanical seals for water injection pumps- A new hard face materials. Lub.Eng., 1978, **33**, 6, 320-326.

34. Metcalfe, L. End face seals in high pressure water - learning from those failures. Lub. Eng., 1976, **32**, 12, 625-636

35. Wasil, T.J. and McCleary, G.P. Corrosion and the carbides.Materials Protection, 1965, **4**, 12, 54-56

36. Wasil, T.J. and McCleary, G.P. Sealing corrosive materials with hard carbon alloys. Lub. Eng., 1967, **23**, 6, 234-240

37. Wallace, N. Personal communications. Flexibox L.t.d., Nash road, Manchester

38. Hirano, F. Starting torque of a mechanical seal. 2 nd Int.Conf. on Fluid Sealing, B.H.R.A., paper **D2**, 1964.

39. Wilikson, S.C.W. The application of face type mechanical seals to super heated water. 2 nd Int.Conf. on Fluid Sealing, B.H.R.A., paper **D1**, 1964.

40. Wood, T.H. Mechanical shaft seals in the chemical industry. Trans. Instn. Chem. Engrs., 1954, **32**, 73-80

41. Sherpherd, K. Sealing in the petrochemical industry. Lub. Eng., 1980, **36**, 1, 40-44

42. Norton, R.D. Mechanical seals for handling abrasive liquids. Chem. Eng., 1956, **9**, 199-210

43. Tankus, H. End face seals in abrasive service. Lub. Eng., 1963, **10**, 403-409

44. Trytek, J.J. The application of mechanical end face seals for hot water service. Lub. Eng., 1973, **29**, 1, 17-23

45. Shiro, K. and Schoeenherr, K. Sealing Boric acid solutions with mechanical seals in nuclear service. Lub.Eng., 1979, **33**, 12, 425-432

46. Paxton, R.R., Massaro, A.J. and Strugala, E.W. The performance of siliconised graphite as mating face in mechanical seals. Lub. Eng., 1977, **33**, 12, 650-656

47. Mowrey, C.C. High speed seal development salt water and ammonia service - what customers want today. Lub. Eng., 1979, **35**, 10, 564-567

48. Schopplein, W. Application of mechanical seals to slurries with particular reference to pumps and agitators on flue gas desulphurization plants.Trib. Int., 1986, **19**, 4, 187-192

49. Tribe, F.J. Sea water - lubricated mechanical seals and bearings associated material problems.Lub. Eng., 1983, **39**, 5, 292-299

50 Lansdown, A.R. and Price, A.L. Materials to resist wear. A guide to their selection and use. Pergamon Press L.t.d., 1986.

51 Lancaster,J.K. Wear mechanisms of metal and polymers. Trans. Int. Met. Fin., 1978, **56**, 57-65

52 de Gee, A.W. Friction and wear as related to the composition, structure, and properties of metals. Int. Met. Rev., 1979, **24**, 2, 57-65.

53 Yust, C.S. Tribology and Wear. Int. Met. Rev., 1985, **30**, 3, 141-153.

54 Bowden, F.P. and Tabor, D. The friction and Lubrication of solids. Oxford University Press (1964).

55 Upsan, C. Adhesive and abrasive wear. Mach. Des. 1969, **41**, 12, 74-77.

56 Bayer, G. Understanding the fundementals of wear. Mach. Des., 1956, **28**, 12, 73-76.

57 Askwith, T.C. The basic mechanisms of wear. Surfacing Journal, 1980, **11**, 4, 2-6.

58 Archard, J.F. Contact and rubbing of flat surfaces. J.App.Physics, 1953, **24**, 8, 981-988.

60 Eyre, T.S. The mechanisms of wear. Trib. Int., 1978, **11**, 5, 91-96.

61 Habig, K.H. Wear protection of steels by boriding, vanadising, nitriding, carburising, etc. Materials in Engineering, 1980, **2**, 12, 83-92.

62 Welsh, N.C. The dry wear of steels. Phil. Trans. Roy. Soc., 1965, **257**, 31-70.

63 Rabinowitz, E. Wear mechanism for lightly loaded surfaces. Proceed. Inst. Mech. Engrs., 1967-1968, **182**, part 3A, 409-410.

64 Precise measurement of wear. Midlands Technology Digest. Published by Technology Exchange Unit, Aston University, Birmingham. July 1979, No 4, 1.

65 Suh, N.P. Delamination theory of wear. Wear, 1973, **25**, 111-124.

66 Rabinowicz, E. Friction and Wear of materials, Wiley publication, 1965.

67 Kruschov, M.M. and Babichem, N.A. Resistance of metals to wear abrasion as related to hardness. Proc.I.Mech.E. Conf. on Lubrication and wear, 1957, 655.

68 Richardson, R.C. Wear of metals by soft abrasives. Wear, 1968,**11**, 245.

69 Flitney, R.K. and Nau, B.S. Seal survey: Part 1-rotary mechanical face seals. B.H.R.A. report CR 1386, Dec.,1976.

70 Nau,B.S. Vibration and rotary mechanical seals. Trib.Int., 1981, **14**, 2, 55-59.

71 Hurricks, P.L. The mechanism of Fretting- A review. Wear, 1970, **15**, 389-409

72 Waterhouse,R.B. Fretting Corrosion. Pergamon Press, Oxford (1972).

73 Gould, A.J. Some mechanical and electrochemical properties of electroless nickel. Ph.D Thesis, Nottingham University, 1982.

74 Tomlinson, G.A. The rusting of steel surface in rubbing contact. Proc. Roy. Soc.(London), 1927, **A115**, 472-483.

75 Godfrey, D. and Bisson, E.E. N.A.C.A. studies of mechanism of Fretting (Fretting Corrosion) and principles of mitigation. Lub. Eng., 1952, **10**, 241-262

76 Barnett, R.S. Fretting Corrosion. Lub. Eng., 1952, **8**, 186-189.

77 Feng, I. and Uhlig, H.H. Fretting Corrosion of mild steel in air and nitrogen. J.App.Mech., 1954, **21**, 12, 395-400.

78 Uhlig, H.H. Mechanisim of Fretting Corrosion. J.App.Mech., 1954, **21**, 12, 401-407.

79 Halliday, J.S. and Hirst,W. The Fretting Corrosion of mild steel. Proc.Roy.Soc. (London), 1956, **A236**, 411-425.

80 Ohmae, N. and Tsukizoe, T. The effect of slip amplitude on Fretting. Wear, 1974, **27**, 281-294.

81 Feng, I. and Rightmire, B.G. The mechanism of Fretting. Lub.Eng., 1953, **9**, 134-140.

82 Waterhouse, R.B. and Taylor, D.E. Fretting debris and the delamination theory of wear. Wear, 1974, **29**, 337-344.

83 Sproles, E.S. and Duquette, D.J. The mechanism of material removal in Fretting. Wear, 1978, **49**, 339-352.

84 Kayaba, T. and Iwabuchi,A. Effect of hardened steels and the action of oxides on the Fretting wear. Wear, 1981, **66**, 27-41.

85 Waterhouse, R.B. Fretting Fatigue. Applied Science Publishers L.t.d., London 1981.

86 Wranglen, G. An introduction to corrosion and protection of metals. London: Champan and Hall, 1985.

87 Shier, L.L. (ed.) Corrosion, vols 1 and 2. London : Newnes- Butterworth, 1963

88 Fontanna, M.G. and Greene, N.D. Corrosion Engineering 2nd Edition, McGraw-Hill International Book company.

89 Pludek, V.R. Design and Corrosion Control. Basingstoke, Macmillan Publishers.

90 Skold, R.V. and Larson, T.E. Measurement of Instantenous corrosion rates by means of polarisation data. Corrosion N.A.C.E., 1957, **13**, 139t-142t

91 Stern, M. and Geary, A.L. Electrochemical Polarization 1. A theoretical analysis of the shape of Polarization curves. J. Electrochem.Soc., 1957, **104**, 1, 56-69

92 Hoar, T.P. On the relation between corrosion rate and polarisation resistance. Corros. Sci., 1967, **7**, 455-458.

93 Jones, D.A.. and Greene, N.D. Electrohemical measurements of low corrosion rates. Corrosion N.A.C.E., 1966, **198**, 198-202.

94 Legault, R.A. and Walker, M.S. Linear polarisation measurements in the study of corrosion inhibitors. Corrosion N.A.C.E., 1963, **19**, 222t - 226t.

95 Jones, D.A. and Greene, N.D. Electrochemical detection of localised corrosion. Corrosion N.A.C.E., 1969, **25**, 9, 367-370.

96 Jones, D.A. Polarisation in high resisivity media. Corrosion Sci., 1968, **8**, 19, 8-27

97 Mansfeld, F. Advances in Corrosion Science and Corrosion Engineering, Vol 8, M, Fontanna and R, Staehle eds., Plenum Press, New York, 1978.

98 Leroy, R.L. The range of validity of Linear Polarization method for measurement of instantaneous corrosion rates. Corrosion-N.A.C.E., 1973 **29**, 7, 272-275.

99 Leroy, R.L. Evaluation of Corrosion rates from polarization measurements. Corrosion-N.A.C.E., 1975, **31**, 5, 173-177.

100 Oldham, K.B. and Mansfeld, F. Corrosion rates from polarization curves: A new method. Corros.Sci., 1973, **13**, 813-819.

101 Mansfeld, F. Simultaneous determinations of instantaneous corrosion rates and Tafel slopes from polarization resistance measurements. J.Electrochem.Soc., 1973, **120**, 4, 515-518.

102 Roy, S.K and Sircar, S.C. Determination of Tafel slopes and corrosion rates from cathodic polarization curves: A graphical method. Br.Corros.J., 1978, **13**, 4, 193-194.

103 de Damborena, J., Ruiz, J. and Vazquez, J. Calculation of corrosion rates by computer : Possible inaccuracies. Br.Corros.J., 1984, **19**, 2, 95-97.

104 Oldham, K.B. and Mansfeld, F. Technical note : On the so-called Linear Polarisation method for measurement of corrosion rates. Corrosion-N.A.C.E., 1971, **21**, 10, 434-435.

105 Department of Trade and Industry. Wear resistance Surfaces in Engineering, a guide to their production, properties and selection. H.M.S.O. Books,1986.

106 National Physical Laboratory in Association with the Institute of Meatal Finishing. Guide to Practice in corrosion control No 16, Engineering coatings-their application and properties. H.M.S.O. Books, 1987.

107 Wyatt, L.M., editor., Fulmer Materials Optimiser (2nd Edition), volume 1 part 2: Comparision of materials. Fulmer Research Institute L.t.d., 1979, printed by Osco L.t.d., England.

108 Child, H.C. Surface Treatments for Tribology problems. Seminar on "Coatings for high temperature applications ," at the High Temperature Materials Information Centre, Petten, Holland, 1982. Applied Science Publishers L.t.d., 1983.

109 Biddulph, R.H. Boronising. Surfacing Journal, 1975, **5**, 2, 5-9.

110 Biddulph, R.H. Boronising. Heat Treatment of Metals, **1974.3**, 95-97.

111 Fichtl, W. Boronising. Ind.Prod.Eng., 1980, **1**, 113.

112 Linial, A.V. and Lavella, J.P. New process for obtaining increased hardness and reduced friction properties by Boronising: Part 1. Ind.Heating, 1973, **40**, 12, 9.

113 Eyre, T.S. and Morri, J. The metallurgy and wear characteristics of boride coatings. Heat Treatment of Metals, **1978.4**, 103-105.

114 Eyre, T.S. Effects of boronising on Friction and Wear characteristics of ferrous metals. Wear, 1975, **34**, 383-397.

115 Takeuchi, E., Fujii, K. and Katagiri, T. Sliding Wear characteristics of Gas Boronized steel. Wear, 1979, **55**, 121-130.

116 Sridar, D. and Iyer, L. Wear studies on Boronised steel. Tool and Alloy Steels, 1980, **14**, 12, 397-401.

117 Fichtl, W. Boronising and its practical application. Mat.Eng., 1981, **12**, 12, 276-286.

118 Method of forming a Carbide Layer. U.K. Patents 1378478 and 1411927.

119 Arai, T. Carbide coating process by use of molten borax bath part 2. Practical and applications to Cold Forging dies in Japan. Wire, 1981 **31**, 5, 208-210.

120 Arai, T. and Komatsu, N. Development and industrial application of carbide coating process using molten borax bath. Metals Australia, 1983, **15**, 8, 8-11.

121 Arai, T. Carbide coating process by use of molten borax bath in Japan. J. Heat treating, 1979, **1**, 2, 15-22.

122 Arai, T. Carbide coating process by use of molten borax bath part 1. Process and application to Cold Forging dies in Japan. Wire, 1981,**31**, 3, 102-104.

123 Yee, K.K. Protective coatings for metals by Chemical Vapour Deposition. Int.Met.Rev., 1978, **23**,1, 9-41.

124 Matthews, A. Titanium Nitride coatings technology. Surface Engineering, 1985, **1**, 2, 93-103.

125 Jacobson, B.E., Nimmagadda,R. and Bunshah, R.F. Microstructure of TiN and $Ti_2N$ deposits prepared by Activated Reactive Evapouration. Thin Solid Films, 1979, **63**, 333-339.

126 Buhl, R. and Puker, H.K.and E. Moll. TiN coatings on steel. Thin Soild Films, 1981, **80**, 265-300.

127 Bucher, J.P., Ackermann, K.P. and Bushor, F.W. R.F. sputtered TiN : Characterization and adhesion to materials of technical interest. Thin Solid Films, 1984, **122**, 63-71.

128 Ramaligam, S. and Winer, W.O. Reactively sputtered TiN coatings for tribological applications. Thin Solid Films, 1980, **73**, 267-274.

129 Hibb, M.K. The microstructure of Reactively sputtered TiN films. Thin Solid Films, 1983, **107**, 149-157.

130 Nethercott, R.B. Advances in surface processing by Physical Vapour Deposition. Metals Australia, 1984, **16**, 6, 10-12.

131 Hinterman, H.E. Adhesion, friction and wear of thin hard films. Wear, 1984, **100**, 381-397

132 Sundquist, H.A., Sirvio, E.H. and Kurkinen, M.T. Wear of metal working tools ion plated with titanium nitride. Proc.Conf. on Ion assisted surface treatments, techniques, and processes. Warwick University 1982, paper 7, published by the Metal Soceity 1982.

133 Sirvio, E.H. and Sulonen, M. Abrasive wear of Ion plated titanium nitride coatings on plasma nitrided surface. Thin Solid Films, 1982, **96**, 93-101.

134 Goldstein, A.W.., Rostoker, W. and Schossberger, K. Structure of chemically deposited nickel. J. Electrochem.Soc., 1957, **104**, 2, 104-110.

135 Graham, A.H., Lindsay, W.R. and Read, H.J. The Structure and mechanical properties of Electroless Nickel. J.Electrochem.Soc., 1965, **112**, 4, 401-412.

136 Randin, J.P. and Hinterman, H.E. Electroless Nickel deposisted at controlled pH, mechanical properties as a function of phosphours content. Plating, 1967, **54**, 523-532.

137 Parker, K. Hardness and wear resistance tests of Electroless Nickel deposits. Plating, 1974, **61**, 834-840.

138 Tope, N.A. and Baker, E.A. and Jackson, B.C. Evaluation of wear properties of Electroless Nickel. Plat.Surf.Fin. 1976, **63**, 10, 30-34.

139 Ma, U. and Gawne, D.T. Effects of counterface materials on the wear of Electroless Nickel - Phosphorus coatings. Trans.Int.Met.Fin., 1986, **64**, 4, 129-133.

140 Parker, K. Effects of heat treatment on the properties of Electroless Nickel deposits. Plat.Surf., 1981, **68**, 12, 71-77.

141 de Minjer, C.H. and Brenner, A. Studies on Electroless Nickel plating. Plating, 1957, **44**, 1297-1305.

142 Mallory, G.O. Influence of Electroless Nickel plating bath on the corrosion resistance of the deposits. Plating, 1974, **61**, 1005-1014.

143 Sadeghi, M., Longfield, P.D. and Beer, C.F. Effects of heat treatment on the structure, corrosion, resistance, and stripping of Electroless Nickel coatings. Trans.Int.Met.Fin., 1983, **61**, 141-146.

144 Trudgeon, M.A. and Griffiths, J.R. Corrosion resistance of Electroless Nickel coatings in Mining enviroments. Br.Corrs.J., 1986, **2**, 113-118.

145 Van Gool, A.P., Boden, P.J. and Harris, S.J. Corrosion behaviour of some Electroless Nickel-Phosphorus coatings. The Institute of Metal Finishing 1987 Annual Technical Conference.

146 Feldstein, N., Lansek, T. and Lindsay, D. Electroless Nickel Composite Plating Met.Fin., 1983, **81**, 8, 35-41.

147 Tulsi, S.S. Composite P.T.F.E.- Nickel coatings for low friction applications. Materials & Design, 1984, **4**, 12, 919-923.

148 Tulsi, S.S. Electroless Nickel-P.T.F.E. Composite coatings. Trans.Met.Fin., 1983, **61**, 147-149.

149 Thomas, R. Master of Philosophy Thesis, Aston University 1988.

150 Edenhofer, B. The Ionitriding Process-Thermochemical treatment of steel and cast iron materials. The Metallurgist and Materials Technologist, 1976, **8**, 8, 421-426.

151 Edenofer, B. Physical and Metallurgical aspects of Ionitriding. Heat Treatment of Metals, **1974.1**, 23-38.

152 Zang, Z.I. and Bell, T. Structure and Corrosion Resistance of Plasma Nitrided Stainless Steels. Surface Engineering, 1985, **1**, 131-136.

153 Ramchandani, A. Nitriding of austenitic stainless steels. Master of Philosophy Thesis, Aston University, 1986.

154 Wood, G.W., co-ordinator, Metals Handbook (ninth edition), volume 5, Surface cleaning, finishing, and coating, p 361-374. A.S.M. publication, 1982, Metals Park, Ohio 44073.

155 Nicoll, A.R., Gruner, H., Prince, R. and Wuest, G. Thermal spraying coatings for high temperature protection. Surface Engineering, 1985, **1**, 1, 59-71.

156 Smart, R.F. and Catherall, J.A. Plasma spraying. M&B Technical Libary-Mechanical Engineering, 1970.

157 Malik, M.P. Plasma sprayed coatings in aircraft and engine components. 7 th Int. Conf. on Metal Spraying, London, 10-14 th Sept 1973, volume 1, 257-267, Published by The Welding Institute, Cambrigde, U.K., 1974.

158 Kreye, H., Fandrich, D., Mullerm H.H. and Reiners, G. Microstructure and Bond Strength of WC-Co coatings deposited by Hypersonic Flame spraying(Jet-Kote process). Advances in Thermal Spraying, Pergamon Press, New York, U.S.A., 1986, 121-128.

159 Arata, Y., Ohmori, A. and Gofuku, E. Studies of WC-Co system coating by High Energy Thermal Spraying. Advances in Thermal Spraying, Pergamon Press, New York, U.S.A., 1986, 873-833.

160 Rao, K.V., Somerville, D.A. and Lee, D.A. Properties and characterization of coatings made using the Jet-Kote termal spraying technique. Advances in Thermal Spraying, Pergamon Press, New York, U.S.A., 1986,873-883.

161 Stern, M. A method for determining corrosion rates from linear polarisation. Corrosion N.A.C.E., 1958, **14**, 440t - 443t.

162 Bowden, F.P. and Tabor, D. Friction-An Introduction to Tribology. Heinman Educational Books.

163 Bowden, F.P. and Leben, L. The nature of sliding and analysis of friction. Proy. Roy. Soc., 1939, **A169**, 371-390.

164 Gaung-Xi, L., Geng-Fu, L. and Fu-Chang, Y. The effect of phosphorus content and heat treatment on the wear resistance of elecroless nickel deposits Ni-P alloys. Wear, 1985, **103**, 269-279.

165 Gawne, D.T. and Ma, U. Wear mechanisms in Electroless Nickel coatings. Wear, 1987, **120**, 125-149.

166 Evans, A.G. and Wilshaw, T.R. Quasi-static solid particle damage in brittle solids: Observations, analysis, and implications. Acta Metallurgica, 1976, **24**, 935-956.

167 Tomlinson, W.J. and Mayor, J.P. Formation, microstructure, surface roughness, and porosity of electroless nickel coatings. Surface Engineering, 1988, **4**, 3, 235-238.

168 Beer, C.F. How to improve the quality of electroless nickel deposits. Trans. Inst. Met. Fin., 1987, **66**, 140-142.

169 Brown, L.D. Factors affecting the corrosion resistance of electroless nickel coatings. Electroless Nickel 87, one day Symposium organised by the I.M.F. and B.E.N.S. held at Aston University on October 21st 1987.

170 Flis, J. and Duquette, D.J. Effects of phosphorus on anodic dissolution and passivation of nickel in near-neutral solutions. Corrosion N.A.C.E., 1985, **41**, 12, 700-706

171 Pai, S.T. and Marton, J.P. The Composition of oxides formed on electroless Ni-P deposits. J. Electrochem. Soc., 1973, **120**, 1280-1281.

172 Hochmann, R.F., Kim, H.J. and Marek, M. Corrosion of ion plated metal surfaces. Proc. Conf. on the Application of Ion Plating and Implantation to materials. Atlanta, Georgia, U.S.A., June 1985, Hochmann, R.F., Editor. Published by A.S.M. 1986.

173 Alina, W., Erdemir, A. and Hochmann, R.F. The friction wear and corrosion properties of ion plated TiN.Proc. Conf. on the Application of Ion Plating and Implantation to materials. Atlanta, Georgia, U.S.A., June 1985, Hochmann, R.F., Editor. Published by A.S.M. 1986.

174 Stevens, K.T. P.V.D. coatings- Their properties and potential applications. Plasma Assisted Coatings Technology Seminar (P.A.C.T.) organised by the National Centre for Tribology (N.C.T.) on 12 June, 1986.

## 9.4 APPENDICES

### APPENDIX ONE

### TAFEL EXTRAPOLATION TECHNIQUE

#### Theory

The tafel equations may be derived from the Volmer-Butler equation. The latter relates the net current density of the electrochemical reaction to the overpotential.

#### Volmer-Butler Equation

$$I = I_o \{\exp [(1-\beta) F \phi / R T] - \exp [-\beta F \phi / R T]\} \qquad (A1.1)$$

$I$ = Net current density

$I_o$ = Exchange current density

$\beta$ = Symmetry factor

$F$ = Faraday's constant

$\phi$ = Overpotential and $\phi = \phi_{APP} - \phi_{CORR}$

$R$ = Gas constant

$T$ = Temperature (K)

$\phi_{APP}$ = Potential applied to specimen

$\phi_{CORR}$ = Corrosion potential

For an electrochemical reaction occuring at large anodic overpotentials i.e. at $\phi = >>RT$

The second term in the Volmer-Butler equation can be neglected, so that:

$$I = I_o \exp [(1 - \beta) F \phi / R T] \qquad (A1.2)$$

For electrochemical reactions occuring at high cathodic overpotentials i.e. at $\phi << RT$

The first term in the Volmer-Butler equation may be neglected, so that:

$$I = I_o \exp (-\beta F \phi / R T) \qquad (A1.3)$$

Equations (A1.2) and (A1.3) may be re-written as:

for $\phi >> R T$

$$\phi = \frac{-2.3 R T}{(1 - \beta) F} \log I_o + \frac{2.3 R T}{(1 - \beta) F} \log I \qquad (A1.4)$$

for $\phi << R T$

$$\phi = \frac{-2.3 R T}{\beta F} \log I_o + \frac{2.3 R T}{\beta F} \log (-I) \qquad (A1.5)$$

The above equations are called Tafel equations after J.Tafel, who proposed an equation of similar form in 1904, to express the hydrogen overpotential as a function of current density. The relationships described so far are dependent only on activation overpotential. This measurement may be complicated by two, interfering phenomenon: concentration polarization and resistance drop effects.

## APPENDIX TWO

### LINEAR POLARISATION TECHNIQUE

The derivation of the polarisation resistance ($R_p$) parameter by Stern and Geary is outlined below:

In a corroding system, two co-existing electrochemical reactions are present

$$M \longrightarrow M^+ + e^- \qquad (I_{1a})$$

$$M^+ + e^- \longrightarrow M \qquad (I_{2c})$$

$$Z \longrightarrow Z^+ + e^- \qquad (I_{2a})$$

$$Z^+ + e^- \longrightarrow Z \qquad (I_{2c})$$

Where M is a corroding metal and Z is usually a species in solution. When the corrosion potential ($\phi_{CORR}$) is sufficiently removed from the equilibrium potentials of M and Z; $\phi_{01}$ and $\phi_{02}$ respectively. The rate of reduction of $M^+$ ($I_{1c}$) becomes insignificant to the rate of oxidation of M ($I_{1a}$), and the rate of oxidation of Z ($I_{2a}$) becomes insignificant with respect to the rate of reduction of $Z^+$ ($I_{2c}$). The corrosion potential is the potential at which the rate of oxidation of M ($I_{1a}$) is equal to the rate of reduction of $Z^+$ ($I_{2c}$). Since the net current is the difference between the oxidation and reduction currents, the current measured with an external device will be zero.

$$I = I_{1a} - I_{2c} = 0 \qquad \text{at } \phi_{CORR} \qquad (A2.1)$$

$$\text{also } I_{CORR} = I_{1a} = |I_{2c}| \qquad (A2.2)$$

Assuming that the anodic and cathodic currents obey Tafel kinetics, then:

$$\phi = BA.\log\frac{I_{1a}}{I_{CORR}} \qquad \text{(Anodic reaction)} \qquad \text{(A2.3)}$$

$$\phi = BC.\log\frac{I_{2c}}{I_{CORR}} \qquad \text{(Cathodic reaction)} \qquad \text{(A2.4)}$$

re-arranging the above equations

$$\log\frac{I_{1a}}{I_{CORR}} = \frac{\phi}{BA} \qquad \text{(A2.5)}$$

$$\log\frac{I_{2c}}{I_{CORR}} = \frac{\phi}{BC} \qquad \text{(A2.6)}$$

Since $\log x = y$ is same as $10^y = x$, the above equations may be expressed as follows:

$$10^{\phi/BA} = \frac{I_{1a}}{I_{CORR}} \qquad \text{(A2.7)}$$

$$10^{\phi/BC} = \frac{I_{2c}}{I_{CORR}} \qquad \text{(A2.8)}$$

Substitution of equations (A2.7) and (A2.8) into equation (A2.1) gives:

$$I = I_{CORR}\,(10^{\phi/BA} - 10^{-\phi/BC}) \qquad \text{(A2.9)}$$

$10^x$ can be approximated by the following power series:

$$10^x = 1 + 2.3x + \frac{(2.3x)^2}{2!} \ldots\ldots\ldots\ldots \frac{(2.3x)^n}{n!}$$

If x is small, the 3rd and latter terms of series can be neglected without significant error

i.e.

$$10^{\phi/BA} = 1 + 2.3\,\phi / BA \qquad \text{(A2.10)}$$

$$10^{\phi/BC} = 1 + 2.3\,\phi / BC \qquad \text{(A2.11)}$$

Substituting equations (A2.10 & A2.11) into equation (A2.9) leads to the Stern-Geary equation:

$$\frac{\phi}{I} = \frac{(B\,A\,.\,B\,C)}{2.3\,I_{CORR}\,(B\,A + B\,C)} \qquad \text{(A2.12)}$$

or

$$\frac{\Delta\phi}{\Delta I} = R_p = \frac{(B\,A\,.\,B\,C)}{2.3\,I_{CORR}\,(B\,A + B\,C)} \qquad \text{(A2.13)}$$

The derivation of equation (A2.13) assumes:

1. The Volmer-Butler equations of electrochemical kinetics are applicable.
2. Ohmic drops in the electrolyte and in surface films are absent.
3. Concentration polarization is absent
4. The corrosion potential does not lie close to the reversible potentials of either of the two reactions occurring

5. The whole metal functions simultaneously as a cathode and an anode rather than being a mosaic of separate cathodic and anodic areas.
6. There are no secondary electrochemical reaction occurring.

The Stern-Geary equation (A2.13) is only valid if $\phi/BA$ and $\phi/BC$ are small. This means $\phi$ must be small compared to BA or BC. A typical value of BA is 100 mV/decade, the overpotential in this case should be less than 10 mV. In general, to construct a linear polarisation plot, the potential is scanned over a range $\pm$ 10 mV with respect to the corrosion potential. If the Tafel slopes are known, or may be assumed, the determined polarisation resistance, $R_p$, can be computed into the Stern-Geary equation to calculate the corrosion current density.

The derivation of the Stern-Geary equation is based on an approximation involving the difference of two power terms. In contrast, the derivation by Oldham and Mansfeld[104] avoids the approximation made by Stern and Geary[91].

Derivation by Oldham and Mansfeld[104]

Equations (A1.1) and (A2.1) may be expressed as:

$$I_{CORR} = I_{1a} = (I_{2c})$$

$$I_{CORR} = I_{01} \exp\frac{(\phi_{CORR} - \phi_{01})}{B\,A'} = I_{02} \exp\frac{(-\phi_{CORR} - \phi_{02})}{B\,C'} \qquad (A2.14)$$

and

$$I = I_{1a} - I_{2c} = 0 \quad \text{at } \phi_{CORR}$$

becomes

$$I = I_{01} \exp\frac{(\phi_x - \phi_{01})}{B\,A'} - I_{02} \exp\frac{(-\phi_x - \phi_{02})}{B\,C'} \qquad (A2.15)$$

$\phi_x$ = Potential

$\phi_{01}$ = Reversible potential for metal M

$\phi_{02}$ = Reversible potential for species Z

$I_{01}$ = Exchange current density for metal M

$I_{02}$ = Exchange current density for species Z

Differentiation of equation (A2.15) with respect to the potential $\phi_x$ gives:

$$\left(\frac{dI}{d\phi}\right)_{\phi_x} = \frac{I_{01}}{BA'} \exp\frac{(\phi_x - \phi_{01})}{B\,A'} + \frac{I_{02}}{BC'} \exp\frac{(\phi_{02} - \phi_x)}{B\,C'} \qquad (A2.16)$$

At the corrosion potential ($\phi_x = \phi_{CORR}$) the gradient of the current potential curve dI / $d\phi$ becomes:

$$\left(\frac{dI}{d\phi}\right)_{\phi_{CORR}} = \frac{I_{01}}{BA'} \exp\frac{\phi_{CORR} - \phi_{01}}{B\,A'} + \frac{I_{02}}{BC'} \exp\frac{(\phi_{02} - \phi_{CORR})}{B\,C'} \quad (A2.17)$$

Equation (A2.14) may be expressed as:

$$I_{01} = I_{CORR} \exp\frac{(\phi_{01} - \phi_{CORR})}{B\,A'} \quad (A2.18)$$

$$I_{02} = I_{CORR} \exp\frac{(\phi_{CORR} - \phi_{02})}{B\,C'} \quad (A2.19)$$

Combining the above equations with Eq.(A2.17) leads to:

$$\left(\frac{d\,I}{d\,\phi}\right)_{\phi_{CORR}} = R_p = I_{CORR}\left(\frac{1}{B\,A} + \frac{1}{B\,C}\right) \quad (A2.20)$$

also $B\,A = 2.303.\,B\,A'$ (A2.21)

$B\,C = 2.303.\,B\,C'$ (A2.22)

so that equation (A2.20) can be formulated as:

$$\left(\frac{d\,I}{d\,\phi}\right)_{\phi_{CORR}} = R_p = I_{CORR}\,\frac{2.3\,(B\,A + B\,C)}{B\,A\,.\,B\,C} \quad (A2.23)$$

# APPENDIX 3

## DIGITAL LOGIC METHOD

Given five material requirements, then the number of possible decisions is given by the following equation:

$$N = n(n - 1) / 2 \qquad (A3.1)$$

where

N, is the number of decisions

n, is the number of material requirements.

In the above case $n = 5$ therefore,

$$N = 5 \times 4/2 = 10$$

| material requirement | 1 | 2 | 3 | 4 | 5 | 6 | 7 | 8 | 9 | 10 | positive decisions | |
|---|---|---|---|---|---|---|---|---|---|---|---|---|
| req. 1 | 2 | 2 | 3 | 3 | | | | | | | 10 | 0.31 |
| req. 2 | 1 | | | | 2 | 2 | 3 | | | | 8 | 0.25 |
| req. 3 | | 1 | | | 1 | | | 2 | 2 | | 6 | 0.20 |
| req. 4 | | | 1 | | | 1 | | 1 | | 1 | 4 | 0.12 |
| req. 5 | | | | 1 | | | 1 | | 1 | 1 | 4 | 0.12 |
| | | | | | | | | | | | --- | --- |
| | | | | | | | | | | | 32 | 1.00 |

The above table represents an example where there are five different material requirements. Each requirement is compared in turn with the other and given a value 1, 2 or 3. Thus $\alpha$ values are calculated. The material properties are converted to $\beta$ values (a common base) using the following equations:

$$\beta = \frac{\text{numerical value of the property} \times 100}{\text{maximum value of the property in the list}} \qquad \text{(A3.2)}$$

or for the properties where a low property value is preferred:

$$\beta = \frac{\text{lowest value of the property in the list} \times 100}{\text{numerical value of the property}} \qquad \text{(A3.3)}$$

The next stage in the analysis is to multipy each $\beta$ value with the corresponding $\alpha$ value, the product is termed the $\gamma$ value. The products are then summed and the material having the largest $\Sigma\gamma$ is the preferred material.